UNIVERSIDADE FEDERAL DE ITAJUBÁ

PROGRAMA DE PÓS-GRADUAÇÃO EM

MEIO AMBIENTE E RECURSOS HÍDRICOS

VALIDATION OF SEASONAL CLIMATE PREDICTIONS FOR SOUTH AMERICA: ECMWF-SEAS5 GLOBAL MODEL

Glauber Willian de Souza Ferreira

Itajubá/MG

2021

UNIVERSIDADE FEDERAL DE ITAJUBÁ

PROGRAMA DE PÓS-GRADUAÇÃO EM

MEIO AMBIENTE E RECURSOS HÍDRICOS

Glauber Willian de Souza Ferreira

Validation of seasonal climate predictions for South America: ECMWF-SEAS5 global model

Dissertation submitted to the Postgraduate Program in Environment and Water Resources in partial fulfilment of the requirements for the degree of Master in Environment and Water Resources

Concentration Area: Environment and Water Resources

Advisor: PhD Michelle Simões Reboita

Itajubá/MG

2021

UNIVERSIDADE FEDERAL DE ITAJUBÁ

PROGRAMA DE PÓS-GRADUAÇÃO EM

MEIO AMBIENTE E RECURSOS HÍDRICOS

Glauber Willian de Souza Ferreira

Validation of seasonal climate predictions for South America: ECMWF-SEAS5 global model

Dissertation approved by the examining committee on December 16, 2021, granting the author the title of Master of Science in Environment and Water Resources.

Examining Comitee:

Dr. Michelle Simões Reboita (Advisor)
Federal University of Itajubá

Dr. Roger Rodrigues Torres
Federal University of Itajubá

Dr. Rosmeri Porfírio da Rocha
University of São Paulo

Dr. Natália Machado Crespo
University of São Paulo

Itajubá/MG
2021

DEDICATION

“Dedicated to my Mom.”

ACKNOWLEDGMENTS

I am pretty grateful to my advisor and professor, Michelle Reboita, for the opportunity for a Master's degree, for her patience and confidence, all the knowledge and support offered since Graduation.

I am grateful to my parents and siblings for their love and support. Special thanks to my mother for her companionship and unconditional love.

I thank the professors Rosmeri da Rocha, Natália Crespo and Roger Torres for their evaluation, review of the dissertation and valuable suggestions for the work.

I thank the Postgraduate Program in Environment and Water Resources (POSMARH) for the opportunity for a Master's degree and apprenticeship.

I thank the Coordination for the Improvement of Higher Education Personnel (CAPES) for the scholarship provided.

I thank all professors from the POSMARH for their knowledge and experience.

I thank the European Centre for Medium-Range Weather Forecasts and the Climate Prediction Center for providing the data used in this study.

"Climate lasts all the time and weather only a few days."
Mark Twain, *English as She is Taught*

"Even as I speak, the very last polar bear may be dying of hunger on account of climate change, on account of us. And I sure miss the polar bears. Their babies are so warm and cuddly and trusting, just like ours."
Kurt Vonnegut, *Armageddon in Retrospect*

ABSTRACT

This work evaluated the quality of ECMWF-SEAS5 seasonal precipitation and 2 m temperature predictions for South America. For this purpose, datasets of hindcasts from 1993 to 2016 and forecasts from 2017 to 2020 were used. The predictions were validated against CPC precipitation and temperature analyses. The average seasonal fields indicated that the model has a good representation of the seasonal rainfall patterns in South America, adequately simulating the wet and dry phases of the monsoon. However, the hindcasts present systematic overestimation of rain in the Amazon, South Brazil, Southeast Brazil, and northern South America sectors. In addition, the model also presents an underestimation of rain in Northeast Brazil and southeastern South America. Regarding the temperature results, the model showed a systematic cold bias over most of the continent, except for portions of Northeast Brazil and southeastern South America. The skill score evaluation showed that the main correlations of precipitation and temperature anomaly occur in regions of high climate predictability, such as the tropical latitudes of the continent. The regionalized mean anomalies indicated that ECMWF-SEAS5 has a good performance to simulate the interannual variability of rainfall and temperature, especially in transition seasons. However, hindcasts were not efficient for predicting anomalous events such as the 2014/2015 drought in Southeast Brazil and the 2015 drought in the east of the Amazon. The analysis of the forecasts from 2017 to 2020 showed that systematic errors of overestimation (underestimation) of rainfall persist in regions such as the Amazon, Southeast Brazil, South Brazil, and northern South America (Northeast Brazil and southeastern South America). Similarly, temperature underestimation (overestimation) errors in most of the continent (Northeast Brazil and southeastern South America) remain in the real-time forecasts. Overall, it is concluded that the ECMWF-SEAS5 model performs seasonal rainfall and temperature predictions for South America with considerable dexterity and potential for diverse applications. However, its limitations and errors must be considered for the best use of its predictions.

Keywords: Seasonal climate prediction; South America; Precipitation; Temperature; Global model; Climatology; Teleconnections.

RESUMO

Este trabalho avaliou a qualidade das previsões climáticas sazonais de precipitação e temperatura do ar do ECMWF-SEAS5 para a América do Sul. Para isso, foram utilizados conjuntos de dados de *hindcasts* de 1993 a 2016 e de *forecasts* de 2017 a 2020. As previsões foram validadas mediante comparação com análises de precipitação e temperatura do CPC. Os campos sazonais médios indicaram que o modelo possui boa representação dos padrões sazonais de chuva na América do Sul, simulando adequadamente a fase úmida e seca da monção. Apesar disso, os *hindcasts* apresentam superestimativa sistemática de chuva em setores como a Amazônia, Sul e Sudeste brasileiros e norte da América do Sul. Além disso, o modelo também apresenta subestimativa de chuva no Nordeste do Brasil e sudeste da América do Sul. Para a temperatura, o modelo apresentou viés frio sistemático sobre a maior parte do continente, com exceção de porções do Nordeste do Brasil e sudeste da América do Sul. A avaliação da performance do modelo mostrou que as principais correlações de anomalia de precipitação e temperatura ocorrem em regiões de alta previsibilidade climática como as latitudes tropicais do continente. As anomalias médias regionalizadas indicam que o modelo possui boa capacidade de simular a variabilidade interanual de chuva e temperatura, principalmente em estações de transição. Entretanto, os *hindcasts* não se mostraram eficientes para a previsão de eventos anômalos como a seca de 2014/2015 no Sudeste brasileiro e a seca de 2015 no leste da Amazônia. A análise das previsões prognósticas de 2017 a 2020 mostrou que os erros sistemáticos de superestimativa (subestimativa) de precipitação persistem em regiões como Amazônia, Sudeste e Sul do Brasil e norte da América do Sul (Nordeste brasileiro e sudeste da América do Sul). Similarmente, erros de subestimativa (superestimativa) de temperatura na maior parte do continente (Nordeste brasileiro e sudeste da América do Sul) permanecem nas previsões prognósticas. De forma geral, conclui-se que o modelo ECMWF-SEAS5 executa previsões sazonais de precipitação e temperatura para a América do Sul com considerável destreza e potencial para aplicações diversas. Entretanto, devem ser consideradas suas limitações e erros para melhor utilização de suas previsões.

Palavras-chave: Previsão climática sazonal; América do Sul; Precipitação; Temperatura; Modelo global; Climatologia; Teleconexões.

LIST OF FIGURES

LIST OF ABBREVIATIONS AND ACRONYMS

AGCMs – Atmospheric general circulation models

AMIP – Atmospheric Model Intercomparison Project

AMJ – April-May-June

AMZ – Amazon

ASO – August-September-October

BH – Bolivian High

C3S – Copernicus Climate Change Service

CanSIPS – Canadian Seasonal to Interannual Prediction System

CFSv2 – Climate Forecast System version 2

CMC – Canadian Meteorological Center

CMCC – Centro Euro-Mediterraneo sui Cambiamenti Climatici

CMIP5 – Coupled Model Intercomparison Project Phase 5

COLA – Center for Ocean-Land-Atmosphere Studies

CPC – Climate Prediction Center

CPTEC – Center for Weather Forecast and Climate Studies

d – Willmott's Index of Agreement

DJF – December-January-February

DWD – Deutscher Wetterdienst

ECCC – Environment and Climate Change Canada

ECWMF – European Centre for Medium-Range Weather Forecasts

ECMWF-MOFC – ECMWF Monthly Weather Forecast

ENSO – El Niño-Southern Oscillation

EWDs – Easterly wave disturbances

FCDO – Foreign Commonwealth and Development Office

FMA – February-March-April

Funceme – Cearense Foundation of Meteorology and Water Resources

GCMs – General circulation models

GDP – Gross Domestic Product

GFDL MOM4 – Geophysical Fluid Dynamics Laboratory Modular version 4.0

GrEC – Climate Studies Group

IFS – Integrated Forecast System

ILs – Instability lines

Inmet – National Institute of Meteorology

INPE – Brazilian National Institute for Space Research

IOD – Indian Ocean Dipole

IRI – International Research Institute for the Climate and Society

ITCZ – Intertropical Convergence Zone

JAS – July-August-September

JFM – January-February-March

JJA – June-July-August

JMA – Japan Meteorological Agency

KGE – Kling-Gupta Efficiency

LLJs – Low-Level Jets

MAE – Mean Absolute Error

MAM – March-April-May

MCCs – Mesoscale convective complexes

McICA – Monte Carlo Independent Column Approximation method

MCSs – Mesoscale convective systems

MJJ – May-June-July

MJO – Madden-Julian Oscillation

NCEP – National Centers for Environmental Prediction

NDJ – November-December-January

NEB – Northeast of Brazil

NEMO – Nucleus for European Modelling of the Ocean

NMME – North American Multimodel Ensemble

NOAA – National Oceanic and Atmospheric Administration

NPSH – North Pacific Subtropical High

NSA – Northern South America

NSE – Nash-Sutcliffe Efficiency

OND – October -November-December

r – Pearson's Coefficient of Correlation

R^2 – Coefficient of Determination

RCMs – Regional climate models

RE – Relative Error

RMSE – Root Mean Square Error

SA – South America

SACZ – South Atlantic Convergence Zone

SAM – Southern Annular Mode

SASA – South Atlantic Subtropical Anticyclone

SB – South of Brazil

SEAS4 – ECMWF System 4

SEAS5 – ECMWF System 5

SEB – Southeast of Brazil

SESA – Southeastern South America

SI – Seasonality Index

SON – September-October-November

SST – Sea surface temperature

ULCVs – Upper-level cyclonic vortices

USP – University of São Paulo

WMO LC-LRFMME – World Meteorological Organization Lead Center for the Long-Range Forecast Multi-Model Ensemble

SUMMARY

1. INTRODUCTION

South America (SA) is a continent with a broad latitudinal extension and diversity of biomes, favouring different climates within its territory. In addition, climatic conditions directly influence the main socioeconomic activities developed in the region. These activities include agriculture, power generation, fishing, tourism, and the textile industry. Consequently, information derived from seasonal climate predictions is vital for different sectors of South American society.

Due to the chaotic internal dynamics of the atmosphere, the prediction of detailed evolution of meteorological events is limited from a few days to two weeks (LORENZ, 1965). However, the statistical behaviour of the weather, expressed by its temporal and spatial averages, can be predicted on time scales of a season or longer (LEE; WANG, 2012). The mathematical models used for weather and climate prediction are based on the same physical principles and sets of equations (KALNAY, 2003; VITART; ROBERTSON, 2019). The primary difference is that climate models need additional climate system components, such as oceans, land, cryosphere, atmospheric chemistry (including aerosols, ozone, greenhouse gases), and a more detailed representation of the stratosphere (VITART; ROBERTSON, 2019).

Pioneering studies (CHARNEY; SHUKLA, 1981; HOSKINS; KAROLY, 1981; WEBSTER, 1972) laid the theoretical foundations for the numerical climate prediction progress (SAMPAIO; SILVA DIAS, 2014). This type of forecast derives mainly from the predictability of the boundary conditions, such as sea surface temperature (SST), sea ice, soil moisture, and snow cover, and from the significant influence of these variables in determining future atmospheric conditions (BRANKOVIĆ; PALMER, FERRANTI, 1994; BRANKOVIĆ; PALMER, 1997; PALMER; ANDERSON, 1994; SHUKLA, 1998; SHUKLA et al., 2000a,b; WANG et al., 2009). It is possible to predict SST anomalies associated with El Niño (or its opposite, La Niña) a few months in advance (BARNSTON et al., 2012), leading to the predictability of their atmospheric impacts (AMBRIZZI; SOUZA; PULWARTY, 2004; ANDREOLI; OLIVEIRA; KAYANO, 2016; CAI et al., 2020; COELHO; DRUMOND; AMBRIZZI, 1999; GRIMM; BARROS; DOYLE, 2000; REBOITA et al., 2021a; ROPELEWSKI; HALPERT, 1987; SILVA; AMBRIZZI, 2006).

Seasonal climate forecasts can be performed with atmospheric general circulation models (AGMs) or coupled ocean-atmosphere models. Within this range of models, there are ones with a global resolution, also known as global climate models (GCMs), and others of limited area, also called regional climate models (RCMs) (AMBRIZZI et al., 2018; GIORGI, 2019; REBOITA et al., 2018). The typical horizontal resolution of global models, such as those of the North American Multimodel Ensemble (NMME; KIRTMAN et al., 2014), is 100 km, while regional models have a resolution of a few hundred metres (VITART; ROBERTSON, 2019). In general, RCMs produce more accurate simulations since they have more refined horizontal resolution and physical parameters more suitable for mesoscale atmospheric processes (DICKINSON et al., 1989; GIORGI; MEARNS, 1999; MISRA; DIRMEYER; KIRTMAN, 2003; REBOITA et al., 2018).

Considering AGCMs and coupled models, Lin, Dong, and Fan (2018) evaluated how 27 AGCMs from the Atmospheric Model Intercomparison Project (AMIP) and 34 coupled models from the Coupled Model Intercomparison Project Phase 5 (CMIP5) simulated the seasonal variation of the North Pacific Subtropical High (NPSH) during boreal summer. Results showed that AMIP models could reproduce the NPSH weakening at the beginning of the boreal summer but fail to simulate its weakening at the end of the season. On the other hand, CMIP5 models performed better in reproducing the NPSH magnitude and associated precipitation. Thus, the authors conclude that a good simulation of air-sea interactions is essential and should not be neglected in NPSH studies.

Concerning global and regional models, as Giorgi (2019) stated, both are complementary and should not be seen as competing models. Inversely, GCMs, RCMs, and other downscaling techniques are complementary methods that can help better understand regional climate or climate change processes (GIORGI, 2019). The diversity of models and spatial resolutions allows for different studies and analyses to be carried out, given the potential and limitations of each method.

Within the framework of global climate models, the ECMWF seasonal forecasting system has proven to be one of the best forecasting models of the El Niño-Southern Oscillation (ENSO) (BARNSTON et al., 2012; GUBLER et al., 2020). The ENSO phenomenon is one of the main modes of influence on a seasonal scale over South America (ACEITUNO, 1988; BERRI; BIANCHI; MÜLLER, 2019; CAI et al., 2020; GRIMM, 2003; GRIMM; BARROS; DOYLE, 2000; KOUSKY; KAYANO; CAVALCANTI, 1984; REBOITA et al., 2021a; TEDESCHI;

COLLINS, 2016; VIEGAS et al., 2019), and their correct predictability is fundamental to the assertiveness of the seasonal climate forecast over SA.

Seasonal climate predictions are essential for the electricity sector, as they benefit activities related to the generation, transmission, and distribution of energy. Furthermore, seasonal precipitation predictions are relevant information for the simulation of planning models that define the generation of energy from hydroelectric and thermal plants and the interchanges between the subsystems, optimizing the use of reservoirs and meeting the energy demand in the country (WEBER et al., 2015).

Seasonal climate predictions may also benefit agriculture, another relevant South American economic sector. Agricultural activity has a fundamental role in Brazil's economy, representing 21.4% of the Gross Domestic Product (GDP) and significant importance in global markets (CEPEA/USP-CNA, 2020; MARTINS et al., 2018). Moreover, agriculture is one of the activities most sensitive to climatic effects, given that its productivity depends directly on the temperature and precipitation conditions of the region where it is performed (PIEDRA-BONILLA et al., 2020; TOL, 2009, 2018).

Despite technological advances and increased productivity, the effects of weather and climate have always had a strong influence on agriculture, and several studies have investigated the interaction between climate and agricultural activity (ASSENG et al., 2014; GREATREX, 2012; LENG et al., 2016; LOBELL; FIELD, 2007; WHEELER; VON BRAUN, 2013). Furthermore, precipitation events play an essential role in several stages of agriculture, such as soil preparation, planting, pesticide application, and harvesting (MORETO et al., 2020). In this context, climate predictions on monthly and seasonal scales are of potential value for farmers and decision-makers in the sector (EASTERLING; MJELDE, 1987; SONKA et al., 1992), as they assist in irrigation management, selection of the appropriate crop, choice planting and harvesting time, fertilizer application, grain storage and sales (MORETO et al., 2020).

The application of seasonal climate predictions in impact models for hydrology and agriculture needs to be improved (CHOU et al., 2020). However, several studies have shown that hindcasts provide statistical measures, such as correlations of anomalies, systematic errors and forecasting skills, which allow to assess properties of the forecasting system and improve seasonal predictions (CHOU et al., 2020; DIRMEYER, 2013; DIRMEYER; HALDER, 2017; GUBLER et al., 2020; HAMIL, 2012; PEGION; KUMAR, 2013; RAJAGOPALAN; LALL; ZEBIAK, 2002; STEFANOVA; KRISHNAMURTI, 2002).

Since ECMWF-SEAS5 constitutes the state-of-the-art global modelling of seasonal climate forecasting and robust predictions are necessary for better planning of various strategic sectors, the present study aims to assess the quality of the European global model over SA. For this purpose, statistical and graphical analyses of trimonthly predictions are made for the set of hindcasts (1993-2016) and forecasts (2017-2020). The analyses are regionalized and validated by comparing the precipitation analysis of the Climate Prediction Center (CPC). It is intended to examine the model's performance in predicting precipitation over the continent and which regions have the best results.

Given that seasonal climate forecasting is an activity in constant development by the scientific community and several socioeconomic sectors in SA can benefit from more accurate climate predictions, this study aims to assess the ECMWF-SEAS5 seasonal climate predictions for the South American continent.

2. AIMS

2.1 General aim

To assess the quality of seasonal precipitation and 2 m temperature predictions from the global model ECMWF-SEAS5 over South America.

2.2 Specific aims

- To validate the ECMWF-SEAS5 seasonal precipitation and 2 m temperature predictions, considering the set of hindcasts and forecasts over South America;

- To examine the quality of ECMWF-SEAS5 seasonal climate predictions in different subdomains of South America: Southeast Brazil (SEB), Northeast Brazil (NEB), Amazon (AMZ), South Brazil (SB), Northern South America (NSA), and Southeastern South America (SESA);

- To assess which regions of South America have their seasonal climate better simulated by the ECMWF-SEAS5 model;

- To analyse the model's performance to predict the seasonal climate over South America considering El Niño events.

3. MOTIVATION

Robust seasonal climate forecasts can benefit decision-makers in numerous socioeconomic activities. The potential for good climate predictions extends across a variety of spheres. For example, they can be applied in flood and drought forecasting (HAO; SINGH; XIA, 2018; ROBERTS; WERNSTEDT, 2016; SHAFIEE-JOOD et al., 2014), crop yield modelling (CEGLAR et al., 2018; VAJDA; HYVÄRINEN, 2020), fisheries management (TOMMASI et al., 2017), wildfires forecasting (CHEN et al., 2011, 2020; GUDMUNDSSON et al., 2014; TURCO et al., 2019), seasonal hurricane prediction (BERGMAN et al., 2019; EMANUEL; FONDRIEST; KOSSIN, 2012; VECHI et al., 2011), heat waves forecasting (LOWE et al., 2016), in the sectors of wind energy (CLARK et al., 2017; TORRALBA et al., 2017), insurance (JEWSON; BRIX, 2005), transport (PALIN et al., 2016), health (LOWE et al., 2011; MORSE et al., 2005; THOMSON et al., 2006), among other areas.

Seasonal climate forecasts assist in strategic planning and decision-making to minimize economic and social damage. Chou et al. (2020) state that if the drought of 2014/2015 in Southeastern Brazil (COELHO et al., 2016; OTTO et al., 2015; REBOITA et al., 2015) had been predicted a few months before, the Brazilian government could have better planning for a drier than normal season.

In this context, this study justifies the ECMWF-SEAS5 validation for the following reasons: it is a state-of-the-art model in seasonal climate forecast whose predictions are publicly available, saving time and computational resources to obtain and analyse data; scarcity of studies that assess the ECMWF-SEAS5 performance over SA, considering the entire series of predictions; ECMWF-SEAS5 has a relatively extensive series of hindcasts, allowing a better evaluation of the model.

Lastly, this study is part of the project “Analysis of hydrological pressure based on global models (CONFAP-WATER-JPI)”. This project consists of a partnership between Brazilian and Swedish researchers who seek to evaluate the physical characteristics of the Sapucaí and São Francisco River basins to assist users through indicators of these regions' climatic and hydrological conditions.

4. CLIMATE MODELLING OVERVIEW

4.1 Seasonal Climate Forecast Modelling

Weather and climate forecasts differ by their period of prediction. Whilst the weather forecast seeks to predict meteorological conditions in an extended period of up to 15 days, the climate forecast projects conditions ahead of two weeks and slightly longer than a year (DOBLAS- REYES et al., 2013). Furthermore, unlike weather forecasting, there is no need to accurately forecast an atmospheric system's place and time in climate predictions, but rather whether the phenomenon is well simulated for a given region (YNOUE et al., 2017).

Weather and climate forecast models use the same set of numerical representations, known as the primitive equations (equations that represent the physical and dynamic processes of the atmosphere, such as the equation of state, equation of conservation of motion, energy conservation, conservation of mass, water conservation, among others). However, climate models also require additional climate system components to represent the sources of climate predictability at longer time scales (MEEHL et al., 2021; SAMPAIO; SILVA DIAS, 2014; VITART; ROBERTSON, 2019). These components refer to the ocean, continental surface, cryosphere, atmospheric chemistry (aerosols, ozone, and greenhouse gases), and a more accurate representation of the stratosphere (VITART; ROBERTSON, 2019). As with weather forecasting, climate forecasting is also susceptible to the effect of chaos (LORENZ, 1965, 1982). In order to represent the chaotic nature of the climate system, GCMs systems produce a set of results provided by members of the model ensemble (LI; JIN; BROWN, 2020).

The feasibility of seasonal climate prediction relies on the occurrence of slow variations in soil moisture, snow cover, sea, and continental ice, vegetation, albedo, surface roughness, and SST, and the knowledge of how the atmosphere interacts with and is affected by these boundary conditions (DOBLAS-REYES et al., 2013; FREDERIKSEN et al., 2001; MA et al., 2021; SHUKLA; KINTER, 2006). In this sense, it is more complex to perform seasonal climate forecast than weather forecast, as in addition to requiring accurate initial atmospheric conditions, it also requires the specification of vegetation and initialization of SST and soil moisture, parameters that directly affect the exchanges between surface and atmosphere (DIRMEYER, 2013; LLOPART et al., 2017; LODH, 2020; MA et al., 2021; REBOITA et al., 2018). Reboita et al.

(2018) highlight that the seasonality of soil water storage introduces a "memory effect" of the order of one to two months so that the erroneous initialization of this variable in a climate model can lead to inadequate forecasts of precipitation and soil and air temperature. Hence, the climate model must be initialized with the most realistic and accurate continental surface characteristics (DIRMEYER; HALDER, 2017; DOBLAS-REYES et al., 2013; HALDER et al., 2018; REBOITA et al., 2018). Due to this, climate models require a period to adjust the hydrological cycle that is usually one month before the period to be forecast, also known as spin-up time (GIORGI; MEARNS, 1999; REBOITA et al., 2018).

Statistical and dynamic forecasts are the most used methods developed to produce seasonal climate predictions. Statistical forecasts establish relationships with past observations and use these calculations to predict conditions for upcoming seasons (MACLEOD; KLASSEN, 2019). This type of forecast can be executed with several techniques, including regression analysis (SINGHRATTNA et al., 2005), canonical correlation analysis (LANDMAN; MASON, 1999, 2001), classification methods (DROSDOWSKY; CHAMBERS, 2001), neural networks (ANOCHI; SILVA, 2009; ANOCHI; VELHO, 2020; HASTENRATH; GREISCHAR; VAN HEERDEN, 1995), machine learning (FENG et al., 2020). These predictions have the advantage of their simplicity of implementation and operation, but their limitation stems from the dependence of stationary relationships between the predictor and the forecasted variable, which is not guaranteed in a constantly changing climate (SCHEPEN; WANG; ROBERTSON, 2012).

On the other hand, dynamic forecasts use three-dimensional climate system models to simulate possible changes in the atmosphere and ocean for the coming months based on current conditions (MACLEOD; KLASSEN, 2019). These predictions are based on physical laws, and their main advantages are related to the ability to represent non-linear interactions between the components of the climate system and provide consistent predictions with high temporal resolution (SCHEPEN; WANG; ROBERTSON, 2012). Anyhow, both statistical and dynamic methods require the availability of observations. Therefore, they are complementary, as advances in statistical forecasting are associated with improving climate knowledge, which leads to an improvement in dynamic forecasting (DOBLAS-REYES et al., 2013). Other forecasting methods include local ecological indicators to predict future conditions. For example, a particular bird’s time return to a region may indicate the beginning of the rainy season in that location (MACLEOD; KLASSEN, 2019).

Dobles-Reyes et al. (2013) describe that the technical complexity of dynamic forecasting subdivides it into two types. In tier-two systems, seasonal forecasts are performed using only an

atmospheric model with persistent SST boundary conditions previously provided by statistical or coupled dynamic models. In tier-one systems, a coupled model has all its subsystems (climate system components) interacting simultaneously, which provides relatively more accurate predictions than those obtained by the tier-one system and statistical models (DOBLAS-REYES et al., 2013; KUG; KANG; CHOI, 2008; RODRIGUES; DOBLAS-REYES; COELHO, 2014; VAN OLDENBORGH et al., 2005a,b). As a result, tier-one systems have a relatively higher seasonal predictive skill than tier-two systems and perform better than simple statistical models over the tropical oceans (DOBLAS-REYES et al., 2013).

RCMs generally produce more accurate predictions since they have more refined horizontal resolution and appropriate physical parameterizations to simulate mesoscale atmospheric processes (AMBRIZZI et al., 2018; GIORGI; MEARNS, 1999; REBOITA et al., 2018). On the other hand, GCMs have a good performance in simulating large-scale atmospheric circulation features. Nonetheless, due to their horizontal resolution (100-200 km), such models cannot satisfyingly represent topography gradient, land-ocean contrasts, urban areas, and other relevant factors for mesoscale circulation and regional climate (AMBRIZZI et al., 2018).

Seasonal climate forecasts from GCMs have limitations such as very coarse spatial resolution, imperfect physical parameterization, and sensitivity to disturbances from initial conditions, so their raw use for planning or decision-making at a local scale may be improper (CHOU et al., 2020; DOBLAS-REYES et al., 2013; HARTMANN et al., 2002). Furthermore, GCM with very high spatial resolution is still restricted due to limited computational capability (CHOU et al., 2020). However, the use of the dynamical downscaling technique can provide more detailed forecasts for application on a regional scale (GIORGI, 1990; GIORGI; BATES, 1989; GIORGI; MEARNS, 1999; LAPRISE et al., 2000; MISRA; DIRMEYER; KIRTMAN, 2003; REBOITA et al., 2018; CHOU et al., 2020). The dynamical downscaling technique consists of nesting an RCM to a GCM. Whilst the GCM provides information on initial and boundary conditions, which indicate the state of the atmospheric circulation on a large scale, the RCM simulates the climatic aspects on a regional scale at high resolution (AMBRIZZI et al., 2018; CHOU et al., 2020). Although the focus of the current study is not an RCM or dynamical downscaling, it is relevant to analyse the accuracy of ECMWF-SEAS5 seasonal climate predictions. These results make it possible to evaluate its application in dynamical downscaling studies in Brazilian subdomains.

Another way to use seasonal climate forecasts from GCMs for regional or local application is through statistical post-processing methods (DELSOLE; SHUKLA, 2010;

HEINRICH et al., 2020; LI; JIN; BROWN, 2020; OSMAN; COELHO; VERA, 2021; STONE; MEINKE, 2005). However, while some studies showed that statistical downscaling reduced systematic errors of GCMs, providing better precipitation predictions (CHARLES et al., 2013; CHEN; SUN; WANG, 2012; FRÍAS et al., 2010), others indicated that there was no improvement in temperature and rainfall forecasts (FRÍAS et al., 2010; LI; JIN; BROWN, 2020).

Generally, precipitation seasonal climate predictions are presented as "tercile probabilities", which are categories that refer to the probability of occurrence of above-normal, normal, or below-normal conditions (MACLEOD; KLASSEN, 2019). These categories are defined based on historically recorded precipitation values. A long chain of procedures is required to obtain this final forecast product. The path includes the steps of pre-processing, processing, and post-processing the data. These steps refer to the data assimilation processes, forecasting by numerical modelling, and interpreting the model's outputs. According to Trocolli (2010), the main ingredients of a seasonal forecasting system are: a) a set of climate observations; b) a model that assimilates the observations in order to generate prognostic fields; c) a set of tools to assess the quality of forecasts; d) a set of tools for post-processing forecasts in order to make them useful for specific applications; e) a strategy for disseminating forecasts; f) a strategy for incorporating forecasts into a decision-making context and; g) a set of tools to assess the impact of forecasts on the decision made.

The following sections will provide more detailed descriptions of different GCMs and their generated seasonal climate forecast products. First, the ECMWF-SEAS5 model, this dissertation's main object of study, is described. Next, other relevant GCMs are described. Lastly, it is emphasized that the descriptions presented here do not encompass all existing global models but only provide a brief overview of some of the GCMs currently used by the scientific community.

4.2 ECMWF-SEAS5 Model

The European Centre for Medium-Range Weather Forecasts (ECMWF) has been operating real-time seasonal forecasting systems since 1997, and such systems have been updated approximately every five years (ECMWF, 2017; JOHNSON et al., 2019). In operation since November 2017, ECMWF-System 5 (ECMWF-SEAS5) is the ECMWF's fifth-generation seasonal forecasting system, replacing its predecessor System 4 (SEAS4; MOLTENI et al., 2011), which has been in operation since 2011. In its six years of operation, the SEAS4 model proved to be competitive and presented relevant skills such as high predictability of ENSO (MOLTENI et al., 2011), good performance in stratospheric simulation and prediction of the Quasi-Biennal Oscillation (SCAIFE et al., 2014) and an overall improvement in forecast competence compared to previous models (MOLTENI et al., 2011; WEISHEIMER; PALMER, 2014).

The ECMWF-SEAS5 forecasting system consists of a 51-member ensemble starting every month (on the first day) and integrated for approximately seven months (215 days). In addition, SEAS5 uses retrospective seasonal forecasts from past decades to verify and calibrate the forecasting system compared to historical records. This set of reforecasts, also known as hindcasts, has a 25-member ensemble starting on the first day of months from 1981 to 2016. Even though the entire set of hindcasts is used to verify the forecast system, only the 1993-2016 period subset calculates the forecast anomalies. There are two reasons for this procedure: it prevents the long-term trend of climate change from affecting forecasting products, and the 1993-2016 period coincides with the time interval employed by the Copernicus Climate Change Service multi-seasonal forecast system (JOHNSON et al., 2019).

The ECMWF-SEAS5 model has considerable improvements over its previous generation, including progress in the horizontal and vertical resolution and better simulation of tropical convection (BECHTOLD et al., 2014). For example, the horizontal resolution of the atmospheric and ocean models has improved substantially compared to SEAS4 (from 1 degree to 0.25 degrees in the ocean model and from 80 km to 36 km in the atmospheric model). Besides, ECMWF-SEAS5 also has a sea ice prognostic model, an essential component for seasonal forecasting and absent in the SEAS4 model (JOHNSON et al., 2019). A detailed description of all model’s components configuration and the physical parameterizations employed can be found in ECMWF (2017) and Johnson et al. (2019).

4.2.1 Components of the ECMWF-SEAS5

The atmospheric model used by ECMWF-SEAS5 is the ECMWF Integrated Forecast System (ECMWF-IFS version 43r1), with a horizontal resolution of 0.4° (≈ 36 km) and 91 vertical levels, with the model top in the 0.01 hPa layer of the mesosphere, around 80 km. The initial atmospheric conditions of ECMWF-SEAS5 are provided by the ECMWF operational analyses (ECMWF, 2017). Some of the physical parameterizations include: the cloud-radiation interactions use the Monte Carlo Independent Column Approximation method (McICA; MORCRETTE et al., 2008), the convection parameterization is based on the mass-flow approach (BECHTOLD et al., 2008; TIEDTKE, 1989, 1993), the surface-exchange parameterization uses the approach by Viterbo and Beljaars (1995), representing different sub-grid surface features such as vegetation, bare soil, snow and water bodies. The horizontal spectral resolution used for the main dynamic part of the model calculations is T319 (∼ 0.5625°). All physical parameterizations of the model (including clouds, rain, and continental surface) are calculated on a reduced grid spacing of approximately 36 km (JOHNSON et al., 2019).

The ocean model used by ECMWF-SEAS5 is the Nucleus for European Modelling of the Ocean (NEMO; MADEC, 2016), with a horizontal resolution of 0.25° (≈ 27 km), improving the representation of ocean transport, 75 vertical levels (including 18 vertical levels in the first 50 meters of oceans) and an ocean surface of 1 meter, which makes the representation of the SST diurnal cycle more accurate. The initial conditions of oceans and sea ice in ECMWF-SEAS5 are provided by the new operational ocean analysis system (OCEAN5, 2020), built with historical ocean reanalysis since 1979 (Ocean ReAnalysis System 5 - ORAS5; TIETSCHE et al., 2017; ZUO; BALSAMEDA; MOGENSEN, 2017) and daily ocean analyses in real-time (Ocean5 Near Real-Time Daily-Monitoring – ORTA5).

The ocean-atmosphere coupling is done with the Gaussian method for interpolation, which discards values in the boundary lines of oceanic and atmospheric models. The coupling interval is one hour, allowing the resolution of the diurnal cycle (ECMWF, 2017).

4.2.2 ECMWF-SEAS5 Ensemble Structure

Seasonal climate forecasts start from an observed state of all Earth system components and then evolve over a few months. Thus, errors present at the beginning of the forecast persist or grow during the integration of the model, reaching magnitudes comparable to the forecast signals (ECMWF, 2017). Some of these errors are random, and their effect is quantified through ensembles. Other errors are systematic and are corrected by comparing retrospective forecasts (hindcasts) and observations.

The ECMWF-SEAS5 seasonal forecasts consist of an ensemble made up of 51 members, whereas hindcasts have 25 members. The ensemble is created using perturbations in initial atmospheric conditions, SST, and activation of stochastic physics (ECMWF, 2017).

In this framework, the techniques employed in hindcasts are similar to those in seasonal forecasts. A single forecasting system is run for several initial conditions in the past, similar to a future forecasting system, using the same time horizon in all runs. The data resulting from this set of predictions constitute a “climate” of the model compared to the observed real-world climate. Systematic differences between the model and the real world (known as biases) are quantified and used as the basis for corrections applied to future predictions. Hence, hindcasts play a key role in correcting systematic errors and assessing the robustness of seasonal forecasting models (comparing each of the hindcasts' baseline years with the respective historical records of observed conditions). In this way, a more consistent set of predictions is created to support the decision-making (ECMWF, 2017).

The ensemble technique quantifies the errors’ effects from uncertainties about initial conditions and model deficiencies. The forecast system produces a set of slightly distinct rounds (the ensemble members), so the result of the prediction system is not a single solution but a set of solutions. Since all ensemble members are equally likely, predictions provide a distribution of outcomes rather than a single deterministic solution. With ensembles, probabilistic inferences can be made about the atmospheric state at a given point in time. Additionally, the ensemble provides information about the reliability of the forecast. Differences in results generated by different members can measure forecast accuracy (ECMWF, 2017).

Different techniques are used to build the members of an ensemble forecast. For example, in the case of ECMWF-SEAS5, a method called “burst mode” is used. All members are

initialized on the same date of origin in this procedure but with slightly different initial state conditions (different perturbations) to sample the observations' uncertainties (ECMWF, 2020). Moreover, each ensemble member is disturbed by random numbers representing possible model errors to quantify the errors caused by these uncertainties (ECMWF, 2017).

Regarding the ECMWF-SEAS5 atmospheric module, member 0 of the ensemble is initialized from initial undisturbed atmospheric conditions. The initial conditions for all other members have perturbations applied to some fields to represent the uncertainty of the atmosphere’s initial state. Disturbed fields include all upper air layers and a limited set of soil moisture, soil temperature, snow, sea-ice temperature, and surface temperature fields (ECMWF, 2017; JOHNSON et al., 2019).

In order to sample the knowledge of uncertainty about the oceanic state, the ORAS5 product contains a 5-member ensemble analysis. The perturbation scheme used to generate the reanalysis ensemble consists of two distinct elements: perturbations in the assimilated observations, both at the surface and in-depth, and perturbations in the surface forcing fields (ZUO et al., 2017). First, before starting the forecasts with the coupled model (ocean-atmosphere), the ocean temperature analyses are perturbed so that all members of the seasonal forecast (and hindcasts) ensemble have different initial conditions. Then, using pentadal analysis from the ORAS5 HadISST2 error repository (ZUO et al., 2017), disturbances are applied to the first 22 SST levels and are reduced with increasing depth (ECMWF, 2017; JOHNSON et al., 2019).

4.2.3 Provision of ECMWF-SEAS5 Seasonal Climate Forecasts

The ECMWF-SEAS5 system provides several products generated by the model forecast. The products include graphical outputs that present the forecasts in an easy-to-understand manner. Amongst these outputs are ENSO forecast maps (Niño SST plumes), seasonal forecast maps (which include terciles and ensemble averages maps), anomaly correlation maps, synoptic fields, tropical storm density maps, and other products. An example of this type of information provided by the European centre is in Figure 1, which shows the seasonal precipitation forecast obtained for the JFM season of 2022, considering rain category probabilities.

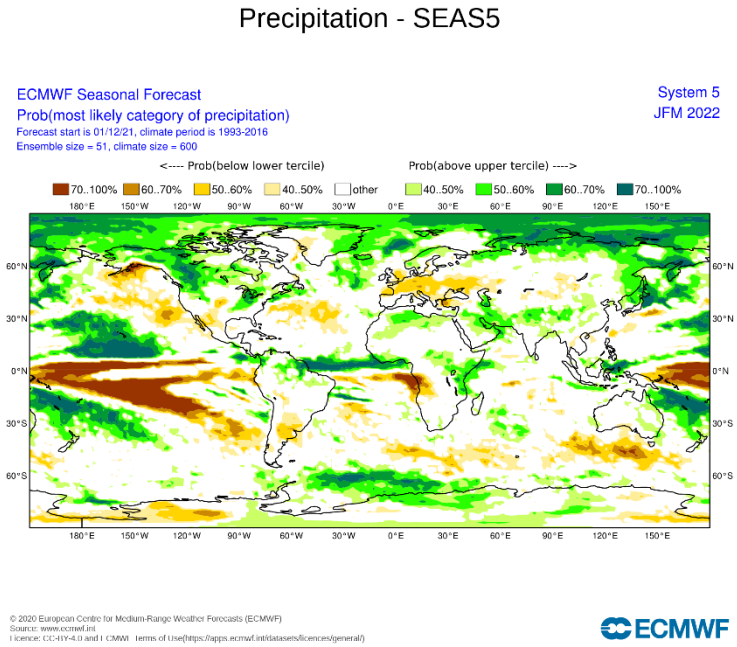

Figure 1 - Example of a seasonal forecast product available by the ECMWF-SEAS5. The map illustrates a forecast initialized in December 2021 for the probability of precipitation for the January-February-March 2022 season. Source: ECMWF-SEAS5 (2021).

A complete catalogue of ECMWF-SEAS5 graphic products available can be found at https://apps.ecmwf.int/webapps/opencharts/. Not only seasonal climate forecasts are provided, but weather forecasts (with a time horizon of up to 15 days) and sub-seasonal forecasts (with a time horizon of up to 42 days) are also offered. In addition to this product suite, ECMWF also provides digital data calculated by ECMWF-SEAS5 and encoded in GRIB format for archiving and distribution. These data help conduct different studies and are open to the public, requiring only the ECMWF data platform registration. A complete catalogue of this dataset (including all forecast timescales) can be found at https://www.ecmwf.int/en/forecasts/datasets/catalogue-ecmwf-real-time-products.

ECMWF SEAS5 is part of the Copernicus Climate Change Service (C3S), a multi-system seasonal forecasting project. In C3S, data produced by seasonal forecasting models developed, implemented, and operated in meteorological centres of several European countries are collected, processed, and combined to allow users different applications. Thereby, multi-system combinations, as well as forecasts from individual systems, are made available. The European centres that provide forecasts to the C3S are European Centre for Medium-Range Weather

Forecasts (ECMWF), UK Met Office, Météo-France, Deutscher Wetterdienst (DWD), and Centro Euro-Mediterraneo sui Cambiamenti Climatici (CMCC). Moreover, C3S also includes forecasts from National Centers for Environmental Prediction (NCEP), Japan Meteorological Agency (JMA), and Environment and Climate Change Canada (ECCC).

Each model (operated by a given meteorological centre) simulates in slightly different ways the earth system processes that influence climate patterns and make relatively different approximations, inducing different types of modelling errors. These errors grow with increasing integration time, so the accumulated errors become significant compared to the signal that the model is expected to predict. Some errors are common to different models, but others are not. Hence, combining results from a larger number of models can allow a more realistic representation of the uncertainties arising from modelling errors. In most cases, the average of the combined predictions is more effective than the prediction of individual models (ECMWF, 2020).

C3S data is grouped into multiple categories or sets defined by variable type (surface level or at different pressure levels) and applied post-processing levels. Data includes forecasts created in real-time (since 2017) and retrospective forecasts (hindcasts) covering the 1993-2016 period, initialized at intervals equivalent to real-time forecasts. A complete catalogue of seasonal climate forecast products provided by C3S can be accessed at https://climate.copernicus.eu/charts/c3s_seasonal/.

4.3 Studies on seasonal climate forecasts for South America

4.3.1 ECMWF-SEAS5

Considering that ECMWF-SEAS5 came into operation at the end of 2017, there is still a paucity of studies that assess the quality of its seasonal rainfall forecasts for specific domains in South America. Nonetheless, Gubler et al. (2020) applied cluster analysis to seasonal precipitation forecasts from ECMWF-SEAS5 hindcasts (from 1981 to 2016), validating them with data from rainfall stations in different regions of SA. Amongst the 15 clusters obtained to

represent the climate zones of the continent, six were inserted in different Brazilian regions: extreme northwest of the Amazon, North Brazil, extreme east of the Northeast Brazil, a region covering the Southeast and areas of the Northeast Brazil, an area comprising portions of the Southeast, South and Midwest Brazil and one last cluster in the extreme south of Brazil.

The results showed that the model's capability to predict rainfall in sectors such as the northwest of the Amazon, Southeast, Midwest, and portions of Southern Brazil was unsatisfactory. The authors associate the poor performance in these regions with factors such as regional topography and influences from other modes of climate variability than ENSO. However, the model showed a remarkable skill in predicting precipitation and temperature in regions such as the north, northeast, and extreme south of Brazil. The better dexterity of the model in those regions stems from the significant influence of the oceanic conditions over these areas and the teleconnection effects (COELHO et al., 2006a,b; WEISHEIMER; PALMER, 2014).

It is worthy of mention that the present work complements the study by Gubler et al. (2020). Here, we seek to assess the quality of ECMWF-SEAS5 hindcasts and forecasts. In addition, different validation metrics than those employed by the authors are used.

4.3.2 CFSv2 Model

The CFSv2 system was developed by the National Centers for Environmental Prediction (NCEP), improving and replacing its previous version (CFSv1), and put into operation in March 2011 (SAHA et al., 2014). CFSv2 is a daily integrated coupled model with a spatial resolution of 0.9°. Its atmospheric component is constituted by the Global Forecast System (GFS) model with T126 triangular truncation (~ 0.937°) of horizontal resolution and 64 vertical levels. The oceanic component of CFSv2 is formed by the Geophysical Fluid Dynamics Laboratory Modular version 4.0 (GFDL MOM4) model, with a resolution of 0.25° latitude by 0.5° longitude and 40 vertical levels. A more detailed description of all system configurations and physical parameterizations can be found in Sahel et al. (2014).

CFSv2 seasonal forecasts have a 6-hour resolution (00, 06, 12, and 18 UTC) and are available every five days. At each initialization, four simulations have different time horizons. In the first forecast run of each synoptic time, the time horizon is nine months, and the initial conditions are undisturbed. In subsequent runs, the initial conditions are disturbed, and the time horizon of the rounds also changes. For example, in the rounds of 00 UTC, the forecasts have a time horizon of three months, and in the rounds of 06, 12, and 18 UTC, the forecasts have a horizon of 45 days (SAHEL et al., 2014). Digital CFSv2 forecast data is available at https://nomads.ncep.noaa.gov/pub/data/nccf/com/cfs/prod/ and has a seven-day rotation. In addition, seasonal forecast graphical products are also provided at https://www.cpc.ncep.noaa.gov/products/CFSv2/CFSv2seasonal.shtml. An example of a CFSv2 seasonal weather forecast graphical product is shown in Figure 2.

Studies have assessed the quality of CFSv2 predictions for SA under different aspects. For example, the model has a good performance to predict rainfall over the Amazon in November (YUAN et al., 2011), but it stills presents errors from CFSv1 like the double-band simulation bias of the Intertropical Convergence Zone (ITCZ) and deficiency in representing the Southern Annular Mode (SAM) (SILVA et al., 2014).

Furthermore, about tropical convection, it was observed that the model's dexterity in representing its development and associated extratropical patterns decreases with the evolution of the forecast horizon. Besides, the model fails in simulating the velocity and propagation direction of the Madden-Julian Oscillation (MJO) (WEBER; MASS, 2017).

Despite CFSv2 presenting deficiencies in the resolution of the hydrological cycle by the model’s atmospheric component, the system is capable of predicting critical hydrological variables such as precipitation and soil moisture as long as the climatological deviation is considered in the analysis (DIRMEYER, 2013; DIRMEYER; HALDER, 2017). Regardless of that, the model has a satisfactory ability to represent the seasonal atmospheric circulation over South America, with a good representation of atmospheric systems such as the South Atlantic Convergence Zone (SACZ), southeast trade winds, and South Atlantic Subtropical Anticyclone (SASA) (DIAS et al., 2017; SILVA et al., 2014).

Further, other studies used the CFSv2 seasonal forecasts in dynamical downscaling with RegCM4.3 (REBOITA et al., 2018), RegCM4.7 (FREITAS et al., 2020), and to estimate monthly flows for reservoirs (PAIVA; MONTENEGRO; CATALDI, 2020).

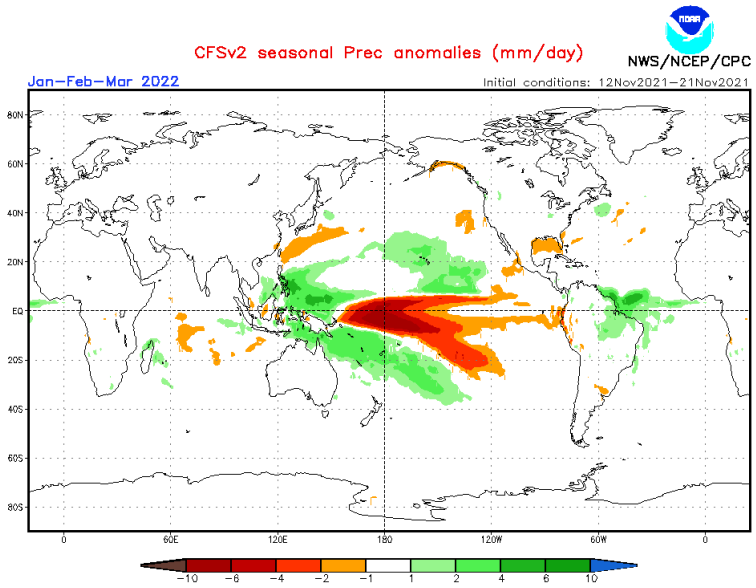

Figure 2 - Precipitation anomaly forecast by CFSv2 for the January-February-March 2022 season, considering an ensemble of 40 members (4 rounds a day for ten consecutive days). The figure corresponds to the normalized anomaly (divided by the climatological standard deviation), calculated to the climatology of the 1991-2020 hindcasts. Source: NCEP-CFSv2 (2021).

4.3.3 CPTEC-COLA Model

The Center for Ocean-Land-Atmosphere Studies (COLA) GCM was developed by the NCEP (SHUKLA et al., 2000), and it is the precursor to the GCM of the Center for Weather Prediction and Climate Studies – Brazilian National Institute for Space Research (CPTEC-INPE/COLA). CPTEC-COLA has been used to perform climate forecasting at CPTEC since January 1995 (CAVALCANTI et al., 2002). The model has a spatial resolution of 1.8º latitude by 1.8º longitude and 28 vertical levels. CPTEC-COLA forecasts are performed daily, and four initial conditions of four consecutive mid-month days are used. The GCM is integrated twice for each initial condition, once with lower boundary conditions given by climatological values of SST and the other with SSTs observed between the date of the initial condition and the month in which the integration is being made, and SST anomalies persisted for the forecast months.

Finally, differences between the forecast-control integrations are averaged to provide the forecast for four months (CAVALCANTI et al., 2002).

CPTEC uses two climate models to perform seasonal forecasts: the GCM CPTEC-COLA and the RCM Eta (CHOU; BUSTAMANTE; GOMES, 2005). Seasonal climate forecasts are made available monthly to the public on http://clima1.cptec.inpe.br/. At the centre, consensus forecasts of a qualitative nature are carried out every month. In these meetings, groups of scientists from CPTEC/INPE, the National Institute of Meteorology (Inmet), and the Cearense Foundation of Meteorology and Water Resources (Funceme) compare the climate forecasts of different models and, with their knowledge on the evolution of atmospheric and oceanic recent conditions, elaborate the seasonal forecast (YNOUE et al., 2017). The forecasts are available at http://clima1.cptec.inpe.br/gpc/pt. However, it is noteworthy that updates of these seasonal forecast products have been interrupted since April 2020.

Further studies corroborated CPTEC-COLA's ability to simulate the annual precipitation cycle in the tropics and austral mid-latitudes, especially in the Northeast of Brazil and Amazon (MARENGO et al., 2003; MISRA, 2006). Nonetheless, the Southeast's acceptable representation of rainfall anomalies was associated with years of extreme El Niño events (MARENGO et al., 2003). Furthermore, the model did not capture the tropical Atlantic SST anomalies, leading to flaws in the simulated precipitation during the northeast’s rainy season (MISRA, 2006).

Regardless of limitations, Coelho et al. (2012) assessed that CPTEC-COLA could predict rainfall anomalies for the three most severe dry seasons in Amazon, from July to September 1997-1998, 2004-2005, and 2009-2010. Moreover, the results indicated that the CPTEC seasonal forecast system produced, one month in advance, drought forecasts for the three investigated events. Such findings were of great relevance for the Brazilian scientific community and local decision-makers as guidance to reduce the harmful impacts of the Amazon drought.

The CPTEC-COLA was also used in dynamical downscaling studies for South America with the RegCM3 (MACHADO; DA ROCHA, 2011) and RegCM4.5 (REBOITA et al., 2018). Both studies indicated that the regional model corrected systematic errors in the global model and presented better rainfall estimates. When RegCM4.5 is nested to CPTEC and uses Emanuel's cumulus convection parameterization, the technique showed remarkable precipitation and air temperature representations in almost all Brazil (REBOITA et al., 2018). However, the air

temperature forecasts in the Southeast region of Brazil carried out by CPTEC proved to be better than those of RegCM (MACHADO; DA ROCHA, 2011; REBOITA et al., 2018).

4.4 Other Global Models and Seasonal Climate Forecasting Products

In addition to the climate models and centres aforementioned, other institutes provide their seasonal climate forecasts for the entire globe. These include the Climate Prediction Center (CPC) of the National Oceanic and Atmospheric Administration (NOAA), the International Research Institute for the Climate and Society (IRI) of Columbia University, the Canadian Meteorological Center (CMC), the UK Met Office, and the National Institute of Meteorology (Inmet).

CPC provides seasonal climate forecasts for SST, air temperature, and precipitation variables with an eight-month time horizon. Since 2011, the centre has been employing the North American Multi-Model Ensemble project (NMME) (KIRTMAN et al., 2014), including seasonal forecasts from six different global models. The project has shown that the predictions obtained by the multi-model ensemble yield superior results than any individual global model. Seasonal forecasts simulated by the ensemble and each global model separately are available at https://www.cpc.ncep.noaa.gov/products/NMME/seasanom.shtml.

Beginning in April 2017, IRI's seasonal forecasts are based on a recalibration of model outputs used in the NMME. First, the predictions of each model are recalibrated, and then the ensemble of the various models is carried out, generating a final product of probabilistic predictions with 1º resolution. The page https://iri.columbia.edu/our-expertise/climate/forecasts/seasonal-climate-forecasts/ provides seasonal precipitation and temperature forecasts for the entire globe with a time horizon of seven months. Besides, seasonal precipitation, air temperature, and geopotential height forecasts for individual GCMs are available at http://iridl.ldeo.columbia.edu/maproom/Global/Forecasts/GCM.html.

In operation since September 1995, CMC's seasonal climate forecasting system has evolved from a single six-member ensemble GCM to a 40-member ensemble multi-model, the

Canadian Seasonal to Interannual Prediction System version 2 (CanSIPSv2) (MERRYFIELD et al., 2013). The page https://climate-scenarios.canada.ca/?page=cansips-global provides seasonal forecasts of various meteorological variables for the entire globe with a forecast horizon of up to 12 months.

Founded in 1854, the Met Office is the UK's national weather service centre and, since the 2015 El Niño event, it has been working in partnership with the UK Government's Foreign, Commonwealth and Development Office (FCDO) and the University of Reading to provide a seasonal weather forecasting service to support decision-making. In this regard, the centre provides seasonal climate forecasts for the entire globe obtained with the multi-system World Meteorological Organization Lead Center for the Long-Range Forecast Multi-Model Ensemble (WMO LC-LRFMME) ensemble, which includes several GCMs operated across the world, including CPTEC-COLA. In addition, seasonal temperature and precipitation forecasts analysed by the Met Office with a time horizon of six months are available on the page https://www.metoffice.gov.uk/services/government/international-development/climate-outlook.

In Brazil, the National Institute of Meteorology (Inmet) employs a statistical climate forecasting model to make seasonal predictions of precipitation and temperature for the entire country, with a forecast horizon of 4 months. This model aggregates point forecasts from stochastic models to obtain the best time projections. Compared to the observed data, the combined model predictions outperform that of each component model (LÚCIO et al., 2010). The institute's forecasts are available at https://clima.inmet.gov.br/. Figure 3 presents the total precipitation forecast by the Inmet for the December/2021-January-February/2022 season.

The Cearense Foundation of Meteorology and Water Resources (Funceme) also performs seasonal climate forecasts, running the global models ECHAM46 and CAM3.1 and the regional model RSM97. In addition, the foundation also provides climate forecasts from several other statistical models on its page http://www.funceme.br/dashboard/climate_forecast, where it is possible to check seasonal forecasts for Brazil with a time horizon of 5 months. Figure 4 illustrates an example of a forecast provided by the centre, using the dynamic model ECHAM46.

Finally, the Climate Studies Group (GrEC) of the Department of Atmospheric Sciences at the University of São Paulo (USP) does not run a climate model but holds monthly climate monitoring meetings and trimonthly climate forecast meetings for Brazil. Based on the products of the climate centres mentioned above, the group of researchers from GrEC makes seasonal

climate forecasts by consensus and provides them on the page http://www.grec.iag.usp.br/data/index_BRA.php.

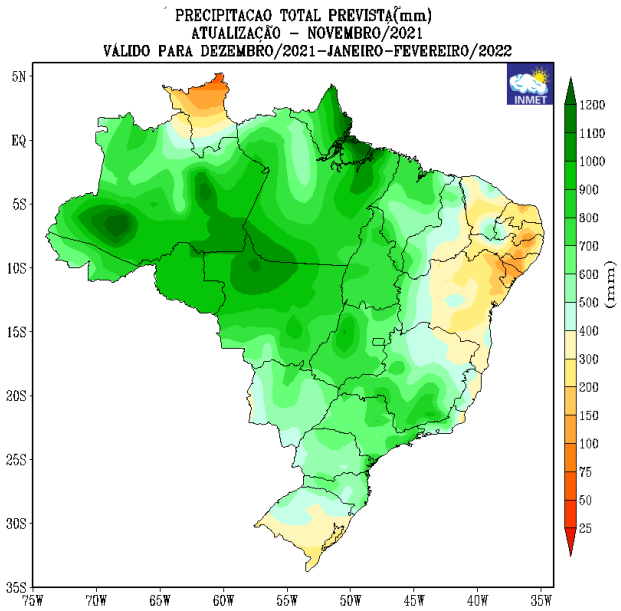

Figure 3 - Seasonal climate forecast of total precipitation (mm) performed by the Inmet statistical climate model for the December/2021-January-February/2022 season. Source: Inmet (2021).

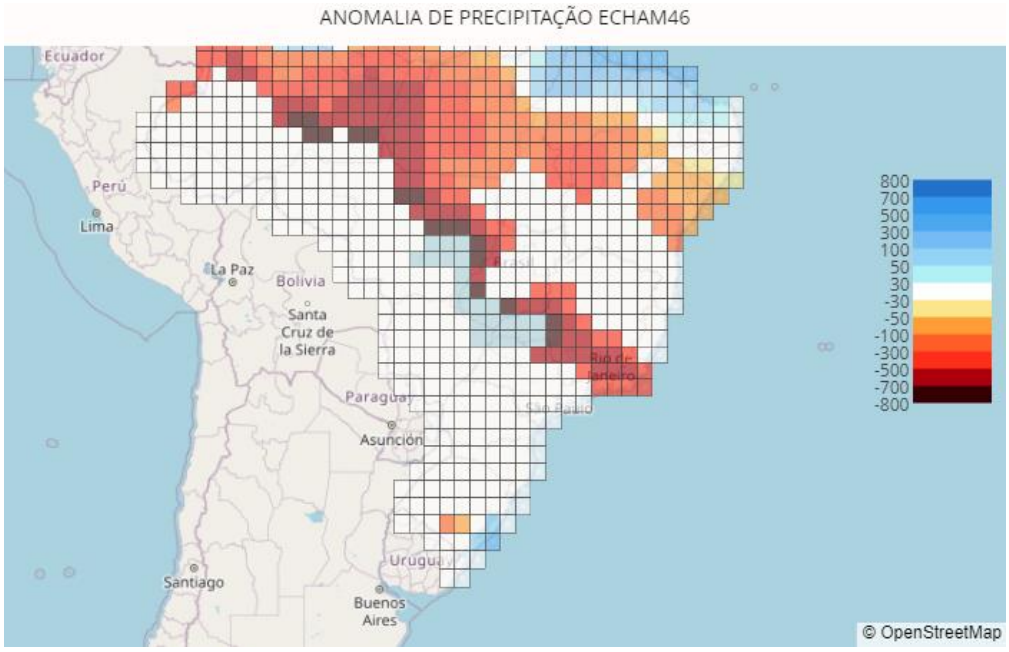

Figure 4 - Precipitation anomaly forecast by the Funceme for the January-February-March 2022 season, derived from the global model ECHAM46. Source: Funceme (2021).

5. METHODOLOGY

5.1 ECMWF-SEAS5 Precipitation and 2 m Temperature Data

This study uses surface data (Seasonal forecast daily data on single levels) of total rainfall (accumulated every 24 hours since the forecast beginning) and 2 m temperature (instantaneous values every 6 hours) from the ECMWF-SEAS5. These data have 1º x 1º horizontal resolution and are available on the page https://cds.climate.copernicus.eu/cdsapp#!/dataset/seasonal-original-single-levels?tab=form. In addition, an explanatory tutorial on obtaining data from the C3S platform is presented in the Appendix section of this document.

The atmospheric model used by ECMWF-SEAS5 is the ECMWF Integrated Forecast System (ECMWF-IFS version 43r1), with a horizontal resolution of 0.4° (≈ 36 km) and 91 vertical levels, with the model top in the 0.01 hPa layer of the mesosphere, around 80 km. The initial atmospheric conditions of ECMWF-SEAS5 are provided by the ECMWF operational analyses (ECMWF, 2017).

The horizontal spectral resolution used for the main dynamic part of the model calculations is T319 (~ 0.5625°). All physical parameterizations of the model (including clouds, rain, and continental surface) are calculated on a reduced grid spacing of approximately 36 km (JOHNSON et al., 2019). Therefore, although the simulations are performed with a finer resolution of 0.4º, they are available with a lower horizontal resolution of 1º.

The ocean model used by ECMWF-SEAS5 is the Nucleus for European Modelling of the Ocean (NEMO; MADEC, 2016), with a horizontal resolution of 0.25° (≈ 27 km), improving the representation of ocean transport, 75 vertical levels (including 18 vertical levels in the first 50 meters of oceans) and an ocean surface of 1 meter, which makes the representation of the SST diurnal cycle more accurate.

In this work, hindcast from January 1993 to December 2016 and forecast from January 2017 to December 2020 are employed. ECMWF-SEAS5 seasonal forecasts are executed once a month, always initialized on the first day of each month (and released on the 13th day), with a time horizon of 215 days (≈ 7 months).

The hindcasts comprise an ensemble formed by 25 members. Additionally, the forecasts are built upon an ensemble formed by 51 members. The ECMWF-SEAS5 ensemble technique applies perturbations in the initial atmospheric conditions, SST, and stochastic physics activation (JOHNSON et al., 2019)

5.2 Construction of the Ensemble

The ECMWF-SEAS5 produces predictions with a forecast length of seven months (215 days). In this work, the first month of the predictions was discarded due to spin-up time (the time necessary for a coupled model to reach a state of statistical equilibrium under the applied forcing; KANTHA; CLAYSON, 2000). Hence, the predictions applied here correspond to the period from the second month after the forecast start, also known as lead time forecast 1 (assuming the month of initialization is the lead time 0). For example, for the forecast that started on January 1st, the first three months from the lead time one were used: February, March, and April (three-month FMA). Table 1 illustrates how the trimesters for each monthly forecast provided by ECMWF-SEAS5 are selected.

Table 1 – Exemplification of the lead times (in months) of ECMWF-SEAS5 seasonal forecasts. This study uses lead times 1, 2, and 3 for trimonthly means.

	LEAD TIME FORECASTING (MONTHS)						
	0	**1**	**2**	**3**	**4**	**5**	**6**
INITIAL MONTH OF PREDICTION	JAN	FEB	MAR	APR	MAY	JUN	JUL
	FEB	MAR	APR	MAY	JUN	JUL	AUG
	MAR	APR	MAY	JUN	JUL	AUG	SEP
	APR	MAY	JUN	JUL	AUG	SEP	OCT
	MAY	JUN	JUL	AUG	SEP	OCT	NOV
	JUN	JUL	AUG	SEP	OCT	NOV	DEC
	JUL	AUG	SEP	OCT	NOV	DEC	JAN
	AUG	FEB	MAR	APR	MAY	JUN	JUL
	SEP	OCT	NOV	DEC	JAN	FEB	MAR
	OCT	NOV	DEC	JAN	FEB	MAR	APR
	NOV	DEC	JAN	FEB	MAR	APR	MAY
	DEC	JAN	FEB	MAR	APR	MAY	JUN

The calculation of the average ensemble is exemplified in Table 2. It shows how the calculation is made for the quarter of February-March-April (FMA), obtained with the seasonal predictions initiated in January. Hindcasts consist of daily predictions generated by the 25-member ensemble (i.e., 25 predictions). Real-time forecasts comprise 51 daily predictions by the 51-member ensemble. Daily arithmetic means of all members were calculated to compute monthly and trimonthly means. As a result, 288 trimesters of hindcasts and 48 trimesters of forecasts were obtained.

Table 2 – Scheme of the ensemble technique used in this study. The example applies to the FMA trimester forecast, obtained with the prediction that started in January.

Prediction Type	**Prediction Start**	**Monthly Means**	**Ensemble Calculation**
Hindcasts	January	$\mathrm{M\_Feb} = \frac{\sum_{i=1}^{i=25} X_i}{25}$ $\mathrm{M\_Mar} = \frac{\sum_{i=1}^{i=25} X_i}{25}$ $\mathrm{M\_Apr} = \frac{\sum_{i=1}^{i=25} X_i}{25}$	$\mathrm{Ensemble\_FMA} = \frac{\mathrm{M\_Feb} + \mathrm{M\_Mar} + \mathrm{M\_Apr}}{3}$
Forecasts	January	$\mathrm{M\_Feb} = \frac{\sum_{i=1}^{i=51} X_i}{51}$ $\mathrm{M\_Mar} = \frac{\sum_{i=1}^{i=51} X_i}{51}$ $\mathrm{M\_Apr} = \frac{\sum_{i=1}^{i=51} X_i}{51}$	$\mathrm{Ensemble\_FMA} = \frac{\mathrm{M\_Feb} + \mathrm{M\_Mar} + \mathrm{M\_Apr}}{3}$

5.3 Data for Validation of ECMWF-SEAS5 Predictions

Seasonal precipitation forecasts from ECMWF-SEAS5 were validated against the Climate Prediction Center (CPC; CHEN et al., 2008) analysis. The CPC Gauge-Based Analysis of Global Daily Precipitation (CPC-Global) dataset is derived from thousands of rain gauges across the globe, cooperative observation networks, and meteorological agencies (TORRES et

al., 2020). Data quality control is carried out through comparisons with historical records, surface measurements, radar and satellite observations, and predictions from numerical models (CHEN et al., 2008).

CPC analysis has a spatial resolution of 0.5º, with a time series of daily data available since 1979 and updated daily at https://ftp.cpc.ncep.noaa.gov/precip/CPC_UNI_PRCP/GAUGE_GLB/RT/. Daily CPC data from January 1993 to April 2021 were used in this study. For comparison, CPC data were interpolated to the spatial resolution of ECMWF-SEAS5 by the bilinear method (PRESS et al., 2007).

The ECMWF-SEAS5 2 m temperature predictions were validated against the CPC Global Daily Temperature data, with a resolution of 0.5°. These data are available at https://psl.noaa.gov/data/gridded/data.cpc.globaltemp.html. For the comparisons, daily averages were taken with the maximum and minimum temperatures provided by the CPC and the bilinear interpolation above.

5.4 Trimonthly Means

With trimonthly means calculated for ECMWF-SEAS5 and CPC, maps were plotted for the seasons January-February-March (JFM), February-March-April (FMA), March-April-May (MAM), April-May-June (AMJ), May-June-July (MJJ), June-July-August (JJA), July-August-September (JAS), August-September-October (ASO), September-October-November (SON), October -November-December (OND), November-December-January (NDJ) and December-January-February (DJF). These maps were built with an average of all the members from hindcasts (25 members) and forecasts (51 members).

Bias maps were also plotted, calculating the difference between the value predicted by ECMWF-SEAS5 and the value obtained by the CPC analysis. Bias measures the correspondence between the predicted value and the observed value of a given parameter (WILKS, 2006). When it is negative, the model underestimates the simulated variable, while its positive result indicates

overestimation. When its result is close to zero, the predicted value approaches the observed value. That is, it is closer to the actual value. Its calculation is given by:

$$\text{Bias} = (\text{Average of the predicted trimester}) - (\text{Average of the observed trimester}) \quad (1)$$

Bias calculations also allow identifying systematic model errors by observing persistent discrepancies in certain regions. In this way, it is possible to assess whether the underestimation or overestimation errors present in the retrospective forecasts are maintained or corrected in the prognostic forecasts.

The ECMWF-SEAS5 trimonthly means were also spatially compared with CPC data, considering their average values in six subdomains of South America (Figure 5; Table 3): Amazon (AMZ), Northeast Brazil (NEB), Southeast Brazil (SEB), South Brazil (SB), Northern South America (NSA) and Southeastern South America (SESA). The choice of these sectors was based on the study by Reboita et al. (2018).

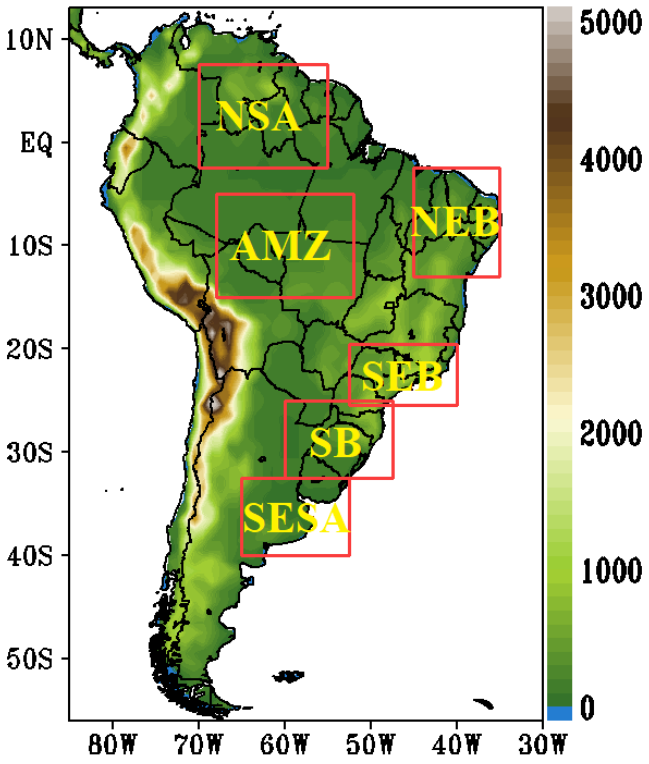

Figure 5 - Selected subdomains for calculating regionalized trimonthly means and statistical parameters. Elevation in colours (m).

Table 3 – Location of sectors used in the study.

Subdomain	Latitude	Longitude
AMZ	5ºS - 15ºS	52ºW - 68ºW
NEB	2.5ºS - 13ºS	35ºW - 45ºW
SEB	19.5ºS - 25.5ºS	40ºW - 52.5ºW
SB	25ºS - 32.5ºS	47.5ºW - 60ºW
SESA	32.5ºS - 40ºS	52.5ºW - 65ºW
NSA	7.5ºN - 2.5ºS	55ºW - 70ºW

5.5 Evaluation of Forecast Skill

The precipitation predictions of ECMWF-SEAS5 hindcasts were also evaluated regarding their seasonal anomaly forecast skill score. Based on the methodology of Chou et al. (2020), these skill scores consist of temporal correlations between predicted and observed anomalies of trimonthly seasonal forecasts, considering the CPC dataset climatological mean from 1993 to 2016. First, temporal correlations of seasonal precipitation and temperature anomalies are calculated to assess the hindcast ensemble. Then, the average temporal correlation value is calculated for the 25 seasonal anomalies. Hence, a single metric value is associated with each grid point at each season. This study calculated skill scores for three-month forecasts starting in lead time 1.

Still following the Chou et al. (2020) methodology, anomaly correlations were also calculated separately for El Niño and La Niña periods compared to the 24 years of hindcasts. For the El Niño events, the DJF and JJA trimesters were selected, and for the La Niña events, the FMA trimester was chosen. The selection of these trimesters was based on the ENSO effects over Brazil in these seasons (CHOU et al., 2020). The DJF, JJA, and FMA periods with El Niño and La Niña events between 1993 and 2016 are listed in Table 4. This table is constructed based on the information provided by the CPC/NOAA on the page https://origin.cpc.ncep.noaa.gov/products/analysis_monitoring/ensostuff/ONI_v5.php. Eight El Niño events in DJF, five El Niño events in JJA, and eight La Niña events in FMA occurred in the period.

Table 4 – Based on the ONI index, the El Niño and La Niña events during DJF, JJA, and FMA from 1993 until 2016. Source: CPC/NOAA

Event	Season	Years
El Niño	DJF	1994/1997/2002/2004 2006/2009/2014/2015
	JJA	1997/2002/2004/2009/2015
La Niña	FMA	1996/1999/2000/2006 2008/2009/2011/2012

5.6 Statistical Parameters

With the trimonthly regionalized means obtained for the AMZ, SEB, NEB, and SB subdomains, different statistical measures were calculated for all trimesters as a way to assess the accuracy of ECMWF-SEAS5 seasonal forecasts:

- **Mean Absolute Error (MAE):** measures the error variability of two datasets through the magnitude of the difference between them, not considering the error underestimation or overestimation (MONTGOMERY; JENNINGS; KULAHCI, 2008).

$$\mathrm{MAE} = \frac{1}{n}\sum_{t=1}^{t=n}|\hat{y}_t - y_t| \qquad (2)$$

where: n: number of samples

t: period

$\hat{y}_t$: value predicted by ECMWF-SEAS5

y_t: value obtained by CPC

- **Root Mean Square Error (RMSE):** measures the error variability of two time series (MONTGOMERY; JENNINGS; KULAHCI, 2008).

$$\mathrm{RMSE} = \sqrt{\frac{1}{n}\sum_{t=1}^{t=n}|\hat{y}_t - y_t|^2} \qquad (3)$$

where: n: number of samples

t: period

$\hat{y}_t$: value predicted by ECMWF-SEAS5

y_t: value obtained by CPC

- **Pearson's Coefficient of Correlation (*r*):** measures the degree of correlation between variables from two datasets, assuming values from -1 to 1. A correlation close to 1 (-1) indicates a very high positive (negative) correlation. (MONTGOMERY; JENNINGS; KULAHCI, 2008).

$$r = \frac{\sum_{t=1}^{t=n}\left[(\hat{y}_t - \bar{\hat{y}})(y_t - \bar{y})\right]^2}{\sqrt{\sum_{t=1}^{t=n}\left|\hat{y}_t - \bar{\hat{y}}\right|^2}\sqrt{\sum_{t=1}^{t=n}|y_t - \bar{y}|^2}} \qquad (4)$$

where: n: number of samples

t: period

$\hat{y}_t$: value predicted by ECMWF-SEAS5

$\bar{\hat{y}}$: average of values predicted by ECMWF-SEAS5

y_t: value obtained by CPC

$\bar{y}$: average of values obtained by CPC

- **Coefficient of Determination (R^2):** measures the fit of the predicted data about the observed ones so that the variation of the forecast information can be explained by the total variation of the observed data (MONTGOMERY; JENNINGS; KULAHCI, 2008). Assuming values between 0 and 1, the higher the value of R^2, the better the fit of forecasts concerning the observations (MORETTIN; BUSSAB, 2017).

$$R^2 = \frac{\left[\sum_{t=1}^{t=n}(\hat{y}_t - \bar{\hat{y}})(y_t - \bar{y})\right]^2}{\sum_{t=1}^{t=n}|\hat{y}_t - \bar{\hat{y}}|^2 \sum_{t=1}^{t=n}|y_t - \bar{y}|^2} \qquad (5)$$

where: n: number of samples

t: period

$\hat{y}_t$: value predicted by ECMWF-SEAS5

$\bar{\hat{y}}$: average of values predicted by ECMWF-SEAS5

y_t: value obtained by CPC

$\bar{y}$: average of values obtained by CPC

- **Relative Error (RE):** given the variability of precipitation and temperature patterns all over SA, the relative error was calculated.

$$RE = \left|\frac{\hat{y}_t - y_t}{y_t}\right| \times 100 \quad (6)$$

where: $\hat{y}_t$: value predicted by ECMWF-SEAS5

y_t: value obtained by CPC

- **Willmott's Index of Agreement (*d*):** evaluates the accuracy of predictions regarding the observations and may assume values between 0 and 1. Values close to 0 indicate disagreement between predicted and observed data, and values close to 1 indicate better prediction accuracy (WILLMOTT, 1981).

$$d = 1 - \frac{\sum_{t=1}^{t=n}(\hat{y}_t - y_t)^2}{\sum_{t=1}^{t=n}(|\hat{y}_t - \bar{y}| + |y_t - \bar{y}|)^2} \qquad (7)$$

where: n: number of samples

t: period

$\hat{y}_t$: value predicted by ECMWF-SEAS5

y_t: value obtained by CPC

$\bar{y}$: average of values obtained by CPC

- **Kling-Gupta Efficiency (KGE):** the Kling-Gupta Efficiency (GUPTA et al., 2009; KLING; FUCHS; PAULIN, 2012) measures the goodness-of-fit between streamflow estimates and gauged observations and is a modified version of the Nash-Sutcliffe efficiency index (NSE). The KGE decomposes the NSE into three independent hydrographic components: linear correlation (r), bias ratio (β) and relative variability between observed and simulated streamflow (α).

KGE values range from -∞ to 1, with values close to 1 indicating better model performance. Towner et al. (2019) classify the KGE with the following categories:

- KGE ≥ 0.75 → Good;
- 0.75 > KGE ≥ 0.5 → Intermediate;
- 0.5 > KGE ≥ 0 → Poor;
- KGE ≤ 0 → Very poor

The KGE index is defined according to equation 9.

$$KGE = 1 - \sqrt{(r-1)^2 + \left(\frac{\sigma_{sim}}{\sigma_{obs}} - 1\right)^2 + \left(\frac{\mu_{sim}}{\mu_{obs}} - 1\right)^2} \qquad (8)$$

where: r: is the linear correlation between observed and simulated values

σ_{sim}: standard deviation of simulations

σ_{obs}: standard deviation of observations

μ_{sim}: mean of simulations

μ_{obs}: mean of observations

- **Seasonality Index (SI):** the Seasonality Index (SI) was proposed by Walsh and Lawler (1981) and quantifies rainfall variability throughout the year, identifying rainfall regimes based on monthly rainfall distribution. The index ranges from zero (when the rain is equally distributed over all months) to 1.83 (when all the rain falls in a single month). Although the method uses the rainfall distribution for all months, a seasonal pattern is detected when the SI value is above 0.6 (DOYLE, 2019). Higher SI values indicate an asymmetry in the distribution of precipitation throughout the year, while values close to zero indicate that there is little or no seasonal variation in rainfall.

The SI is defined as the sum of the absolute values of the differences between the amount of rain in each month and the annual average of total precipitation, divided by the annual precipitation, as expressed by equation 8.

$$SI_i = \frac{1}{R_i}\sum_{n=1}^{12}\left|X_{in} - \frac{R_i}{12}\right| \qquad (9)$$

where: R_i: total annual precipitation in the year i

X_{in}: monthly precipitation occurred in the month n of the year i

5.7 Cluster Analysis

Cluster analysis is an essential statistical tool for grouping the homogenous regions and can be performed using two different methods based on hierarchical and non-hierarchical techniques (WILKS, 2006). This technique was used to group the South American regions with similar patterns of monthly rainfall. The *K*-Means method used for grouping the regimes was employed with the scikit-learn® library, available in the Python software. The *K*-Means is a non-hierarchical clustering method that starts by computing the centroids for each cluster and then calculates the distances between the current data vector and each centroid, assigning the vector to the cluster whose centroid is closest to it. This process is repeated until all vectors are assigned a cluster, and their members are closest to the centroids than to the mean of other clusters (WILKS, 2006).

The analysis used monthly averages from ECMWF-SEAS5 hindcast predictions for the lead time 1-month and CPC monthly averages, considering 1993 to 2016. The number of pre-selected groups for the method was k = 8, based on the qualitative analysis of rainfall regimes in the SA obtained by Reboita et al. (2010a). This work aims to evaluate the homogeneous rainfall patterns on the continent rather than discuss the statistical results obtained by the cluster technique.

6. RESULTS

6.1 Seasonal Means and Errors of Precipitation

In this section, the ECMWF-SEAS5 hindcasts seasonal mean predictions and their comparison with the fields obtained by the CPC are presented. Thus, it is possible to evaluate the model simulations regarding seasonal climate variability and spatial patterns of precipitation prediction.

Figure 6 shows the seasonal mean precipitation forecasts produced by ECMWF-SEAS5, and the mean value is calculated from the 25 members of the ensemble for the 24 years of each retrospective forecast season. That is, the mean value is obtained from 600 seasonal reforecasts of the model. Each season is identified by the initial letters of the three months that comprise the season. For instance, JFM corresponds to the January-February-March season. The Annexe presents maps with rainfall totals obtained by ECMWF-SEAS5 and CPC for all quarters and the resulting biases.

In general, the seasonal forecasts from ECMWF-SEAS5 reproduce the seasonal patterns of precipitation in the country and show good agreement with the fields obtained by CPC. The ECMWF-SEAS5's ability to capture the SACZ (CARVALHO; JONES; LIEBMANN, 2004; KODAMA, 1992) is highlighted in the summer months. In the months of NDJ and DJF (Figures 6k1, 6l1), a band of precipitation extends from the southern Amazon towards the southwestern South Atlantic, passing through Southeastern Brazil. However, CPC results for the same seasons (Figures 6k2, 6l2) show smaller precipitation amounts than ECMWF-SEAS5, indicating that the forecast model tends to overestimate rainfall in the region by up to 2 mm day^{-1}.

In the autumn and winter seasons (from AMJ to JAS), precipitation is reduced in the continent's interior, and the dry season begins in SEB (REBOITA et al., 2010a). Precipitation maxima occur in the northern Amazon Basin, and the seasonal forecasts of ECMWF-SEAS5 reasonably represent these patterns. However, from MJA to NDJ seasons, the model underestimates the rainfall totals in the eastern NEB compared to the CPC fields (Figures 6d2-6k2).

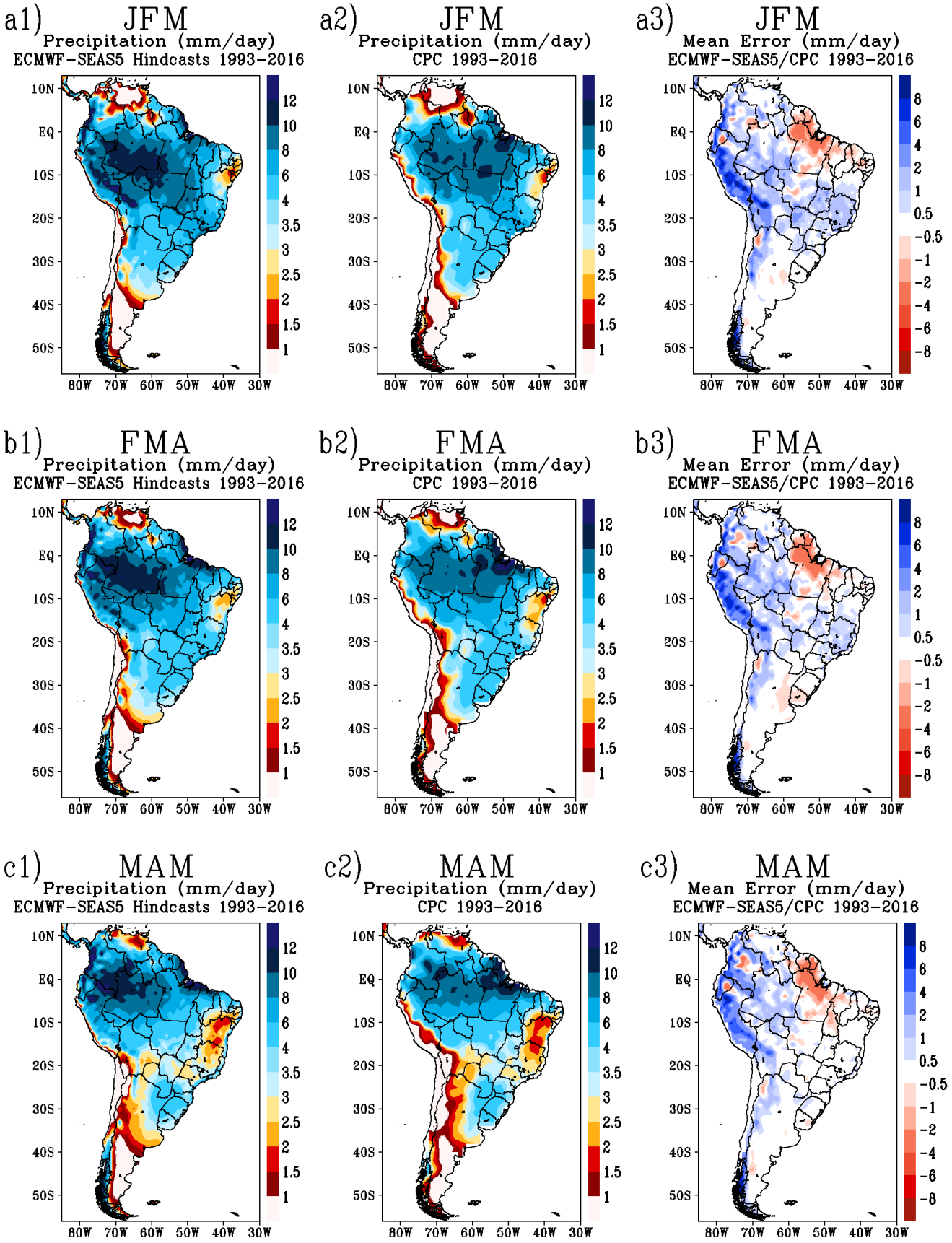

Figure 6 – Left column: seasonal mean precipitation (mm day^{-1}) derived from the ECMWF-SEAS5 hindcasts, averaged for 1993-2016 and over the 25 ensemble members. Center column: CPC seasonal mean precipitation (mm day^{-1}) averaged over 1993-2016. Right column: seasonal precipitation mean errors (mm day^{-1}) obtained by the difference between ECMWF-SEAS5 and CPC and averaged over 1993-2016.

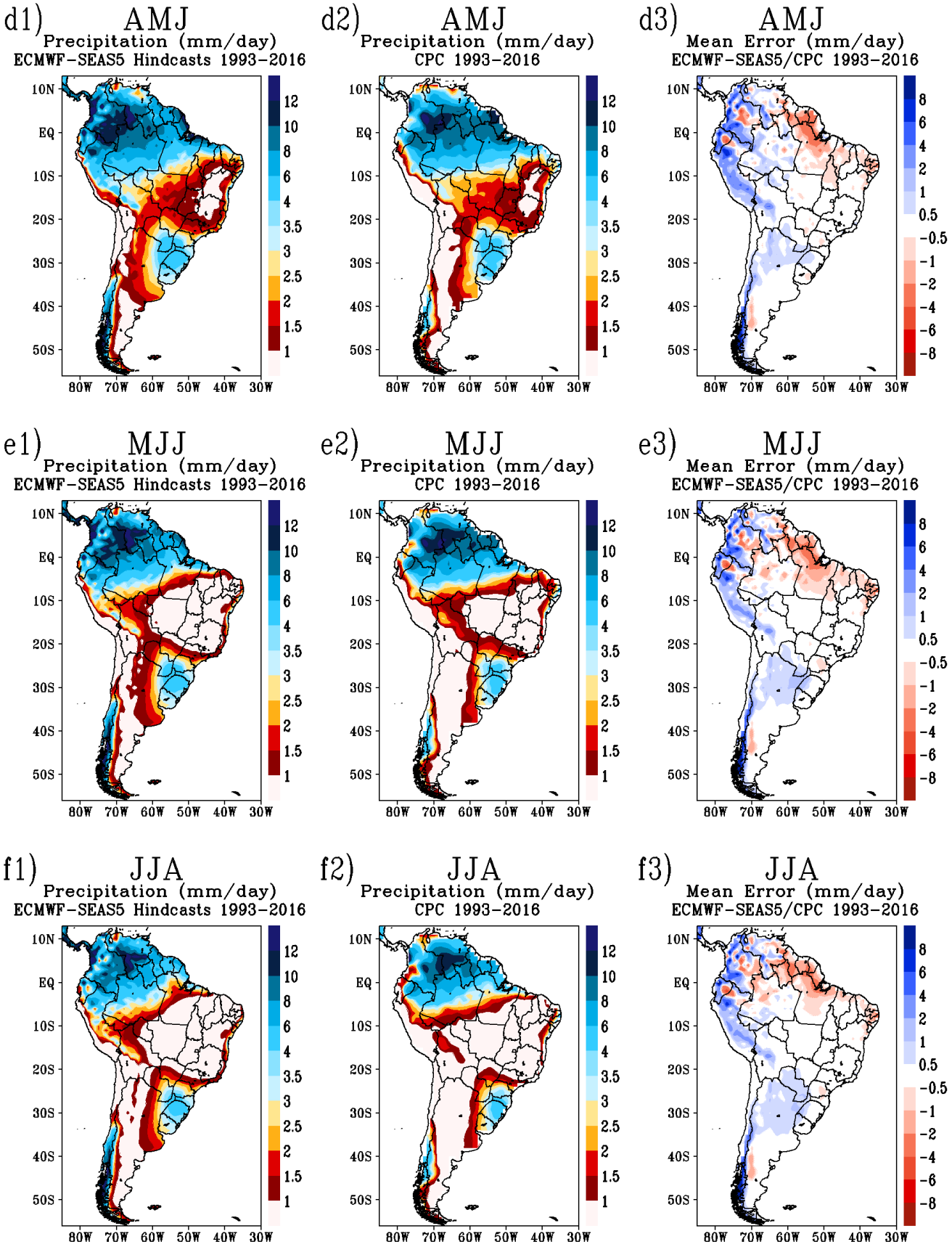

Figure 6 – continued.

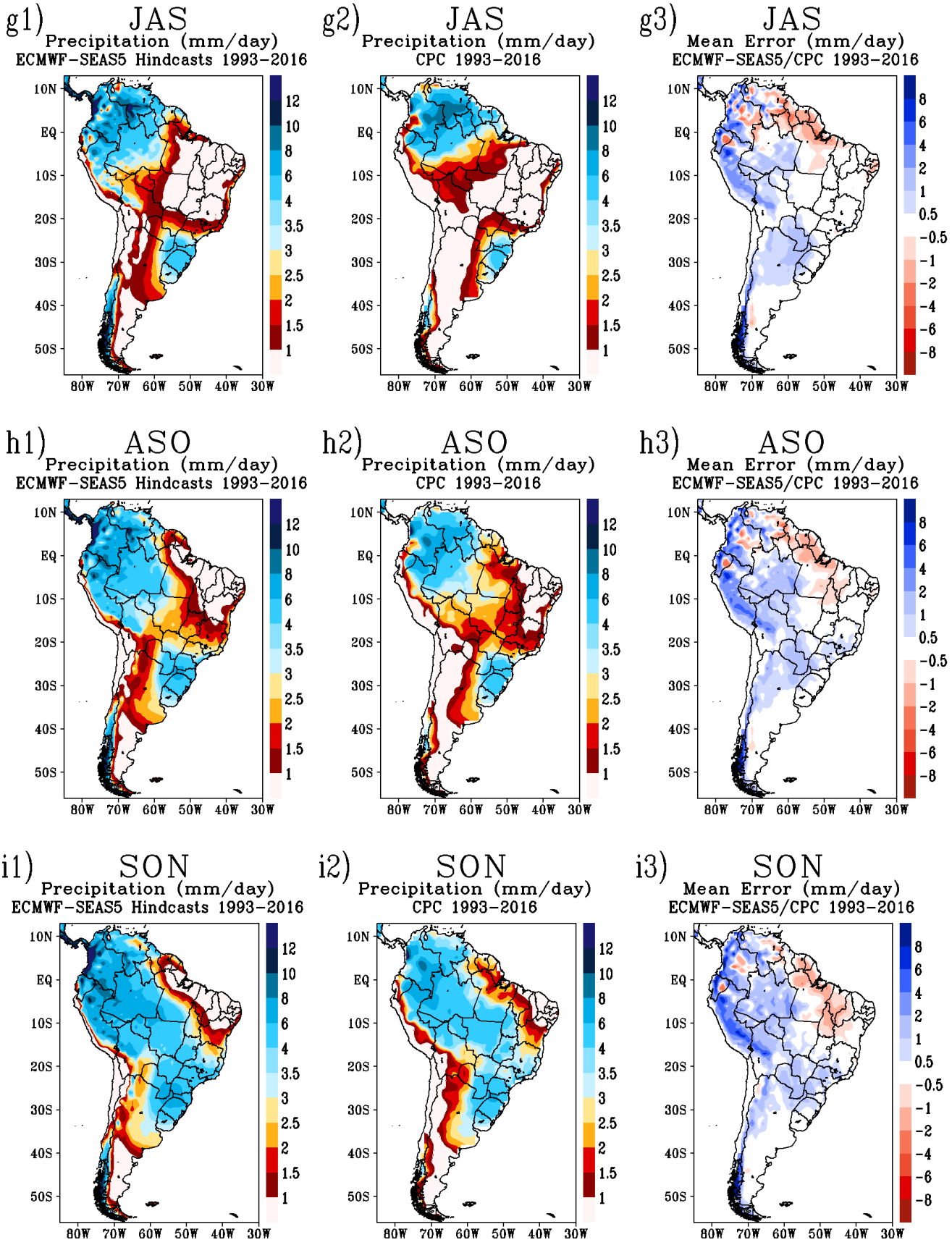

Figure 6 – continued.

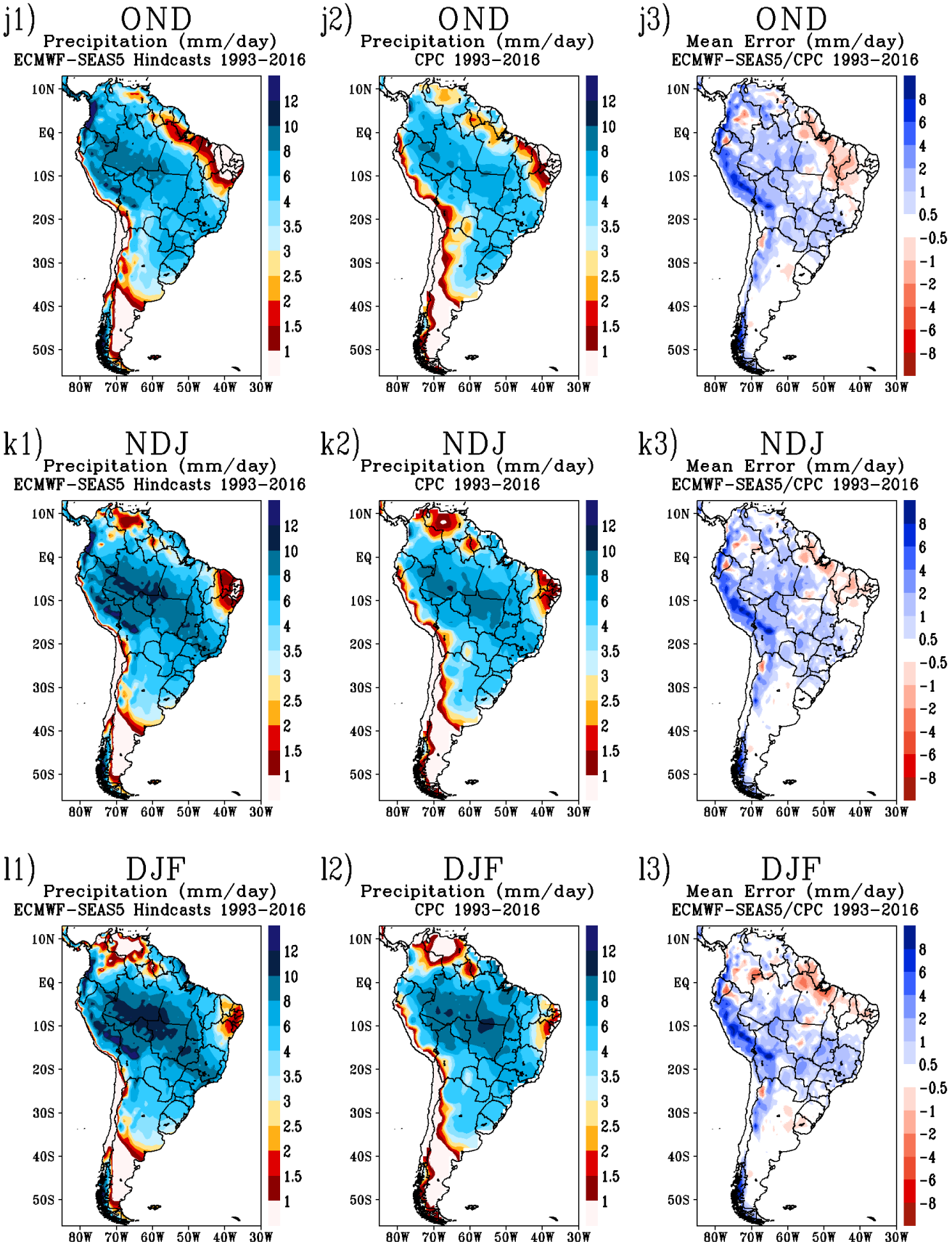

Figure 6 – continued.

In the following trimesters, from ASO to OND, the rainy season starts in most of South America (REBOITA et al., 2010a), and the model appropriately represents the seasonal variability of precipitation. Nevertheless, ECMWF-SEAS5 underestimates rainfall in northern sectors of the NEB (Figures 6h1-6j1). In southern Brazil, seasonal rainfall forecasts show little variability during the year, similar to the patterns obtained by CPC.

Despite the model presenting humid (dry) biases in the Amazon region (Northeast sector) throughout the year, the results indicate that ECMWF-SEAS5 hindcasts satisfactorily simulate the main precipitation patterns and their seasonal variability in Brazil. First, however, it is essential to verify whether the forecasts have systematic errors. Systematic errors can vary over the seasons, as they can be generated by the model's failure to capture predominant meteorological phenomena (CHOU et al., 2020). According to Hoskins, Shopf and Navarra (2008), those errors can be due to the observational data or its assimilation, physical process parameterization and a short timescale spin-up/adjustment process.

The ECMWF-SEAS5 seasonal predictions underestimate precipitation in Brazil's centre during most of the year. In the rainy season quarters, from OND to JFM (Figures 6a3, 6j3-6l3), seasonal forecasts overestimate total rainfall in the Southeast and North regions of the country, with overestimates of up to 4 mm day^{-1} in the Amazon region and up to 2 mm day^{-1} in the central and Southeast regions. Inversely, sectors such as the far north and northeastern Brazil show that seasonal forecasts underestimate rainfall in these regions throughout the year. Precipitation underestimates in the east and interior of the Northeast become more expressive in the austral autumn/winter months (Figures 6b3-6f3), including the rainy season in this region (CHOU et al., 2020; REBOITA et al., 2010).

In the Southeast, seasonal forecasts underestimate rain in the dry seasons up to 1 mm day^{-1} (Figures 6c3-6g3) but overestimate it from the beginning of spring onwards in regions like the south of Minas Gerais and over the whole São Paulo state (Figures 6h3-6j3). Conversely, as described, in the rainy season months, the model's predictions overestimate rainfall occurrence, with notable positive deviations in the regions comprising the SACZ (Figures 6a1, 6j1-6l1).

Southern Brazil indicates that ECMWF- SEAS5 underestimates rainfall in the autumn and winter (Figures 6b1-6g1) and overestimates it in the spring and summer (Figures 6i3-6k3). Besides, seasonal forecasts show a slightly negative bias throughout the year in sectors such as the country's extreme south. However, the magnitude and variability of seasonal forecast errors for the South are smaller than other Brazil regions.

In conclusion, seasonal rainfall forecasts from ECMWF-SEAS5 hindcasts indicate systematic overestimates (underestimates) in the North and Southeast Brazil during the rainy (dry) season and systematic underestimates in the far north SA and Northeast Brazil throughout the year.

6.2 Seasonal Precipitation Skill Score

This section presents the skill scores obtained for ECMWF-SEAS5 hindcasts to evaluate the model's capability to represent the seasonal rainfall variability over SA. Following the methodology of Chou et al. (2020), skill scores are calculated as the temporal correlations between the trimonthly precipitation anomalies predicted by the model and those obtained by CPC, considering the CPC's dataset climatological mean (from 1993 to 2016).

According to Ziervogel et al. (2005), for seasonal climate forecasts to be useful for application at a local scale, they must be accurate at least 60%-70% of the time. In this sense, Gubler et al. (2020) adapted the discrimination score by Ziervogel et al. (2005), converting it to thresholds associated with Pearson's correlation coefficient. For this, a linear model was established between the percentages by Ziervogel et al. (2005) and the correlations of Gubler et al. (2020), and Fisher's transformation was applied to both parameters. The adjusted linear model obtained from the relationship between the two metrics resulted in the following thresholds: accurate seasonal predictions at least 60% of the time correspond to correlations of at least 0.32, whilst accurate seasonal forecasts at least 70% of the time correspond to correlations above 0.58. Thus, correlations below 0.3 were related to potentially harmful predictions, while correlations above 0.6 indicated useful predictions even for application at a local scale (GUBLER et al., 2020). Notwithstanding, the authors emphasize that uncertainties regarding these thresholds should not be neglected.

Given the above, only skill scores equal to or greater than 0.3 are presented in this study. Moreover, Chou et al. (2020) also use the skill score of 0.3 to indicate the usefulness of seasonal forecasts. Figure 7 shows the ECMWF-SEAS5 hindcasts skill scores calculated for all seasons.

North Brazil has skill score values above 0.6 in the seasons from SON to JFM (Figures 7a and 7i-7l). Chou et al. (2020) evaluated the seasonal forecast skill scores of the RCM Eta and

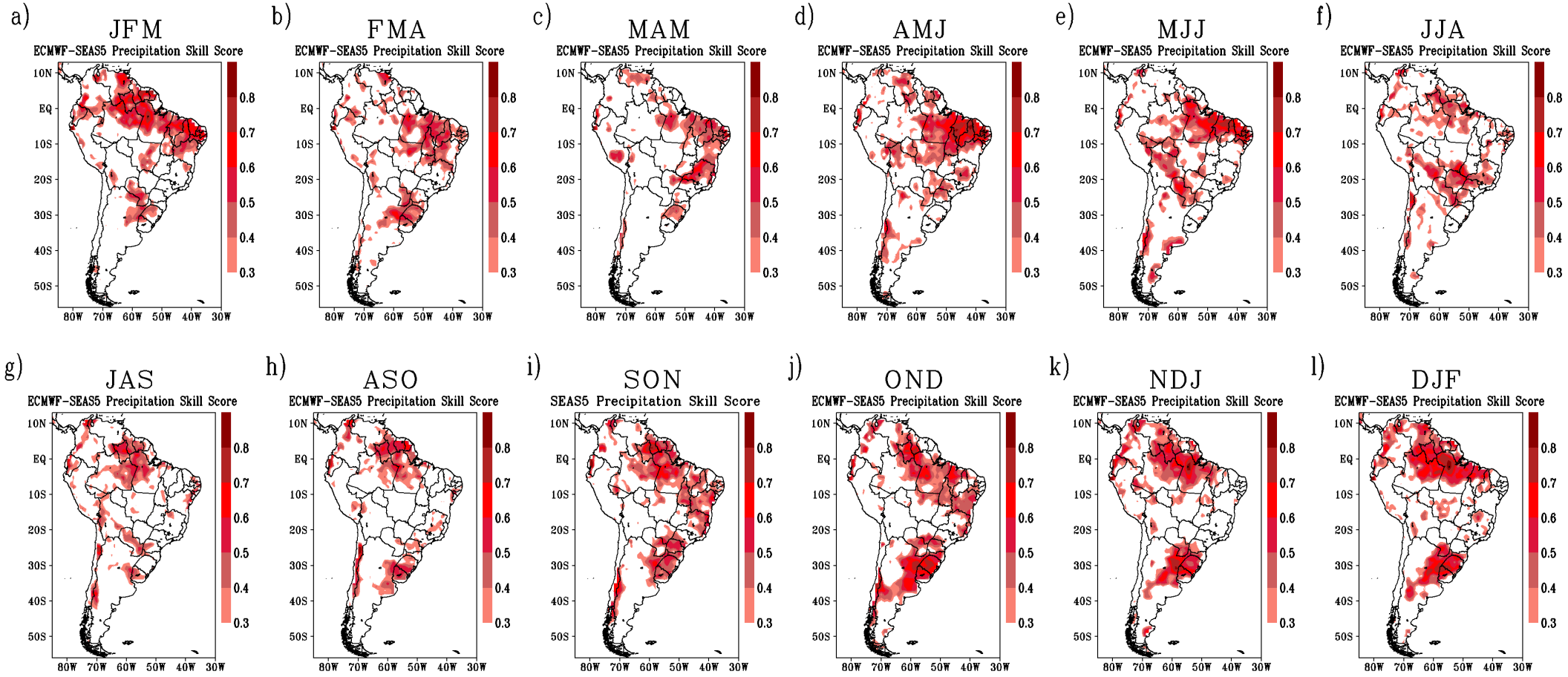

Figure 7 – Seasonal precipitation anomaly skill scores for the ECMWF-SEAS5 hindcasts. Trimesters correspond to reforecasts from the 1–3-month lead times. Only scores equal to or above 0.3 are shown. The score is nondimensional.

the GCM CPTEC-COLA. It is worth noting that the skill scores obtained here for North Brazil in the rainy seasons are similar to those obtained by Chou et al. (2020). The seasons from FMA to JJA (Figures 7b-7f) show moderate skill scores in the northern region, results analogous to those found by Chou et al. (2020) and Gubler et al. (2020). The authors attribute the good performance of forecasts in the region to the ENSO's influence (ACEITUNO, 1988; COELHO et al., 2006a; COELHO; UVO; AMBRIZZI, 2002; ROWELL, 1998; UVO et al., 1998).

Northeast Brazil presents high skill scores (above 0.6) in the wetter seasons of MAM, AMJ and MJJ (Figures 7c-7e), corroborating results obtained by Chou et al. (2020) and Gubler et al. (2020). Besides, the region's MAM skill score (Figure 7c) is remarkable, indicating the model's skilful performance in predicting precipitation anomalies in almost the entire sector. One reason for this may be the strong relationship between tropical Atlantic SST and rainfall in the Northeast during MAM (HASTENRATH; GREISCHAR, 1993; MOURA; HASTENRATH, 2004; PEZZI; CAVALCANTI, 2001; REBOITA et al., 2021a).

Another prominent region that has relevant skill scores is South Brazil. In the seasons from SON to MAM (Figures 7a-7c and 7i-7l), moderate values are observed, with skill scores above 0.6 in the DJF season (Figure 7l). Even though Chou et al. (2020) have not found notable skill scores for this region (except at SON and OND seasons), Gubler et al. (2020) verified an excellent performance of ECMWF-SEAS5 in the sector north of Uruguay in the DJF months, indicating its potential use even for smallholder farmers. It is suggested that the skilful execution of seasonal forecasts in this region may be associated with ENSO's teleconnection effects (COELHO et al., 2006a; GUBLER et al., 2020).

The results indicate low skill scores in Brazil's southeast and central regions throughout the year. Similar results were obtained by Chou et al. (2020) and Gubler et al. (2020). Moreover, despite Coelho et al. (2006b) having suggested moderate climate predictability for the Southeast in summer, in this study, moderate skill scores were only obtained in the region for the JJA trimester (Figure 7f).

The ECMWF-SEAS5 seasonal forecast skill scores showed higher values in Brazil's northern and southern portions and lower ones in central and southeastern sectors. The tropical region has greater climate predictability (ROWELL, 1998), whereas the southern subtropical region has already shown relevant predictability (COELHO et al., 2006b). The results obtained for sectors such as the extreme south and northeastern Brazil may indicate that the ECMWF-

SEAS5 performance does not derive only from ENSO mechanisms but also from other modes of climate predictability that contribute to a better seasonal forecasting skill.

6.3 ENSO Events

The same skill score evaluation methodology presented above is applied in this section, considering only El Niño and La Niña events from 1993 to 2016. Anomaly correlations were also calculated separately for El Niño and La Niña periods compared to the 24 years of hindcasts. For the El Niño events, the DJF and JJA trimesters were selected, and for the La Niña events, the FMA trimester was chosen. The selection of these trimesters was based on the ENSO effects over Brazil in these seasons (CHOU et al., 2020). The DJF, JJA and FMA periods with El Niño and La Niña events between 1993 and 2016 are listed in Table 4. This table is constructed based on the information provided by the CPC/NOAA on the page https://origin.cpc.ncep.noaa.gov/products/analysis_monitoring/ensostuff/ONI_v5.php. Eight El Niño events in DJF, five El Niño events in JJA, and eight La Niña events in FMA occurred in the period.

Figure 8 shows the seasonal rainfall forecast skill scores of ECMWF-SEAS5 during DJF (Figure 8a) and JJA (Figure 8c), considering only El Niño years and during FMA (Figure 8b) computing only La Niña years. Figure 8a indicates moderate skill score values over the central region of Brazil, comprising areas commonly occupied by the SACZ. Nevertheless, this skill is not evident whether the entire DJF dataset is considered (Figure 8l). Furthermore, the high skill scores in South Brazil and the northern part of Northeast Brazil are still apparent in these El Niño compositions.

In the JJA months during El Niño years, the highest skill scores are in Northern Brazil. Compared to the JJA season of the entire data set (Figure 7f), it is observed that the skill scores are more expressive in the country's northern portion. Results obtained here for the El Niño compositions are similar to those of Chou et al. (2020), indicating the ECMWF-SEAS5 ability is equivalent to that of the Eta during ENSO periods.

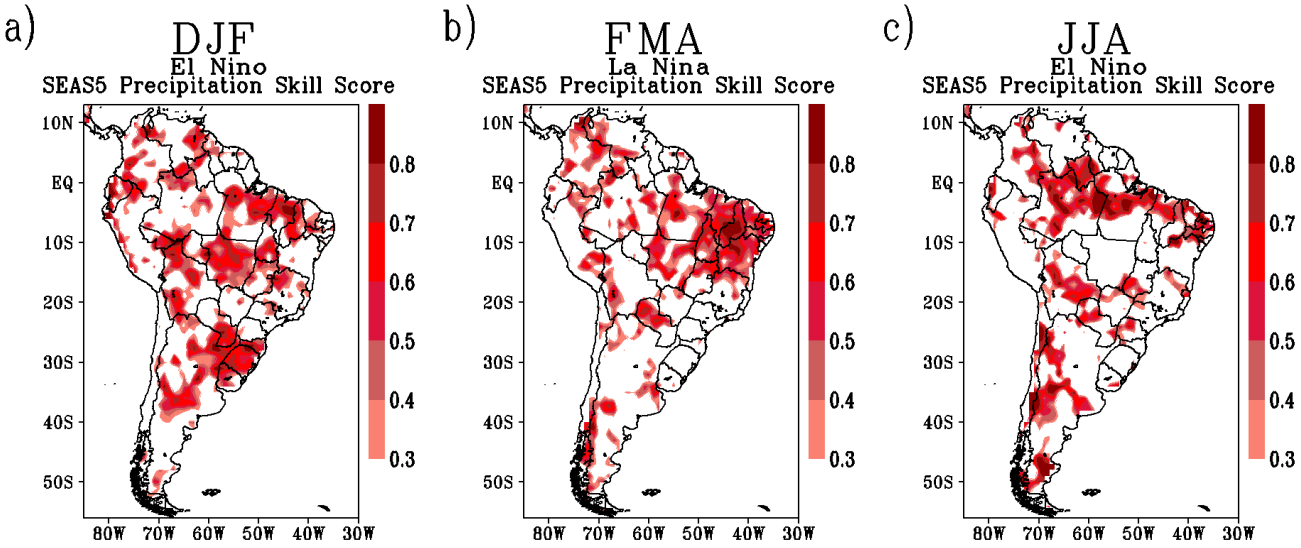

Figure 8 – Seasonal precipitation anomaly skill scores derived from the ECMWF-SEAS5 hindcasts for (a) DJF and (c) JJA for El Niño years; and (b) FMA for La Niña years. Only scores equal to or above 0.3 are shown. The score is nondimensional.

Figure 8b shows the skill scores calculated during the FMA months considering only La Niña years. Compared with the results for FMA of the entire hindcast (Figure 7b), there are higher skill values throughout Northeast Brazil and an absence of skill in the southern region. The best results for the northeast region are also found in Chou et al. (2020).

During Canonical La Niña events (associated with cooling in the eastern sector of the equatorial Pacific), the meridional gradient of SST in the tropical Atlantic often turns negative, with cold anomalies in the tropical North Atlantic and warm anomalies in the tropical South Atlantic, inducing a southward migration of the ITCZ and consequent precipitation in the Northeast Brazil (RODRIGUES; MCPHADEN, 2014). However, studies show that SST cooling in the central and eastern sectors of the equatorial Pacific (indicating a La Niña event with Canonical and Modoki-type features) is related to reduced rainfall in the northeast and increased precipitation in the north, resulting from the ITCZ displacement (TEDESCHI; CAVALCANTI; GRIMM, 2013; WIEDERMANN et al., 2021).

Other studies show that in Canonical La Niña events, there is a trend to decrease precipitation in the southern region of Brazil (ANDREOLI et al., 2018; GRIMM; BARROS; DOYLE, 2000; GRIMM; FERRAZ; GOMES, 1998; TEDESCHI; CAVALCANTI; GRIMM, 2013; WIEDERMANN et al., 2021). Therefore, although La Niña affects the rainfall in southern Brazil, the composition in Figure 8b does not indicate skill improvement in the region.

Besides the inherent difficulty of coupled models in representing different El Niño and La Niña events, there are also limitations in predicting the teleconnection effects, as errors persist even when the simulations eliminate the SST biases (TEDESCHI; COLLINS, 2016). Furthermore, studies show that the representation of El Niño/La Niña different types in climate models is sensitive to the atmospheric response, particularly in convection location (HAM; KUG, 2012; KUG et al., 2012; KUG; HAM, 2011; XU et al., 2014), the ability to represent the teleconnections effects in the Indian Ocean (DU et al., 2013; OKUMURA; DESER, 2010; SANTOSO; ENGLAND; CAI, 2012; WANG, 2019), as well as the different convection parameterization schemes (BELLENGER et al., 2013).

Using global climate models from Coupled Model Intercomparison Project Phase 5 (CMIP5), studies had simulated the difference between the two types of La Niña – the Canonical and Modoki types – (TASCHETTO et al., 2014; TEDESCHI; COLLINS, 2016). However, although the events had been well simulated, most of the models had failed to reproduce the asymmetry between the two types of La Niña, presenting La Niña events in the eastern Pacific more intense than those in the central Pacific, when the opposite occurred in observations (TASCHETTO et al., 2014; TEDESCHI; COLLINS, 2016).

6.4 Regional Precipitation Anomalies

Spatial anomalies of the subdomains illustrated in Figure 5 are calculated and compared to those obtained by the CPC for the same areas. The average anomalies are calculated considering the 1993-2016 climatological mean from ECMWF-SEAS5 and CPC.

For Southeast Brazil (SEB; Figure 9), the ECMWF-SEAS5 seasonal forecasts overestimate precipitation for most of the year, except for the MJJ quarter, where the CPC anomalies are more positive than the simulations (Figure 9c). In general, the series of anomalies obtained by ECMWF-SEAS5 indicates that the model remains stable throughout the integration of forecasts. In the autumn and winter quarters (Figures 9b-9d), the model satisfactorily represents the interannual variability of rainfall anomalies in the region, with some deficiency in simulating the positive precipitation deviations that occurred in the MJJ quarter (Figure 9c).

However, in the spring and summer quarters (Figures 9a, 9e and 9f), the model presents more marked deviations from the CPC. In addition to the overestimation of rainfall in these periods, the model fails to capture the most prominent negative and positive rainfall deviations, as shown by the quarters from ASO (Figure 9d) to FMA (Figure 9a). An example is the drought that occurred in the region in 2013/2014 (COELHO et al., 2016; OTTO et al., 2015; REBOITA et al., 2015), which the model was not able to predict, as shown in Figures 9a and 9f.

Concerning the Amazon subdomain (AMZ), the model adequately performs from SON to DJF (Figures 10e and 10f), with anomalies close to CPC. However, as in the SEB subdomain, the model overestimates rainfall practically throughout the year, with more pronounced deviations in the autumn and winter months (Figures 10b, 10c and 10d). As seen in the previous subdomain, the model fails to capture negative anomalies of greater magnitude, remaining stable during forecast integration and with few prominent variations over the years. Drought events such as in 2005 (MARENGO et al., 2008) and 2015 in Eastern Amazon (region inserted in the AMZ subdomain) (JIMÉNEZ-MUÑOZ et al., 2016) were not well predicted by the ECMWF-SEAS5 hindcasts, which tended to overestimate the rainfall totals in the area.

Unlike the other subdomains, the seasonal forecasts from ECMWF-SEAS5 tend to underestimate precipitation throughout the year in Northeastern Brazil (NEB). As a result, the precipitation anomalies obtained by CPC have positive deviations more prominent in magnitude than those predicted by ECMWF-SEAS5 (Figure 11). However, it appears that the European model can simulate the interannual variability of precipitation anomalies in the region, as illustrated in the quarters from JFM to FMA (Figures 11a and 11b). Nevertheless, hindcast predictions did not simulate extreme drought events in the region, such as those in 1997 (OLIVEIRA; SATYAMURTY, 1998) and 2012 (MARENGO et al., 2013, 2018), as seen in Figure 11c.

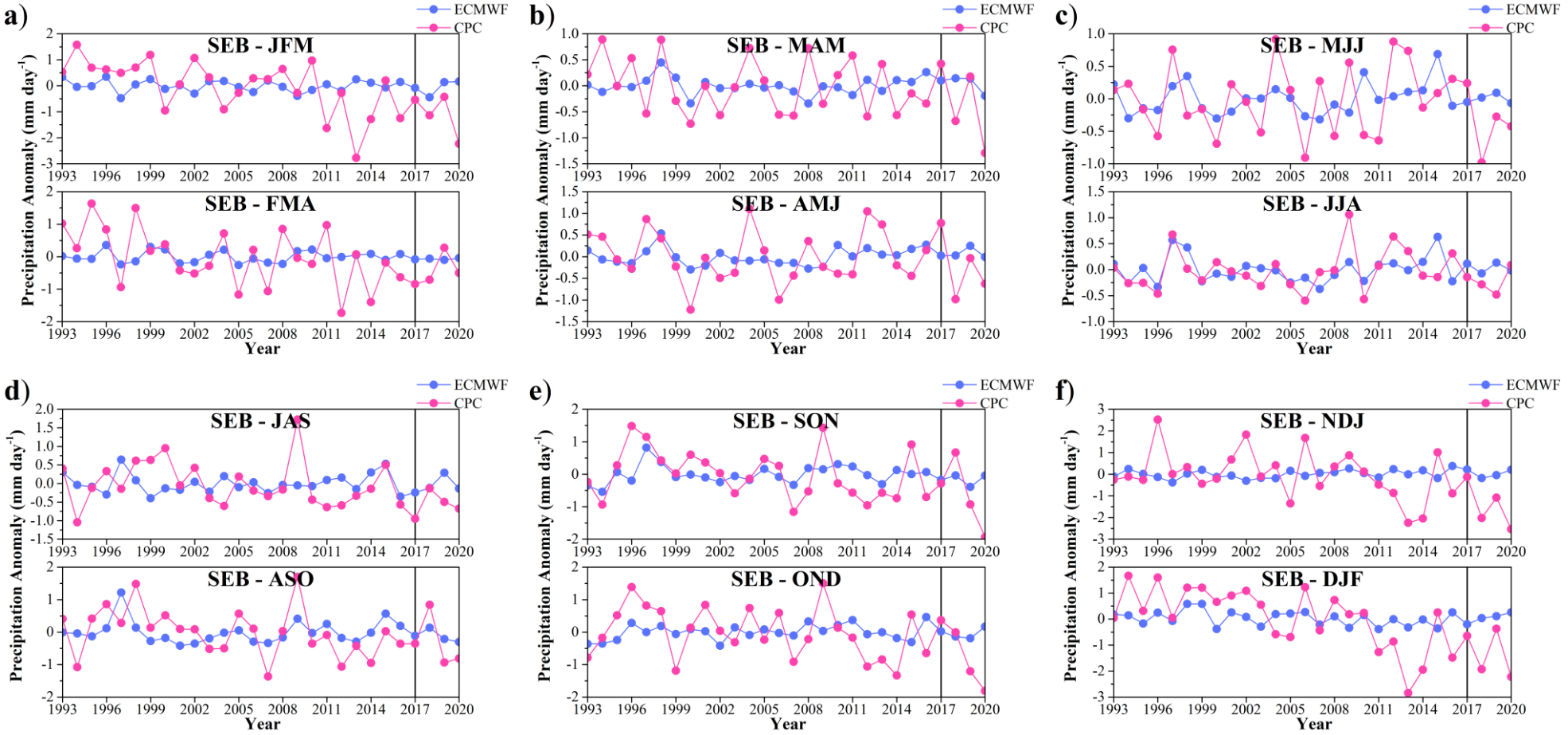

Figure 9 – Average seasonal precipitation anomalies (mm day^{-1}) in the Southeastern Brazil subdomain (SEB). The vertical black line indicates the end of hindcasts and the start of forecasts.

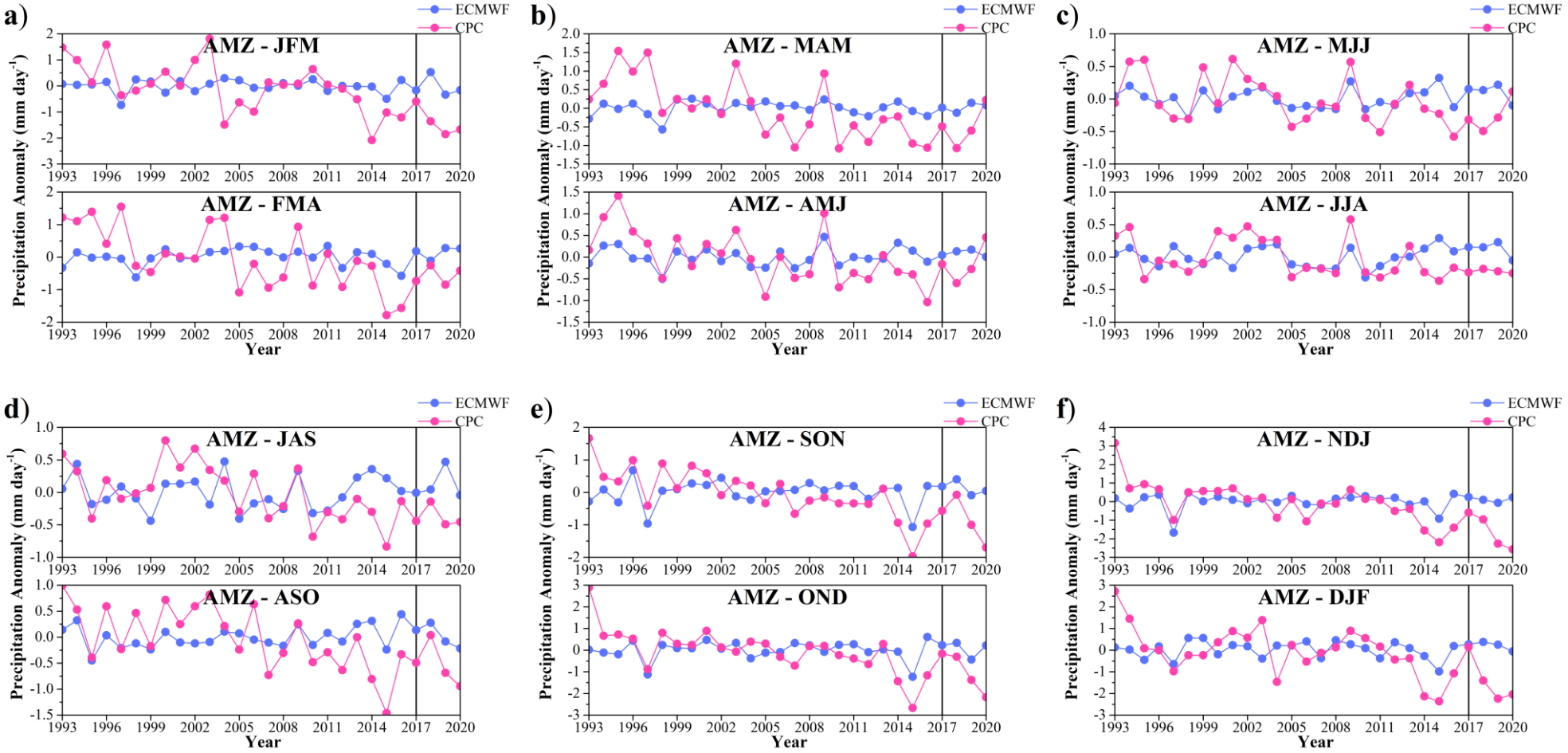

Figure 10 – Similar to Figure 9, except for the Amazon subdomain (AMZ).

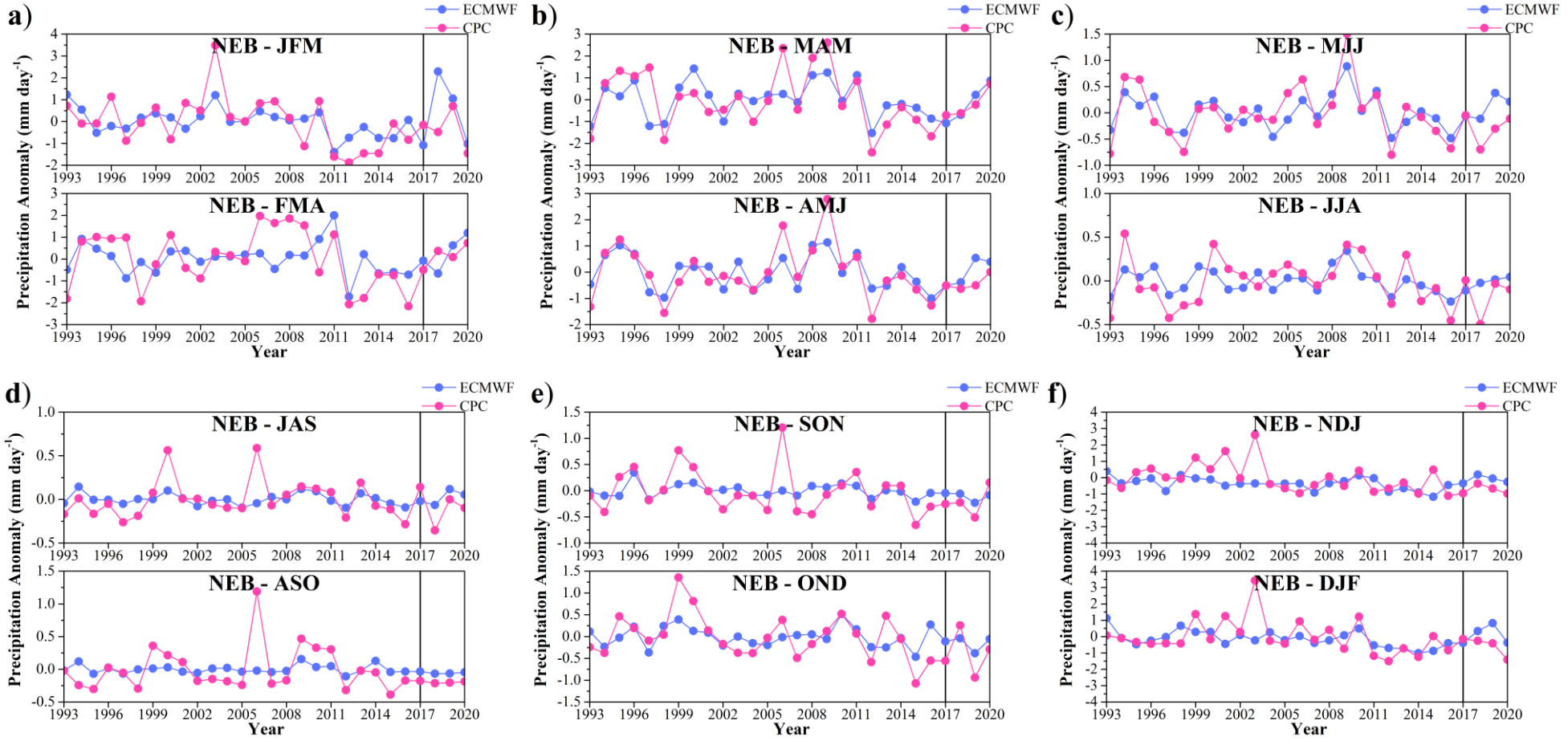

Figure 11 – Similar to Figure 9, except for the Northeast Brazil subdomain (NEB).

In Southern Brazil (SB), ECMWF-SEAS5 indicates adequate performance in simulating interannual rainfall variability in some seasons (Figures 12b and 12e). However, forecasts tend to overestimate rainfall totals throughout the year, with the most expressive deviations in the winter months (Figures 12c and 12d). Despite capturing some precipitation maxima (Figures 12b, 12e and 12f), the model does not satisfactorily represent the interannual rainfall variability in the summer months (Figures 12a and 12f), remaining stable throughout integration in most seasons. The larger negative rainfall anomalies observed in the CPC data are not well simulated by the model, as illustrated in Figures 12c, 12d and 12f.

The model underestimates precipitation throughout the year for the SESA subdomain, with larger deviations in the summer quarters (Figure 13a). Only in the JAS and DJF quarters (Figures 13d and 13f), the model presents a series of anomalies whose interannual variability is similar to that of the CPC. Despite underestimating the precipitation in the SESA, the model does not skillfully reproduce the prominent negative precipitation anomalies obtained by the CPC (Figures 13a, 13c and 13e). Although studies indicate the relationship between the teleconnection effects of ENSO, SAM and Indian Ocean Dipole (IOD) on SESA precipitation (GARBARINI et al., 2016; GONZÁLEZ; VERA, 2010), other works show that few models are capable of capturing rainfall peaks in the region's annual cycle, indicating drier conditions than those observed (DE JESUS et al., 2016; SOLMAN et al., 2013). The underestimation of rainfall in the region is assumed to be due to the failure of models to simulate atmospheric systems at mid-latitudes, such as cold fronts that cross the region (DE JESUS et al., 2016). In this sense, sensitivity tests investigated the behaviour of different models and parameterizations for the region (DE JESUS et al., 2016; REBOITA et al., 2014b; SOLMAN et al., 2013). Considering the studies by Gubler et al. (2020) and Chou et al. (2020), both works did not find a satisfactory performance of the ECMWF-SEAS5 and Eta models in predicting rainfall in the region.

In the NSA subdomain, the model overestimates rainfall throughout the year, but the forecasts have a reasonable ability to simulate the interannual variability of rainfall anomalies. Figure 14 shows that the simulated interannual cycles oscillate similarly to those obtained by the CPC, although with different magnitudes. Besides, in the summer months, the model has a good representation of year-to-year variations in rainfall anomalies (Figures 14a, 14e and 14f). Given the relevant influence of ENSO on this region (CÓRDOBA-MACHADO et al., 2015), Gubler et al. (2020) and Chou et al. (2020) also found a good performance of forecasts for this sector.

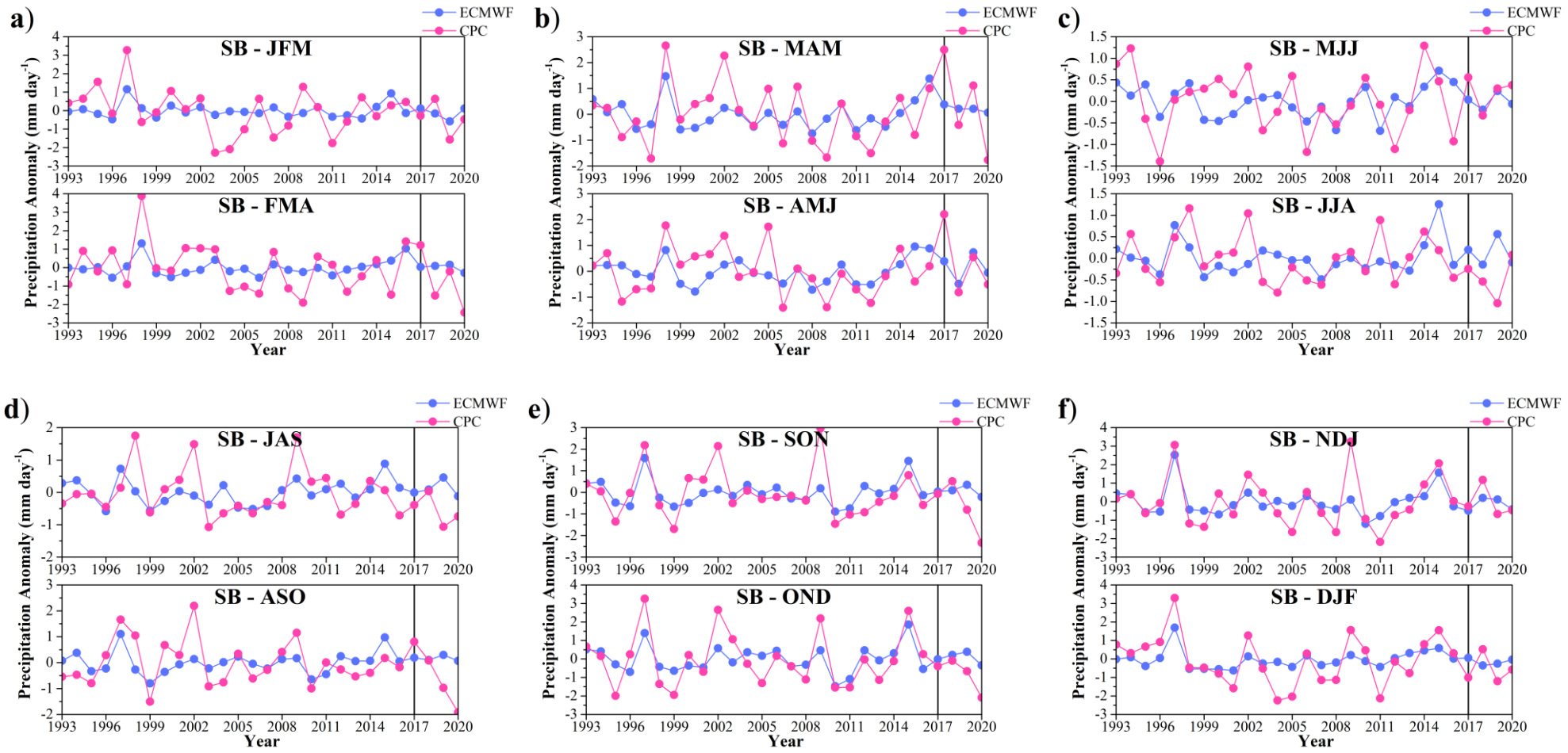

Figure 12 – Average seasonal precipitation anomalies (mm day^{-1}) in the Southern Brazil subdomain (SB). The vertical black line indicates the end of hindcasts and the start of forecasts.

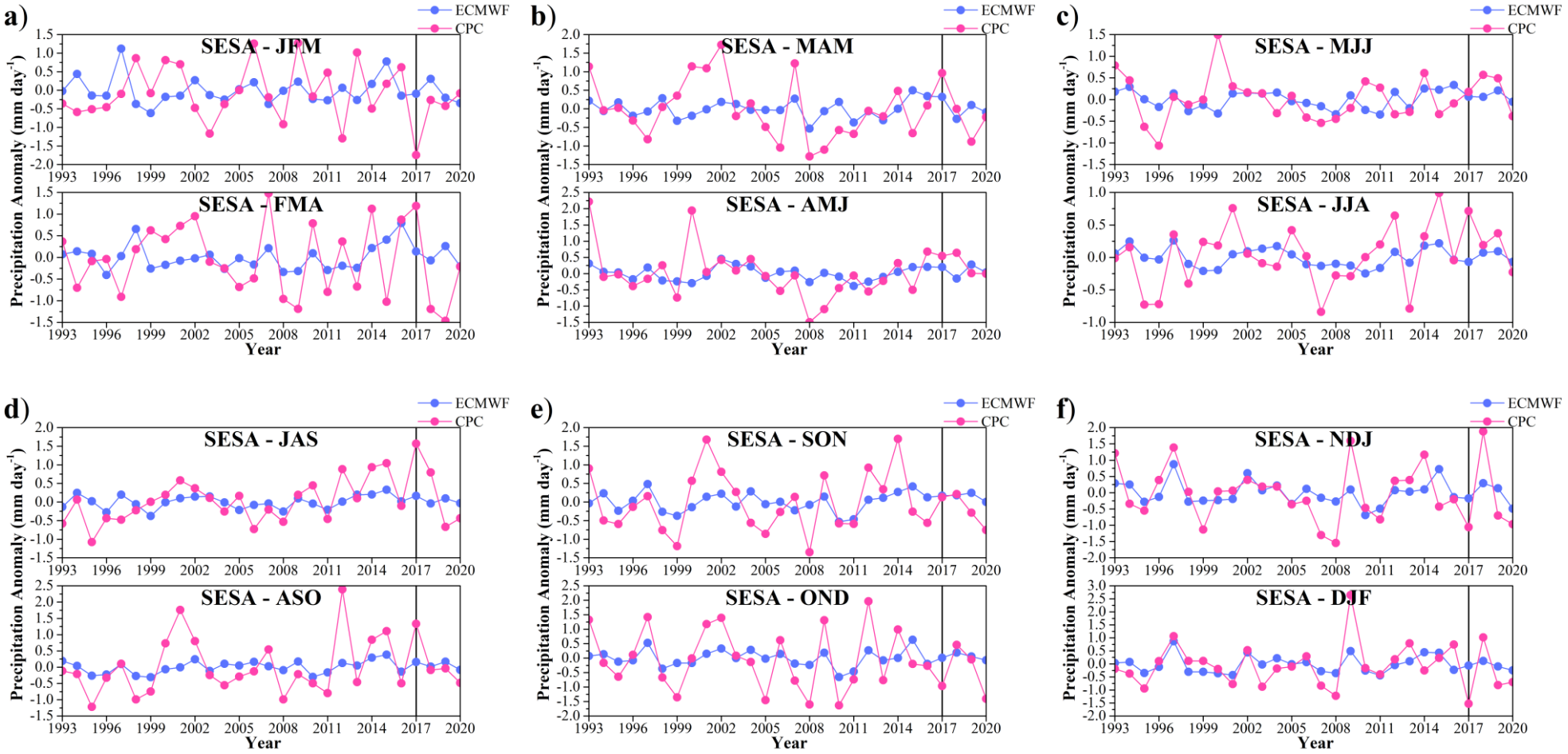

Figure 13 – Similar to Figure 12, except for the Southeastern South America subdomain (SESA).

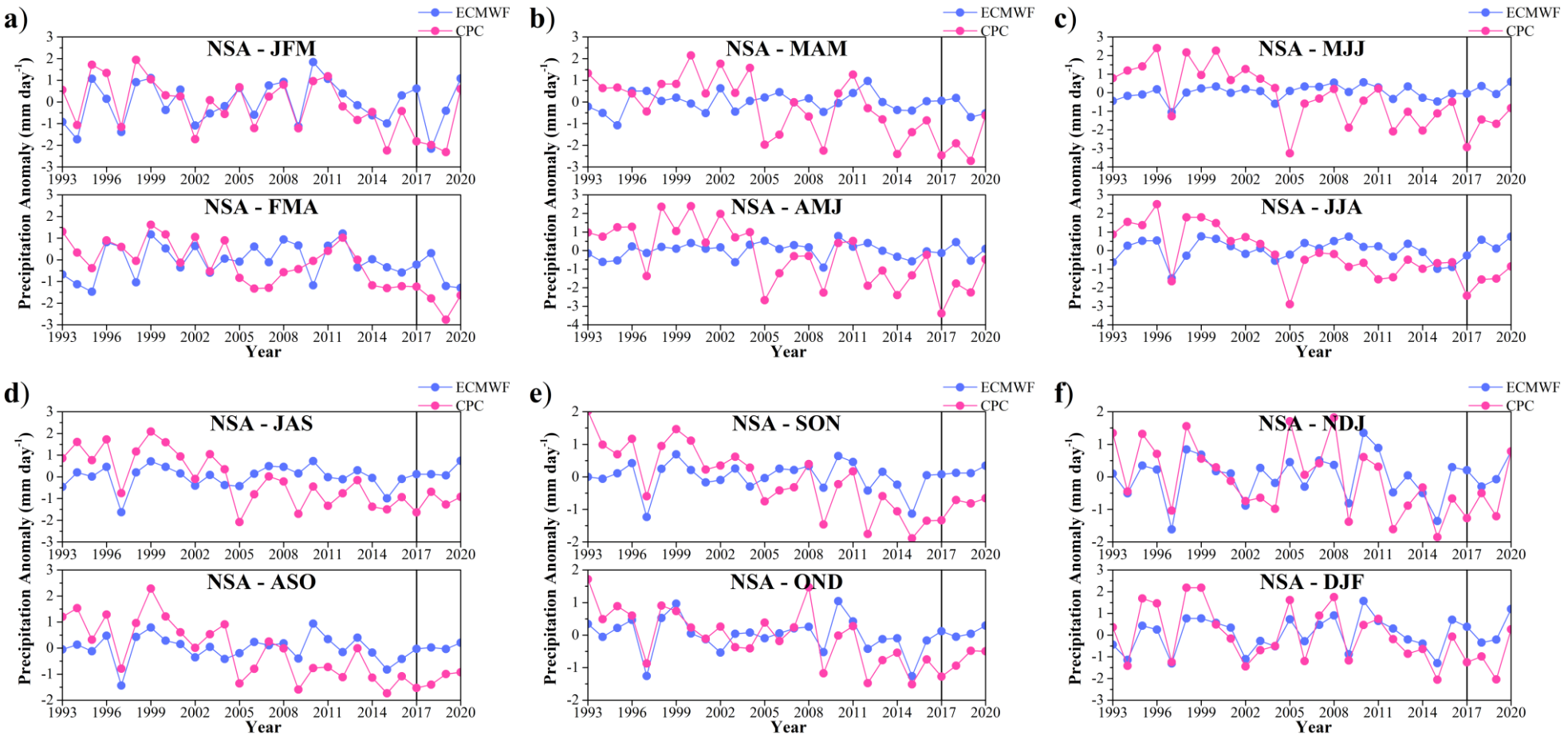

Figure 14 – Similar to Figure 12, except for the Northern South America subdomain (NSA).

6.5 Regional Skill Scores

Section 6.3 presented the temporal correlation analysis between the seasonal precipitation anomalies predicted by the model and those obtained by the CPC. The results indicated that the model has its best forecasting performance in Brazil's north, northeast and south regions. Furthermore, the tropical regions have good forecasting performance practically throughout the year, while the southern region presents better skill values in the spring and summer months (Figure 7). These results corroborate those found by Chou et al. (2020) and Gubler et al. (2020), indicating good prediction ability in regions strongly influenced by the teleconnection effects of ENSO and Tropical Atlantic (ACEITUNO, 1988; COELHO; UVO; AMBRIZZI, 2002; HASTENRATH; GREISCHAR, 1993; REBOITA et al., 2021a; UVO et al., 1998).

The mean regional rainfall anomalies obtained for three different subdomains are analysed in this section. These subdomains were selected according to the best results of the skill score assessment previously performed. The three sectors cover portions of the North (NB2), Northeast (NEB2) and South Brazil (SB2) regions, illustrated in Figure 15 and whose geographic coordinates are indicated in Table 5. The selection was based on sectors with better forecasting skills, and the seasons of DJF, MAM, JJA and SON were chosen.

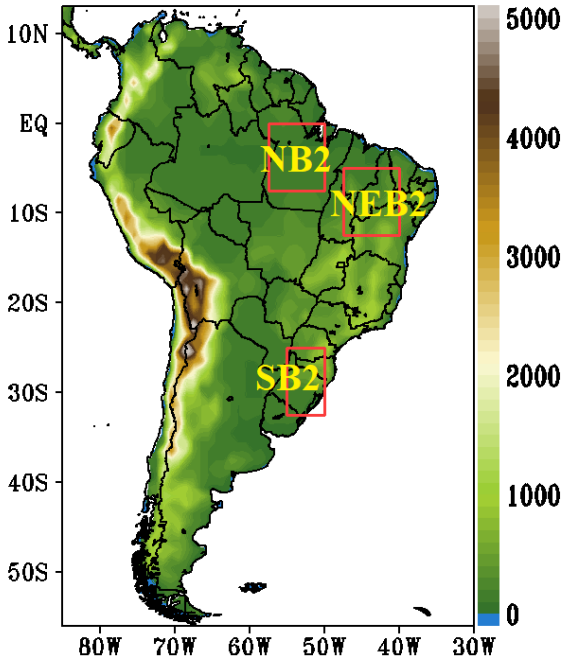

Figure 15 – Selected subdomains for calculating regional skill scores. Elevation in colours (m).

Table 5 – Location of sectors used to calculate seasonal mean anomalies.

Subdomain	Latitude	Longitude
NB2	0º - 7.5ºS	50ºW - 57.5ºW
NEB2	5ºS - 12.5ºS	40ºW - 47.5ºW
SB2	25ºS - 32.5ºS	50ºW - 55ºW

For the NB2 subdomain, belonging to the northern region of Brazil, results indicate that the model has a good capacity to simulate the interannual variability of seasonal rainfall anomalies (Figure 16). Despite underestimating precipitation, the model's ability to represent the oscillations of seasonal rainfall anomalies in the summer and spring seasons is noteworthy. Examples are given in the DJF and SON months from 2008 to 2018. Note that the model captured the most considerable negative rainfall deviations, such as those that occurred in 1997 and 2015. In autumn and winter, the model's forecasts underestimate the rainfall occurrence but coherently simulate the variability of seasonal anomalies, as in MAM from 2012 to 2017 and in JJA from 2000 to 2012.

In the NEB2 subdomain, located in the central region of northeastern Brazil, the model presents an underestimate of precipitation, as illustrated in other results that indicate this systematic error in forecasts for the region (Figures 6 and 11). However, the model's performance in simulating the seasonal anomalies of MAM from 1997 to 2004 and from 2009 to 2020 is notable (Figure 17). Besides, it captures the largest negative deviations in 1997, 2012 and 2015. Also, ECMWF-SEAS5 shows a remarkable ability to represent the rainfall deviations in ENSO periods such as MAM in 1997 and 2012 (MARENGO et al., 2013, 2018; OLIVEIRA; SATYAMURTY, 1998), a characteristic not so evident in the series obtained for the NEB subdomain (Figure 11). In general, dynamic and statistical models have a good predictive capacity in NEB during MAM due to the strong relationship between tropical Atlantic SST and rainfall in the region (DOBLAS-REYES et al., 2013; HASTENRATH; GREISCHAR, 1993; MOURA; HASTENRATH, 2004; UVO et al., 1998).

ECMWF-SEAS5 overestimates rainfall in the SB2 subdomain but fails to capture some precipitation maxima as in the JJA of 2002 and 2011 (Figure 18). The most pronounced negative anomalies, such as those occurring from 2004 onwards, are not well represented by the ECMWF-SEAS5 hindcasts. During the different seasons, the model remains stable throughout the integration of the forecasts, with few jumps in the values of the mean seasonal anomalies. However, some maximums obtained by the CPC are captured by the model, as in JJA and SON from 1997.

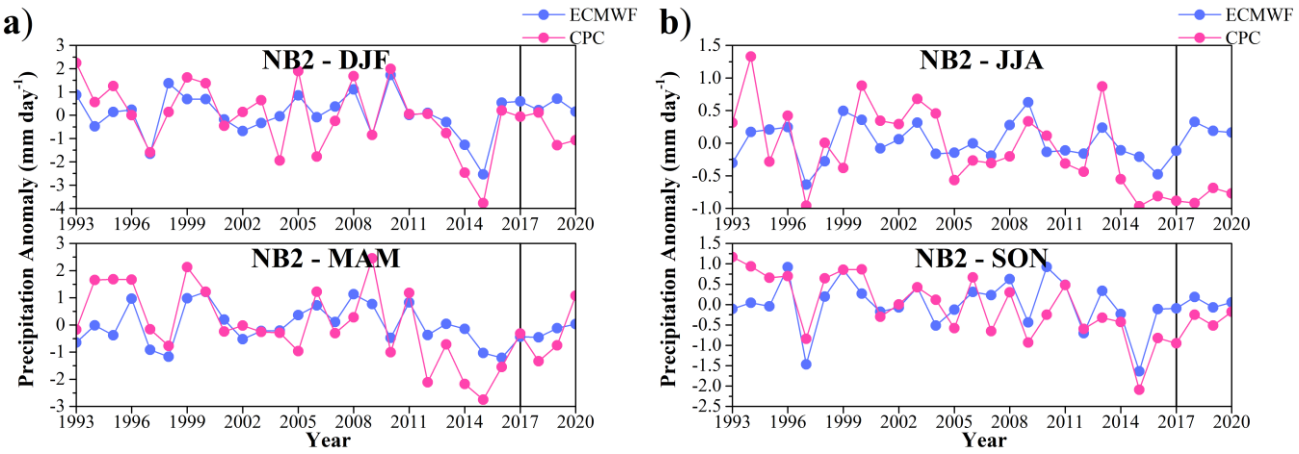

Figure 16 – Average seasonal precipitation anomalies (mm day^{-1}) in the northern Brazil subdomain (NB2). The vertical black line indicates the end of hindcasts and the start of forecasts.

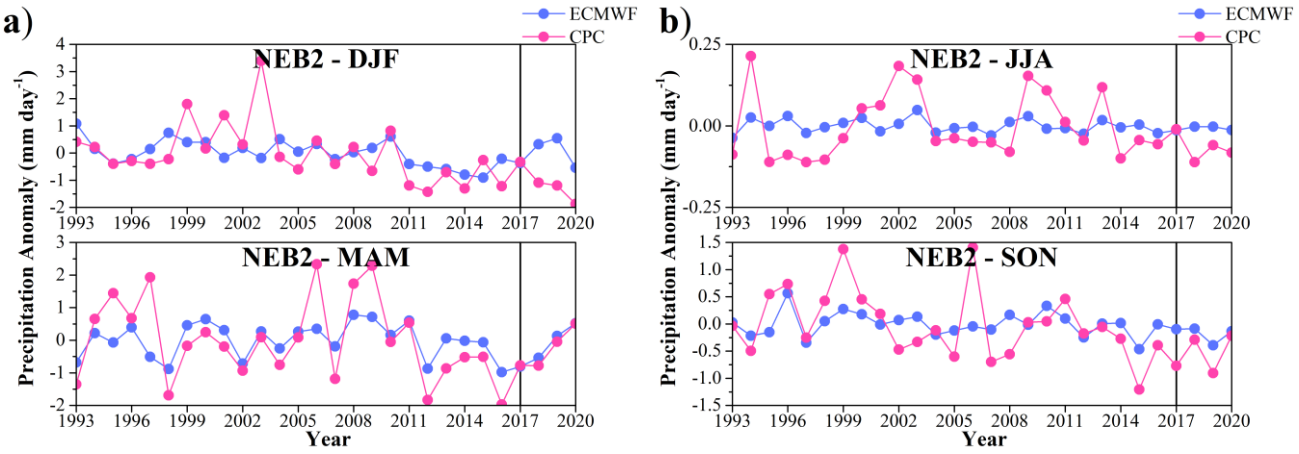

Figure 17 – Similar to Figure 16, except for Northeast Brazil (NEB2).

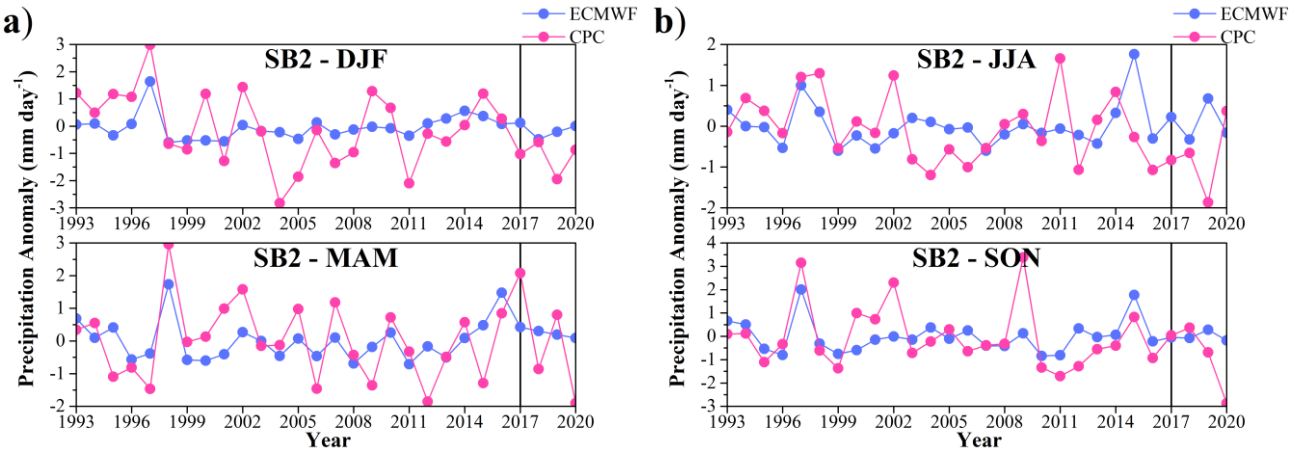

Figure 18 – Similar to Figure 16, except for South Brazil (SB2).

6.6 Statistical Parameters

Different statistical parameters were calculated using the regionalized anomalies to complement the quality analysis. Figure 19 shows the boxplots generated by the parameters calculated for each trimester. Therefore, a boxplot corresponds to all seasons (JFM to DJF). In the Annexe, tables with all the individual parameter values for each subdomain and quarter are presented.

The highest MAE and RMSE values correspond to the NSA subdomain (Figure 19a and 19b). The highest values of MAE and RMSE in AMZ correspond to the seasons of AMJ and MJJ. Despite the SB and SESA subdomains showing the lowest errors variability, the sectors have biases with considerable magnitudes. The NDJ trimester shows the highest RMSE in the SEB subdomain, and the JJA months correspond to the lowest values for SB. Although there is no marked difference between the MAE and RMSE magnitudes, the latter accentuates the most prominent errors, which justifies the larger variability in the NSA (Figure 19b).

The SB, NEB and NSA subdomains indicate the best results for R^2 and *r* (Figures 19c and 19d). The best values for the NEB subdomain correspond to the MJJ season ($R^2 = 0.68$ and $r = 0.82$), while for the SB, they refer to the OND months ($R^2 = 0.55$ and $r = 0.74$). On the other hand, the SEB and AMZ subdomains show the worst results for the JFM season.

The *d* index shows that only SEB and AMZ have values below 0.25. Again, the MJJ trimester indicates the best values for NEB ($d = 0.86$), while the NDJ and JFM trimesters show the worst results for SEB, AMZ and SB.

Considering domains outside Brazil, SESA presents the worst results. For the *d* index, SESA shows variability and the lowest values (Figure 19f). Likewise, the subdomain indicates higher relative error values, reaching 36% in the JJA quarter. On the contrary, the NSA subdomain presents good results of *r*, obtaining 0.80 in DJF and relative errors below 25%.

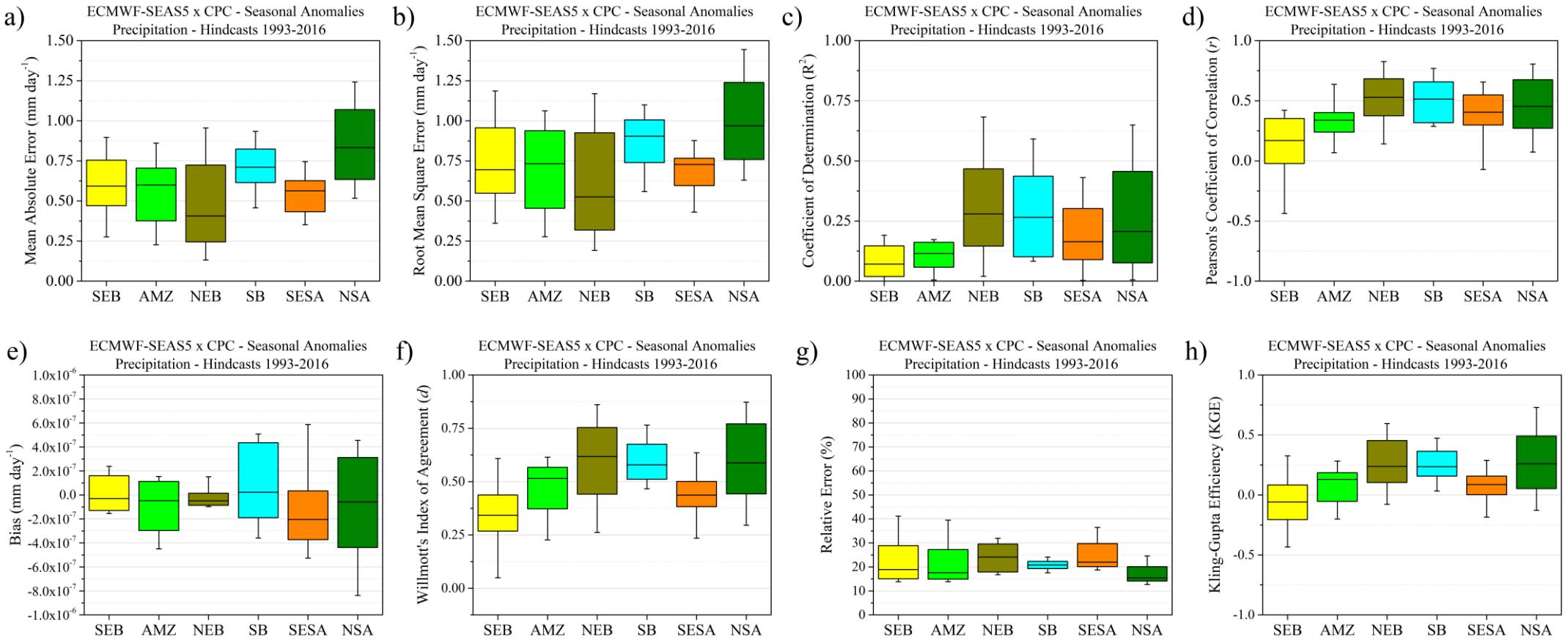

Figure 19 – Boxplots of statistical parameters derived from seasonal precipitation anomalies (JFM to DJF) of the ECMWF-SEAS5 hindcasts (1993-2016) for the SEB, AMZ, NEB, SB, SESA and NSA subdomains. Statistical parameters of relative error (g) and Kling-Gupta Efficiency are calculated from seasonal precipitation means.

Regarding the KGE index (GUPTA et al., 2009), when its value is equal to 1, it indicates perfect agreement between simulations and observations. Some authors report that KGE < 0 indicates that the mean of the observations provides better estimates than the simulations (CASTANEDA-GONZALEZ et al., 2018). Other studies show that KGE > 0.5 indicates good model simulations, while KGE < 0.5 is unsatisfactory and negative values are considered poor (TOWNER et al., 2019). In general, the authors state that positive values close to 1 indicate that the model can represent the observations (KNOBEN; FREER; WOODS, 2019).

The results for the KGE index show that, except for the SB subdomain, all the others have KGE < 0, with emphasis on NEB, SB and NSA, which have the best values (Figure 19h). The NSA subdomain provides the best KGE values, obtaining KGE = 0.73 and KGE = 0.60 for the JFM and DJF quarters, respectively. In the NEB subdomain, the best KGE results occur in the quarters of AMJ (KGE = 0.59) and MJJ (KGE = 0.56). For the SB, higher KGE values occur in the NDJ (KGE = 0.47) and OND (KGE = 0.43) quarters. Subdomains such as SESA and SEB show the worst results for this parameter. In SESA, the highest values obtained are for the DJF quarter, with KGE = 0.28, while the other seasons indicate KGE between -0.18 and 0.26. In SEB, the best result occurs in JJA (KGE = 0.32), and the other seasons show indexes between -0.65 and 0.12.

Different metrics make it possible to analyse subdomains more broadly. An example is the SB subdomain, which provides considerable MAE and RMSE and bias values (Figures 19a, 19b and 19e) but indicates satisfactory values of *r* (Figure 19d), *d* (Figure 19f) and relative error (Figure 19g). In contrast, the SESA presents small MAE and RMSE values (Figures 19a and 19b) but also unsatisfactory results for *d* (Figure 19f) and KGE (Figure 19h), as well as the largest relative errors (Figure 19g).

In general, it is observed that the NEB and NSA subdomains provide the best statistical results, which reiterates previous results indicating the good performance of ECMWF-SEAS5 in tropical regions which are strongly influenced by teleconnection effects from the Pacific and Atlantic oceans. In addition, the good results for the SB subdomain should also be mentioned, as illustrated in the parameters *r* (Figure 19d), *d* (Figure 19f) and relative error (Figure 19g).

6.7 Evaluation of Precipitation Forecasts

After evaluating the quality of ECMWF-SEAS5 hindcasts seasonal predictions for South America, it is worth analysing how the forecasts behave concerning the system's climatological model. Despite systematic overestimation (underestimation) errors in regions such as the North, Southeast and South (Northeast) Brazil, the hindcasts seasonal predictions showed that the model has a satisfactory performance in representing the South-American seasonal climate patterns.

Figure 20 indicates that the forecast prediction fields are similar to those obtained from the hindcasts. Note the characterization of the SACZ in the months from NDJ to JFM (Figures 20a and 20k) and the seasonal rainfall variability in Brazil's interior in the following months (Figure 20e-20j).

Bias maps indicate that some characteristics differ from those found for hindcasts. An example is the far north region of Brazil that has systematic underestimates of precipitation in hindcasts (Figures 6a-6c) but indicates wetter conditions in prognostic forecasts (Figures 20a-20c). Still, the most expressive dry bias in hindcasts in autumn and winter (Figures 6d-6f) is reduced in forecasts (Figures 20d-20f). This change in sign is evident in the Brazilian states of Roraima, Amapá, Pará and Maranhão. On the other hand, portions of Southeast Brazil, such as Minas Gerais and São Paulo, with dry bias in the spring and summer months (Figures 6a-6c, 6j-6l), have a wetter bias in forecasts (Figures 20a-20c, 20j-20l). In addition, regions in the country's centre with drier behaviour during the year (Figure 6d-6i) have their deviation corrected in the forecasts, indicating an adjusted forecast around 0.5 mm day^{-1}.

Seasonal forecasts from the ECMWF-SEAS5 hindcasts have systematic rainfall underestimation over Northeast Brazil. Such a feature is adjusted in forecasts. The very expressive dry biases in the MAM to JAS seasons (Figure 6c-6g) are slightly smoother in the prognostic forecasts (Figure 20c-20g). Howsoever, some portions of the region's interior and the east coast maintain their year-round dry bias, albeit to a lesser extent than the hindcasts. The ECMWF-SEAS5 forecasts reduce dry bias throughout the year for the SESA region, except in the AMJ and NDJ quarters. However, for the northern region of South America, the wet bias present in the hindcasts remains in the forecasts, indicating even wetter conditions as in the MAM and AMJ quarters (Figures 20c and 20d).

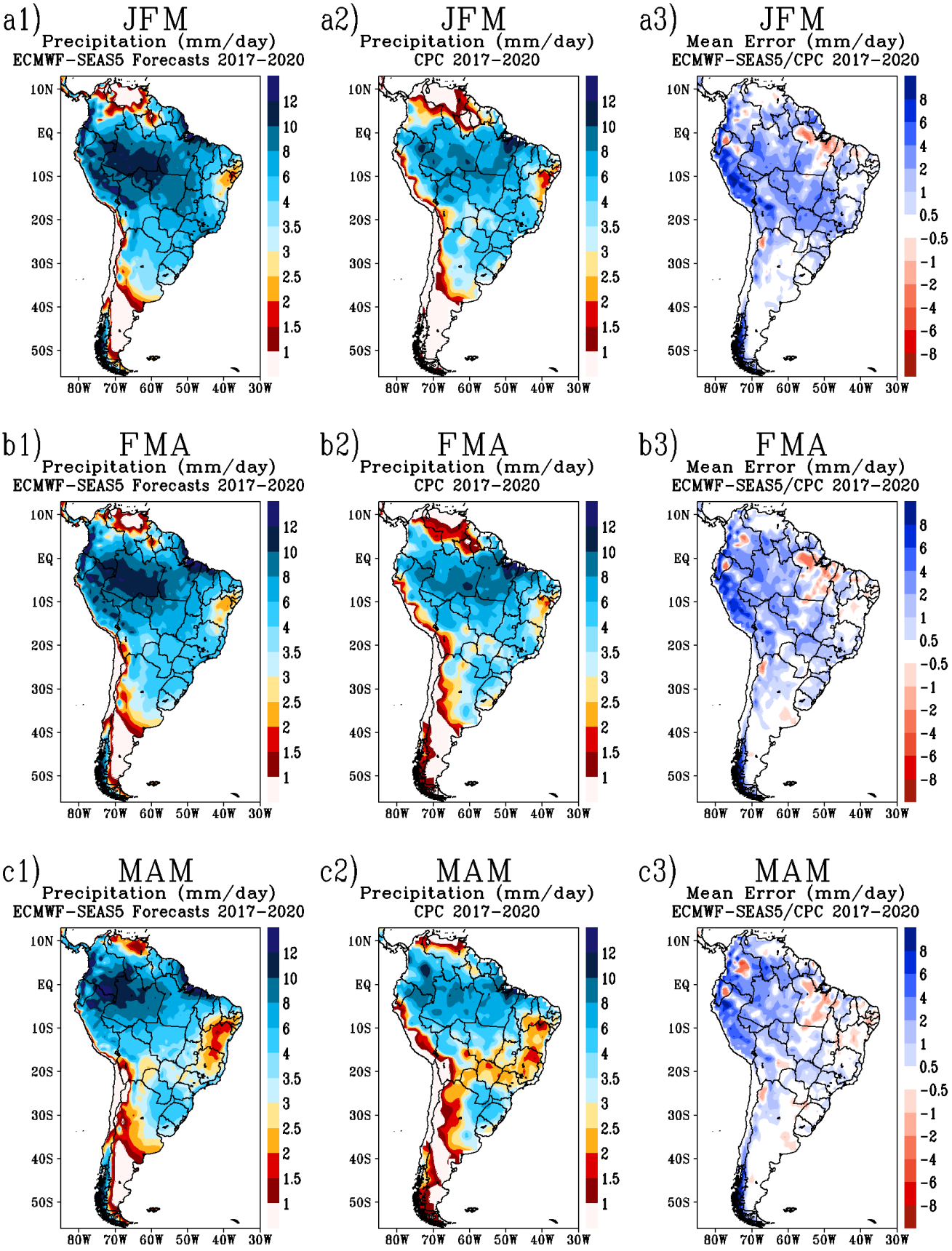

Figure 20 – Left column: seasonal mean precipitation (mm day^{-1}) derived from the ECMWF-SEAS5 forecasts, averaged for 2017-2020 and over the 51 ensemble members. Center column: CPC seasonal mean precipitation (mm day^{-1}) averaged over 2017-2020. Right column: seasonal precipitation mean errors (mm day^{-1}) obtained by the difference between ECMWF-SEAS5 and CPC and averaged over 2017-2020.

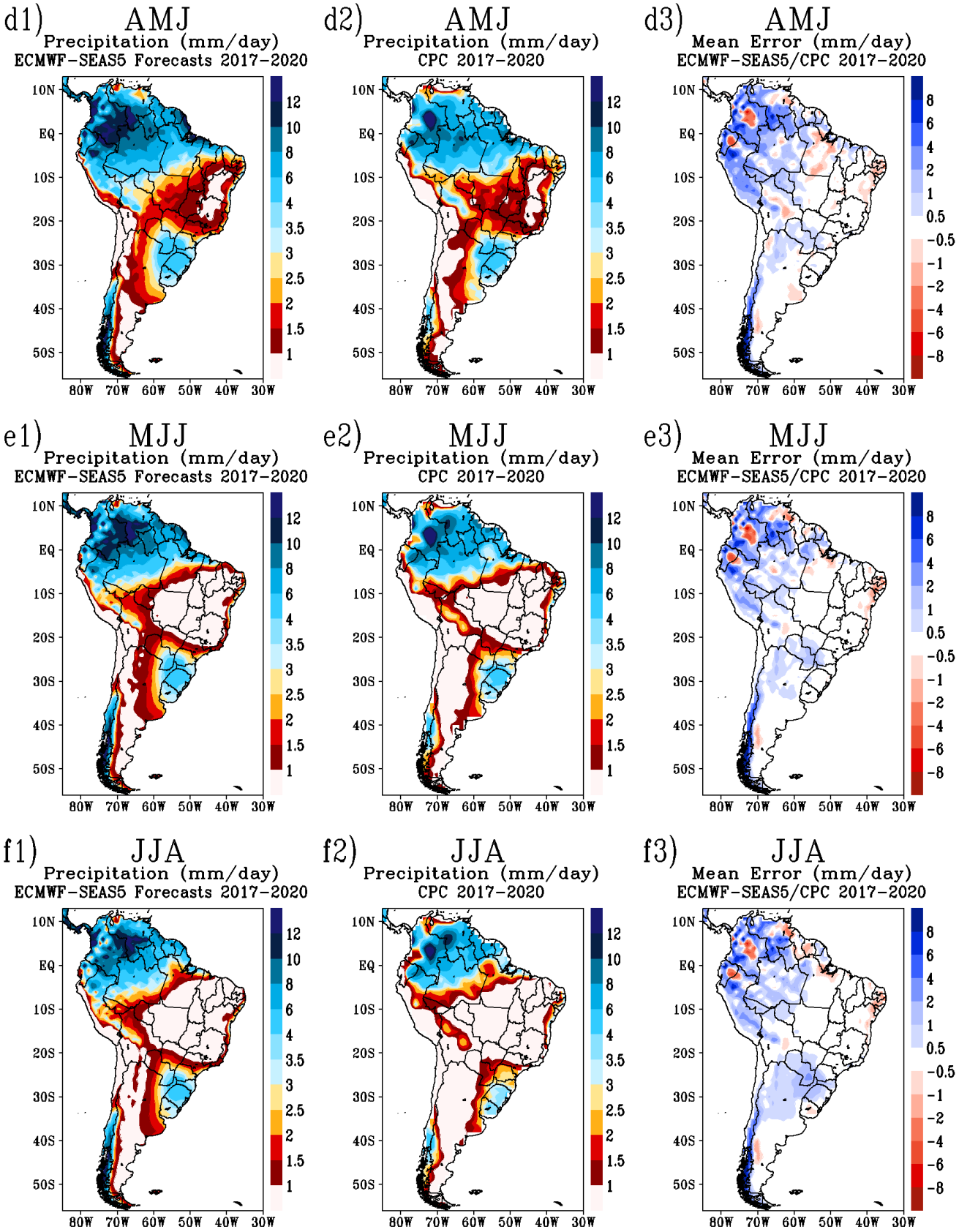

Figure 20 – continued.

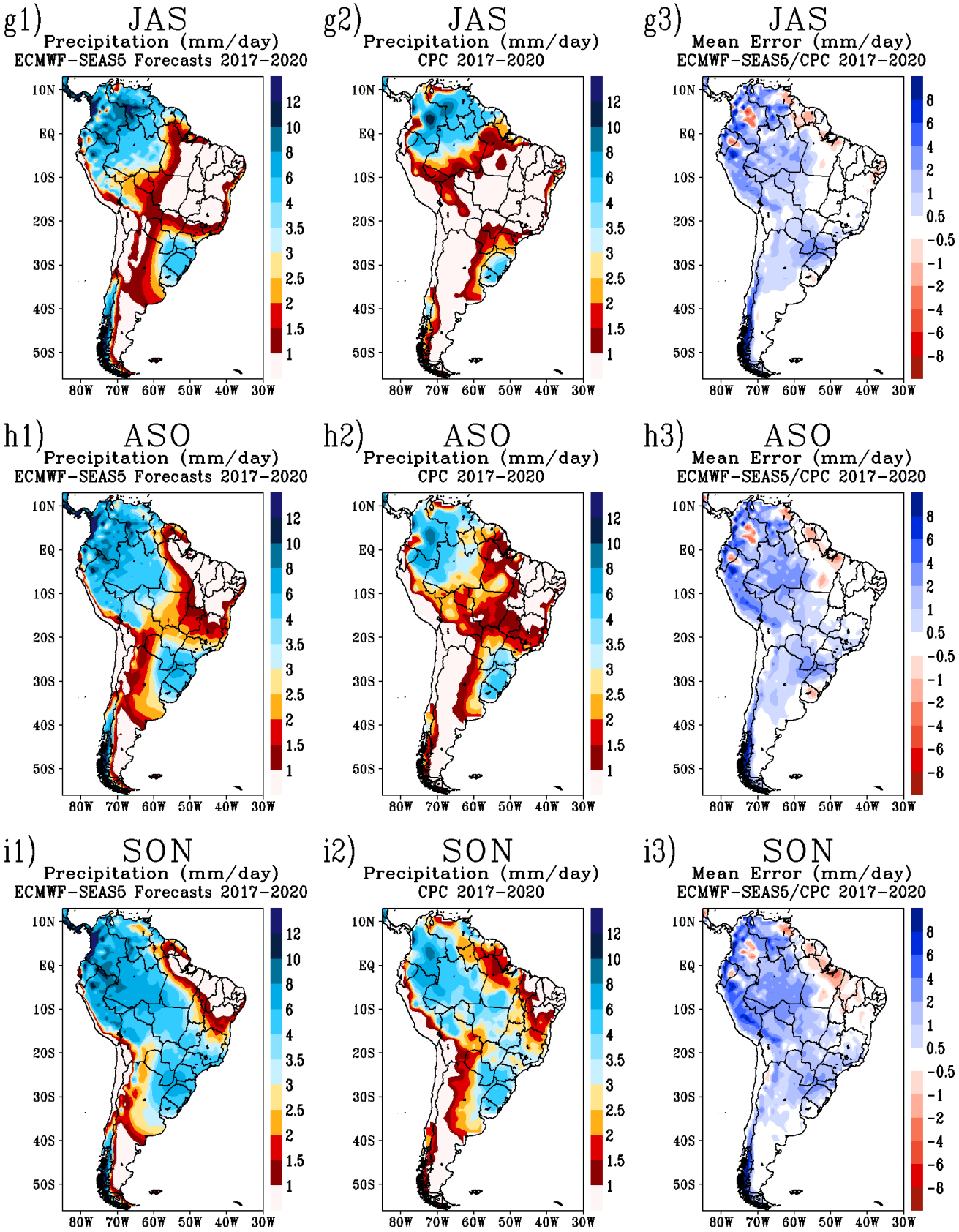

Figure 20 – continued.

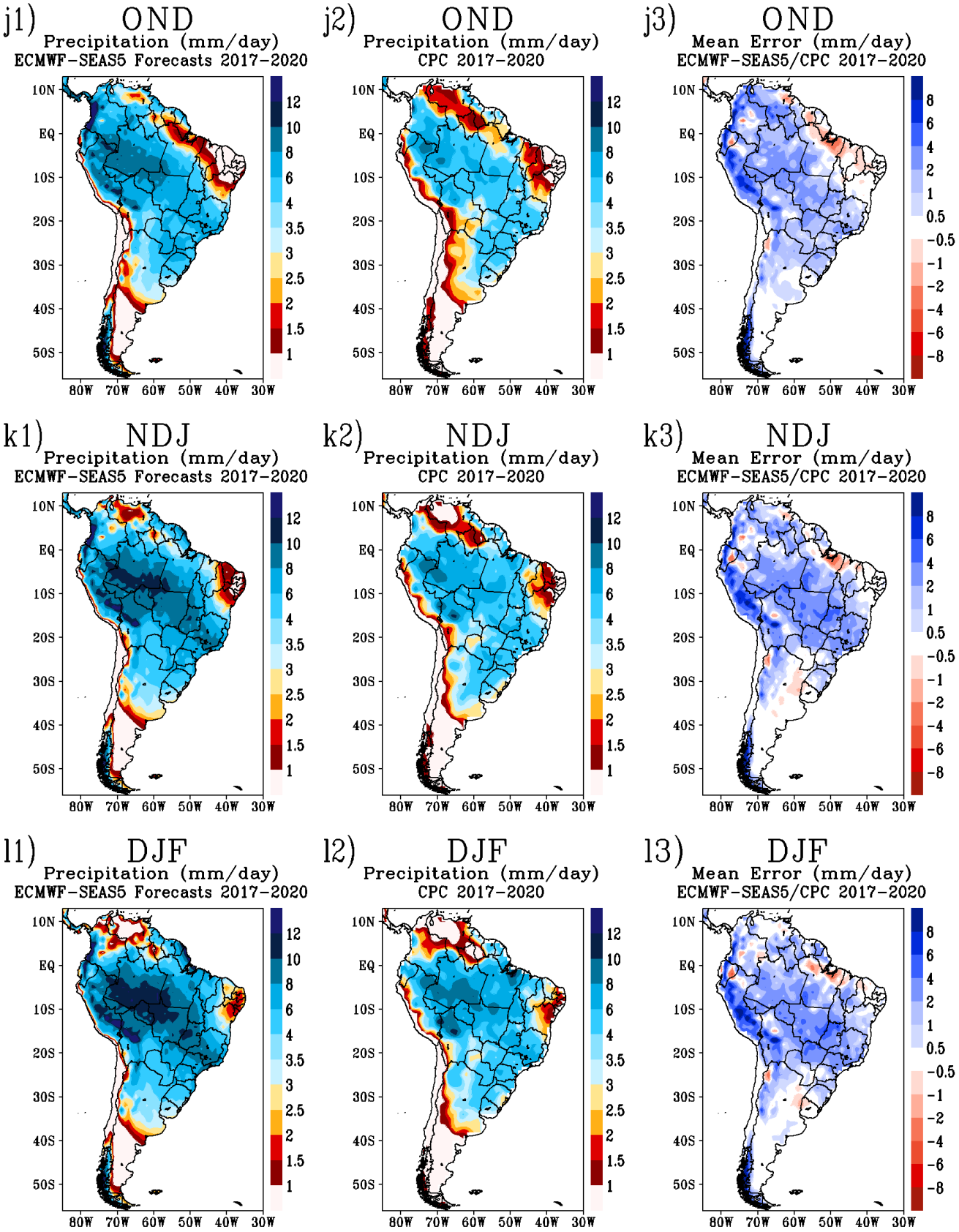

Figure 20 – continued.

It is essential to comparatively evaluate the performance of forecasts and hindcasts since the latter has a more extensive set of predictions, allowing the model to be evaluated using more robust statistics. On the other hand, the retrospective predictions present more idealized conditions than those of the prognostic forecasts since the hindcasts are better calibrated and submitted to complete data ingestion for the initial conditions (RISBEY et al., 2021).

In this context, attention should be paid to the possibility of hindcasts overestimating the forecasts, if they have an "artificial skill", or underestimating if there is variability in the model's skill sampled from different periods (DELSOLE; SHUKLA, 2009; GODDARD et al., 2013; RISBEY et al., 2021). Artificial skill can be understood as a skill of hindcasts that is not achievable by the forecast system due to some aspect of the idealized nature of hindcast predictions, such as the use of unavailable data for a situation of forecast comparison (RIBLEY et al., 2021).

For the ECMWF-SEAS5 seasonal precipitation forecasts, it can be inferred that the addition of twice as many members in the ensemble gives the opposite average results to those obtained in the hindcasts ensemble in several analysed regions. As a result, systematic rainfall underestimation errors in regions such as the North and Southeast of Brazil are reversed, while overestimates in the Amazon region and southern Brazil persist. Moreover, underestimates in portions of the Northeast also remain, although smoother.

Figure 21 illustrates results obtained from the statistical analysis for the ECMWF-SEAS5 forecasts. Although the AMZ subdomain presents MAE and RMSE magnitudes higher than hindcasts (Figures 19a and 19b), better R^2 and r are observed (Figures 21c and 21d). The best results of r and R^2 for AMZ refer to the months of ASO ($R^2 = 0.91$ and $r = 0.95$).

The months of ASO show the best R^2 and r for the SEB subdomain ($R^2 = 0.92$ and $r = 0.96$). NEB presents good R^2 and r for NDJ ($R^2 = 0.96$ and $r = 0.98$), while SB indicates better R^2 and r in the MAM trimester ($R^2 = 0.89$ and $r = 0.94$). AMZ and NSA have the highest magnitude errors (Figure 21a and 21e). This fact is reflected in their d index, which presents shallow values since it is sensitive to the errors' magnitude. In contrast, despite the notable variability, NEB and NSA indicate the best d values for MAM, with $d = 0.94$ and $d = 0.88$, respectively.

It should be mentioned that the analysed subdomains present a greater variability of results than those found in hindcasts. The R^2 index results show considerable variability for NEB

(with R^2 values from 0.01 to 0.96 in JJA and NDJ, respectively) and AMZ (from 0.01 to 0.91 in JFM and ASO, respectively). Similarly, the index *r* also gives a range of values for all regions, mainly SEB (from *r* = -0.55 in MAM and DJF to *r* = 0.96 in ASO) and NEB (from *r* = -0.12 in JJA to *r* = 0.96 in NDJ). The *d* index also indicates variability across regions, with SESA obtaining *d* = 0.58 and SB with *d* = 0.65 in MJJ.

The relative error obtained in forecasts is also greater for all regions, with the NEB indicating the best results, as its entire series of relative errors is below 28%. Regarding the KGE, there is greater variability and worse results for all regions. Highlight for NEB with KGE = 0.86 in ASO and SB with KGE = 0.74 in FMA. Giorgi and Mearns (1999) state that when observations drive climate models, these models can reproduce observed precipitation at the regional and seasonal scales with errors mainly in the range of 5 ± 5-30% for precipitation. The authors also stress that these errors should be evaluated given the uncertainties in observational data sets, which can be high, especially over remote areas or mountainous regions. In this case, it is worth noting that only the NEB obtained a series of relative errors below 30%.

Table 6 summarizes the average results calculated for all statistical parameters in each subdomain.

Table 6 – Average of the statistical parameters calculated for each subdomain's seasonal climate prediction of precipitation. Best (worst) results in blue (red).

	Mean Statistics Parameters 1993-2016 - Precipitation							
	Bias	**R^2**	***r***	**MAE**	**RMSE**	***d***	**RE**	**KGE**
SEB	0,0000000503	0,0152426	0,1234608	0,6091243	0,7859156	0,2975454	22,551762	0,8918813
AMZ	-0,0000001031	0,1033911	0,3215449	0,546149	0,7419804	0,4427837	22,809438	0,8300876
NEB	-0,0000000993	0,3169802	0,5630099	0,4555105	0,6641542	0,6607223	24,000949	0,8779604
SB	0,0000000967	0,3278719	0,572601	0,7140413	0,8959586	0,2361778	21,277709	0,4859299
SESA	0,0000011843	0,1478455	0,3845069	0,5465105	0,6970264	0,4610349	24,846341	0,2976489
NSA	0,0024940700	0,2058382	0,453694	0,8617831	1,0392562	0,5937017	17,023506	0,72096
	Mean Statistics Parameters 2017-2020 - Precipitation							
	Bias	**R^2**	***r***	**MAE**	**RMSE**	***d***	**RE**	**KGE**
SEB	0,60921649	0,001634	0,040423	0,7663843	1,0075352	0,4431906	36,92557	0,7443799
AMZ	0,826997321	0,0259626	0,1611291	0,8606725	1,0939827	0,4529601	43,135062	0,5890117
NEB	0,351766266	0,143797	0,3792057	0,4541163	0,6447355	0,5414132	19,952601	0,7798835
SB	0,355528263	0,1231964	0,3509934	0,8188964	1,0297821	0,4348464	30,402682	0,2349843
SESA	0,189270362	0,1336011	0,3655148	0,6085765	0,7669379	0,3952872	21,841404	0,2142119
NSA	1,366988933	0,2656062	0,51537	1,3740398	1,5535809	0,4934943	34,655973	0,6784748

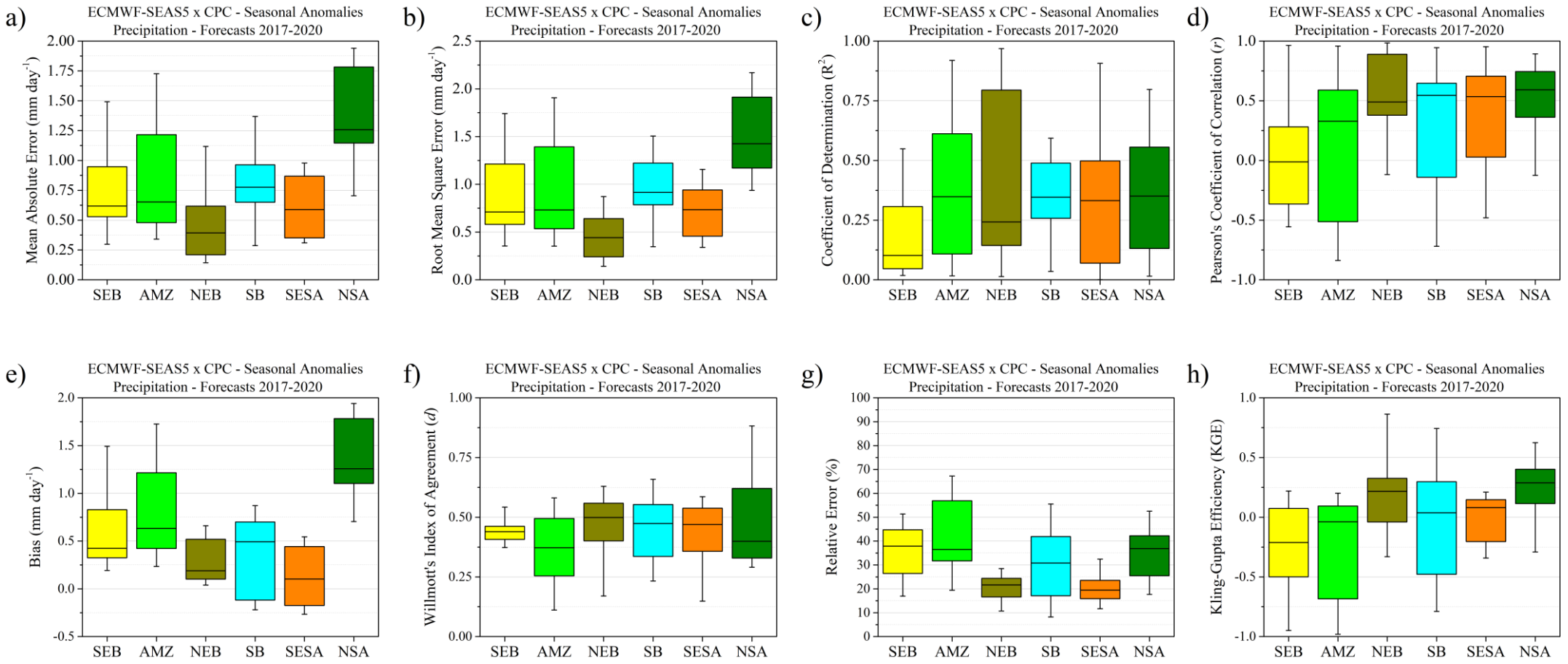

Figure 21 – Boxplots of statistical parameters derived from seasonal precipitation anomalies (JFM to DJF) of the ECMWF-SEAS5 forecasts (2017-2020) for the SEB, AMZ, NEB, SB, SESA and NSA subdomains. Statistical parameters of relative error (g) and Kling-Gupta Efficiency (h) are calculated from seasonal precipitation means.

6.7 Seasonal Means and Errors of Temperature

This section evaluates the seasonal climate predictions of 2 m air temperature obtained by ECMWF-SEAS5 and the CPC analyses. Figure 22 indicates that ECMWF-SEAS5 forecasts have acceptable performance in representing the seasonal temperature variation in the South American continent. However, bias maps show that ECMWF-SEAS5 underestimates temperatures across most of SA throughout the year. Considering Brazil, the model underestimates by up to 3 ºC in portions of the Amazon, the country's northern region, and northern Minas Gerais. In Southeast and South Brazil, the cold bias underestimates by up to 4 °C during spring (Figures 22h-22k). In the summer months, underestimates persist, but the cold bias is reduced, indicating negative deviations of up to 3 ºC in Southeast and South Brazil.

In the autumn and winter seasons, ECMWF-SEAS5 reduces negative deviations, indicating biases of -1 to 1 ºC in the Southeast, South Brazil and Bahia (Figures 22c-22e). In contrast, the North region presents a cold bias throughout the year. Portions of the North and Southeast regions with the highest precipitation overestimates coincide with the temperature underestimates in these sectors, a thermodynamically expected feature, since precipitation energy is used for water evaporation instead of heating the atmosphere via sensible heat (REBOITA et al., 2018).

The Northeast region presents the slightest negative deviations. This feature is evident in the autumn and winter seasons (Figures 22d-22f), showing an overestimate of up to 1°C in most northeastern regions. Similarly, the SESA and Argentina point to overestimates of up to 3 °C in the months from FMA to MJJ (Figures 22b-22e). However, the model’s cold bias also covers these regions from the JJA, indicating underestimates of up to 5 °C in western and southern Argentina (Figures 22f-22l).

Other studies have also found a tendency for different global models to underestimate air temperature prediction in SA. Weigel et al. (2008) evaluated the ECMWF Monthly Weather Forecast (ECMWF-MOFC) and found that the model’s systematic cold bias was present across the continent, with larger negative deviations in northern SA and Northeast Brazil. Manzanas et al. (2013) found that ECMWF-SEAS4 underestimates maximum temperatures across most of the continent.

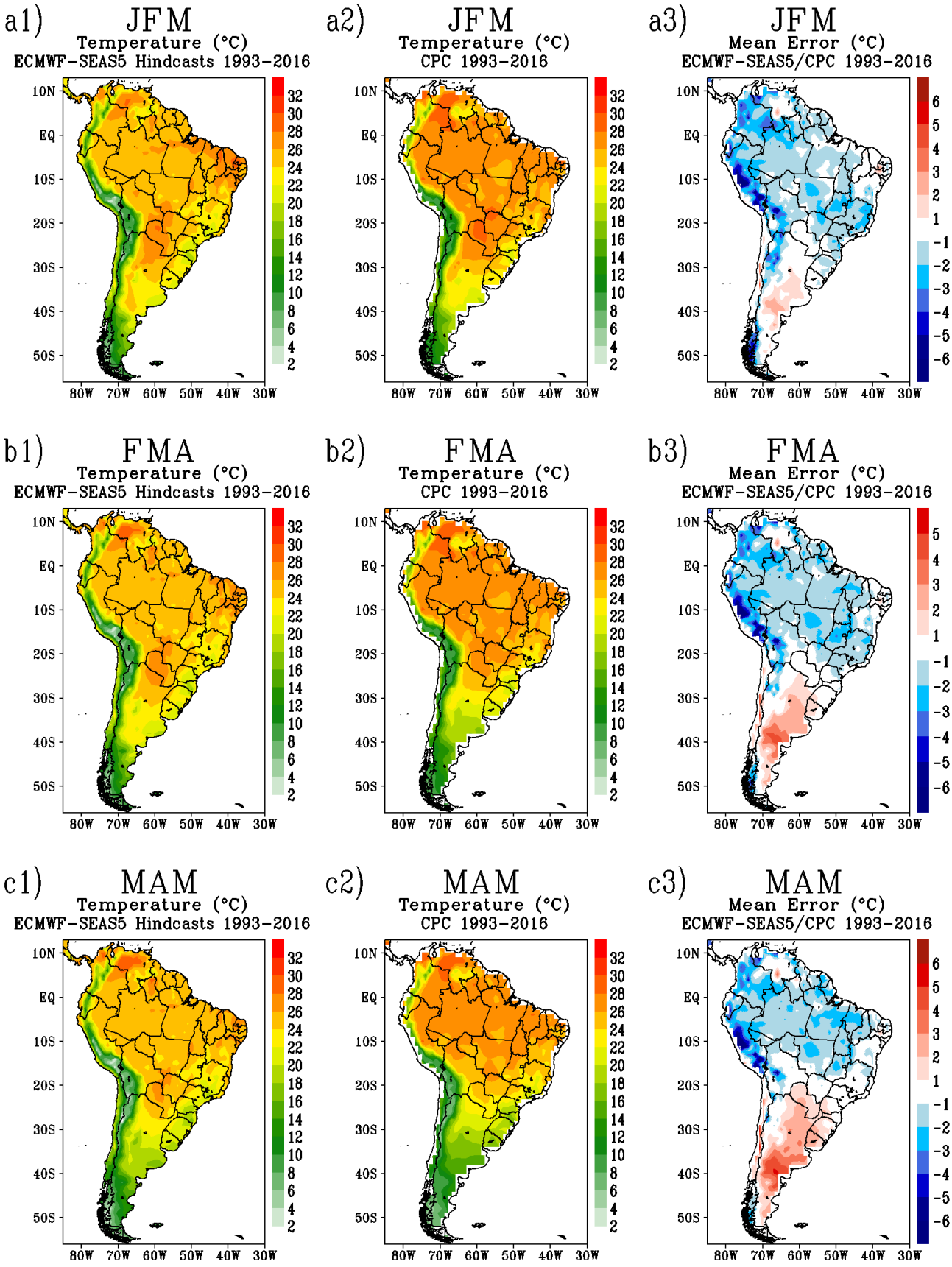

Figure 22 – Left column: seasonal mean 2 m temperature (ºC) derived from the ECMWF-SEAS5 hindcasts, averaged for 1993-2016 and over the 25 ensemble members. Center column: CPC seasonal mean surface temperature (ºC) averaged over 1993-2016. Right column: seasonal temperature mean errors (ºC) obtained by the difference between ECMWF-SEAS5 and CPC and averaged over 1993-2016.

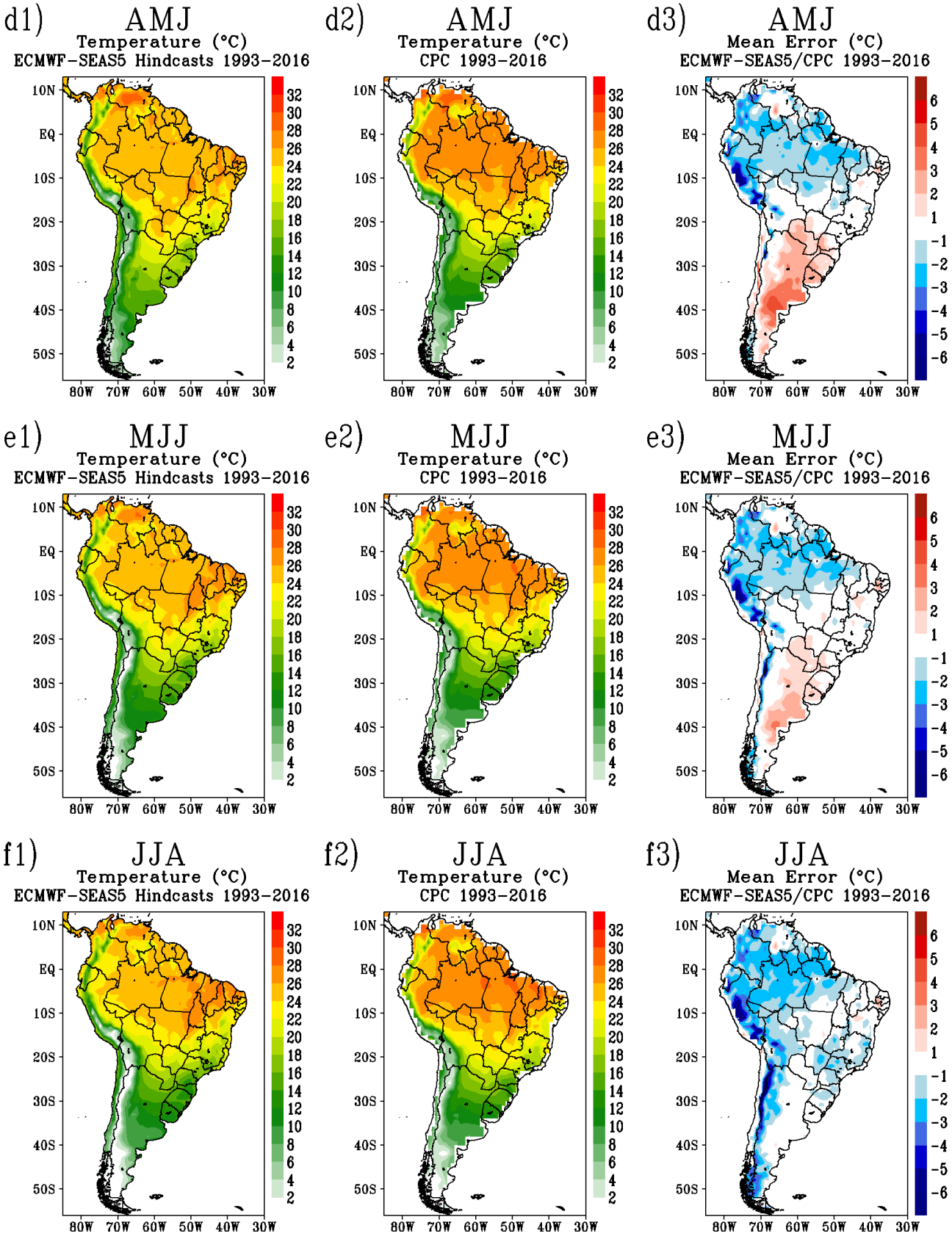

Figure 22 – continued.

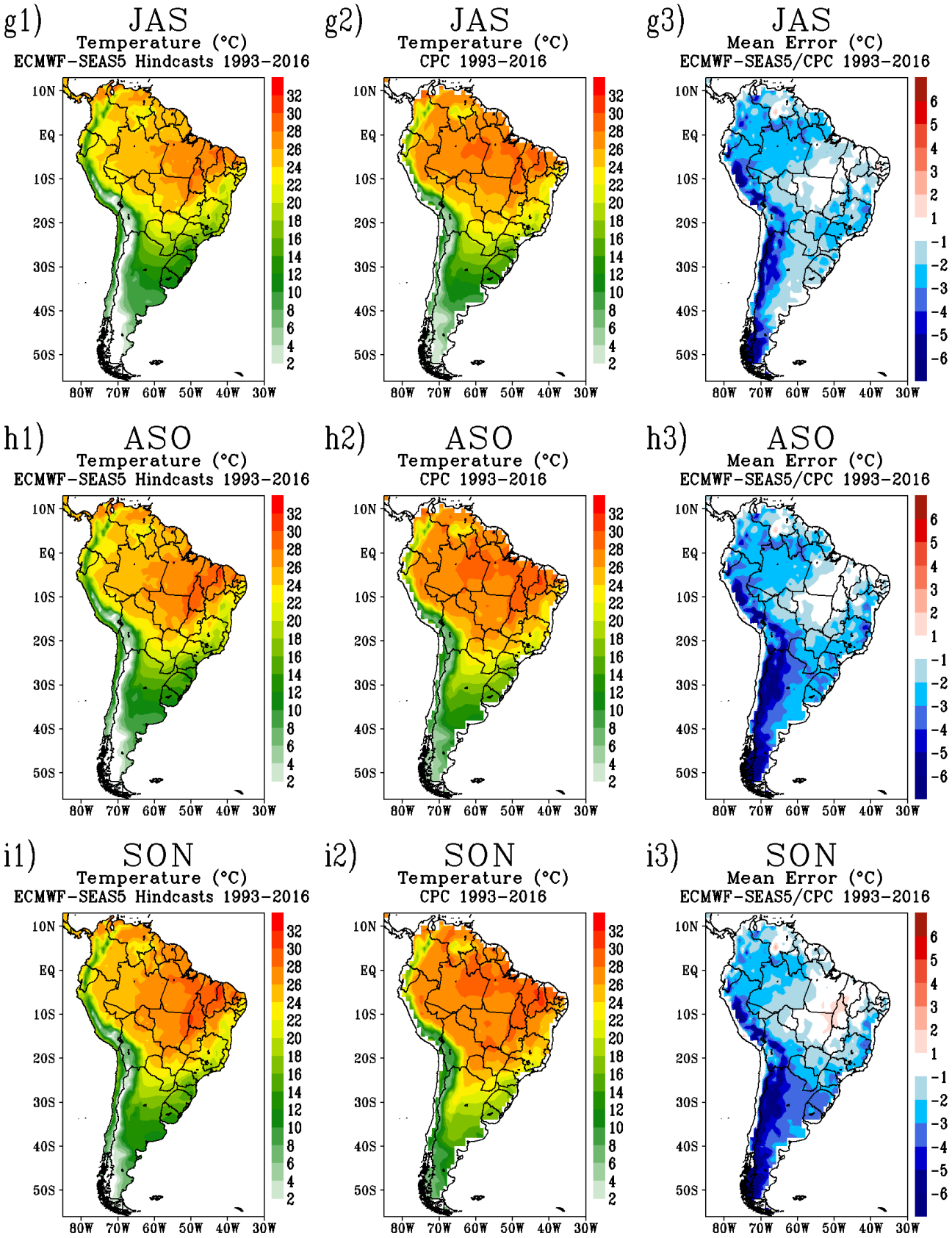

Figure 22 – continued.

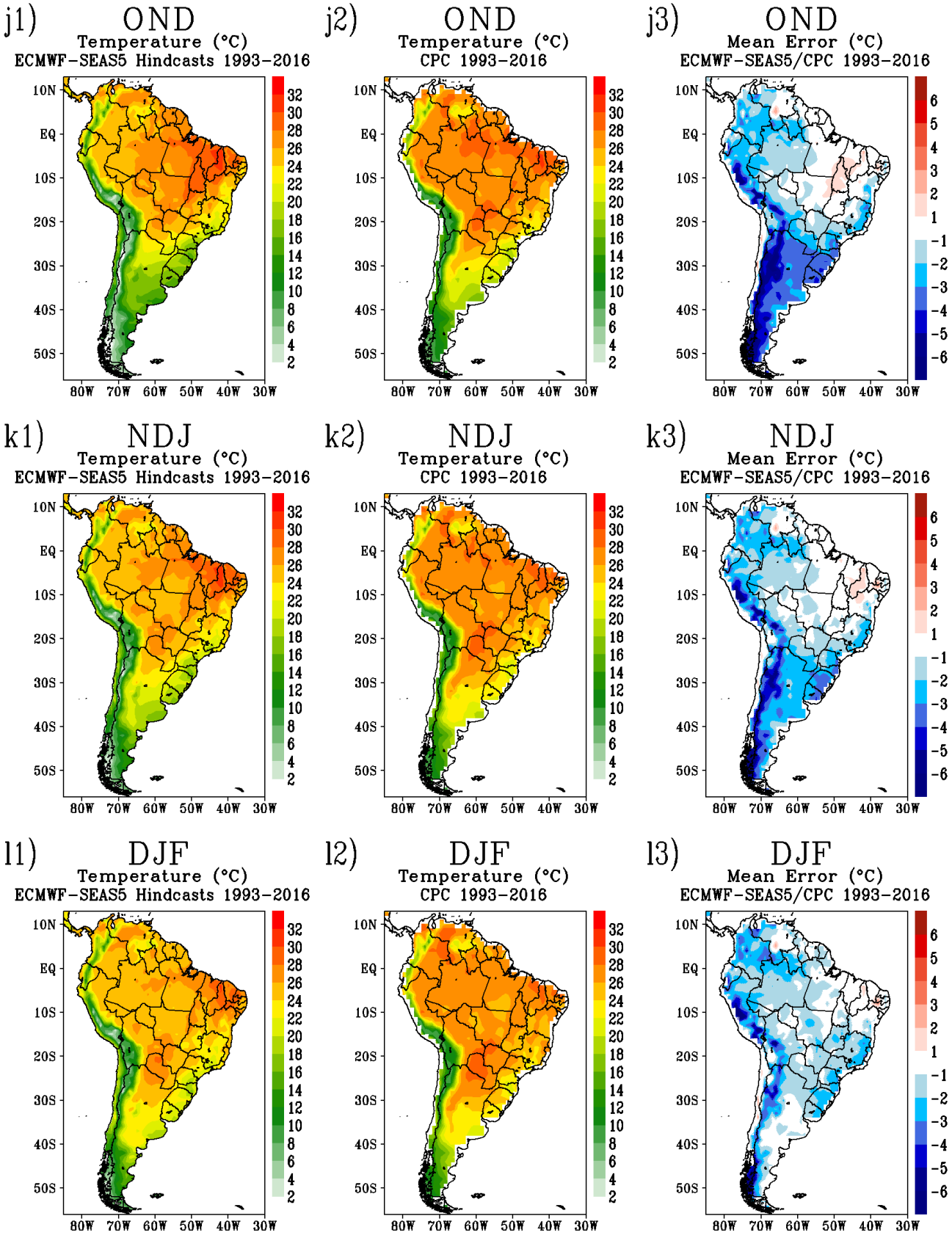

Figure 22 – continued.

Osman and Vera (2016) investigated the performance of nine models from the Climate Historical Forecast Project (CHFP) and concluded that models accentuate the cold bias in periods of both ENSO phases. Reboita et al. (2018) found the systematic cold bias of CFSv2 throughout Brazil, and this error persisted and increased with the RegCM simulations driven by the global model. Kim et al. (2012) analysed the ECMWF-SEAS4 and CFSv2 hindcasts and observed a systematic cold bias of both models in SA. Chou et al. (2020) found a systematic cold bias of the Eta regional model over the entire South American continent. However, the authors observed a warm bias in the SESA region between MAM and MJJ, which agrees with the present results.

6.8 Seasonal Temperature Skill Score

Following the analysis in section 6.2, the ECMWF-SEAS5 skill score results for 2 m air temperature are evaluated. In this case, temporal correlations between temperature anomalies predicted by ECMWF-SEAS5 and those obtained by CPC are calculated. In addition, as with precipitation, temporal correlations are calculated for seasonal predictions for quarters composed of lead-times 1, 2 and 3-months.

Figure 23 illustrates the skill score results for the air temperature, and it is observed that many regions with high precipitation skill score values also result in good values for temperature prediction. In the summer months, ECMWF-SEAS5 can predict the temperature in regions such as northern Brazil and some northeastern states such as Tocantins, Maranhão and Piauí (Figures 23a-23l), whose correlation values are above 0.7. Gubler et al. (2020) also found high correlations in these regions, associating the model's performance with the strong influence of ENSO in these sectors. Considering that Pacific SST influences such regions, temperatures are expected to rise (decrease) in El Niño (La Niña). The best performance in these sectors persists until winter, when lower values are observed from MJJ to SON. From SON onwards (Figure 23i), the best correlations are located in the tropical region of the continent, with the best values obtained in the north of Northeast Brazil in the months from DJF to MAM (Figures 23a-23c, 23l).

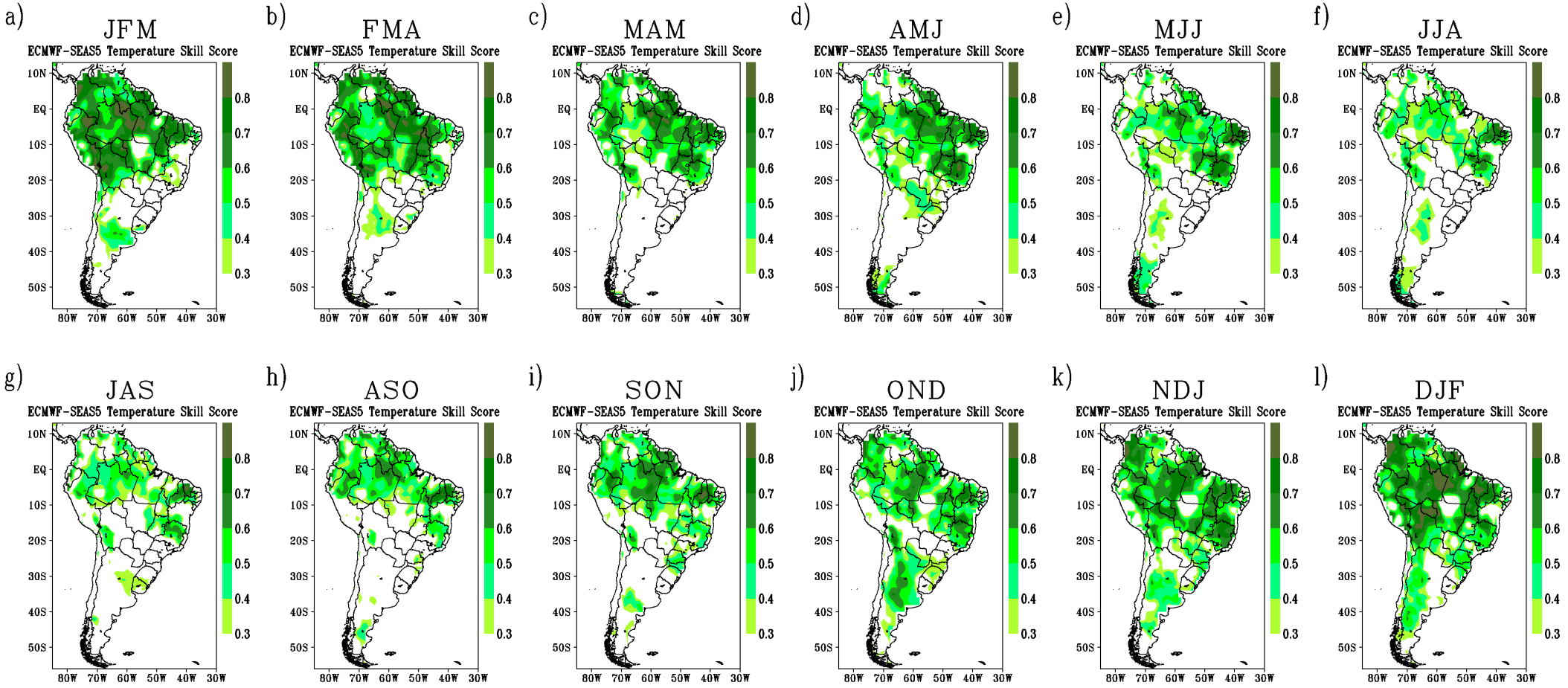

Figure 23 – Seasonal temperature anomaly skill scores for the ECMWF-SEAS5 hindcasts. Trimesters correspond to reforecasts from the 1–3-month lead times. Only scores equal to or above 0.3 are shown. The score is nondimensional.

The Northeast Brazil region provides good skill score results practically throughout the year. An exception occurs for the state of Bahia, which indicates good values only for OND and NDJ (Figures 23j and 23k). The excellent performance of ECMWF-SEAS5 in this sector of Brazil was also observed by Gubler et al. (2020), indicating that ECMWF-SEAS5 performance does not derive only from the strong influence of the Pacific on the region but also from other modes of variability such as the Tropical Atlantic Dipole (MOURA; SHUKLA, 1981; SHIMIZU; ANOCHI; KAYANO, 2021; UVO et al., 1998).

Unlike the precipitation skill score results, in southern Brazil, the model has an unsatisfactory performance almost throughout the year. However, exceptions occur in the quarters from SON to DJF (Figures 23i-23l), which illustrate the model's marginal performance, with skill scores of up to 0.5 in Paraná, Santa Catarina, and the east of Rio Grande do Sul.

The SESA region indicates skill score values above 0.4 in the spring and summer seasons (Figures 23j-23l, 23a) and no appreciable performance for the rest of the year. Although the skill score for precipitation has indicated some ECMWF-SEAS5 performance in the region from OND to DJF (Figures 7j-7l), it is observed that the temperature correlations cover more broad areas than those found. Furthermore, moderate correlations of up to 0.5 are noted in the far south of Argentina in the months from AMJ to JJA (Figures 23d-23f).

As obtained for precipitation, the skill scores for the ECMWF-SEAS5 seasonal temperature forecasts indicate that the best performances occur in regions strongly influenced by ENSO. Furthermore, regions such as SESA also presented a moderate performance in temperature prediction, a result obtained by Weisheimer and Palmer (2014), who found a moderate performance of ECMWF-SEAS4 in the region in the DJF months.

6.9 Regional Temperature Anomalies

Spatial temperature anomalies were calculated and compared to those obtained by CPC for the same areas.

For Southeastern Brazil (SEB; Figure 24), ECMWF-SEAS5 underestimates temperature practically the entire year. In the spring and summer months (Figures 24d-24f and 24a), the errors

reach -1.5°C, whilst in the autumn and winter (Figures 24b and 24c), the model indicates mixed signs of overestimation and underestimation, failing to capture the main negative deviations, as in MJJ of 1999 and 2004.

In the AMZ subdomain (Figure 25), ECMWF-SEAS5 underestimates the temperature throughout the year, with mean negative deviations of up to 1.5 ºC in the summer and spring months (Figures 25a and 25f). In transition seasons (Figures 25b-25d), the deviations decrease in magnitude, and ECMWF-SEAS5 reasonably simulates the interannual temperature cycle, except from 2008 onwards when deviations become more expressive. However, it is noteworthy that the model captured some maximums, such as in OND and NDJ from 1997, an aspect associated with the strong El Niño that occurred in this period (OLIVEIRA; SATYAMURTY, 1998). Furthermore, it is observed that from 2017 onwards, the deviations become slighter.

In Northeastern Brazil (NEB; Figure 26), ECMWF-SEAS5 underestimates the temperature throughout the year, but their deviations are minor than those of the two previous subdomains. The model's ability to simulate the annual variation of temperature anomalies in the spring and summer months is remarkable (Figures 26a, 26e and 26f). The model also represents the interannual cycle with dexterity in the transition seasons, as evident in the quarters from AMJ to JJA (Figures 26b and 26c). ECMWF-SEAS5 presents larger deviations from JAS to SON (Figures 26d and 26e) but maintains its good performance in simulating the interannual variation. It is also noteworthy that the model captures the most prominent observed anomalies, as those that occurred in 1997.

For Southern Brazil (SB; Figure 27), ECMWF-SEAS5 shows mixed signs of underestimation and overestimation. While in the FMA to MJJ months (Figures 27b and 27c), the model tends to overestimate the temperature by up to 1.5 °C, it underestimates the variable in the JJA to JFM with the same magnitude, reaching larger deviations in the spring and summer months (Figures 27e and 27f). Briefly, it is noted that ECMWF-SEAS5 does not reasonably simulate the interannual variability of temperature, except in MAM and AMJ (Figure 27b).

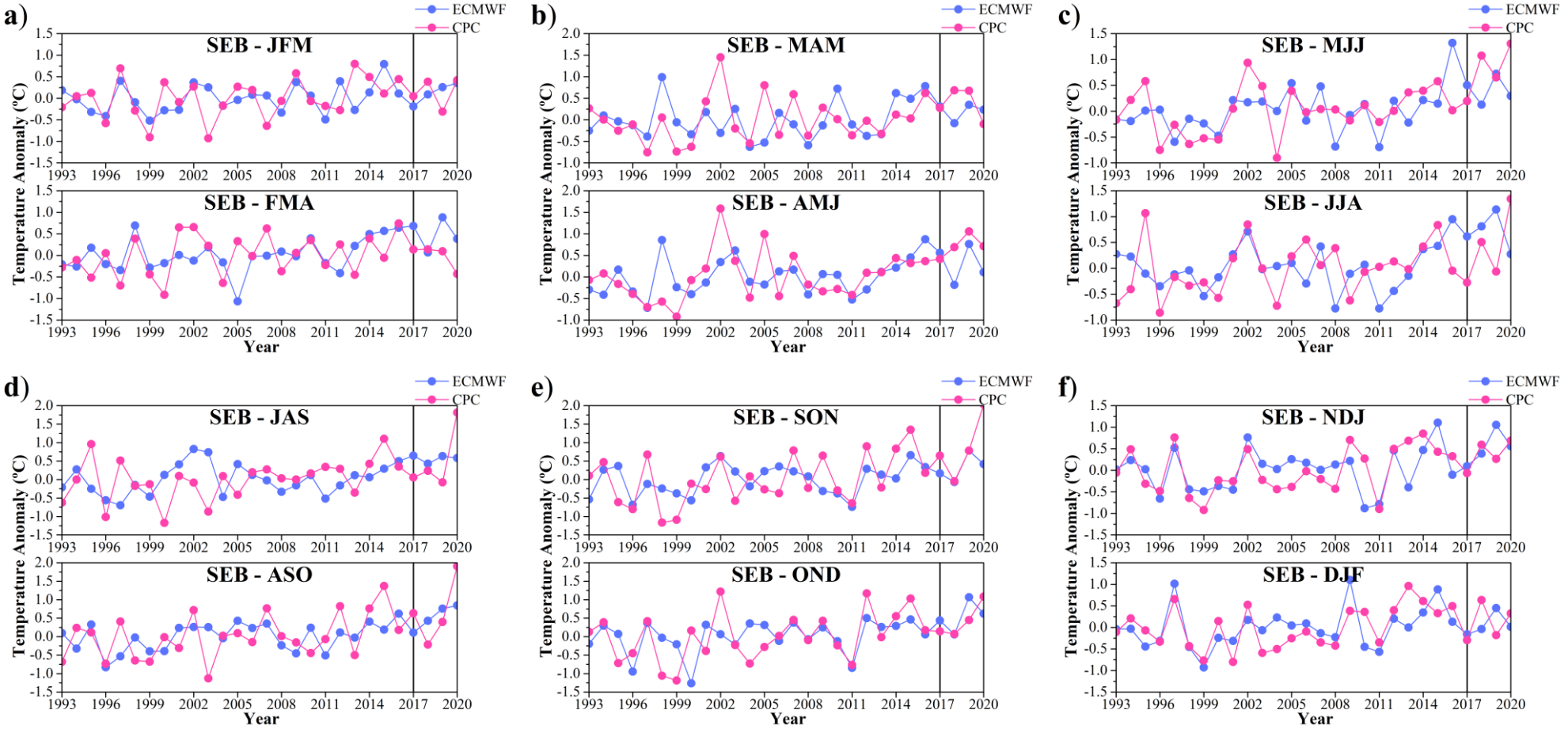

Figure 24 – Average seasonal temperature anomalies (°C) in the Southeastern Brazil (SB) subdomain. The vertical black line indicates the end of retransmissions and the beginning of predictions.

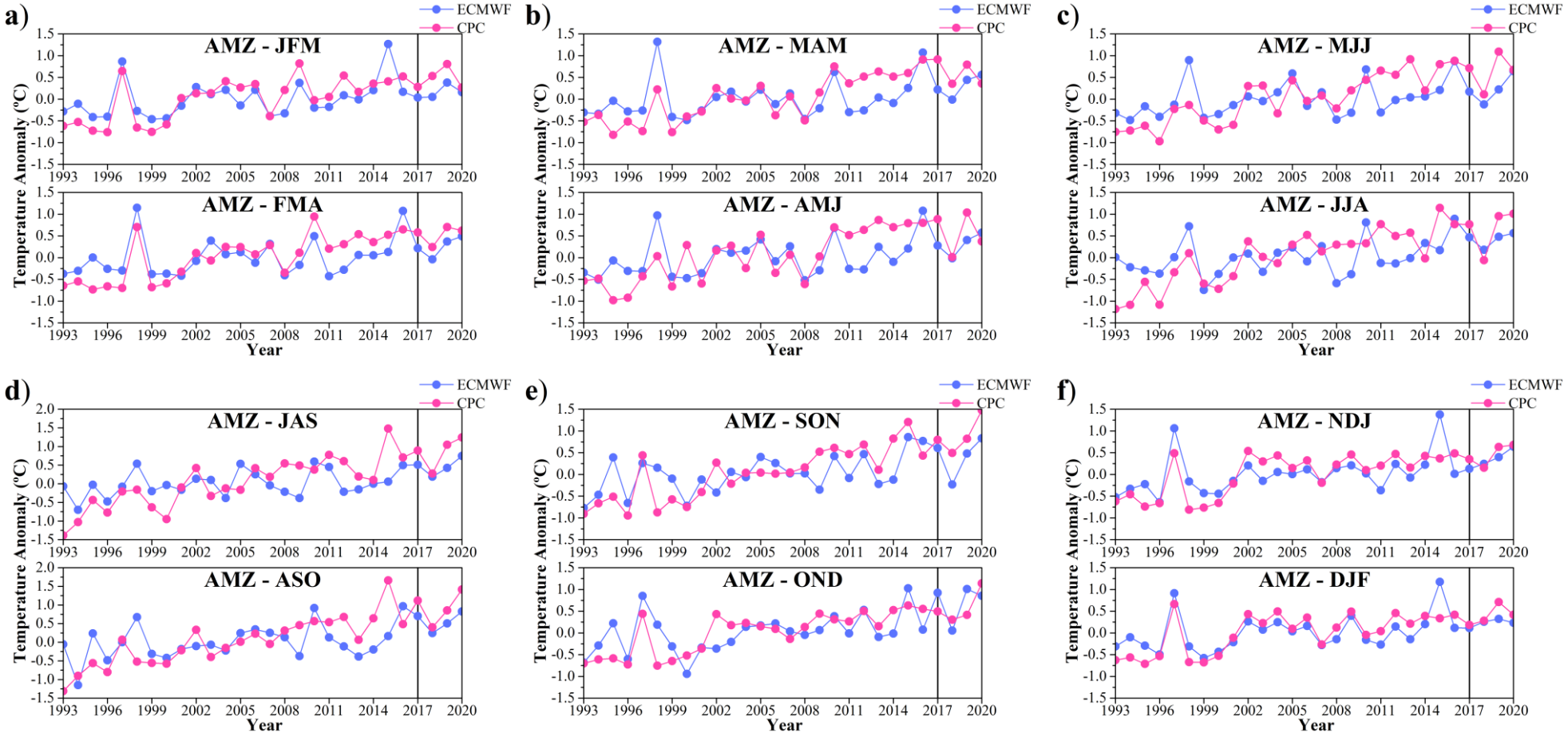

Figure 25 – Similar to Figure 24, except for the Amazon subdomain (AMZ).

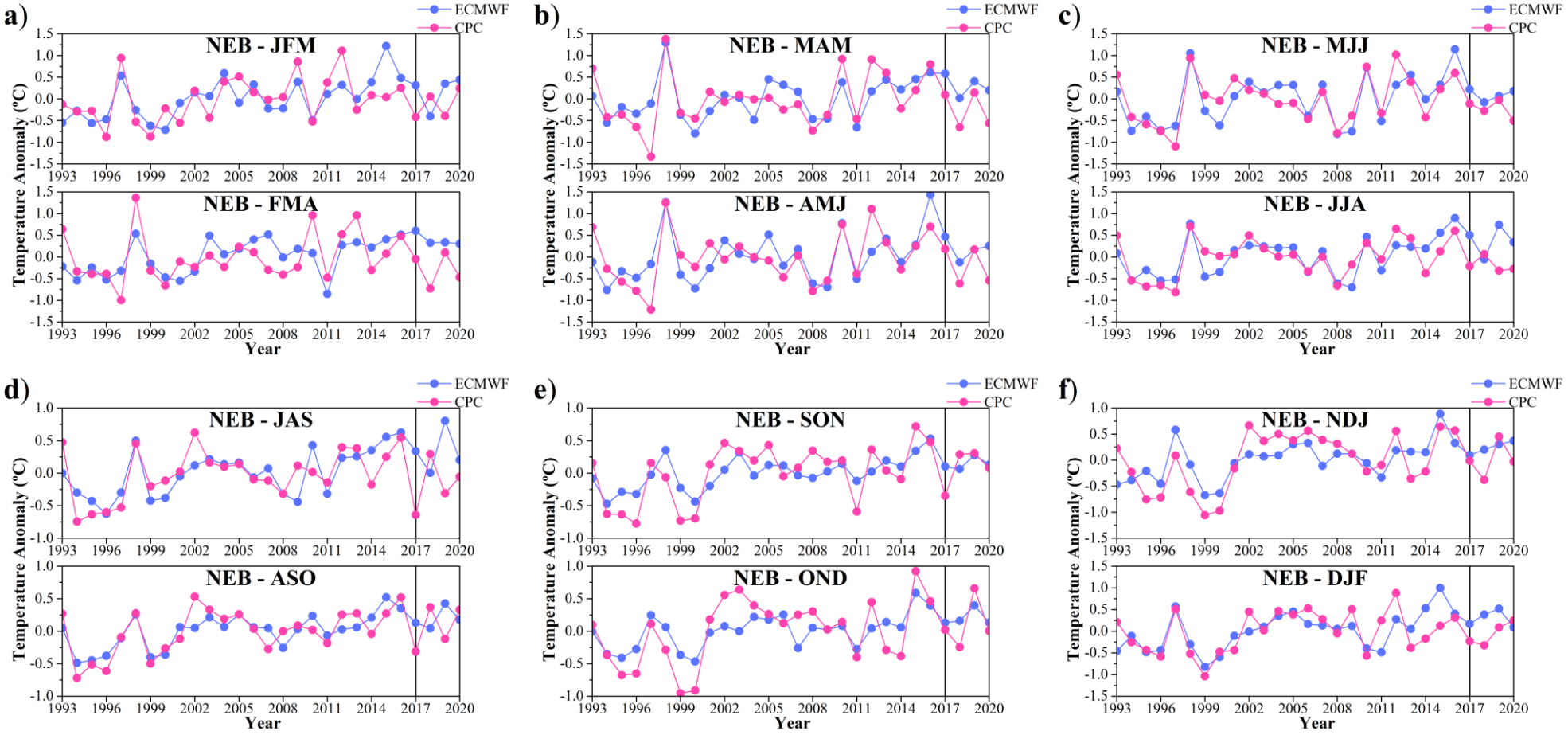

Figure 26 – Similar to Figure 24, except for the Northeast Brazil subdomain (NEB).

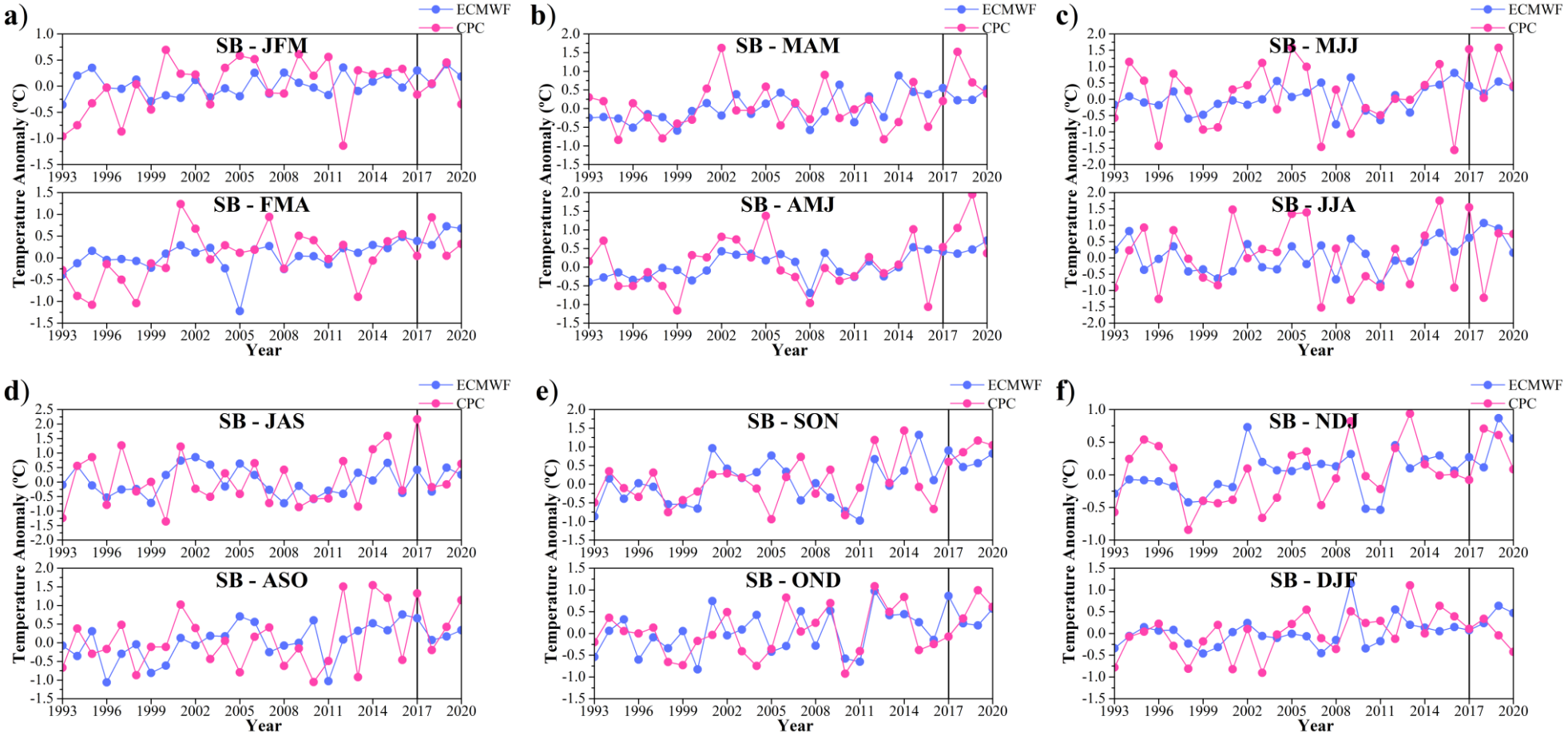

Figure 27 – Similar to Figure 24, except for the Southern Brazil subdomain (SB).

In the SESA subdomain (Figure 28), ECMWF-SEAS5 predictions overestimate the temperature from JFM to JJA (Figures 28a-28c) and underestimate it from JAS to DJF (Figures 28d-28f). In addition, as in the SB subdomain, the model fails to simulate the interannual variability of temperature anomalies for most of the year, except from OND to DJF (Figures 28e and 28f), when the simulated series indicate some correspondence with the values obtained by the CPC.

In Northern South America (NSA; Figure 29), ECMWF-SEAS5 forecasts underestimate the temperature throughout the year. Despite the deviations, it is noted that ECMWF-SEAS5 reasonably reproduces the temperature's interannual variability throughout most of the year. As in the other subdomains, there is a better quality of forecasts from 2017 onwards, indicating that the climatological mean of ECMWF-SEAS5 hindcasts is coherent with that obtained by the CPC.

6.10 Statistical Parameters

Statistical parameters were calculated for the selected subdomains. In Annexe, tables with all the individual parameter values for each subdomain and quarter are presented.

Figures 30a, 30b and 30e show that the SB and SESA subdomains have the largest errors in temperature predictions, which confirms the results described early. The NEB and NSA subdomains have the smallest errors, reflected in better values of R^2 and r. In AMZ, the best coefficients occur in DJF ($R^2 = 0.57$ and $r = 0.76$) and in NEB during MJJ ($R^2 = 0.66$ and $r = 0.81$). Although the NSA subdomain has considerable MAE and RMSE (Figures 30a and 30b), its relative error is small (Figure 30g), associated with the high totals of rainfall in the tropical region. Thus, the good correlation results for this region are justified, with its best coefficient of $r = 0.84$ in JFM.

Considering the d index, NEB and NSA indicate the best results, with NEB obtaining $d = 0.89$ in MJJ and NSA with $d = 0.91$ in JFM. Similarly, the best KGE results correspond to these subdomains and AMZ, giving KGE = 0.83 in JFM for NSA, KGE = 0.80 in MJJ for NEB, and KGE = 0.73 in DJF for AMZ.

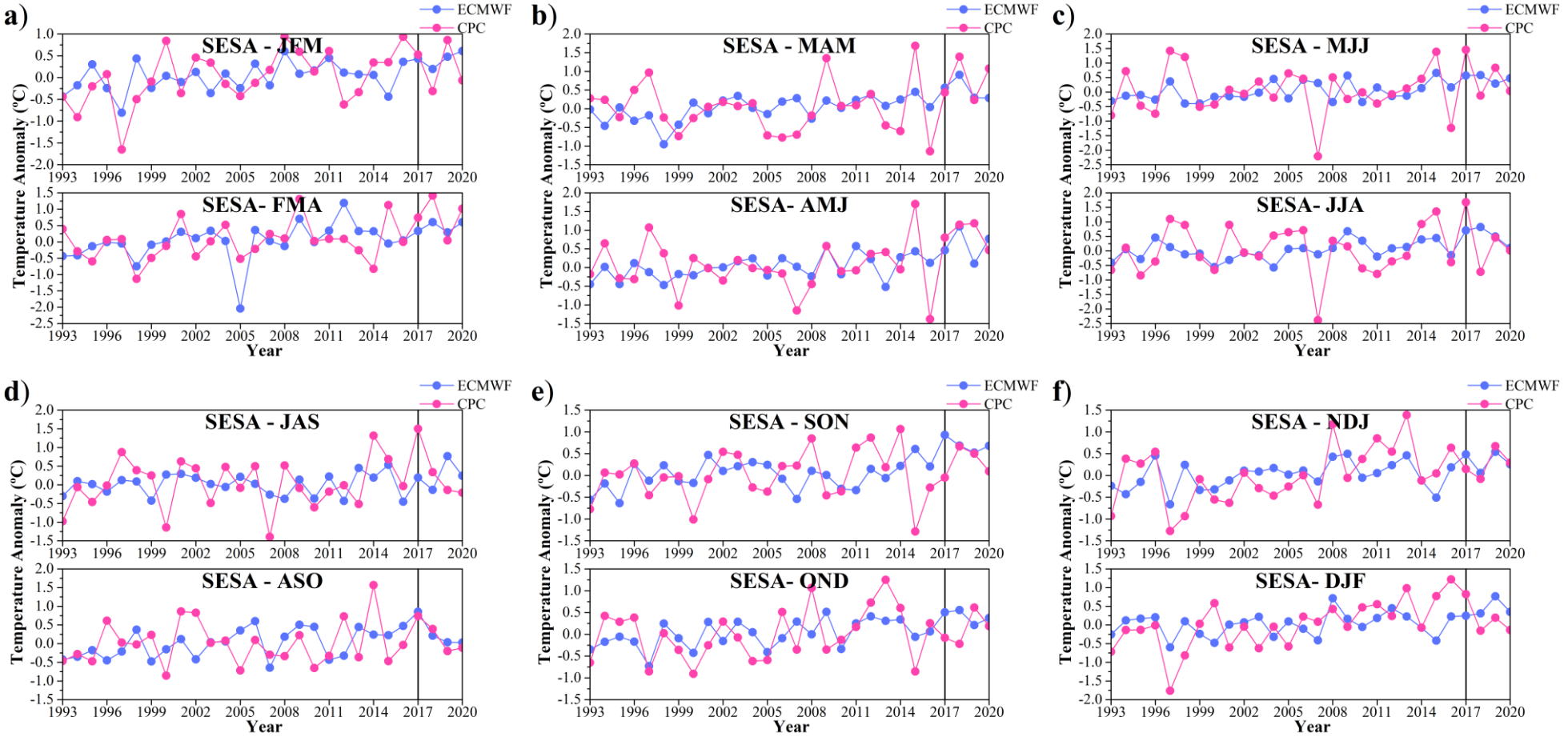

Figure 28 – Average seasonal temperature anomalies (°C) in the Southeastern South America subdomain (SESA). The vertical black line indicates the end of hindcasts and the start of forecasts.

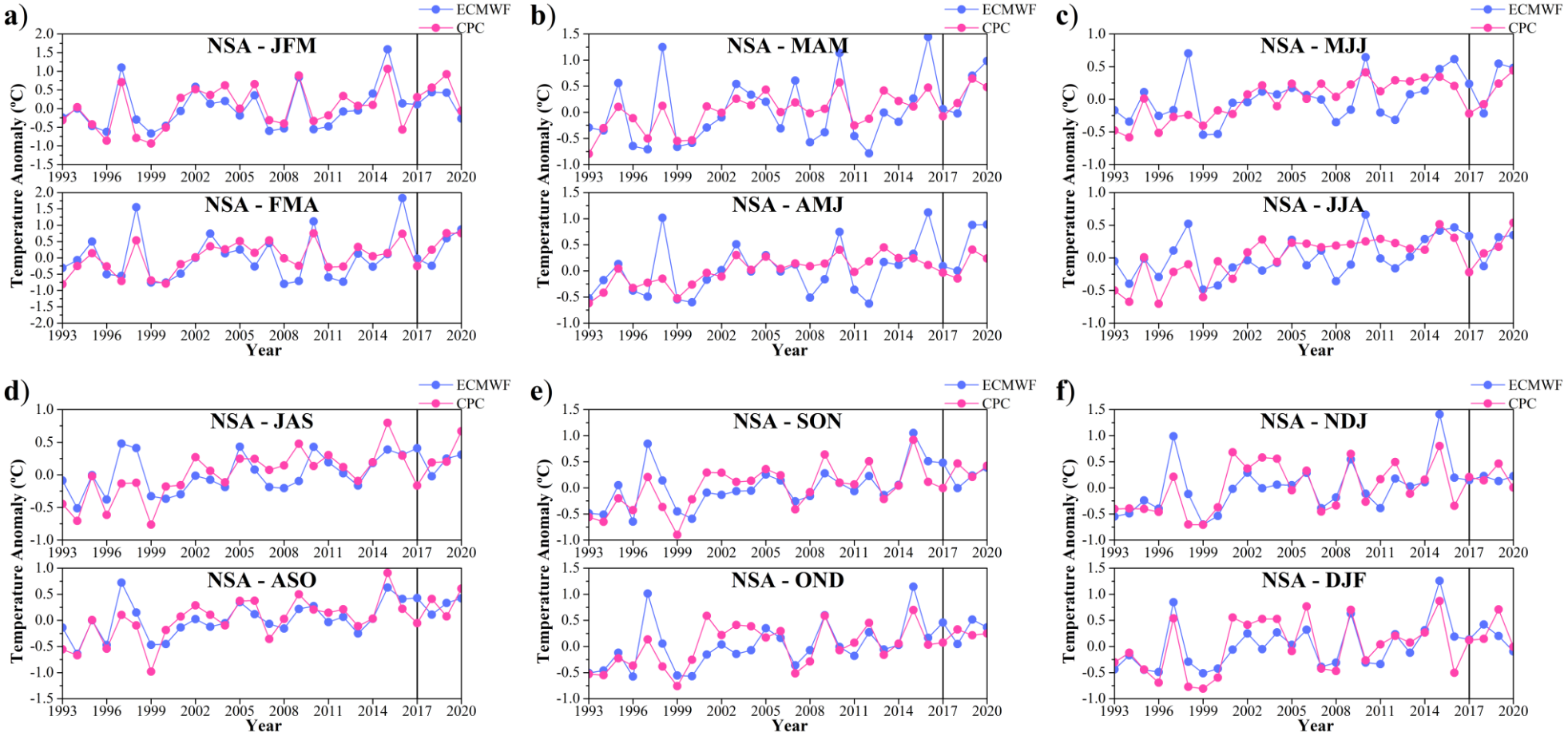

Figure 29 – Similar to Figure 28, except for the Northern South America subdomain (NSA).

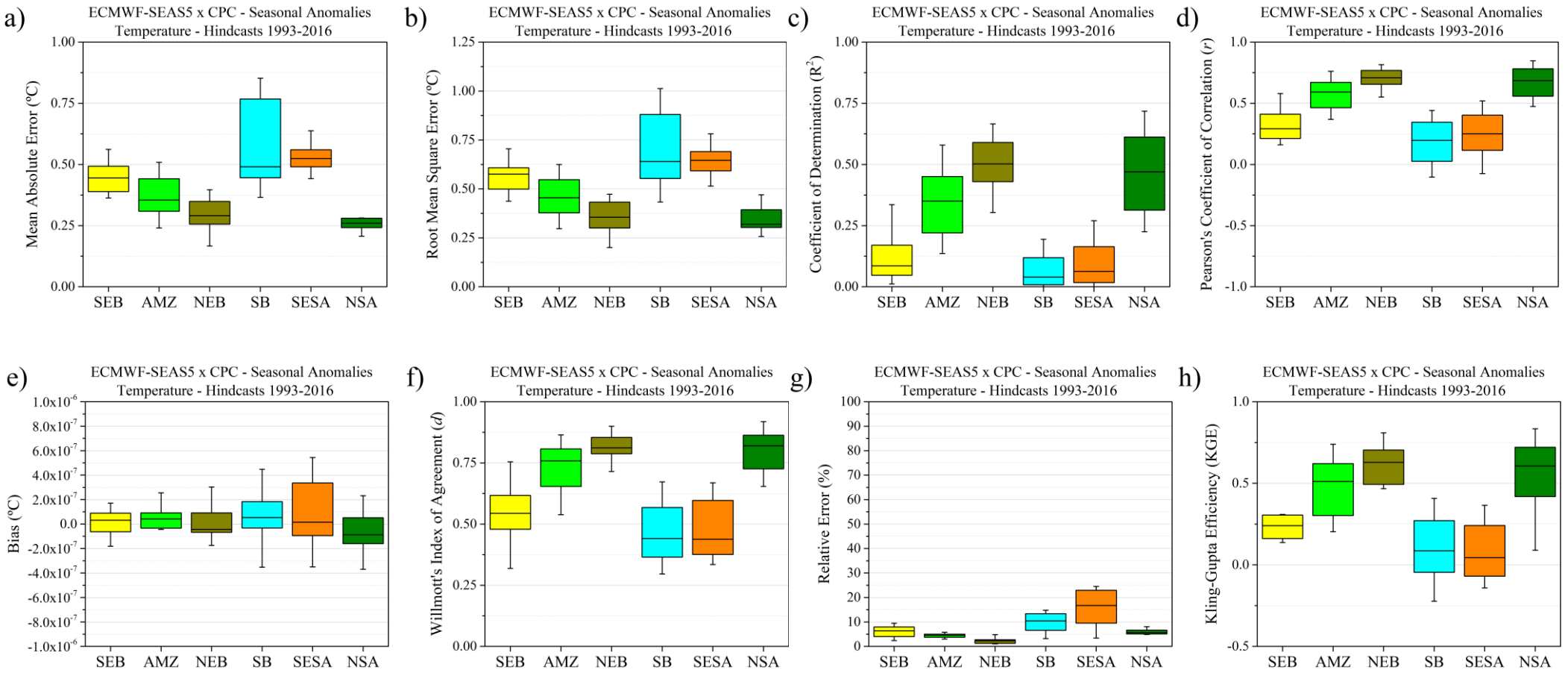

Figure 30 – Boxplots of statistical parameters derived from seasonal mean temperature anomalies (JFM to DJF) of the ECMWF-SEAS5 hindcasts (1993-2016) for the SEB, AMZ, NEB, SB, SESA and NSA subdomains. Statistical parameters of relative error (g) and Kling-Gupta Efficiency (h) are calculated from seasonal temperature means.

The SEB, SB and SESA subdomains present the worst results. They indicate high MAE, RMSE and bias values, despite SEB showing relative errors below 10% for all seasons. The poor ECMWF-SEAS5's performance in predicting temperature anomalies in these regions is reflected in the worst results of R^2, *r*, *d* and KGE.

6.11 Evaluation of Temperature Forecasts

Figure 31 presents the ECMWF-SEAS5 forecasts for 2017-2020 and the biases obtained. In general, it is observed that prognostic predictions are not very different from retrospective predictions. The cold bias of ECMWF-SEAS5 persists across most of the South American continent, with larger negative deviations in northern Brazil and northwestern South America. The warm bias in the SESA region also holds up in the reforecasts from JFM to MJJ (Figures 22a-22e). From JJA (Figure 31f), positive temperature deviations can be seen in the region, a pattern also found in hindcasts.

Some differences occur in the NEB and SEB. For SEB, there are slight reductions in the cold bias in FMA (Figure 31b), but underestimates remain throughout the year. In NEB, there is a reduction in the cold bias mainly in Bahia and portions of Piauí during the autumn and winter seasons (Figures 31b-31f), but the temperature underestimation remains in the prognostic forecasts, although with a lower magnitude compared to hindcasts.

A possible cause for the persistence of systematic errors is associated with the initial soil moisture conditions used in the model. Wang et al. (2010) evaluated the CFS seasonal temperature predictions and inferred that the model's cold bias was related to positive soil moisture anomalies in the initial conditions of the predictions. Soil moisture modifies the temperature amplitude at the surface level, as the increase in soil moisture induces a reduction in temperature differences between day and night (AL-KAYSSI et al., 1990). Another reason for the systematic cold bias may be associated with the model using fixed concentrations of greenhouse gases (WANG et al., 2010).

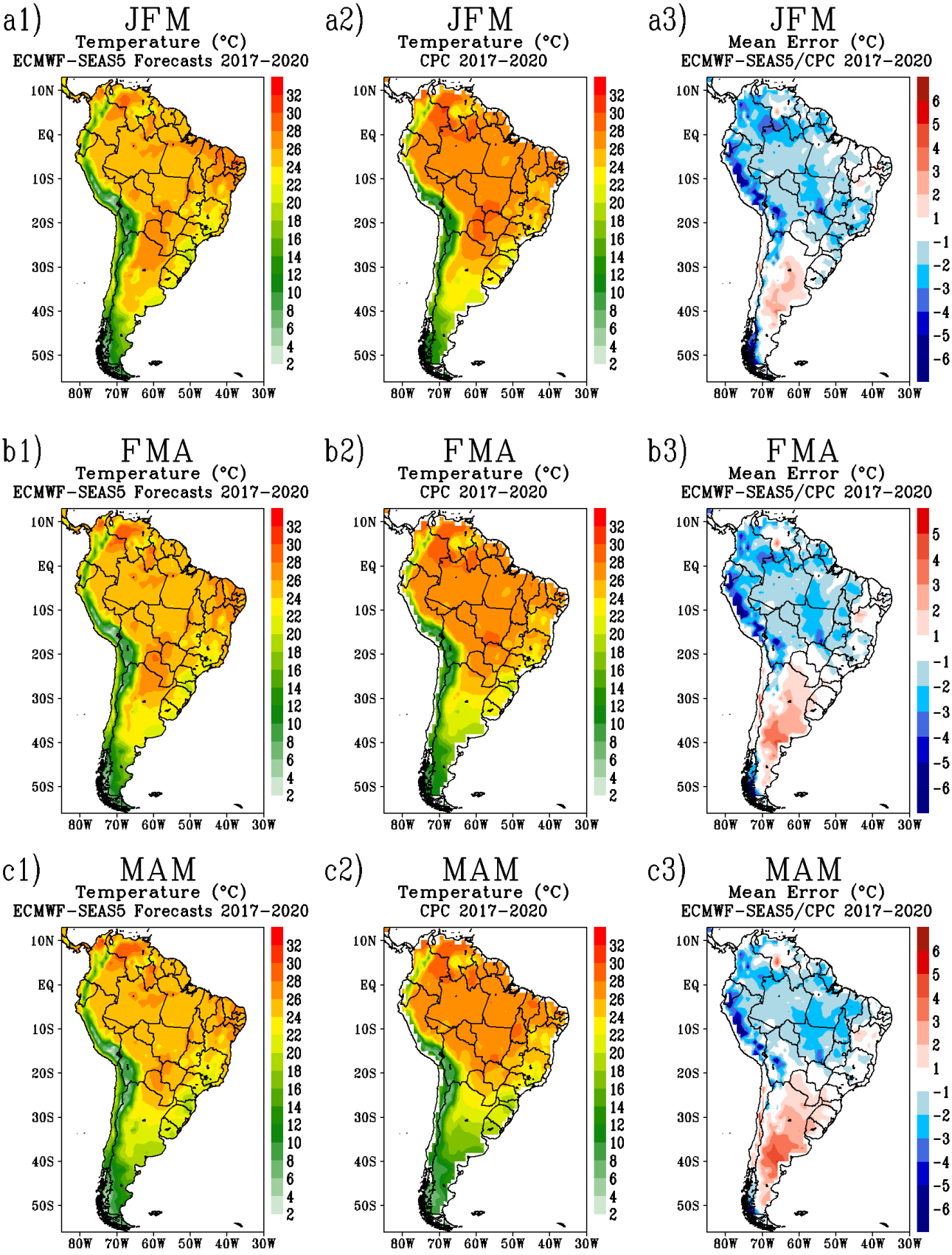

Figure 31 – Left column: seasonal mean 2 m temperature (°C) derived from the ECMWF-SEAS5 forecasts, averaged over the 2017-2020 period and the 51 ensemble members. Center column: CPC seasonal mean surface temperature (°C) averaged over 2017-2020. Right column: seasonal temperature mean errors (°C) obtained by the difference between ECMWF-SEAS5 and CPC and averaged over 2017-2020.

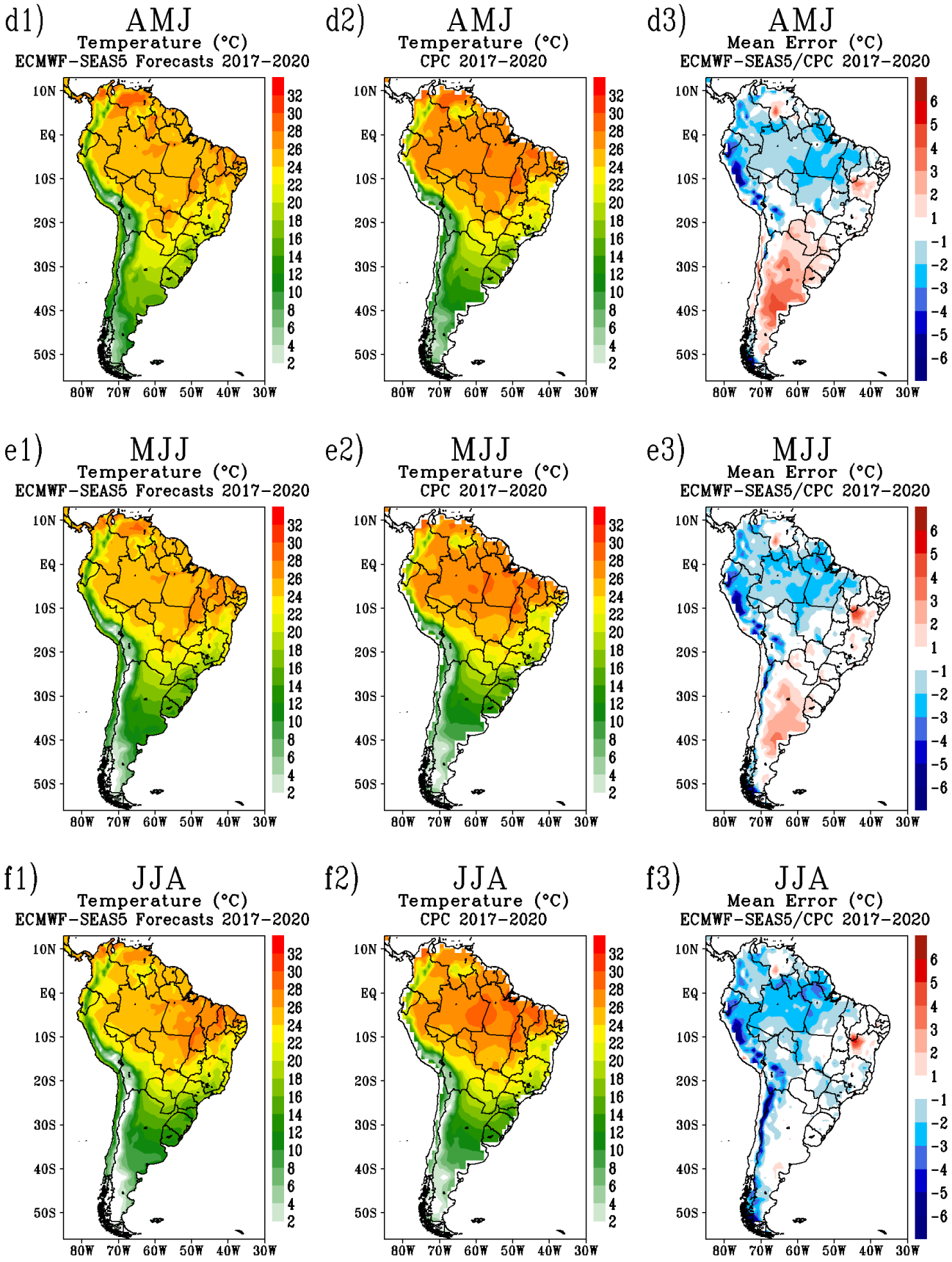

Figure 31 – continued

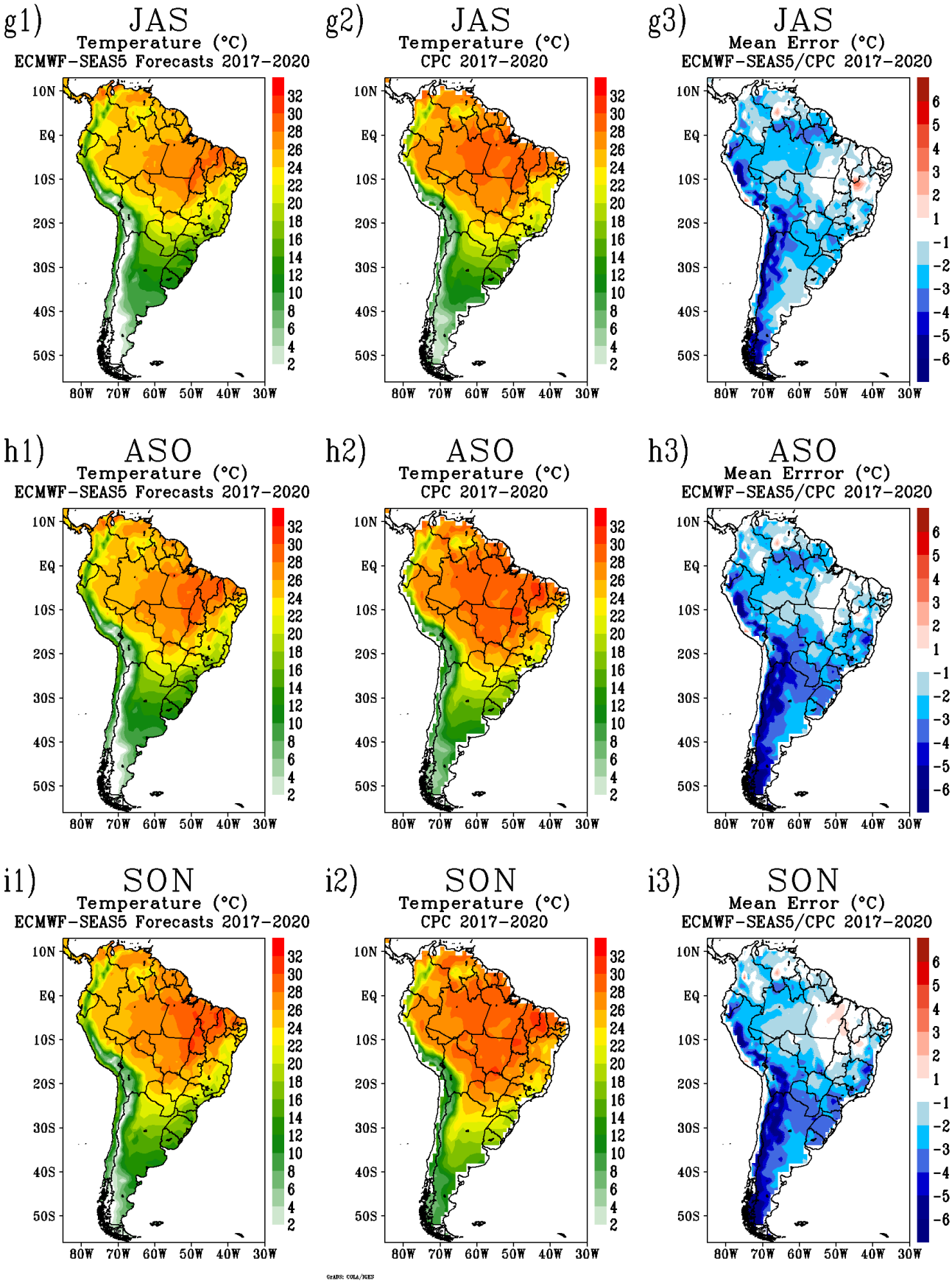

Figure 31 – continued.

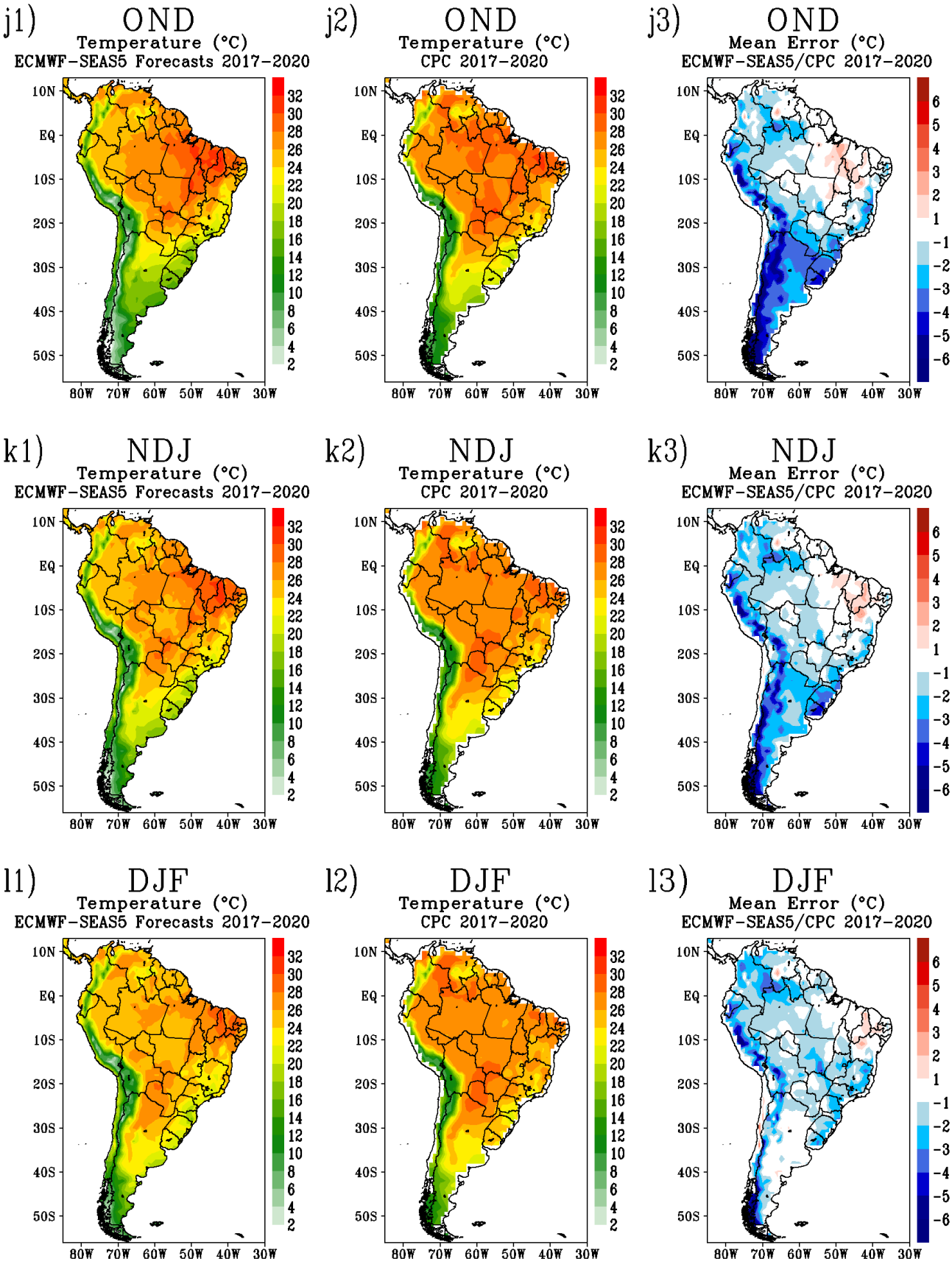

Figure 31 – continued.

Figure 32 presents the statistical parameters calculated for the seasonal temperature predictions from the ECMWF-SEAS5 forecasts. The MAE and RMSE results indicate that the worst results are in the SEB, SB and SESA regions. On the other hand, the AMZ and NSA regions have the smallest MAE and RMSE values and minor amplitudes. Although NEB indicates considerable MAE and RMSE, its relative error is the smallest of all subdomains. The same pattern is found for SEB, which indicates a series of relative errors below 15%.

Concerning the R^2 and *r* coefficients, all subdomains show great variability. The best R^2 scores correspond to 0.91 in AMJ for NSA, 0.99 in OND for SESA, and 0.99 in ASO for AMZ. About the *r* index, better results for ASO in AMZ (*r* = 0.99), for ASO in SESA (*r* = 0.91) and for AMJ in NSA (*r* = 0.95). Regarding the *d* index, AMZ stands out providing only values above 0.4 (with *d* = 0.83 in NDJ), while NEB (*d* = 0.70 in OND), SESA (*d* = 0.94 in MAM) and NSA (*d* = 0.89 in JFM) also show reasonable results. For the KGE index, AMZ, SESA and NSA show the best results, with AMZ obtaining KGE = 0.81 in FMA, SESA with KGE = 0.74 in ASO and NSA with KGE = 0.78 in JJA. There is a slight improvement in the statistical results for the SESA subdomain regarding hindcasts.

Table 7 summarizes the average results calculated for all statistical parameters in each subdomain.

Table 7 – Average of the statistical parameters calculated for each subdomain's seasonal climate prediction of temperature. Best (worst) results in blue (red).

	Mean Statistics Parameters 1993-2016 - Temperature							
	BIAS	**R^2**	***r***	**MAE**	**RMSE**	***d***	**RE**	**KGE**
SEB	0,0000001586	0,095170246	0,3084968	0,4460686	0,5647102	0,5673772	6,081173	0,709267
AMZ	-0,0020051516	0,302381022	0,5498918	0,3706053	0,4709386	0,7224057	4,4597635	0,7281013
NEB	0,0000000347	0,474580049	0,6888977	0,2943599	0,3683702	0,8160128	2,3366193	0,753294
SB	0,0000000559	0,023942783	0,1547346	0,5716087	0,7235233	0,4498924	9,6940547	0,7856497
SESA	0,0000000849	0,056236048	0,2371414	0,5288944	0,6597429	0,4766107	15,834389	0,7650634
NSA	-0,0000000623	0,475347101	0,6894542	0,2712302	0,3505969	0,8199282	5,9756084	0,6250002
	Mean Statistics Parameters 2017-2020 - Temperature							
	BIAS	**R^2**	***r***	**MAE**	**RMSE**	***d***	**RE**	**KGE**
SEB	-0,044959977	0,010982894	0,1047993	0,5087382	0,6314448	0,3957513	5,6913143	0,6693692
AMZ	-0,268639402	0,364125564	0,6034282	0,3416169	0,3987162	0,676517	5,3840539	0,776433
NEB	0,349932341	0,0000081788	-0,0028599	0,4398089	0,5276349	0,4037853	1,9962468	0,6588615
SB	-0,101136142	0,000655706	0,0256068	0,5383082	0,711663	0,3299496	9,164447	0,8011808
SESA	0,028741756	0,028078225	0,1675656	0,4604395	0,5786382	0,4560274	14,540904	0,7925213
NSA	0,041106966	0,18763748	0,4331714	0,2589827	0,3103535	0,6547435	5,7651331	0,5632199

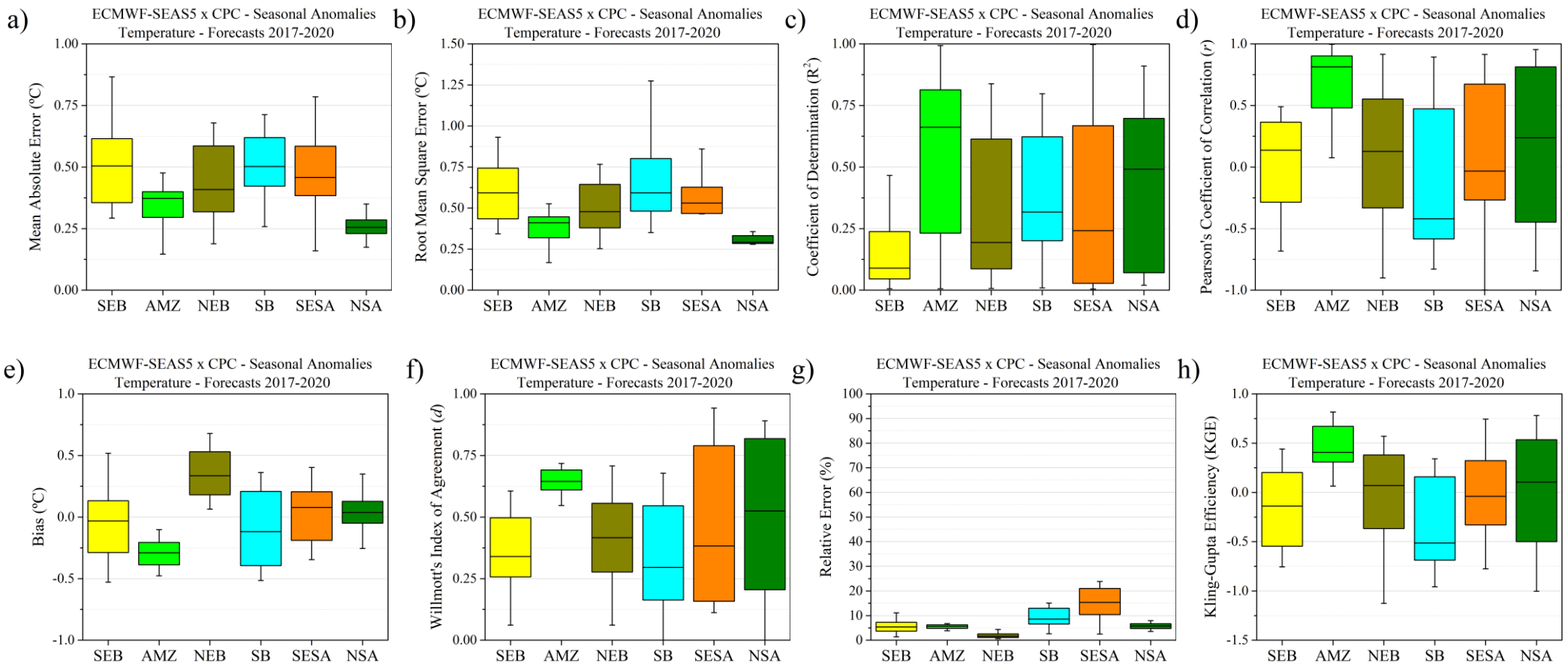

Figure 32 – Boxplots of statistical parameters derived from seasonal mean temperature anomalies (JFM to DJF) of the ECMWF-SEAS5 forecasts (2017-2020) for the SEB, AMZ, NEB, SB, SESA and NSA subdomains. Statistical parameters of relative error (g) and Kling-Gupta Efficiency (h) are calculated from seasonal temperature means.

6.12 The Seasonality Index (SI)

The Seasonality Index (SI) was proposed by Walsh and Lawler (1981), and it measures the monthly rainfall variability throughout the year, where the result is the degree of seasonality ranging from zero, for a homogeneous monthly rainfall distribution, to 1.83, where rain occurs for a single month (WALSH; LAWLER, 1981). The SI index classifies climate types concerning water availability so that the higher the SI of a region, the greater the variability of water resources and seasonal scarcity, which accentuates the area's vulnerability to desertification (PATIL, 2015). In Table 6, a qualitative classification of degrees of seasonality is indicated

Figure 33 shows the SI results obtained for SA, considering the seasonal predictions of ECMWF-SEAS5 hindcasts and the precipitation analysis from the CPC. The maps indicate many similarities between the two types of outputs, showing that ECMWF-SEAS5 satisfactorily represents the seasonal contrasts of precipitation on the continent. The most remarkable differences occur in the centre of Northeastern Brazil, where ECMWF-SEAS5 points to a larger extension of the area of $0.80 \leq SI \leq 0.99$, whose classification is markedly seasonal with a long drier season. Other differences are found in southern Argentina, where ECMWF-SEAS5 indicates a region with $0.20 \leq SI \leq 0.39$, classified as homogeneous with a defined wet season. In the CPC, this region yields $0.4 \leq SI \leq 0.59$, categorized as quite seasonal with a shorter dry season. Differences also occur in the region to the west of the Andes, covering the extreme northwest of Argentina and the extreme southwest of Bolivia, where the ECMWF-SEAS5 indicates values of $1.0 \leq SI \leq 1.19$, while the CPC gives values of $0.8 \leq SI \leq 0.99$. These differences are assumed to be due to systematic errors in SEAS5, as the model underestimates the precipitation in the mountain range region in the autumn and winter months and overestimates it in the spring and summer months shown in Figure 6.

Differences aside, it is observed that the two outputs generate very similar fields. The SEB region falls into the seasonal and very seasonal categories with a short drier season (values of $0.4 \leq SI \leq 0.79$), which is expected since this sector is influenced by the monsoon system (CARVALHO; JONES; LIEBMANN, 2004). An exception occurs in the extreme northwest of Minas Gerais, where the two fields indicate the classification of markedly seasonal with a long drier season, a regime verified in other studies that show this sector as the driest in Minas Gerais (PEREIRA et al., 2018; SILVA; REBOITA, 2013).

Table 6 – Classification of Seasonality Index (SI) according to Walsh and Lawler (1981).

Rainfall Regime	SI Class Limits
Very equable	≤ 0.19
Equable but with a definite wetter season	0.20 – 0.39
Rather seasonal with a short drier season	0.40 – 0.59
Seasonal	0.60 – 0.79
Markedly seasonal with a long drier season	0.80 – 0.99
Most rain in 3 months or less	1.00 – 1.19
Extreme, almost all rain in 1-2 months	≥ 1.20

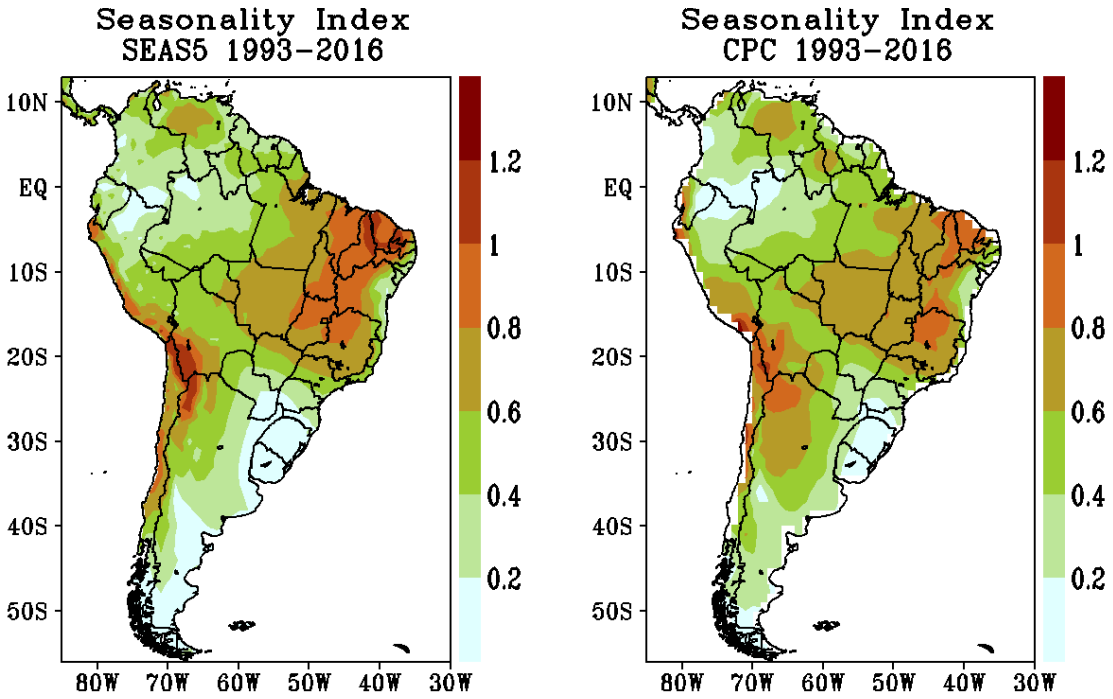

Figure 33 – Seasonality Index (SI) derived from the ECMWF-SEAS5 hindcasts and CPC over 1993-2016 for South America.

Figure 34 shows the interannual SI series obtained for the SEB with ECMWF-SEAS5 and CPC. ECMWF-SEAS5 provided an interval of $0.35 \leq SI \leq 0.55$, with a mean of $\overline{SI} = 0.49$, and CPC $0.38 \leq SI \leq 0.68$, with $\overline{SI} = 0.54$. What is observed is that ECMWF-SEAS5 results in smaller SI values, a consequence of the model's wet bias in this region, as shown in the precipitation compositions (Figures 6, 9, 19e, 20 and 21e). However, the CPC series exhibits interannual variations in seasonality (as in 2000, 2003, 2006, 2007, 2011, 2018 and 2020) that are not reproduced by the ECMWF-SEAS5. However, despite the deviations, it is noted that ECMWF-SEAS5 reasonably simulates the seasonal contrasts of rainfall in the SEB. Walsh and Lawler (1981) stated that the precise thresholds of the SI categories should not be interpreted with intrinsic significance.

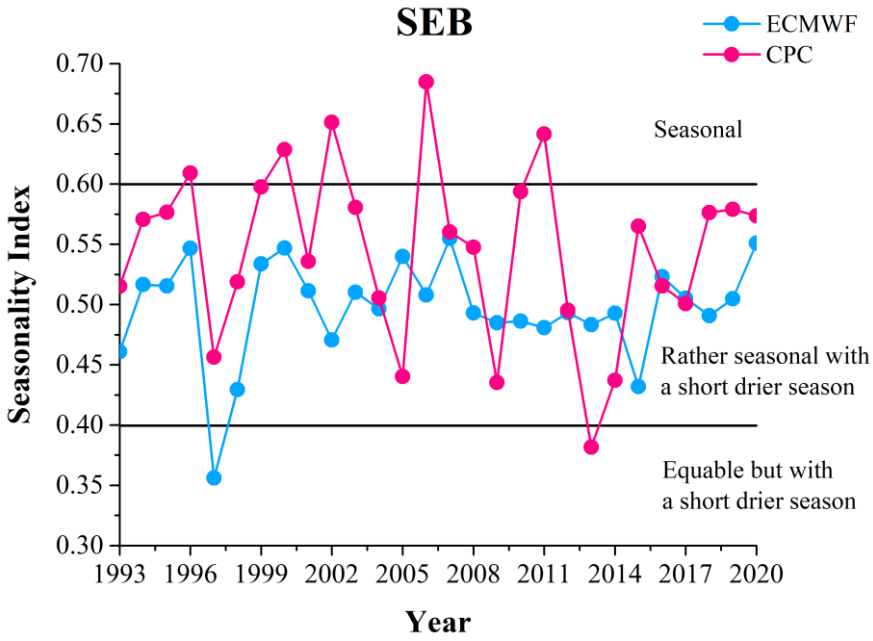

Figure 34 – Seasonality Index (SI) derived from the ECMWF-SEAS5 hindcasts and CPC over 1993-2020 for the SEB domain.

Considering the AMZ domain, both fields indicate values of $0.20 \leq SI \leq 0.59$, corresponding to the categories of equable with a definite wetter season and rather seasonal with a short drier season (Figure 33). This domain is characterized by spatial and temporal heterogeneity of rainfall. In southern Amazonia, the dry season usually occurs from July to September and the rainy season from January to March, while the northern portion has the opposite seasonality (BAGLEY et al., 2014).

Figure 35 shows that ECMWF-SEAS5 remained close to CPC in the seasonal rainfall representation. Most years correspond to rather seasonal with a short drier season. Despite moderately representing the interannual variation of the index, it is noted that ECMWF-SEAS5 provides higher SI values, which may be due to the model overestimating rainfall in the spring and summer months and underestimating it in the autumn and winter months (Figure 6). The series resulting from ECMWF-SEAS5 has an interval of $0.52 \leq SI \leq 0.60$ and $\overline{SI} = 0.56$, while the CPC provided $0.47 \leq SI \leq 0.64$ and $\overline{SI} = 0.57$, indicating reasonable proximity between the values.

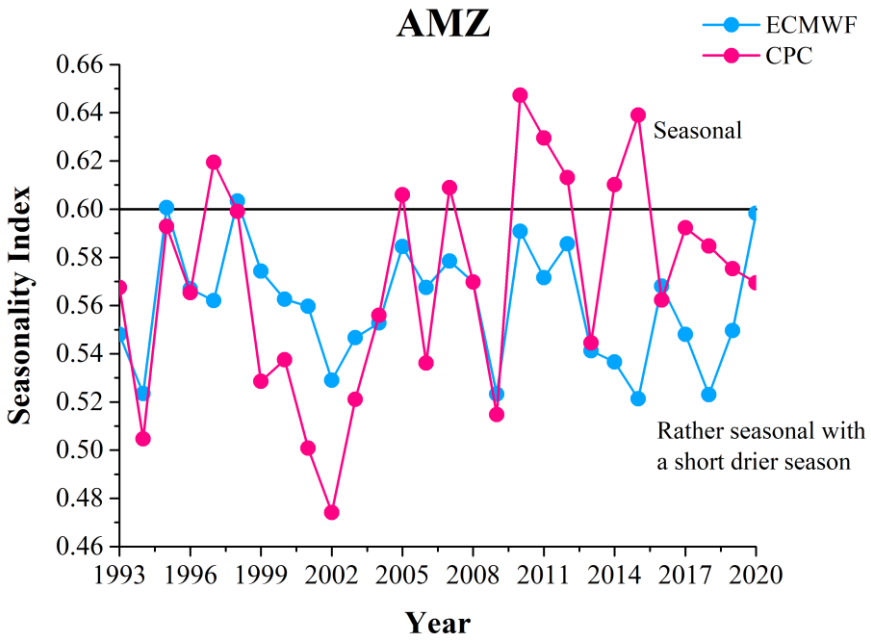

Figure 35 – Similar to Figure 34, except for the AMZ subdomain.

For the NEB subdomain, the maps show that both ECMWF-SEAS5 and CPC indicate categories of $0.8 \leq SI \leq 0.99$ (markedly seasonal with a long drier season) in regions such as the central and northern NEB (with ECMWF-SEAS5 indicating a more extensive area under this rating) and $0.4 \leq SI \leq 0.59$ (rather seasonal with a short drier season) in the east of the region (Figure 33). The systematic dry bias of ECMWF-SEAS5 in the region (Figures 6, 11 and 19e) is reflected in the highest SI values provided, resulting in $0.62 \leq SI \leq 0.75$ and $\overline{SI} = 0.68$, while the CPC resulted in $0.40 \leq SI \leq 0.85$ e $\overline{SI} = 0.64$ (Figure 36).

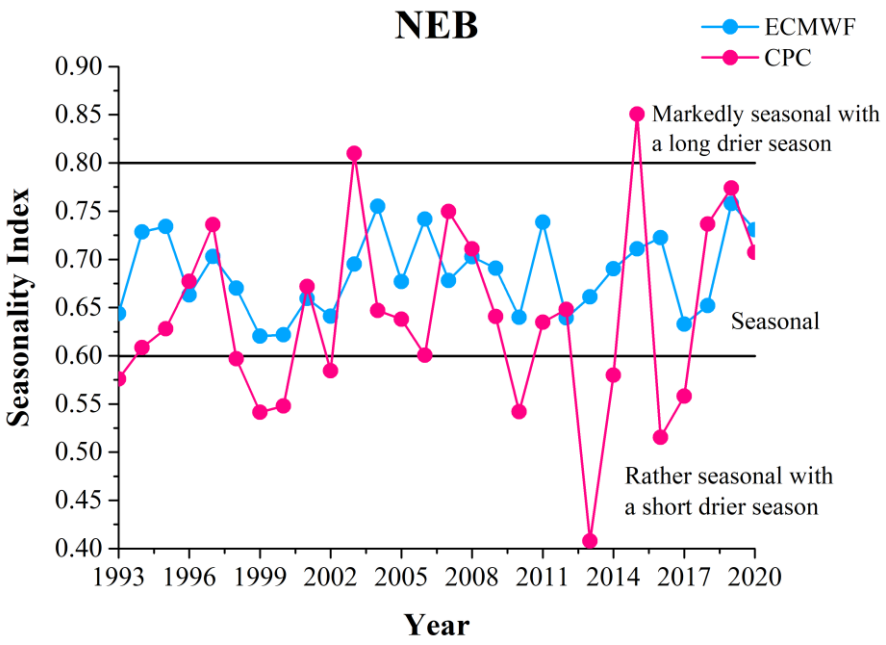

Figure 36 – Similar to Figure 34, except for the NEB subdomain.

In the SB region, both maps (Figure 33) indicate a predominance of SI ≤ 0.19, considered very equable, indicating that rainfall is evenly distributed over all months. However, some portions like north of Santa Catarina and Paraná are 0.20 ≤ SI ≤ 0.39 (equable but with a short drier season). As seen in the seasonal rainfall fields of the hindcasts (Figure 6), ECMWF-SEAS5 underestimates the variable in autumn and winter and overestimates it in spring and summer. Here, the model provides SI series all located in the very equable class (Figure 37), similar to the result of the 1993-2016 composition (Figure 33), but different from the series provided by the CPC, which is in the range of equable but with a short drier season. ECMWF-SEAS5 provides 0.08 ≤ SI ≤ 0.21 and $\overline{SI}$ = 0.13, and the CPC gives 0.27 ≤ SI ≤ 0.32 and $\overline{SI}$ = 0.31, indicating the disparity between the indices obtained annually.

The ECMWF-SEAS5 and CPC series discrepancy is more notable in the SESA subdomain than in the SB one (Figure 38). The maps in Figure 33 indicate reasonable similarity between the two outputs, with ECMWF-SEAS5 showing the region with 0 ≤ SI ≤ 0.39 and CPC with 0.20 ≤ SI ≤ 0.39. However, the interannual series resulting from the CPC falls almost entirely in the rather seasonal class with a short drier season, while ECMWF-SEAS5 presents its series in the very equable class. The ECMWF-SEAS5 results in a series with 0.07 ≤ SI ≤ 0.19 and $\overline{SI}$ = 0.10, and the CPC gives 0.20 ≤ SI ≤ 0.53 and $\overline{SI}$ = 0.37, showing considerable asymmetry between the indices obtained by the two series.

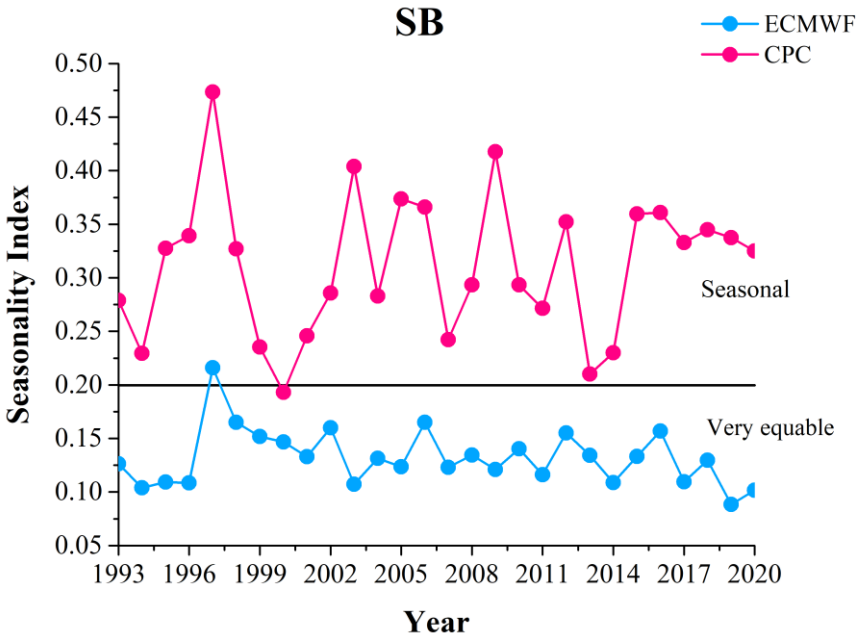

Figure 37 – Similar to Figure 34, except for the SB subdomain.

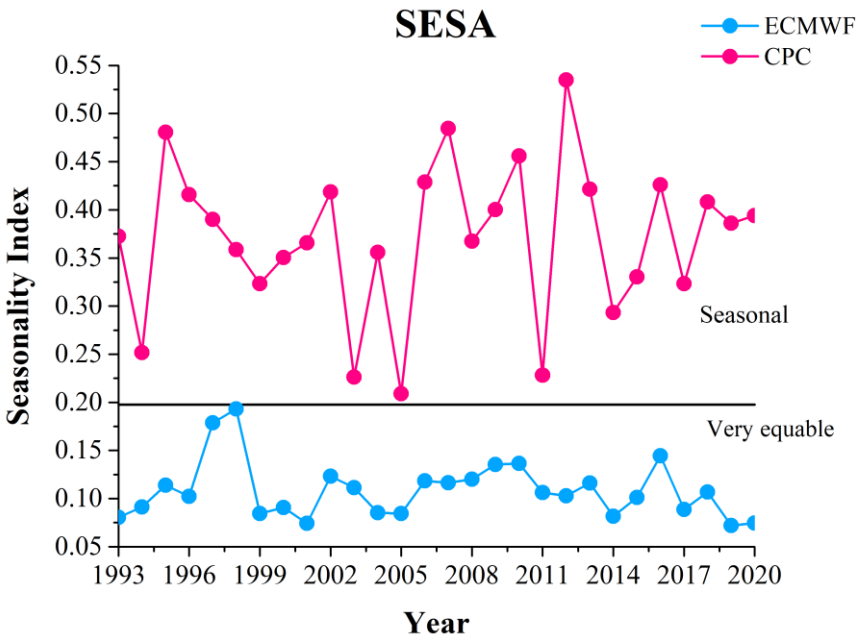

Figure 38 – Similar to Figure 34, except for the SESA subdomain.

In the NSA domain, both ECMWF-SEAS5 and CPC indicate regions with 0.2 ≤ SI ≤ 0.59, values corresponding to the categories of equable but with a short drier season and rather seasonal with a short drier season (Figure 33). In the CPC, small portions of Venezuela and Guyana are in the range of 0.6 ≤ SI ≤ 0.79 (seasonal), a characteristic not found by ECMWF-SEAS5. The series provided by ECMWF-SEAS5 indicates 0.18 ≤ SI ≤ 0.36 and $\overline{SI}$ = 0.24, and the CPC gives 0.23 ≤ SI ≤ 0.46 and $\overline{SI}$ = 0.31, indicating relative symmetry between the two series.

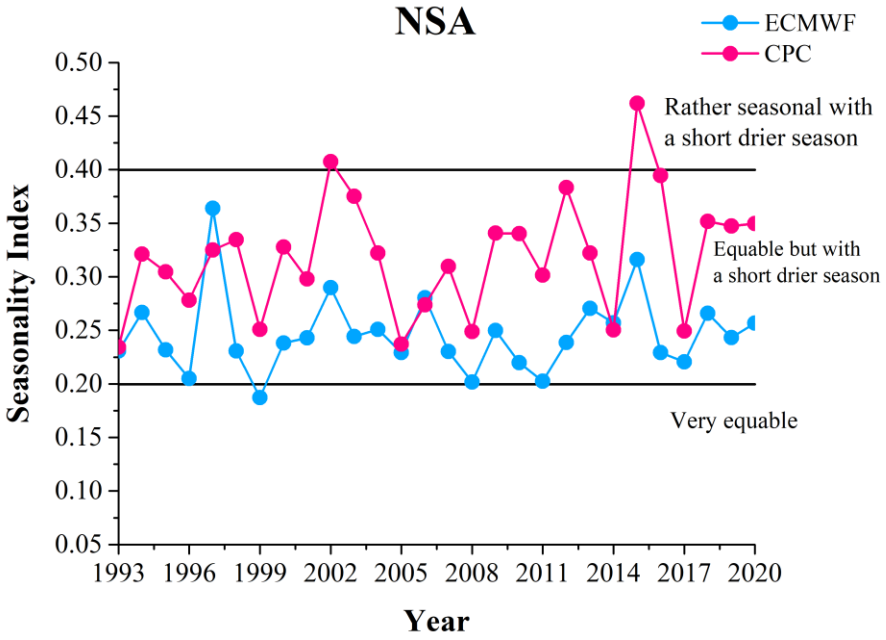

Figure 39 – Similar to Figure 34, except for the NSA subdomain.

Finally, the SI index is a simple metric for mapping large areas regarding their seasonal variation in precipitation. The ECMWF-SEAS5 results show that the model presented an acceptable representation of SI in the SEB, AMZ, NEB and NSA regions. On the other hand, regions such as SB and SESA indicated considerable disparity between the series compared to the CPC, which may be due to the model's deficiency in representing mid-latitude atmospheric systems (DE JESUS et al., 2016).

6.13 Precipitation Regimes in South America

This section presents the results obtained by the cluster analysis performed with monthly ECMWF-SEAS5 predictions (lead time 1-month) and monthly CPC analyses for 1993-2016. The previous choice of k = 8 resulted in eight rainfall regimes in SA, consistent with the qualitative analysis carried out by Reboita et al. (2010a).

a) – R1 – Southwest South America

R1 comprises sectors of southwestern SA such as central-southern Chile and far-western southern Argentina (Figure 40). In this region, the annual rainfall cycle presents maximum in winter and minimum in summer, except in the southernmost part, where precipitation is homogeneously distributed throughout the year (REBOITA et al., 2010a, 2012).

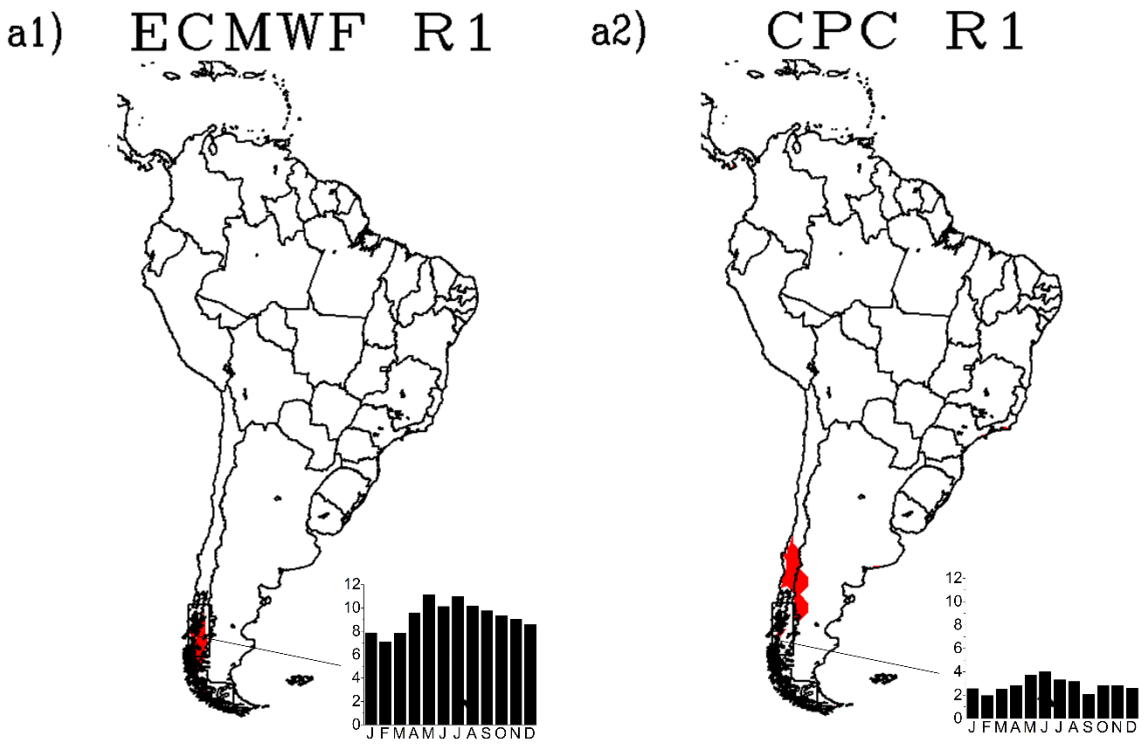

Figure 40 – R1 formed by southwestern South America and annual precipitation cycle (mm day^{-1}).

Precipitation in this region is mainly influenced by the South Pacific Subtropical Anticyclone (SPSA) (BARRETT; HAMEED, 2017; FAHAD et al., 2021; FLORES-AQUEVEQUE et al., 2020; ZOU; XI, 2021), a centre of semi-permanent high pressure caused by the subsiding movement of the Hadley cell. The SPSA is located further north during winter, allowing transient systems and the anticyclone's west-south winds to reach the Andes, favouring precipitation west of the mountain range (ESPINOZA et al., 2020; GARREAUD; MUÑOZ, 2005; VIALE et al., 2019). However, in summer, SPSA is located in its southernmost position, so its southeast sector acts on, inhibiting the passage of transient systems and the development of cloudiness and decreasing precipitation rates in this season.

Figure 40 illustrates the monthly rainfall cycle in R1 obtained by ECMWF-SEAS5 and CPC, and the results are discrepant. The CPC indicates slight total rainfall and shows that the larger rainfall rates occur in winter, with a maximum of 4 mm day^{-1} in June. In contrast, ECMWF-SEAS5 overestimates rainfall throughout the year, with maximums of 11 mm day^{-1} in May and July. The model's poor performance in this region is also indicated in the skill score results (Figure 7). In addition, ECMWF-SEAS5 points to R1 in the extreme south of Chile and Argentina, and CPC points to R1 further north.

b) – R2 – Northern Chile, Northwest and Central-South Argentina

The R2 sector is formed by northern Chile, northwestern and central-south Argentina. In the northern sector of R2, the subsiding movements of the SPSA inhibit the occurrence of rain, responsible for the extreme aridity of northern Chile (ACEITUNO et al., 2021; ANCAPICHÚN; GARCÉS-VARGAS, 2015; GREZ et al., 2020; MESEGUER- RUIZ et al., 2020a; VALDÉS-PINEDA et al., 2016) and the existence of the Atacama Desert (BÖHM et al., 2020; GONZÁLEZ-PINILLA et al., 2021; MESEGUER-RUIZ et al., 2020b; VELOSO et al., 2020).

The annual rainfall cycle obtained by the CPC (Figure 41-b2) illustrates this arid behaviour of the northern region of R1, with monthly rainfall totals below 0.12 mm day^{-1} throughout the year. However, as previously verified, ECMWF-SEAS5 overestimates the rainfall in the region throughout the year, indicating totals of up to 0.75 mm day^{-1}.

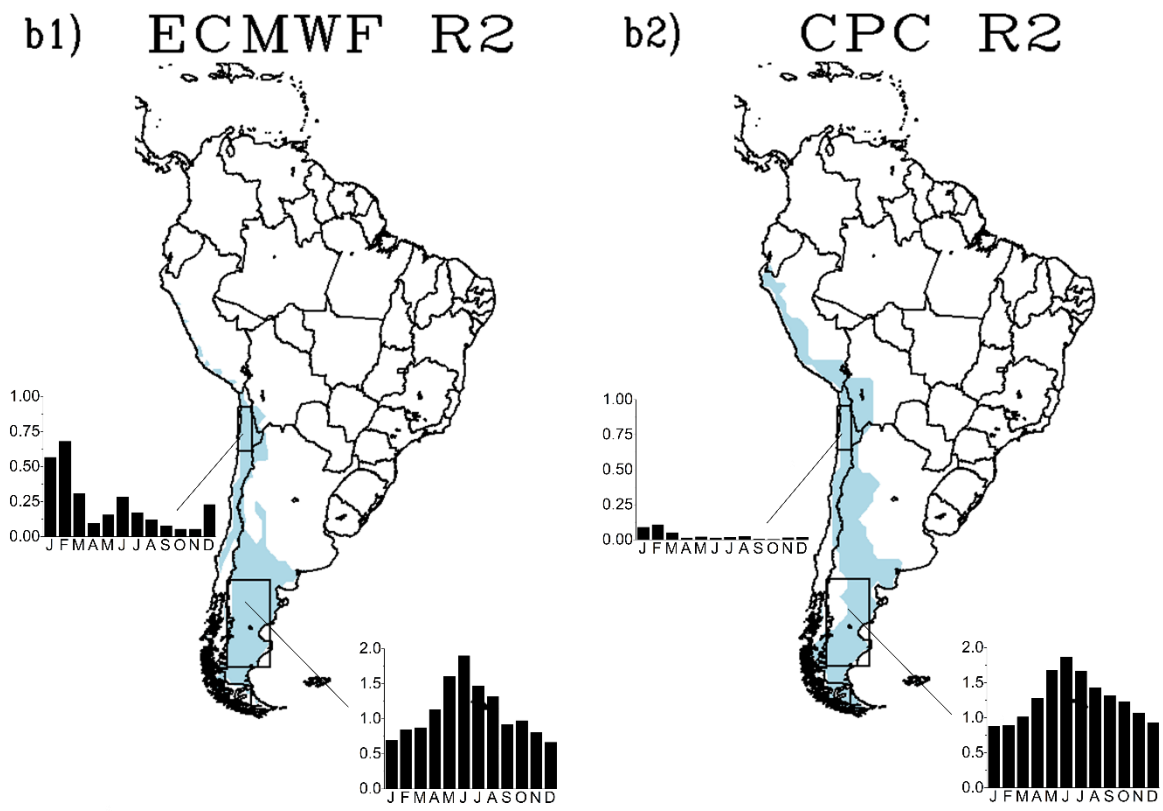

Figure 41 – R2 formed by northern Chile, northwest and central-south Argentina and annual precipitation cycle (mm day^{-1}).

In the southern sector of R2, ECMWF-SEAS5 consistently reproduces the annual rainfall variation (Figure 41-b1), indicating pronounced rainfall totals from May to August. Furthermore, the regions have relatively similar spatial delimitation between the two types of data, except that CPC extends the R2 to the entire marine coast of Peru and southwestern Bolivia.

The south of R2, formed by northwestern and south-central Argentina, is located in the lee of the Andes Mountains, which is unfavourable to rain in the sector (REBOITA et al., 2010a). The rains in this region are due to the action of frontal and cyclonic systems since the southeast coast of Argentina is a frontogenetic and cyclogenetic region (BLÁZQUEZ; SOLMAN, 2016; CARDOZO; REBOITA; GARCIA, 2015; CRESPO et al., 2021; DA ROCHA et al., 2018; DE JESUS et al., 2016, 2021; GOZZO et al., 2014; REBOITA et al., 2009, 2010, 2019). Furthermore, as the southern temperature gradients are relatively intense in this region, it is conducive to forming cyclones and frontal systems (REBOITA et al., 2010a).

Cyclones are closed circulation centres with lower central pressure than on their periphery and play an essential role in global thermal regulation (YNOUE et al., 2017). Finally, frontal

systems are common transient disturbances in atmospheric circulation and increase precipitation in the regions they pass through (CARDOZO; REBOITA; GARCIA, 2015 ESCOBAR; REBOITA; SOUZA, 2019). More detailed descriptions of the cyclones and frontal systems can be found in Palmén and Newton (1969), Peixoto and Oort (1992), Hartmann (1994), Wallace and Hobbs (2006), Ahrens (2009) and Ynoue et al. (2017).

c) – R3 – West of Peru, West and South of Bolivia, North and Center-East of Argentina and North-Central Paraguay

The R3 sector comprises western Peru, western and southern Bolivia, northern and central-eastern Argentina and central-northern Paraguay (Figure 42), with larger totals of rain in the summer months and smaller ones in the winter months (REBOITA et al., 2010a). The spatial configuration of R3 is similar between the two fields, but the CPC indicates portions of this group in Peru, which is not found in the ECMWF-SEAS5 results. The European model reasonably simulates the annual precipitation cycles, except in Peru, where ECMWF-SEAS5 considerably overestimates the variable. ECMWF-SEAS5 overestimates also occur in Bolivia and Argentina but to a lesser extent. In the northern sector of R3, the low-level jets (LLJs) constitute a crucial atmospheric system, as they transport moisture to the region (AGUIRRE et al., 2021; ARRAUT et al., 2012; JONES, 2019; MARDONES et al., 2021; MONTINI; JONES; CARVALHO, 2019), favouring the formation of mesoscale convective complexes (MCCs) (PIERSANTE et al., 2021).

Low-Level Jets (LLJs) are a narrow region of anomalously strong winds that blow into the lower troposphere, along the east side of mountain ranges such as the Rocky Mountains in the United States and the Andes in South America (HODGES; PU, 2019; MARENGO, 2004; MARENGO; AMBRIZZI; SOARES, 2009; NASCIMENTO; HERDIES; SOUZA, 2016; STENSRUD, 1996). From November to February, LLJs are more frequent north of 20ºS (Bolivia region), while in southern latitudes, they are frequent throughout the year (REBOITA et al., 2010a; SANTOS; REBOITA, 2018). However, its moisture transport from the tropics to the subtropics is more intense in summer (MARENGO et al., 2004).

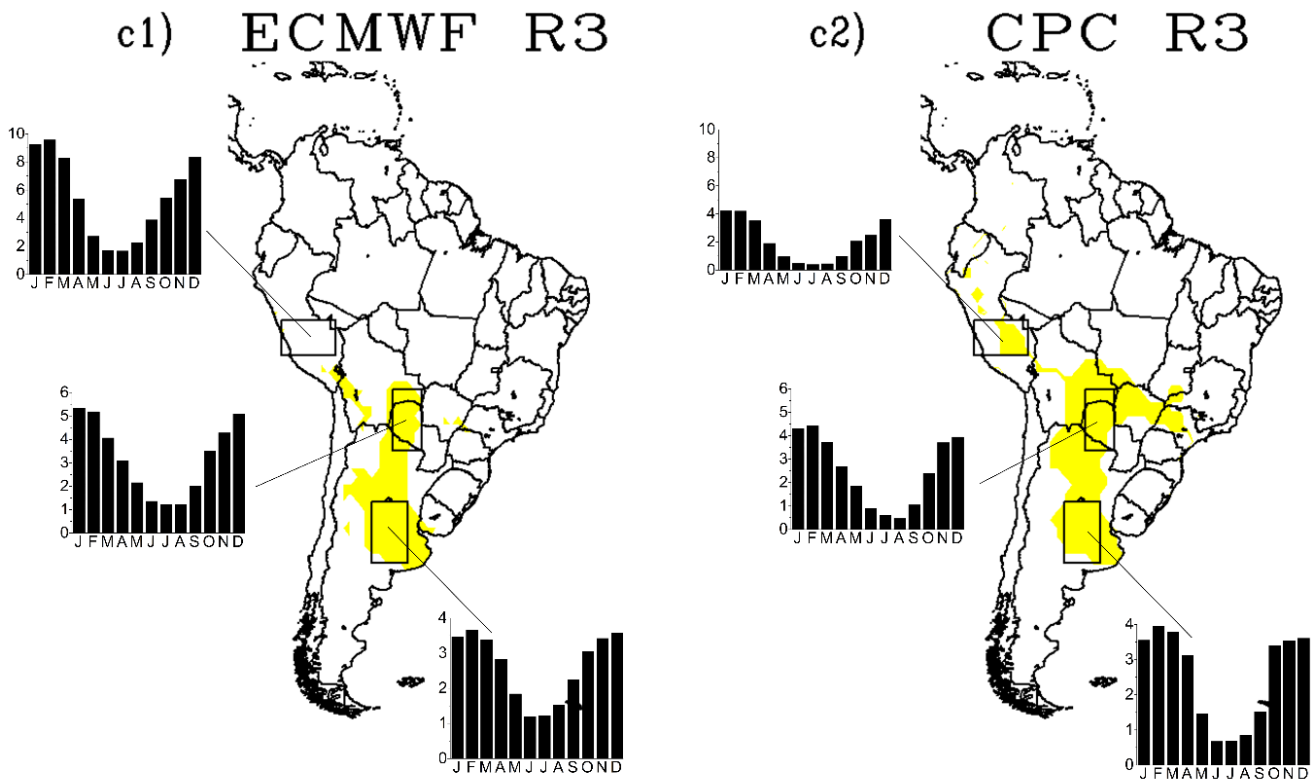

Figure 42 – R3 formed by west of Peru, west and south of Bolivia, north and centre-east of Argentina, north-central Paraguay, and annual precipitation cycle (mm day^{-1}).

In summer, there is more significant moisture transport from the Atlantic Ocean to the Amazon Basin by the trade winds, and such moisture can be channelled by LLJs to the subtropics, favouring the development of mesoscale convective complexes (MCCs) in south-central Brazil (REBOITA et al., 2010a). Mesoscale convective systems (MCCs) are constituted by an agglomerate of convective clouds that present an area with continuous precipitation, which may have various forms such as partially stratiform or partially convective (HOUZE, 2004). In the north of R3, the LLJs favour the formation of mesoscale convective complexes (MCCs) (PIERSANTE et al., 2021; RASMUSSEN et al., 2016).

In the south-central part of R3, precipitation can be caused by different factors such as frontal systems (BLÁZQUEZ; SOLMAN, 2016; CARDOZO; REBOITA; GARCIA, 2015; ESCOBAR; REBOITA; SOUZA, 2019), cyclones (CRESPO et al., 2021; DA ROCHA et al., 2019; DE JESUS et al., 2016, 2021; MENDES et al., 2010; REBOITA; AMBRIZZI; DA ROCHA, 2009; REBOITA et al., 2021b) and subtropical upper-level cyclonic vortices (CAMPETELLA; POSSIA, 2007; PINHEIRO et al., 2016; PINHEIRO; HODGES; GAN, 2020; PORTMANN; SPRENGER; WERNLI, 2021; REBOITA et al., 2010b; SATYAMURTY;

SELUCHI, 2007). Upper-level cyclonic vortices (ULCVs) are low-pressure synoptic systems formed in the upper troposphere and whose closed cyclonic circulation has a colder centre than its periphery (KOUSKY; GAN, 1981).

d) – R4 – Southern Brazil, Southern Paraguay and Uruguay

The R4 region, formed by southern Brazil, southern Paraguay and Uruguay, has rainfall well distributed throughout the year (NERY; CARFAN, 2014; REBOITA et al., 2010a). Figure 43 shows that ECMWF-SEAS5 satisfactorily reproduces the annual rainfall cycle in the region, despite overestimating the totals in the winter months. Furthermore, the precipitation regime fields are very similar between ECMWF-SEAS5 and CPC, an aspect also found in the analysis of the SI index (Figure 33).

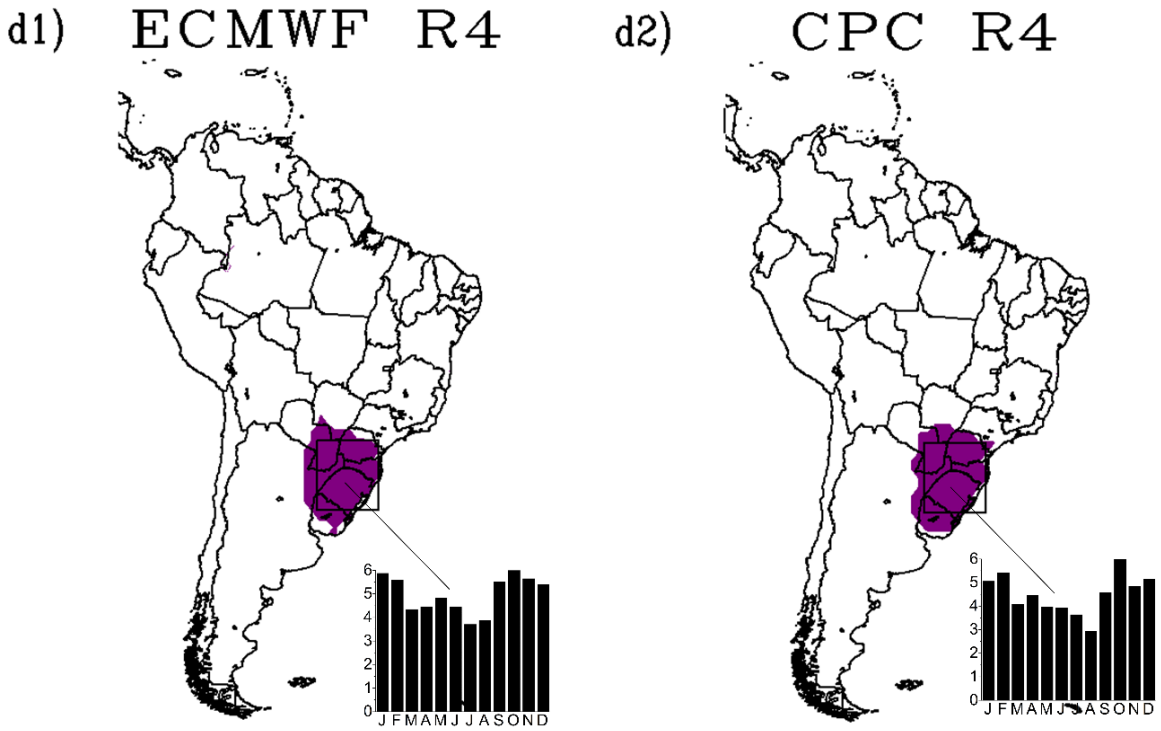

Figure 43 – R4 formed by southern Brazil, southern Paraguay, Uruguay and north-central Paraguay and annual precipitation cycle (mm day^{-1}).

Amongst the main atmospheric phenomena acting in the region are frontal systems (CARDOZO; REBOITA; GARCIA, 2015; ESCOBAR; REBOITA; SOUZA, 2019; REBOITA; KRUSCHE; PICOLLI, 2006; RODRIGUES; FRANCO; SUGAHARA, 2004), cyclones (CRESPO et al., 2021; DA ROCHA et al., 2019; DE JESUS et al., 2016, 2021; DIAS PINTO; DA ROCHA, 2011; DIAS PINTO; REBOITA; DA ROCHA, 2013; GAO; RAO, 1991; GOZZO et al., 2014; IWABE; DA ROCHA, 2009; MENDES et al., 2010; REBOITA; AMBRIZZI; DA ROCHA, 2009; REBOITA; DA ROCHA; OLIVEIRA, 2019; REBOITA et al., 2021b), subtropical ULCVs (PINHEIRO et al., 2016; PINHEIRO; HODGES; GAN, 2020; PORTMANN; SPRENGER; WERNLI, 2021; REBOITA et al., 2010b), MCCs (CAMPOS; EICHHOLZ, 2011; DURKEE; MOTE, 2010; DURKEE; MOTE; SHEPHERD, 2009; EICHHOLZ; CAMPOS, 2014; SILVA DIAS; ROZANTE; MACHADO, 2009; MORAES et al., 2020; PIERSANTE et al., 2021; SALIO; NICOLINI; ZIPSER, 2007), atmospheric blockings (RODRIGUES; WOOLINGS, 2017), breezes (TRUCOLLO, 2011).

Furthermore, R4 may also be indirectly influenced by the South Atlantic Convergence Zone (SACZ) (CAVALCANTI, 2012; FERNANDES; RODRIGUES, 2017; PEDRON et al., 2016). Although SACZ acts climatologically in southeastern Brazil, it can induce subsiding movements in southern Brazil, inhibiting the occurrence of rain (REBOITA et al., 2010a). In addition, the region is also impacted by ENSO episodes, such that wet (dry) conditions occur in El Niño (La Niña) episodes, as discussed in many studies (BUENO et al. 2020; CAI et al. 2020; CIRINO et al., 2015; GRIMM, 2003; GRIMM et al., 2000, 2020; GRIMM; TEDESCHI, 2009; HURTADO; AGOSTA, 2020).

e) – R5 – Northwest to Southeast of Brazil, including Ecuador and northern Peru

The R5 covers a wide area of SA as it extends from Ecuador and northern Peru to southeastern Brazil. In this region, total rainfall is maximum in summer and minimum in winter. This pattern is evident in Figure 44, which shows the annual precipitation series in three distinct regions of the R5: Southeast, Midwest and North Brazil. ECMWF-SEAS5 skillfully reproduces the region's seasonal rainfall cycle, although it overestimates more intensely in the Amazon region.

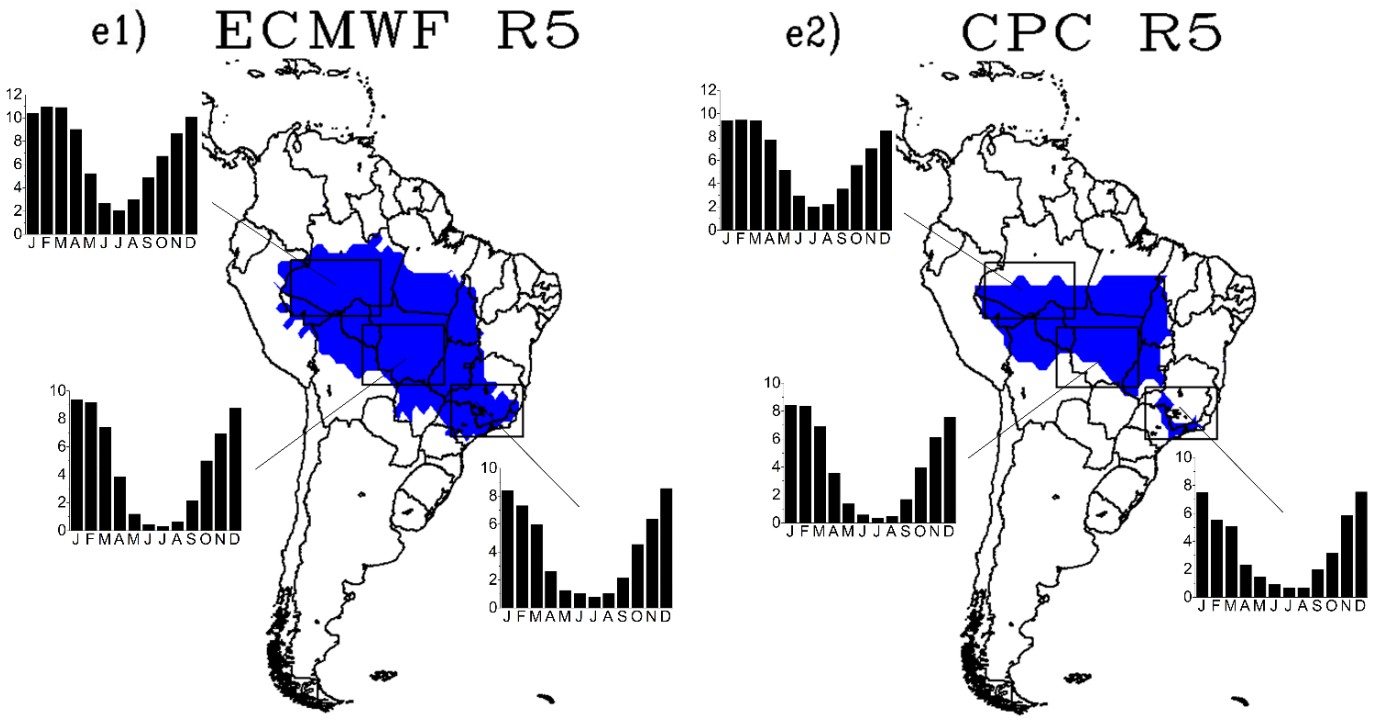

Figure 44 – R5 formed by Northwest to Southeast Brazil, including Ecuador and northern Peru and annual precipitation cycle (mm day^{-1}).

Southeast Brazil is a particular area from a climatic point of view. This peculiarity is due to the region being inserted in transition areas between the tropics and extratropics, presenting a warm climate of low latitudes and a temperate climate of mid-latitudes (NIMER, 1989). The summer is humid due to the South American monsoon system (ASHFAQ et al., 2020; DA ROCHA et al., 2012; GRIMM, 2019; GRIMM; SABOIA, 2015; MARENGO et al., 2012; PASCALE et al., 2019; REBOITA et al., 2014b; TEODORO et al., 2021; VERA et al., 2006) and to the SACZ occurrence (CARVALHO; JONES; LIEBMANN, 2004; ESCOBAR; REBOITA, 2020; SILVA; MARRAFON; REBOITA, 2020; REBOITA; ESCOBAR, 2019).

SACZ plays a key role in the rainy season in Southeast Brazil (AGUIAR; CATALDI, 2021; CARVALHO; JONES; LIEBMANN, 2004; ESCOBAR; REBOITA, 2020; GRIMM, 2011; KODAMA, 1992; KOUSKY, 1988; MARRAFON; REBOITA, 2020; QUADRO et al., 2012), accounting for 25% of rainfall from October to April (NIELSEN et al., 2019). SACZ is characterized as a cloudiness band extending from the Southern Amazon to the southwest of the Atlantic Ocean, passing through Southeastern Brazil and remaining stationary over these regions for periods equal to or greater than three days (YNOUE et al., 2017). The formation of SACZ is

associated with the convergence between the transport of moisture and heat from the Amazon region by the LLJs east of the Andes and the transport of humid air from the South Atlantic Ocean to the continent by the northwest winds of the South Atlantic Subtropical Anticyclone (SASA) (MARENGO et al., 2004; PENNA et al., 2021; REBOITA et al., 2010a). LLJs are essential for moisture transport from the Amazon Basin to Southeastern Brazil, contributing to the region's monsoon system (REHBEIN et al., 2018). In SACZ episodes, it is also possible to observe a stationary cold front over the South Atlantic Ocean associated with this system (YNOUE et al., 2017).

Inversely, Southeast Brazil's winter is dry under the SASA influence, which reaches its westernmost position in the colder months (REBOITA et al., 2019). The SASA is a semi-permanent anticyclone with seasonal variability, extending over the Southeast during winter and displacing east during summer (CARPENEDO; AMBRIZZI, 2020; REBOITA et al., 2019). In winter, SASA inhibits the influence/formation of other atmospheric systems such as frontal systems, reducing rainfall in the Southeast and configuring drier conditions (CARPENEDO; AMBRIZZI, 2020; YNOUE et al., 2017). In summer, as the SASA is far from the Brazilian coast, its circulation contributes to moisture transport from the Atlantic Ocean to the continent's interior, favouring precipitation (YNOUE et al., 2017). In the western sector of the South Atlantic Basin, SASA also affects rainfall in Southeastern Brazil through its impact on SST and SACZ (BOMBARDI et al., 2014; SUN; COOK; VIZY, 2017). It is noticeable that in the summer of 2014, the SASA was in an anomalous position to the west, which induced an intense drought over the Southeast (COELHO et al., 2016; REBOITA et al., 2015, 2019).

Southeast Brazil is also influenced by other systems such as prefrontal instability lines, cold fronts (CAVALCANTI; KOUSKY, 2009; FOSS; CHOU; SELUCHI, 2016), MCCs (SIQUEIRA; MARQUES, 2021), cyclones (REBOITA et al., 2020), atmospheric blockings (MARENGO et al., 2021; RODRIGUES et al., 2019) and breezes (RIBEIRO et al., 2018; VEMADO; FILHO, 2016).

Precipitation in central-western Brazil is maximum in summer, influenced by the monsoon system (GAN; KOUSKY; ROPELEWSKI, 2004; PRADO et al., 2021). The northern portion is impacted by systems that act in the Amazon, such as MMCs (REBOITA et al., 2010a), and the southern sector is affected by extratropical atmospheric systems such as frontal systems (ESCOBAR; VAZ; REBOITA, 2019). The region is also strongly influenced by ENSO (BORGES; BERNHOFER; RODRIGUES, 2018; HEINEMANN et al., 2021; SANTOS et al., 2021).

North Brazil has the highest annual rainfall (NIMER, 1989) and spatial rainfall heterogeneity (MARENGO, 1995). Its precipitation regime is influenced by different atmospheric systems such as the Intertropical Convergence Zone (MARENGO, 1995; MARENGO; HASTENRATH, 1993; RAO; HADA, 1990; TEODORO; REBOITA; ESCOBAR, 2019), frontal systems (ESCOBAR; VAZ; REBOITA, 2019; KOUSKY; FERREIRA, 1981), instability lines (BEZERRA et al., 2021; COHEN; SILVA DIAS; NOBRE, 1995; NESTARES, 2017; OLIVEIRA; OYAMA, 2019; SOUSA, 2020; SOUSA; CANDIDO; SATYAMURTY, 2021), MCCs (ANSELMO et al., 2021; JARAMILLO; POVEDA; MEJÍA, 2017; SALIO; NICOLINI; ZIPSER, 2007), the Pacific and Atlantic SST (WANG et al., 2018), the Bolivian High (FERREIRA et al., 2012; KOUSKY; KAYANO, 1981; LENTERS; COOK, 1997).

The Intertropical Convergence Zone (ITCZ) configures a band of convective clouds extending along the equatorial sector. It constitutes a region where the trade winds from the northern and southern hemispheres converge close to the equator at low levels in the atmosphere. This convergence makes the warm and humid air of the tropics ascend and promotes moisture transport from the ocean to the upper levels, favouring the formation of a cloud band with great vertical development (YNOUE et al., 2017). Thus, ITCZ greatly influences the rainy season of the northern Northeast and the northeastern semiarid (COELHO; GAN; CONFORTE, 2004; TEODORO; REBOITA; ESCOBAR, 2019). ITCZ is a thermally induced low-pressure system since it is positioned over oceanic areas with positive SST anomalies and negative sea level pressure anomalies (HASTENRATH, 1991). The system acts in the North and Northeast Brazil in two ways: through agglomerates of convective clouds that form along with the band and move west, reaching the Amazon Basin, and through the interaction of trade winds with sea breeze circulation, forming instability lines that enter the continent (REBOITA et al., 2010a).

The Bolivian High (BH) is an anticyclonic circulation in the upper troposphere, centred on average over the Bolivian Highlands. Elevated plateaus such as the Bolivian Highlands act as heat sources in the middle troposphere during the summer, and intense storms occur in the vicinity of these uplands (VIRJI, 1981), contributing to rainfall in North and Northeast Brazil (REBOITA et al., 2010a). According to Virji (1981), the latent and sensible heat release to the atmosphere in these regions helps maintain the anticyclone in the upper troposphere during summer. Lenters and Cook (1997) investigated the influence of South American topography on BH formation and concluded that the system forms in response to the precipitation over the Amazon Basin, central Andes, SACZ, and precipitation over Africa. Thus, the BH position is

primarily determined by rainfall in Amazonia, while the topographic effect of the Andes Mountains plays a secondary role in rainfall variability.

The cold fronts also reach North Brazil (MARENGO; NOBRE; CULF, 1997; NETO; SATYAMURTY; CORREIA, 2015), a phenomenon known as “friagens”.

f) – R6 – Northern Brazil and the coast of northeastern Brazil

The R6 comprises northern Brazil and the coast of northeastern Brazil, with maximum rainfall in the first half of the year. Figure 45 shows that although ECMWF-SEAS5 underestimates the rainfall in the region throughout the year, the model simulates the annual cycle appropriately.

The R6 is mainly influenced by the ITCZ's annual displacement (CAVALCANTI, 2015; HASTENRATH, 2006, 2012; HOUNSOU-GBO et al., 2015; KUCHARSKI; POLZIN; HASTENRATH, 2008; MOURA; SHUKLA, 1981; TEODORO; REBOITA; ESCOBAR, 2019; MARENGO et al., 2018; SHIMIZU; ANOCHI; KAYANO, 2021; UTIDA et al., 2019; UVO et al., 1998; WU et al., 2020). ITCZ reaches its southernmost position between austral summer and autumn (between February and April), locating approximately around 4º S, and contributing to the maximum rainfall that occurs in the northern and coastal regions of the Northeast during the first semester of the year (REBOITA et al., 2010a).

The east of R6 can also be affected by other atmospheric systems such as sea and land breezes (ANJOS et al., 2020; KOUSKY, 1980; SOUZA; OYAMA, 2017), frontal systems (ESCOBAR; REBOITA; SOUZA, 2020; FEDOROVA; LEVIT ; DA CRUZ, 2016; KOUSKY, 1979), instability lines (OLIVEIRA; OYAMA, 2019; SILVA DIAS, 1987; SOUSA, 2020), MCCs (SOUSA, 2020), tropical ULCVs (FERREIRA; REBOITA; DA ROCHA, 2019; KOUSKY ; GAN, 1981; MORAIS; GAN; YOSHIDA, 2020; RAMÍREZ; KAYANO; FERREIRA, 1999), and EWDs (GOMES et al., 2015, 2019; SILVA; DA ROCHA; GOMES, 2020; TORRES; FERREIRA, 2011).

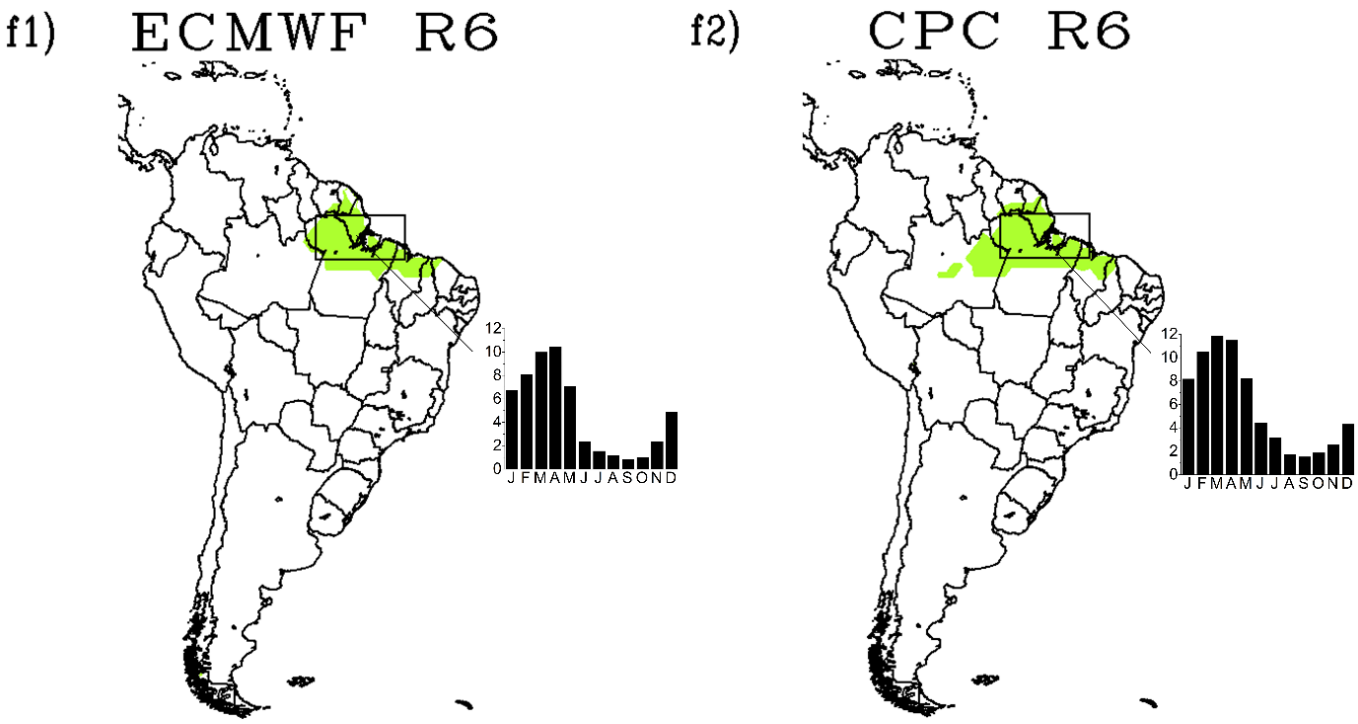

Figure 45 – R6 formed by northern Brazil and the coast of northeastern Brazil and annual precipitation cycle (mm day^{-1}).

ULCVs distinguish from other atmospheric systems by presenting favourable or unfavourable conditions for the occurrence of precipitation (FERREIRA; REBOITA; DA ROCHA, 2019). On the systems' periphery, there are upward movements and the formation of convective clouds. Conversely, there are subsiding movements and inhibition of convective activity. On tropical ULCVs, their development is mainly due to the joint action of BH with the Northeast trough (KOUSKY; GAN, 1981). However, the interaction with the flow of mid-latitudes plays a relevant role in forming the systems (FERREIRA; REBOITA; DA ROCHA, 2019; PAIXÃO; GANDU, 2000).

Easterly wave disturbances (EWDs) are waves that propagate from West Africa to the tropical Atlantic, characterized by disturbances in the trade wind regime, with an average period of 5.5 days and maximum occurrence in the austral winter (GOMES et al. 2019; MACHADO et al., 2009; TORRES; FERREIRA, 2011). When EWDs interact with the local circulation induced by the topography, there can be convergence at low levels and increased precipitation over the east and north coasts of the Northeast (GOMES et al., 2015, 2019).

EWDs are vital as they transport large amounts of moisture to generally dry regions (GOMES et al., 2015, 2019). In this context, the precipitation produced by EWDs can benefit

activities related to agriculture and energy, but it is also responsible for flash floods, landslides in risk areas, erosion and, consequently, several harmful impacts on society and economy (GOMES et al., 2015, 2019; SILVA; DA ROCHA; GOMES, 2020; TORRES; FERREIRA, 2011). EWDs cause rain mainly in the Zona da Mata, which extends from the Recôncavo Baiano to the coast of Rio Grande do Norte State, and, in the centre-north of Ceará, State when atmospheric and oceanic conditions are favourable (FERREIRA; MELO, 2005).

g) – R7 – Brazil's northeastern hinterland

The R7 covers the hinterland of Northeast Brazil, a region with slight total rainfall, between 200 to 500 mm (REBOITA et al., 2010a). Despite systematic underestimation errors in the region, ECMWF-SEAS5 consistently reproduces the annual rainfall cycle in the sector. The northeastern hinterland area presents the minor total rainfall resulting from the subsiding movements of Hadley and Walker cells in the region, whose influence exceeds that of the Borborema Highlands in inhibiting convection in this sector (REBOITA et al., 2016).

The R7 region presents a remarkable interannual rainfall variability, with arid and rainy years (MARENGO et al., 2020, 2021). Such variability is attributed to teleconnection mechanisms such as the SST variation in the tropical Pacific and Atlantic. In addition, during El Niño events, the subsidence cell acting on the region inhibits convective activity over the western tropical Atlantic and reduces precipitation in the Northeast (ANDREOLI; KAYANO, 2007; COSTA et al., 2021; JARDIM et al., 2021; MARENGO et al., 2018; RODRIGUES et al., 2011; RODRIGUES; MCPHADEN, 2014; SHIMIZU; ANOCHI; KAYANO, 2021; UVO et al., 1998).

Furthermore, the southern gradient of SST in the tropical Atlantic affects the latitudinal displacement of the ITCZ, so that the migration of this system induces precipitation in the Northeast (CAVALCANTI, 2015; HOUNSOU-GBO et al., 2015; KUCHARSKI; POLZIN; HASTENRATH, 2008; MARENGO et al., 2018; UTIDA et al., 2019; UVO et al., 1998; WU et al., 2020).

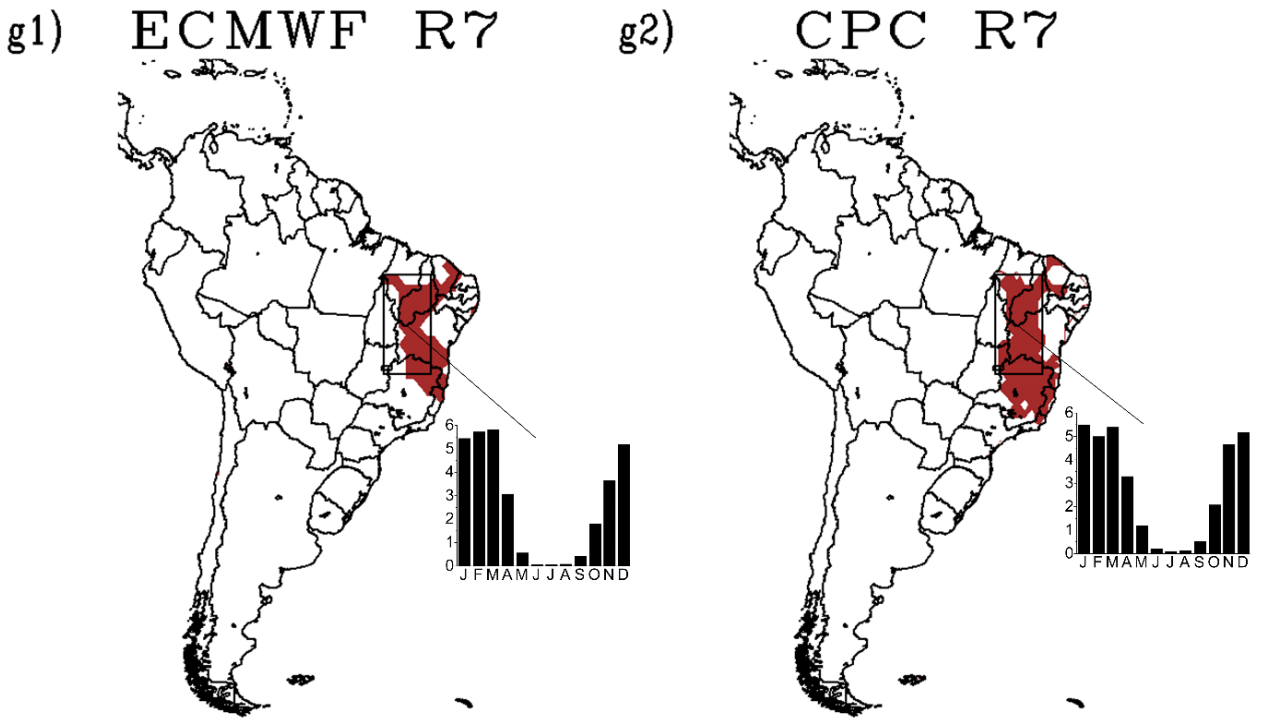

Figure 46 – R7 formed by Brazil's northeastern hinterland and annual precipitation cycle (mm day^{-1}).

h) – R8 – Northern South America

The R8 region covers the north of SA, where rainfall is high throughout the year but has larger values in winter. This behaviour is due to ITCZ acting in its northernmost position, directly influencing R8. Conversely, in summer, when the ITCZ moves to the south, the rainfall in that region is somewhat unfavourable.

In addition to the ITCZ (HOYOS et al., 2018, 2019; SATYAMURTY; ROSA, 2019; URREA; UCHOA; MESA, 2019), eastern waves (RYDBECK; MALONEY; ALAKA JR., 2017), local convection, CCM, breeze circulation (PÉREZ et al., 2018; YEPES et al., 2017) and instability lines are systems that contribute to precipitation in R8.

In summary, Figure 48 schematically illustrates the major synoptic systems for regional circulation over SA.

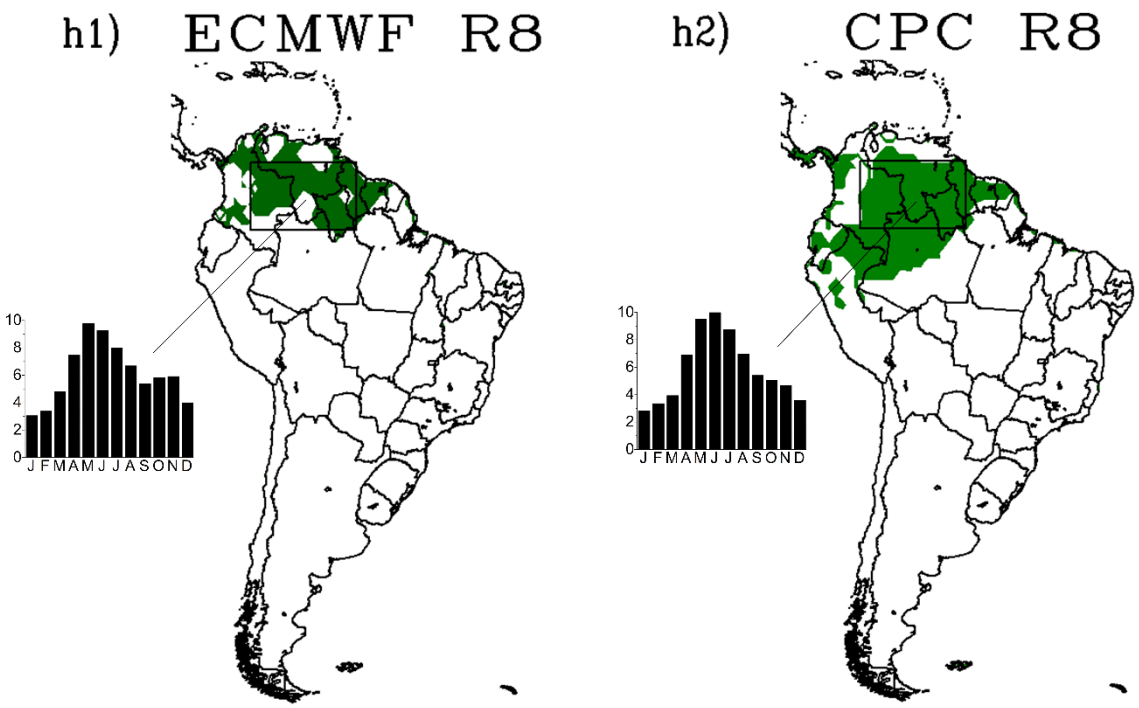

Figure 47 – R8 formed by the north of South America and annual precipitation cycle (mm day^{-1}).

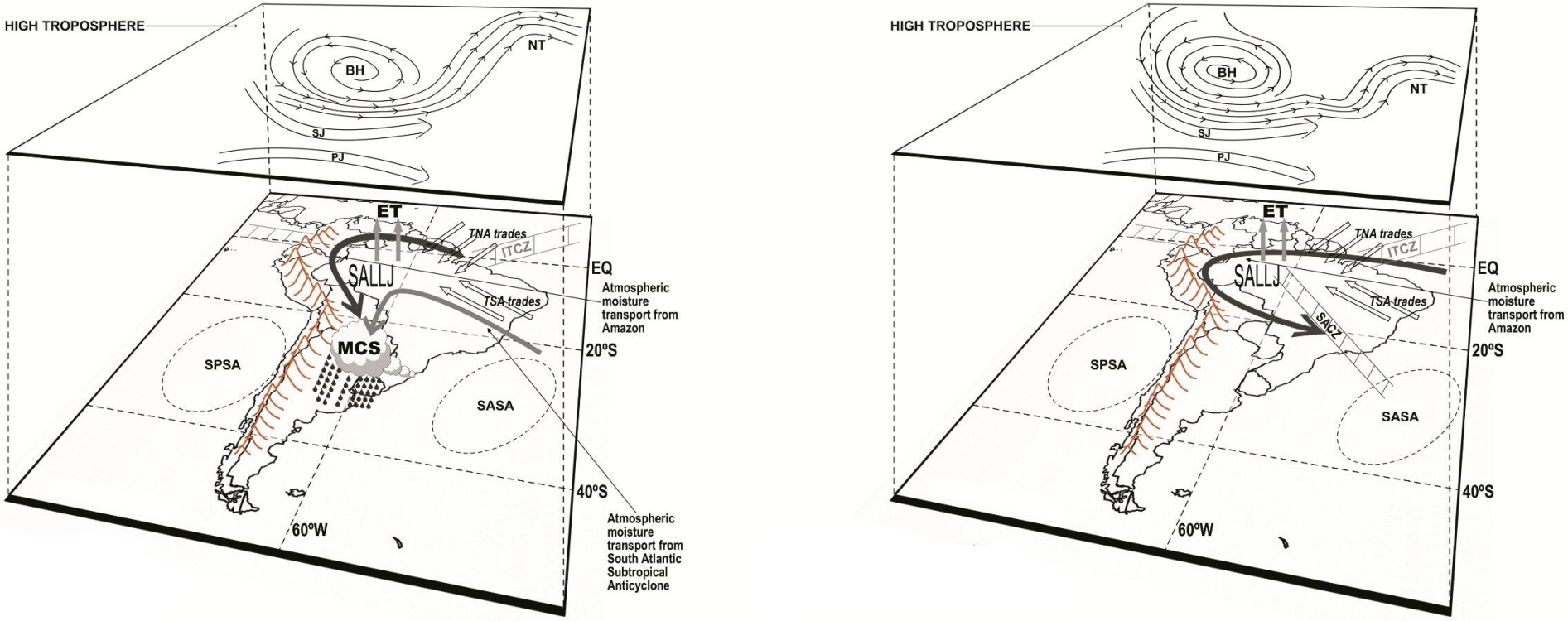

Figure 48 – Schematic sketch of important atmospheric circulation features over the South American region, considering events with (right) and without (left) SACZ. SALLJ = South American Low-Level Jet East of the Andes; TNA trades = Tropical North Atlantic trade winds; TSA trades = Tropical South Atlantic trade winds; ET = evapotranspiration from Amazon forests; MCS = Mesoscale Convective Systems; ITCZ = Intertropical Convergence Zone; SPSA = South Pacific Subtropical Anticyclone; SASA = South Atlantic Subtropical Anticyclone; NT = Northeast Trough; BH = Bolivian High; SJ = Subtropical Jet; PJ = Polar Jet. Adapted from Satyamurty, Nobre and Silva Dias (1998) and Silva, Reboita and Escobar (2019).

7. CONCLUSIONS

The present work aimed to evaluate the quality of seasonal precipitation and 2 m temperature predictions from ECMWF-SEAS5 over South America. Hence, their hindcasts from 1993 to 2016 and forecasts from 2017 to 2020 were validated.

The seasonal mean precipitation forecast fields indicated an appropriate simulation of the seasonal patterns over Brazil, satisfactorily representing the monsoon system and the rainfall variability in the country's interior. Nevertheless, the reforecasts have systematically overestimated rainfall predictions in the Amazon region and South and Southeast Brazil. Conversely, the model also has systematic underestimation errors in predicting rainfall over Northeast Brazil.

The temperature fields indicate that the model has a systematic cold bias over most of South America. However, exceptions occur in NEB and SESA, where the model overestimates the temperature. In general, the cold bias of the model tends to be accentuated in the austral summer months, covering regions with a warm bias such as SESA.

The skill score evaluation showed that the main seasonal correlations of precipitation and temperature anomaly occur in high climate predictability areas such as the more tropical latitudes of North and Northeast Brazil and subtropical latitudes in the continent's south. Furthermore, the temperature skill scores showed that ECMWF-SEAS5 could predict this variable in regions with poor rainfall prediction performance, such as SESA.

Seasonal anomalies of precipitation and temperature predictions were also calculated for South American subdomains. The model showed a competence to simulate the interannual variability of rainfall, especially in transition seasons. However, hindcasts were not efficient in capturing anomalous climate events like the 2013/2014 Southeast Brazil drought, the 1997/1998 drought in Northeast Brazil, and the Eastern Amazon and Northeast Brazil drought in 2015. For temperature, the best simulations were obtained for NEB and NSA, where the model skillfully represented their interannual variability.

Statistical parameters calculated for regionalized seasonal precipitation and temperature mean anomalies indicated considerable variability of metrics between subdomains, among which NEB, SB and NSA indicate the best results for precipitation. However, despite the low

precipitation predictability, the AMZ subdomain performed better concerning the temperature predictions.

Seasonal rainfall predictions from the 2017-2020 set of real-time forecasts were also examined to assess their systematic errors. Biases fields indicated that predictions with overestimated rainfall in the south and Amazon regions persist. Furthermore, systematic underestimates of rainfall predictions in the northeastern sectors remain in the ECMWF-SEAS5 real-time forecasts. Regarding temperature forecasts, systematic underestimates in the South American continent persist, with slight reductions in SEB and NEB and intensification of overestimates in SESA.

Seeking physical explanations for the model errors is beyond the scope of this work. Despite numerous advances and constant development of climate modelling, errors are intrinsic to the process. However, several studies point to different causes for the errors, such as deficiency in SST simulation, errors in the initialization of soil moisture conditions, inappropriate physical parameterization (MA et al., 2021, MEEHL et al., 2021; RISBEY et al., 2021). In this context, the ECMWF-SEAS5 seasonal climate forecasts seek to quantify the associated error by expanding the ensemble.

Finally, it is concluded that the ECMWF-SEAS5 model effectively predicts seasonal precipitation and temperature over South America and has potential application to guide decision-making, provided that its limitations and appropriate conditions for use are observed (such as regions and periods with better performance). Some issues for future ECMWF-SEAS5 studies include:

- analyse the model's performance to predict the onset, demise and duration of the South American Monsoon System;

- analyse the model's performance to predict cold waves on the continent;

- bias correction of the predictions for hydrological purposes;

- probabilistic analysis with upper and lower precipitation quantiles;

- analysis of seasonal SST predictions and their relationship with teleconnection patterns acting on the continent.

REFERENCES

ACEITUNO, P. On the functioning of the Southern Oscillation in the South American sector. Part I: surface climate. **Monthly Weather Review**, v. 116, p. 505-524, 1988.

ACEITUNO, P.; BOISIER, J. P.; GARREAUD, R.; RONDANELLI, R.; RUTLLANT, J. A. Climate and weather in Chile. *In*: FERNÁNDEZ, B..; GIRONÁS, J. **Water Resources of Chile**. Springer, 2021, p. 7–29.

AGUIAR, L. F.; CATALDI, M. Social and environmental vulnerability in Southeast Brazil associated with the South Atlantic Convergence Zone. **Natural Hazards**, v. 109, p. 2423-2437, 2021.

AGUIRRE, C.; FLORES-AQUEVEQUE, V.; VILCHES, P.; VÁSQUEZ, A.; RUTLLANT, J. A.; GARREAUD, R. Recent changes in the low-level jet along the subtropical west coast of South America. **Atmosphere**, v. 12, 465, 2021.

AHRENS, C. D. **Meteorology today – An introduction to weather, climate and the environment**. Belmont: Cengage Learning. 2009, 624 p.

AL-KAYSSI, A. W.; AL-KARAGHOULI, A. A.; HASSON, A. M.; BEKER, S. A. Influence of soil moisture content on soil temperature and heat storage under greenhouse conditions. **Journal of Agricultural Engineering Research**, v. 45, p. 241-252, 1990.

AMBRIZZI, T.; REBOITA, M. S.; DA ROCHA, R. P. LLOPART, M. The state-of-the-art and fundamental aspects of regional climate modeling in South America. **Annals of the New York Academy of Sciences, Special Issue: Climate Sciences**: 1-23, 2018.

AMBRIZZI, T.; SOUZA, E. B.; PULWARTY, R. S. The Hadley and Walker regional circulations and associated ENSO impacts on the South American Seasonal Rainfall. *In*: DIAZ, H. F.; BRADLEY, R. S. **The Hadley Circulation: Present, Past and Future**. Kluwer Academic Publishers, 2004, p. 203–235.

ANCAPICHÚN, S.; GARCÉS-VARGAS, J. Variability of the Southeast Pacific Subtropical Anticyclone and its impact on sea surface temperature off north-central Chile. **Ciencias Marinas**, v. 41, p. 1-20, 2015.

ANDREOLI, R. V.; KAYANO, M. T. A importância relativa do Atlântico tropical sul e Pacífico leste na variabilidade de precipitação do Nordeste do Brasil. **Revista Brasileira de Meteorologia**, v. 22, p. 63-74, 2007.

ANDREOLI, R. V.; KAYANO, M. T.; SILVA, J. V.; OLIVEIRA, S. S.; SOUZA, R. A. F.; GARCIA, S. R.; REGO, W. H. T.; OLIVEIRA, M. B. L. Effects of two different La Niña types on the South American rainfall. **International Journal of Climatology**, v. 39, p. 1415-1428, 2018.

ANDREOLI, R.V.; OLIVEIRA, S. S.; KAYANO, M. T.; VIEGAS, J.; SOUZA, R. A. F.; CANDIDO, L. A. The influence of different El Niño types on the South American rainfall. **International Journal of Climatology**, v. 37, n. 3, p. 1374–1390, 2016.

ANOCHI, J. A.; SILVA, J. D. S. Uso de redes neurais artificiais e teoria de conjuntos aproximativos no estudo de padrões climáticos sazonais. **Learning and Nonlinear Models – Revista da Sociedade Brasileira de Redes Neurais**, v. 7, p. 83-91, 2009.

ANOCHI, J. A.; VELHO, H. F. C. Neural network for seasonal climate precipitation prediction on the Brazil. **Ciência e Natura**, v. 42, 2020.

ANSELMO, E. M.; MACHADO, L. A. T.; SCHUMACHER, C; KILADIS, G. N. Amazonian mesoscale convective systems: life cycle and propagation characteristics. **International Journal of Climatology**, v. 41, p. 3968-3981, 2021.

ARRAUT, J. M.; NOBRE, C.; BARBOSA, H. M. J.; OBREGON, G.; MARENGO, J. Aerial rivers and lakes: looking at large-scale moisture transport and its relation to Amazonia and to subtropical rainfall in South America. **Journal of Climate**, v. 25, p. 543-556, 2012.

ASHFAQ, M.; CAVAZOS, T.; REBOITA, M. S.; TORRES-ALAVEZ, J. A.; IM, E.; OLUSEGUN, C. F.; ALVES, L.; KEY, K.; ADENIYI, M. O.; TALL, M.; SYLLA, M. B.; MEHMOOD, S.; ZAFAR, Q.; DAS, S.; DIALLO, I.; COPPOLA, E.; GIORGI, F. Robust late 21st century shift in regional monsoons in RegCM-CORDEX simulations. **Climate Dynamics**, 2020.

ASSENG, A.; EWERT, F.; MARTRE, P.; RÖTTER, R. P.; LOBELL, D. B.; CAMMARANO, D.; KIMBALL, B. A.; OTTMAN, M. J.; WALL, G. W.; WHITE, J. W.; REYNOLDS, M. P.; ALDERMAN, P. D.; PRASAD, V. V.; AGGARWAL, P. K.; ANOTHAI, J.; BASSO, B.; BIERNATH, C.; CHALLINOR, A. J.; DE SANCTIS, G.; DOLTRA, J.; FERERES, E.; GARCIA-VILA, M.; GAYLER, S.; HOOGENBOOM, G.; HUNT, L. A.; IZAURRALDE, R.

C.; JABLOUN, M.; JONES, C. D.; KERSEBAUM, K. C.; KOEHLER, A. -K.; MÜLLER, C.; KUMAR, S. N.; NENDEL, C.; O'LEARY G.; OLESEN, J. E.; PALOSUO, T.; PRIESACK, E.; EYSHI REZAEI. E.; RUANE, A. C.; SEMENOV, M. A.; SHCHERBAK, I.; STÖCKLE, C.; STRATONOVITCH, P.; STRECK, T.; SUPIT, I.; TAO, F.; THORBURN, P. J.; WAHA, K.; WANG, E.; WALLACH, D.; WOLF, J.; ZHAO, Z.; ZHU, Y. Rising temperatures reduce global wheat production. **Nature Climate Change**, 2014.

BAGLEY, J. E.; DESAI, A. R.; HARDING, K. J.; SNYDER, P. K.; FOLEY, J. A. Drought and deforestation: has land cover change influenced recent precipitation extremes in the Amazon? **Journal of Climate**, v. 27, p. 345-361, 2014.

BARNSTON, A. G.; TIPPETT, M. K.; L'HEUREUX, M. L.; LI, S.; DE WITT, D. G. Skill of real-time seasonal ENSO model predictions during 2002-2011 – Is our capability increasing? **Bulletin of the American Meteorological Society**, v. 93, n. 5, p. 631-651, 2012.

BARRETT, B. S.; HAMEED, S. Seasonal variability in precipitation in central and southern Chile: modulation by the South Pacific High. **Journal of Climate**, v. 30, p. 55-69, 2017.

BECHTOLD, P.; KÖHLER, M.; JUNG, T.; DOBLAS-REYES, F.; LEUTBECHER, M.; RODWELL, M. J.; VITART, F.; BALSAMO, G. Advances in simulating atmospheric variability with the ECMWF model: from synoptic to decadal time-scales. **Quarterly Journal of the Royal Meteorological Society**, v. 134, p. 1337-1351, 2008.

BECHTOLD, P.; SEMANE, N.; LOPEZ, P.; CHABOUREAU, J. -P.; BELJAARS, A.; BORMANN, N. Representing equilibrium and nonequilibrium convection in large-scale models. **Journal of the Atmospheric Sciences**, v. 71, p. 734-753, 2014.

BELLENGER, H.; GUILYARDI, E.; LELOUP, J.; LENGAIGNE, M.; VIALARD, J. ENSO representation in climate models: from CMIP3 to CMIP5. **Climate Dynamics**, v. 42, p. 1999-2018, 2014.

BERGMAN, D. L.; MAGNUSSON, L.; NILSSON, J.; VITART, F. Seasonal forecasting of tropical cyclone landfall using ECMWF's System 4. **Weather and Forecasting**, v. 34, p. 1239-1255, 2019.

BERRI, G. J.; BIANCHI, E.; MÜLLER, G. V. El Niño and La Niña influence on mean river flows of southern South America in the 20th century. **Hydrological Sciences Journal**, v. 64, n. 8, p. 900-909, 2019.

BLÁZQUEZ, J.; SOLMAN, S. A. Interannual variability of the frontal activity in the Southern Hemisphere: relationship with atmospheric circulation and precipitation over southern South America. **Climate Dynamics**, v. 48, p. 2569-2579, 2017.

BÖHM, C.; REYERS, M.; SCHWEEN, J. H.; CREWELL, S. Water vapor variability in the Atacama Desert during the 20th century. **Global and Planetary Change**, v. 190, 103192, 2020.

BOMBARDI, R. J.; CARVALHO, L. M. V.; JONES, C.; REBOITA, M. S. Precipitation over eastern South America and the South Atlantic sea surface temperature during neutral ENSO periods. **Climate Dynamics**, v. 42, p. 1553-1568, 2014.

BORGES, P. A.; BERNHOFER, C.; RODRIGUES, R. Extreme rainfall indices in Distrito Federal, Brazil: trends and links with El Niño southern oscillation and Madden-Julian oscillation. **International Journal of Climatology**, v. 38, p. 4550-4567, 2018.

BRANKOVIĆ, Č.; PALMER, T. N. Atmospheric seasonal predictability and estimates of ensemble size. **Monthly Weather Review**, v. 125, n. 5, p. 859-874, 1997.

BRANKOVIĆ, Č.; PALMER, T. N.; FERRANTI, L. Predictability of seasonal atmospheric variations. **Journal of Climate**, v. 7, n. 5, p. 217-237, 1994.

BUENO, N. M. M.; JADOSKI, S. O.; LIMA, V. A.; BUENO, J. C. M. El Niño-Oscilação Sul e ocorrência de geadas na região de Guarapuava – PR. **Research, Society and Development**, v. 9, e689119596, 2020.

CAI, W.; MCPHADEN, M. J.; GRIMM, A. M.; RODRIGUES, R. R.; TASCHETTO, A. S.; GARREAUD, R. D.; DE WITTE, B.; POVEDA, G.; HAM, Y. -G.; SANTOSO, A.; NG, B.; ANDERSON, W.; WANG, G.; GENG, T.; JO, H. -S.; MARENGO, J. A.; ALVES, L. M.; OSMAN, M.; LI, S.; WU, L.; KARAMPERIDOU, C.; TAKAHASHI, K.; VERA, C. Climate impacts of the El Niño-Southern Oscillation on South America. **Nature Reviews Earth & Environment,** v. 1, p. 215-231, 2020.

CAMPETELLA, C. M.; POSSIA, N. E. Upper-level cut-off lows in southern South America. **Meteorology and Atmospheric Physics**, v. 96, p. 181-191, 2007.

CAMPOS, C. R. J.; EICHHOLZ, C. W. Características físicas dos sistemas convectivos de mesoescala que afetaram o Rio Grande do Sul no período de 2004 a 2008. **Revista Brasileira de Geofísica**, v. 29, p. 331-345, 2011.

CARDOZO, A. B.; REBOITA, M. S.; GARCIA, S. R. Climatologia de frentes frias na América do Sul e sua relação com o Modo Anular Sul. **Revista Brasileira de Climatologia**, v. 17, p. 9-26, 2015.

CARPENEDO, C. B.; AMBRIZZI, T. Anticiclone subtropical do Atlântico Sul associado ao Modo Anular Sul e impactos climáticos no Brasil. **Revista Brasileira de Meteorologia**, v. 35, p. 605-613, 2020.

CARVALHO, L. M. V.; JONES, C.; LIEBMANN, B. The South Atlantic Convergence Zone: intensity, form, persistence, and relationships with intraseasonal to interannual activity and extreme rainfall. **Journal of Climate**, v. 17, p. 88-108, 2004.

CASTANEDA-GONZALEZ, M.; POULIN, A.; ROMERO-LOPEZ, R.; ARSENAULT, R.; BRISSETTE, F.; CHAUMONT, D.; PAQUIN, D. Impacts of regional climate model spatial resolution on summer flood simulation. **EPiC Series in Engineering**, v. 3, p. 372-380, 2018.

CAVALCANTI, I. F. A. Large scale and synoptic features associated with extreme precipitation over South America: a review and case studies for the first decade of the 21st century. **Atmospheric Research**, v. 118, p. 27-40, 2012.

CAVALCANTI, I. F. A. The influence of extratropical Atlantic ocean region on wet and dry years in North-Northeastern Brazil. **Frontiers in Environmental Science**, v. 3, 2015.

CAVALCANTI, I. F. A.; KOUSKY, V. E. Frentes frias sobre o Brasil. *In*: CAVALCANTI, I. F. A.; FERREIRA, N. J.; SILVA, M. G. A. J.; SILVA DIAS, M. A. F. **Tempo e Clima no Brasil**. São Paulo: Oficina de Textos, 2009, p. 135-147.

CAVALCANTI, I. F. A.; MARENGO, J. A.; SATYAMURTY, P.; NOBRE, C. A.; TROSNIKOV, I.; BONATTI, J. P.; MANZI, A. O.; TARASOVA, T.; PEZZI, L. P.; D'ALMEIDA, C.; SAMPAIO, G.; CASTRO, C. C.; SANCHES, M. B.; CAMARGO, H. Global climatological features in a simulation using the CPTEC-COLA AGCM. **Journal of Climate**, v. 15. N. 21, p. 2965-2988, 2002.

CEGLAR, A., TORETI, A.; PRODHOMME, C.; ZAMPIERI, M.; TURCO, M.; DOBLAS-REYES, F. J. Land-surface initialization improves seasonal climate prediction skill for maize yield forecast. **Scientific Reports**, v. 8, n. 1322, 2018.

Centro de Estudos Avançados em Economia Aplicada – CEPEA-USP-CNA, 2020. PIB do Agronegócio: 1995–2019. Disponível em: http://cepea.esalq.usp.br/pib/

CHARLES, A.; TIMBAL, B.; FERNANDEZ, E.; HENDON, H. Analogue downscaling of seasonal rainfall forecasts in the Murray Darling basin. **Monthly Weather Review**, v. 141, p. 1099-1117, 2013.

CHARNEY, J. G.; SHUKLA, J. Predictability of monsoons. *In*: LIGHTHILL, J.; PEARCE, R. **Monsoon Dynamics**. Cambridge: Cambridge University Press, 1981, p. 99-109.

CHEN, H.; SUN, J.; WANG, H. A statistical downscaling model for forecasting summer rainfall in China from DEMETER hindcast datasets. **Weather and Forecasting**, v. 27, p. 608-628, 2012.

CHEN, M.; SHI, W.; XIE, P.; SILVA, V. B. S.; KOUSKY, V. E.; HIGGINS, R. W.; JANOWIAK, J. E. Assessing objective techniques for gauge-based analyses of global daily precipitation. **Journal of Geophysical Research**, v. 113, D04110, 2008.

CHEN, Y.; RANDERSON, J. T.; MORTON, D. C.; DEFRIES, R. S.; COLLATZ, J.; KASIBHATLA, P. S.; GIGLIO, L.; JIN, Y.; MARLIER, M. E. Forecasting fire season severity in South America using sea surface temperature anomalies. **Science**, v. 334, p. 787-791, 2011.

CHEN, Y.; RANDERSON, J. T.; COFFIELD, S. R.; FOUFOULA-GEORGIOU, E.; SMYTH, P.; GRAFF, C. A.; MORTON, D. C.; ANDELA, N.; VAN DER WERF, G. R.; GIGLIO, L.; OTT, L. E. Forecasting global fire emissions on subseasonal to seasonal (S2S) time scales. **Journal of Advances in Modelling Earth Systems**, v. 12, 2020.

CHOU, S. C.; BUSTAMANTE, J. F.; GOMES, J. L. Evaluation of Eta Model seasonal precipitation forecasts over South America. **Nonlinear Processes in Geophysics**, v. 12, p. 537-555, 2005.

CHOU, S. C.; DERECZYNSKI, C.; GOMES, J. L.; PESQUERO, J. F.; AVILA, A. M. H.; RESENDE, N. C.; ALVEZ, L. P.; RUIZ-CÁRDENAS, R.; SOUZA, C. R..; BUSTAMANTE, J. F. Ten-year seasonal climate reforecasts over South America using the Eta regional climate model. **Anais da Academia Brasileira de Ciências**, v. 92, n. 3, 2020.

CIRINO, P. H.; FÉRES, J. G.; BRAGA, M. J.; REIS, E. Assessing the impacts of ENSO-related weather effects on the Brazilian agriculture. **Procedia Economics and Finance**, v. 24, p. 146-155, 2015.

CLARK, R. T.; BETT, P. E.; THORNTON, H. E.; SCAIFE, A. A. Skillful seasonal predictions for the European energy industry. **Environmental Research Letters**, v. 12, 2017.

COELHO, C. A. S.; CAVALCANTI, I. F. A.; COSTA, S. M. S.; FREITAS, S. R.; ITO, E. R.; LUZ, G.; SANTOS, A. F.; NOBRE, C. A.; MARENGO, J. A.; PEZZA, A. B. Climate diagnostics of three major drought events in the Amazon and illustrations of their seasonal precipitation predictions. **Meteorological Applications**, v. 19, p. 237-255, 2012.

COELHO, C. A. S.; DRUMOND, A. R. M.; AMBRIZZI, T. Estudo climatológico sazonal da precipitação sobre o Brasil em episódios extremos da Oscilação Sul. **Revista Brasileira de Meteorologia**, v. 14, n. 1, p. 49-65, 1999.

COELHO, C. A. S.; OLIVEIRA, C. P.; AMBRIZZI, T.; REBOITA, M. S.; CARPENEDO, C. B.; CAMPOS, J. L. P. S.; TOMAZIELLO, A. C. N.; PAMPUCH, L. A.; CUSTÓDIO, M. S.; DUTRA, L. M. M.; DA ROCHA, R. P.; REHBEIN, A. The 2014 southeast Brazil austral summer drought: regional scale mechanisms and teleconnections. **Climate Dynamics**, v. 46, p. 3737-3752, 2016.

COELHO, C. A. S.; STEPHENSON, D. B.; DOBLAS-REYES, F. J.; BALSAMEDA, M. The skill of empirical and combined/calibrated coupled multi-model South American seasonal predictions during ENSO. **Advances in Geosciences**, v. 6, p. 51-55, 2006a.

COELHO, C. A. S.; STEPHENSON, D. B.; BALSAMEDA, M.; DOBLAS-REYES, F. J.; VAN OLDENBORGH, G. J. Toward an integrated seasonal forecasting system for South America. **Journal of Climate**, v. 19, p. 3704-3721, 2006b.

COELHO, C. A. S.; UVO, C. B.; AMBRIZZI, T. Exploring the impacts of the tropical Pacific SST on the precipitation patterns over South America during ENSO. **Theoretical and Applied Climatology**, v. 71, p. 185-197, 2002.

COELHO, M. S.; GAN, M. A.; CONFORTE, J. C. Estudo da variabilidade da posição e da nebulosidade associada à ZCIT do Atlântico, durante a estação chuvosa de 1998 a 1999 no Nordeste do Brasil. **Revista Brasileira de Meteorologia**, v. 19, p. 23-34, 2004.

COHEN, J. C. P.; SILVA DIAS, M. A. F.; NOBRE, C. A. Environmental conditions associated with Amazonian squall lines: a case study. **Monthly Weather Review**, v. 123, p. 3163-3174, 1995.

COHEN, J.; CAVALCANTI, I. F. A; BRAGA, R. H. M.; NETO, L. S. Linhas de instabilidade na costa norte-nordeste da América do Sul. *In*: CAVALCANTI, I. F. A.; FERREIRA, N. J.; SILVA, M. G. A. J.; SILVA DIAS, M. A. F. **Tempo e Clima no Brasil**. São Paulo: Oficina de Textos, 2009, p. 75-93.

CÓRDOBA-MACHADO, S.; PALOMINO-LEMUS, R.; GÁMIZ-FORTIS, S. R.; CASTRO-DÍEZ, Y.; ESTEBAN-PARRA, M. J. Influence of tropical Pacific SST on seasonal precipitation in Colombia: prediction using El Niño and El Niño Modoki. **Climate Dynamics**, v. 44, p. 1293-1310, 2015.

COSTA, M. S.; OLIVEIRA-JÚNIOR, J. F.; SANTOS, P. J.; CORREIA FILHO, W. L. F.; GOIS, G.; BLANCO, C. J. C.; TEODORO, P. E.; SILVA JÚNIOR, C. A.; SANTIAGO, D. B.; SOUZA, E. O.; JARDIM, A. M. R. F. Rainfall extremes and drought in Northeast-Brazil and its relationship with El Niño-Southern Oscillation. **International Journal of Climatology**, v. 41, p. E2111-E2135, 2021.

CRESPO, N. M.; DA ROCHA, R. P.; SPRENGER, M.; WERNLI, H. A potential vorticity perspective on cyclogenesis over center-eastern South America. **International Journal of Climatology**, v. 41, p. 663-678, 2021.

DA ROCHA, R. P.; CUADRA, S. V.; REBOITA, M. S.; KRUGER, L. F.; AMBRIZZI, T.; KRUSCHE, N. Effects of RegCM3 parameterizations on simulated rainy season over South America. **Climate Research**, v. 52, ´. 253-265, 2012.

DA ROCHA, R. P.; REBOITA, M. S.; GOZZO, L. F.; DUTRA, L. M. M.; DE JESUS, E. M. Subtropical cyclones over the oceanic basins: a review. **Annals of the New York Academy of Sciences**, v. 1436, p. 138-156, 2018.

DE JESUS, E. M.; DA ROCHA, R. P.; CRESPO, N. M.; REBOITA, M. S.; GOZZO, L. P. Multi-model climate projections of the main cyclogenesis hot-spots and associated winds over the eastern coast of South America. **Climate Dynamics**, v. 56, p. 537-557, 2021.

DE JESUS, E. M.; DA ROCHA, R. P.; REBOITA, M. S.; LLOPART, M.; DUTRA, L. M. M.; REMEDIO, A. R. C. Contribution of cold fronts to seasonal rainfall in simulations over the southern La Plata Basin. **Climate Research**, v. 68, p. 243-255, 2016.

DELSOLE, T.; SHUKLA, J. Model fidelity versus skill in seasonal forecasting. **Journal of Climate**, v. 23, p. 4794-4806, 2010.

DIAS, C. G.; REBOITA, M. S.; DUTRA, L. M. M.; DA ROCHA, R. P. Destreza de dois modelos climáticos globais em prever a circulação geral da atmosfera. **Revista Brasileira de Geografia Física**, v. 10, p. 1090-1099, 2017.

DIAS PINTO, J. R.; DA ROCHA, R. P. The energy cicle and structural Evolution of cyclones over southeastern South America in three case studies. **Journal of Geophysical Research**, v. 116, D14112, 2011.

DIAS PINTO, J. R.; REBOITA, M. S.; DA ROCHA, R. P. Synoptic and dynamical analysis of subtropical cyclone Anita (2010) and its potential for tropical transition over the South Atlantic ocean. **Journal of Geophysical Research**, v. 118, p. 10870-10883, 2013.

DICKINSON, R. E.; ERRICO, R. M.; GIORGI, F.; BATES, G. T. A regional climate model for the western United States. **Climatic Change**, v. 15, p. 383-422, 1989.

DIRMEYER, P. A. Characteristics of the water cycle and land-atmosphere interactions from a comprehensive reforecast and reanalysis data set: CFSv2. **Climate Dynamics**, v. 41, p. 1083-1097, 2013.

DIRMEYER, P. A.; HALDER, S. Application of the land-atmosphere coupling paradigm to the operational Coupled Forecast System, version 2 (CFSv2). **Journal of Hydrometeorology**, v. 18, p. 85-108, 2017.

DOBLAS-REYES, F. J.; GARCÍA-SERRANO, J.; LIENERT, F.; BIESCAS, A. P.; RODRIGUES, L. R. L. Seasonal climate predictability and forecasting: status and prospects. **WIREs Climate Change**, v. 4, p. 245-268, 2013.

DOYLE, M. E. Observed and simulated changes in precipitation seasonality in Argentina. **International Journal of Climatology**, v. 40, p. 1716-1737, 2019. January-February-March season 2022

DROSDOWSKY, W.; CHAMBERS, L. E. Near-global sea surface temperature anomalies as predictors of Australian seasonal rainfall. **Journal of Climate**, v. 14, p. 1677-1687, 2001.

DU, Y.; XIE, S-P.; YANG, Y-L.; ZHENG, X-T.; LIU, L.; HUANG, G. Indian Ocean variability in the CMIP5 multimodel ensemble: the basin mode. **Journal of Climate**, v. 26, p. 7240-7266, 2013

DURKEE, J. D.; MOTE, T. L. A climatology of warm-season mesoscale convective complexes in subtropical South America. **International Journal of Climatology**, v. 30, p. 418-431, 2010.

DURKEE, J. D.; MOTE, T. L.; SHEPERD, J. M. The contribution of mesoscale convective complexes to rainfall across subtropical South America. **Journal of Climate**, v. 22, p. 4590-4605, 2009.

EASTERLING, W. E.; MJELDE, J. W. The importance of seasonal climate prediction lead time in agricultural decision making. **Agricultural and Forest Meteorology**, v. 40, p. 37-50, 1987.

EICHHOLZ, C. W.; CAMPOS, C. R. J. Características físicas dos sistemas convectivos de mesoescala que afetaram o Rio Grande do Sul em 2006. **Anuário do Instituto de Geociências**, v. 37, p. 70-80, 2014.

ESCOBAR, G. C. J.; REBOITA, M. S. Relationship between daily atmospheric circulation patterns and South Atlantic Convergence Zone (SACZ) events. **Atmósfera**, 2020.

ESCOBAR, G. C. J.; REBOITA, M. S.; SOUZA, A. Climatology of surface baroclinic zones in the coast of Brazil. **Atmósfera**, v. 32, p. 129-141, 2019.

ESPINOZA, J. C.; GARREAUD, R.; POVEDA, G.; ARIAS, P. A.; MOLINA-CARPIO, J.; MASIOKAS, M.; VIALE, M.; SCAFF, L. Hydroclimate of the Andes part I: main climatic features. **Fronters in Earth Science**, v. 8, 64, 2020.

European Centre for Medium-Range Weather Forecasts System 5 (ECMWF SEAS5) User Guide. 2017.

European Centre for Medium-Range Weather Forecasts (ECMWF). Seasonal Forecasts Daily Data on Single Levels Documentation. 2020.

EMANUEL, K. F.; FONDRIEST, F.; KOSSIN, J. Potential economic value of seasonal hurricane forecasts. **Weather, Climate and Society**, v. 4, p. 110-117, 2012.

FAHAD, A. A.; BURLS, N. J.; SWENSON, E. T.; STRAUS, D. M. The influence of South Pacific Convergence Zone heating on the South Pacific Subtropical Anticyclone and Southern Hemisphere storm tracks. **Journal of Climate**, v. 34, p. 3787-3798, 2021.

FEDOROVA, N.; LEVIT, V.; DA CRUZ, C. D. On frontal zones analysis in the tropical region of the Northeast Brazil. **Pure and Applied Geophysics**, v. 173, p. 1403-1421, 2016.

FENG, P.; WANG, B.; LIU, D. L.; JI, F.; NIU, X.; RUAN, H.; SHI, L.; YU, Q. Machine learning-based integration of large-scale climate drivers can improve the forecast of seasonal rainfall probability in Australia. **Environmental Research Letters**, v. 15, 084051, 2020.

FERNANDES, L. G.; RODRIGUES, R. R. Changes in the patterns of extreme rainfall events in southern Brazil. **International Journal of Climatology**, v. 38, p. 1337-1352, 2017.

FERREIRA, A. G.; MELLO, N. G. S. Principais sistemas atmosféricos atuantes sobre a região Nordeste do Brasil e a influência dos oceanos Pacífico e Atlântico no clima da região. **Revista Brasileira de Climatologia**, v. 1, p. 15-28, 2005.

FERREIRA, G. W. S.; REBOITA, M. S.; DA ROCHA, R. P. Vórtices ciclônicos de altos níveis nas cercanias do Nordeste do Brasil: climatologia e análise da vorticidade potencial isentrópica. **Anuário do Instituto de Geociências**, v. 42, p. 568-585, 2019.

FERREIRA, W. R. S.; VITORINO, M. I.; SOUZA, E. B.; CARMO, A. M. C. Sazonalidade da precipitação para a Amazônia usando o modelo RegCM3: avaliando apenas a forçante do Atlântico equatorial. **Revista Brasileira de Meteorologia**, v. 27, p. 435-446, 2012.

FLORES-AQUEVEQUE, V.; ROJAS, M.; AGUIRRE, C.; ARIAS, P. A.; GONZÁLEZ, C. South Pacific Subtropical High from late Holocene to the end of the 21st century: insights from climate proxies and general circulation models. **Climate of the Past**, v. 16, p. 79-99, 2020.

FOSS, M.; CHOU, S. C.; SELUCHI, M. E. Interaction of cold fronts with the Brazilian Plateau: a climatological analysis. **International Journal of Climatology**, v. 37, p. 3644-3569, 2016.

FREDERIKSEN, C. S.; ZHANG, H.; BALGOVIND, R. C.; NEVILLE, N.; DROSDOWSKY, W.; CHAMBERS, L. Dynamical seasonal forecasts during the 1997/98 ENSO using persisted SST anomalies. **Journal of Climate**, v. 14, p. 2675-2695, 2001.

FREITAS, I. G. F.; GOMES, H. B.; MARIANO, G. L.; SILVA, M. C. L.; LYRA, M. J. A.; NOVA, T. S. V.; SILVA, F. D. S.; RIBEIRO, L. E.; OLIVEIRA, C. P. Downscaling dinâmico através do modelo RegCM para diferentes inicializações utilizando dados do CFSv2. **Revista Brasileira de Meteorologia,** 2020.

FRÍAS, M. D.; HERRERA, S.; COFIÑO, A. S.; GUTIÉRREZ, J. M. Assessing the skill of precipitation and temperature seasonal forecasts in Spain: windows of opportunity related to ENSO events. **Journal of Climate**, v. 23, p. 209-220, 2010.

GAN, M. A.; KOUSKY, V. E.; ROPELEWSKI, C. F. The South America Monsoon circulation and its relationship to rainfall over West-Central Brazil. **Journal of Climate**, v. 17, p. 47-66, 2004.

GAN, M. A.; RAO, V. B. Surface cyclogenesis over South America. **Monthly Weather Review**, v. 119, p. 1293-1302, 1991.

GARBARINI, E.; SKANSI, M. M.; GONZALEZ, M. H.; ROLLA, A. ENSO influence over precipitation in Argentina. *In*: DANIELS, J. A. **Advances in Environmental Research**. Nova Science Publisher, 2016, p. 223-246.

GARREAUD, R. D.; MUÑOZ, R. C. The low-level jet off the west coast of subtropical South America structure and variability. **Monthly Weather Review**, v. 133, p. 2246-2261, 2005.

GIORGI, F. Simulation of regional climate using a limited area model nested in a general circulation model. **Journal of Climate**, v. 3, p. 941-963, 1990.

GIORGI, F. Thirty years of regional climate modeling: where are we and where are we going next: **Journal of Geophysical Research: Atmospheres**, v. 124, p. 5696-5723, 2019.

GIORGI, F.; BATES, G. T. The climatological skill of a regional model over complex terrain. **Monthly Weather Review**, v. 117, p. 2325-2347, 1989.

GIORGI, F.; MEARNS, L. O. Introduction to special section: regional climate modeling revisited. **Journal of Geophysical Research**, v. 104, p. 6335-6352, 1999.

GODDARD, L.; KUMAR, A.; SOLOMON, A.; SMITH, D.; BOER, G.; GONZALEZ, P.; KHARIN, V.; MERRYFIELD, W.; DESER, C.; MASON, S. J.; KIRTMAN, B. P.; MSADEK, R.; SUTTON, R.; HAWKINS, E.; FRICKER, T.; HEGERI, G.; FERRO, C. A. T.; STEPHENSON, D. B.; MEEHL, G. A.; STOCKDALE, T.; BURGMAN, R.; GREENE, A. M.; KUSHNIR, .; NEWMAN, M.; CARTON, J.; FUKUMORI, I.; DELWORTH, T. A verification framework for interannual-to-decadal predictions experiments. **Climate Dynamics**, v. 40, p. 245-272.

GOMES, H. B.; AMBRIZZI, T.; HERDIES, D. L.; HODGES K.; SILVA, B. F. P. Easterly waves disturbances over Northeast Brazil: an observational analysis. **Advances in Meteorology**, v. 2015, 176238, 2015.

GOMES, H. B.; AMBRIZZI, T.; SILVA, B. F. P.; HODGES, K.; SILVA DIAS, P. L.; HERDIES, D. L.; SILVA, M. C. L.; GOMES, H. B. Climatology of easterly waves disturbances over the tropical South Atlantic. **Climate Dynamics**, v. 53, p. 1393-1411, 2019.

GONZÁLEZ, M. H.; VERA, C. S. On the interannual wintertime rainfall variability in the Southern Andes. **International Journal of Climatology**, v. 30, p. 643-657, 2010.

GONZÁLEZ-PINILLA, F. J.; LATORRE, C.; ROJAS, M.; HOUSTON, J.; ROCUANT, M. I.; MALDONADO, A.; CALOGERO, M. S.; QUADE, J.; BETANCOURT, J. L. High-and-low

latitude forcings drive Atacama Desert rainfall variations over the past 16000 years. **Science Advances**, v. 7, eabg1333, 2021.

GOZZO, L. F.; DA ROCHA, R. P.; REBOITA, M. S.; SUGAHARA, S. Subtropical cyclones over the Southwestern South Atlantic: climatological aspects and case study. **Journal of Climate**, v. 27, p. 8543-8562, 2014.

GREATREX, H. **The application of seasonal rainfall forecasts and satellite rainfall estimates to seasonal crop yield forecasting for Africa**. 2012. Thesis of Meteorology – University of Reading, Reading, 2012.

GREZ, P. W.; AGUIRRE, C.; FARÍAS, L.; CONRTRERAS-LÓPEZ, M.; MASOTTI, I. Evidence of climate-driven changes on atmospheric hydrological, and oceanographic variables along the Chilean coastal zone. **Climatic Change**, v. 163, 633-652, 2020.

GRIMM, A. M. The El Niño impact on the summer monsoon in Brazil: regional processes versus remote influences. **Journal of Climate**, v. 16, p. 263-280, 2003.

GRIMM, A. M. Interannual climate variability in South America: impacts on seasonal precipitation, extreme events and possible effects of climate change. **Stochastic Environmental Research and Risk Assessment**, v. 25, p. 537-554, 2011.

GRIMM, A. M. South American Monsoon and its extremes. *In*: VENUGOPAL, V.; SUKHATME, J.; MURTUGUDDE, R.; ROCA, R. Tropical Extremes – Natural Variability and Trends. Elsevier, 2019, p. 51-93.

GRIMM, A. M.; ALMEIDA, A. S.; BENETI, C. A. A.; LEITE, E. A. The combined effect of climate oscillations in producing extremes: the 2020 drought in southern Brazil. **Revista Brasileira de Recursos Hídricos**, v. 25, e48, 2020.

GRIMM, A. M.; BARROS, V. R.; DOYLE, M. E. Climate variability in Southern South America associated with El Niño and La Niña events. **Journal of Climate**, v. 13, p. 35-58, 2000.

GRIMM, A. M.; FERRAZ, S. E. T.; GOMES, J. Precipitation anomalies in Southern Brazil associated with El Niño and La Niña events. **Journal of Climate**, v. 11, p. 2863-2880, 1998.

GRIMM, A. M.; SABOIA, J. P. J.; Interdecadal variability of the South American precipitation in the monsoon system. **Journal of Climate**, v. 28, p. 755-775, 2015.

GRIMM, A. M.; TEDESCHI, R. ENSO and extreme rainfall events in South America. **Journal of Climate**, v. 22, p. 1589-1609, 2009.

GUBLER, S.; SEDLMEIER, K.; BHEND, J.; AVALOS, G.; COELHO, C. A. S.; ESCAJADILLO, Y.; JACQUES-COPER, M.; MARTINEZ, R.; SCHWIERZ, C.; DE SKANSI, M.; SPIRIG, C. Assessment of ECMWF-SEAS5 seasonal forecast performance over South America. **Weather and Forecasting**, v. 35, p. 561-584, 2020.

GUDMUNDSSON, L.; REGO, F. C.; ROCHA, M. SENEVIRATNE, S. I. Predicting above normal wildfire activity southern Europe as a function of meteorological drought. **Environmental Research Letters**, v. 9, 2014.

GUPTA, H. V.; KLING, H.; YILMAZ, K. K.; MARTINEZ, G. F. Decomposition of the mean squared error and NSE performance criteria: implications for improving hydrological modeling. **Journal of Hydrology**, v. 377, 2009.

HALDER, S.; DIRMEYER, P. A.; MARX, L.; KINTER, J. L. Impact of land surface initialization and land-atmosphere coupling on the prediction of the Indian summer monsoon with the CFSv2. **Frontiers in Environmental Science**, v. 5, p. 1-19, 2018.

HAM, Y-G.; KUG, J-S. How well do climate models simulate two types of El Niño? **Climate Dynamics**, v. 39, p. 383-398, 2012.

HAMILL, T. M. Verification of TIGGE multimodel and ECMWF reforecast-calibrated probabilistic precipitation forecasts over the contiguous United States. **Monthly Weather Review,** v. 140, p. 2232-2252, 2012.

HAO, Z.; SINGH, V. P.; XIA, Y. Seasonal drought prediction: advances, challenges, and future prospects. **Reviews of Geophysics**, v. 56, p. 108-141, 2018.

HARTMANN, D. L. **Global physical climatology**. New York: Academic Press, 1994, 411 p.

HARTMANN, H. C.; PAGANO, T. C.; SOROOSHIAN, S.; BALES, R. Confidence builders: evaluating seasonal climate forecasts from user perspectives. **Bulletin of the American Meteorological Society**, v. 83, p. 683-698, 2002.

HASTENRATH, S. **Climate dynamics of the tropics**. Dordrecht: Kluwer Academic Publishers, 1991, 488 p.

HASTENRATH, S. Circulation and teleconnection mechanisms of Northeast Brazil droughts. **Progress in Oceanography**, v. 70, p. 407-415, 2006.

HASTENRATH, S. Exploring the climate problems of Brazil's Nordeste: a review. **Climatic Change**, v. 112, p. 243-251, 2012.

HASTENRATH, S.; GREISCHAR, L. Further work on the prediction of Northeast Brazil anomalies. **Journal of Climate**, v. 6, p. 743-758, 1993.

HASTENRATH, S.; GREISCHAR, L.; VAN HEERDEN, J. Prediction of the summer rainfall over South Africa. **Journal of Climate**, v. 8, p. 1511-1518, 1995.

HEINEMANN, A. B.; RAMIREZ-VILLEGAS, J.; STONE, L. F.; SILVA, A. P. G. A.; MATTA, D. H.; DIAZ, M. E. P. The impact of El Niño Southern Oscillation on cropping season rainfall variability across Central Brazil. International Journal of Climatology, v. 41, p. E283-304, 2020.

HEINRICH, C.; HELLTON, K. H.; LENKOSKI, A.; THORARINSDOTTIR, T. L. Multivariate postprocessing methods for high-dimensional seasonal weather forecasts. **Journal of the American Statistical Association**, 2020.

HODGES, D.; PU, Z. Characteristics and variations of low-level jets and environmental factors associated with summer precipitation extremes over the Great Plains. Journal of Climate, v. 32, p. 5123-5144, 2019.

HOSKINS, B. J.; KAROLY, D. J. The steady linear response of a spherical atmosphere to thermal and orographic forcing. **Journal of the Atmospheric Sciences**, v. 38, p. 1179-1196, 1981.

HOSKINS, B.; SCHOPF, P.; NAVARRA, A. Modelling the atmospheric, oceanic and coupled system. *In*: TROCCOLI, A.; HARRISON, M.; ANDERSON, D. L. T.; MASON, S. J. **Seasonal climate: forecasting and managing risk**. Dordrecht: Springer, 2008, p. 127-161.

HOUNSOU-GBO, G. A.; ARAUJO, M.; BOURLÈS, B.; VELEDA, D.; SERVAIN, J. Tropical Atlantic contributions to strong rainfall variability along the Northeast Brazilian coast. **Advances in Meteorology**, v. 2015, 902084, 2015.

HOUZE, R. A. Mesoscale convective systems. **Reviews of Geophysics**, v. 42, 2004.

HOYOS, I.; CAÑÓN-BARRIGA, J.; ARENAS-SUÁREZ, T.; DOMINGUEZ, F.; RODRÍGUEZ, B. A. Variability of regional atmospheric moisture over Northern South America: patterns and underlying phenomena. Climate Dynamics, v. 52, p. 893-911, 2019.

HOYOS, I.; DOMINGUEZ, F.; CAÑÓN-BARRIGA, J.; MARTÍNEZ, J. A.; NIETO, R.; GIMENO, L.; DIRMEYER, P. A. Moisture origin and transport processes in Colombia, northern South America. Climate Dynamics, v. 50, p. 971-990, 2018.

HURTADO, S. I.; AGOSTA, E. A. El Niño Southern Oscillation-related precipitation anomaly variability over eastern subtropical South America: atypical precipitation seasons. International Journal of Climatology, v. 41, p. 3793-3812, 2020.

IWABE, C. M. N.; DA ROCHA, R. P. An event of stratospheric air intrusion and its associated secondary surface cyclogenesis over the South Atlantic Ocean. **Journal of Geophysical Research,** v. 114, D09101, 2009.

JARAMILLO, L.; POVEDA, G.; MEJÍA, J. F. Mesoscale convective systems and other precipitation features over the tropical Americas and surrounding areas as seen by TRMM. **International Journal of Climatology**, v. 37, p. 380-397, 2017.

JARDIM, A. M. R. F.; SILVA, M. V.; SILVA, A. R.; SANTOS, A.; PANDORFI, H.; OLIVEIRA-JÚNIOR, J. F.; LIMA, J. L. M. P.; SOUZA, L. S. B.; ARAÚJO JÚNIOR, G. N.; LOPES, P. M. O.; MOURA, G. B. A.; SILVA, T. G. F. Spatiotemporal climatic analysis in Pernambuco State, Northeast Brazil. **Journal of Atmospheric and Solar-Terrestrial Physics**, v. 223, 105733.

JEWSON, S.; BRIX, A. **Weather Derivative Valuation: The Meteorological, Statistical, Financial and Mathematical Foundations.** Cambridge: Cambridge University Press, 2005.

JIMÉNEZ-MUÑOZ, J. C.; MATTAR, C.; BARICHIVICH, J.; SANTAMARÍA-ARTIGAS, A.; TAKAHASHI, K.; MALHI, Y.; SOBRINO, J. A.; VAN DER SCHRIER, G. Record-breaking warming and extreme drought in the Amazon rainforest during the course of El Niño 2015-2016. **Scientific Reports**, v. 6, 2016.

JONES, C. Recent changes in the South America low-level jet. **npj Climate and Atmospheric Science**, 2, 20, 2019.

JOHNSON, S. J.; STOCKDALE, T. N.; FERRANTI, L.; BALSAMEDA, M. A.; MOLTENI, F.; MAGNUSSON, L.; TIETSCHE, S.; DECREMER, D.; WEISHEIMER, A.; BALSAMO, G.;

KEELEY, S. P. E.; MOGENSEN, K.; ZUO, H.; MONGE-SANZ, B. M. SEAS5: the new ECMWF seasonal forecast system. **Geoscientific Model Development**, v. 12, p. 1087-1117, 2019.

KAYANO, M. T.; ANDREOLI, R. V. Clima da região Nordeste do Brasil. *In*: CAVALCANTI, I. F. A.; FERREIRA, N. J.; SILVA, M. G. A. J.; SILVA DIAS, M. A. F. **Tempo e Clima no Brasil**. São Paulo: Oficina de Textos, 2009, p. 15-21.

KALNAY, E. **Atmospheric modeling, data assimilation and predictability**. Cambridge: Cambridge University Press, 2003, 341 p.

KANTHA, L. H.; CLAYSON, C. A. **Numerical models of oceans and oceanic processes**. San Diego: Academic Press, 2000, 940 p.

KIM, H-M.; WEBSTER, P. J.; CURRY, J. A. Seasonal prediction skill of ECMWF System 4 and NCEP CFSv2 retrospective forecast for the Northern Hemisphere winter. **Climate Dynamics**, v. 39, p. 2957-2973, 2012.

KIRTMAN, B. P.; MIN, D.; INFANTI, J. M.; KINTER III, J. L.; PAOLINO, D. A.; ZHANG, Q.; VAN DEN DOOL, H.; SAHA, S.; MENDEZ, M. P.; BECKER, E.; PENG, P.; TRIPP, P.; HUANG, J.; DE WITT, D. G.; TIPPETT, M. K.; BARNSTON, A. G.; LI, S.; ROSATI, A.; SCHUBERT, S. D.; RIENECKER, M.; SUAREZ, M.; LI, Z. E.; MARSHAK, J.; LIM, Y. -K.; TRIBBIA, J.; PEGION, K.; MERRYFIELD, W. J.; DENIS, B.; WOOD, E. F. The North American Multimodel Ensemble – Phase-1 Seasonal-to-interannual prediction; Phase-2 toward developing intraseasonal prediction. **Bulletin of the American Meteorological Society**, v. 95, n. 4, p. 585-601, 2014.

KLING, H.; FUCHS, M.; PAULIN, M.; Runoff conditions in the upper Danube basin under and ensemble of climate change scenarios. **Journal of Hydrology**, p. 264-277, 2012.

KNOBEN, W. J. M.; FREER, J. E.; WOODS, R. A. Technical note: inherent benchmark or not? Comparing Nash-Sutcliffe and Kling-Gupta efficiency scores. **Hydrology and Earth System Sciences**, v. 23, p. 4323-4331, 2019.

KODAMA, Y. Large-scale common features of subtropical precipitation zones (the Baiu Frontal Zone, the SPCZ, and the SACZ). Part I: characteristics of subtropical frontal zones. **Journal of the Meteorological Society of Japan**, v. 70, p. 813-836, 1992.

KOUSKY, V. E. Frontal influences on Northeast Brazil. **Monthly Weather Review**, v. 107, p. 1140-1153, 1979.

KOUSKY, V. E. Diurnal rainfall variation in Northeast Brazil. **Monthly Weather Review**, v. 108, p. 488-498, 1980.

KOUSKY, V. E. Pentad outgoing longwave radiation climatology for the South American sector. **Revista Brasileira de Meteorologia**, v. 3, p. 217-231, 1988.

KOUSKY, V. E.; FERREIRA, N. J. Interdiurnal surface pressure variations in Brazil: their spatial distributions, origins and effects. **Monthly Weather Review**, v. 109, p. 1999-2008, 1981.

KOUSKY, V. E.; GAN, M. A. Upper tropospheric cyclonic vortices in the tropical South Atlantic. **Tellus**, v. 36, p. 538-551, 1981.

KOUSKY, V. E.; KAYANO, M. T. A climatological study of the tropospheric circulation over the Amazon region. **Acta Amazonica**, v. 11, p. 743-758, 1981.

KOUSKY, V. E.; KAYANO, M. T.; CAVALCANTI, I. F. A. A review of the Southern Oscillation: oceanic-atmospheric circulation changes and related rainfall anomalies. **Tellus**, v. 36, p. 490-504, 1984.

KUCHARSKI, F.; POLZIN, D.; HASTENRATH, S. Teleconnection mechanisms of Northeast Brazil droughts: modelling and empirical evidence. **Revista Brasileira de Meteorologia**, v. 23, p. 115-125, 2008.

KUG, J-S.; HAM, Y-G. Are there two types of La Niña? **Geophysical Research Letters**, v. 38, L16704, 2011.

KUG, J-S.; HAM, Y-G.; LEE, J-Y.; JIN, F-F. Improved simulation of two types of El Niño in CMIP5 models. **Environmental Research Letters**, v. 7, 034002, 2012.

KUG, J. S.; KANG, I. S.; CHOI, D. H. Seasonal climate predictability with tier-one and tier-two prediction systems. **Climate Dynamics**, v. 31, p. 403-416, 2008.

LANDMAN, W. A.; MASON, S. J. Operational long-lead prediction of South African rainfall using canonical correlation analysis. **International Journal of Climatology**, v. 19, p. 1073-1090, 1999.

LANDMAN, W. A.; MASON, S. J. Forecasts of near-global sea surface temperatures using a canonical correlation analysis. **Journal of Climate**, v. 14, p. 3819-3833, 2001.

LAPRISE, R.; VARMA, M. R.; DENIS, B.; CAYA, D.; ZAWADZKI, I. Predictability of a nested limited-area model. **Monthly Weather Review**, v. 128, p. 4149-4154, 2000.

LEE, J.-Y; WANG, B. Seasonal climate prediction and predictability of atmospheric circulation. *In*: DRUYAN, L. **Climate Models**. IntechOpen, 2012, p. 19-42.

LENG, G.; ZHANG, X.; HUANG, M.; ASRAR, G. R.; LEUNG, L. R. The role of climate covariability on crop yields in the conterminous United States. **Scientific Reports**, v. 6, 2016.

LENTERS, J. D.; COOK, K. H. On the origin of the Bolivian High and related circulation features on the South American climate. **Journal of the Atmospheric Sciences**, v. 54, p. 656-677, 1997.

LI, M.; JIN, H.; BROWN, J. N. Making the output of seasonal climate models more palatable to agriculture: a copula-based postprocessing method. **Journal of Applied Meteorology and Climatology**, v. 59, p. 497-515, 2020.

LIN, R.; DONG, X.; FAN, F. Can coupled models perform better in the simulation of sub-seasonal evolution of the western North Pacific subtropical high than atmospheric models in boreal summer? **Atmospheric Science Letters**, v. 19, e862, 2018.

LLOPART, M.; DA ROCHA, R. P.; REBOITA, M. S.; CUADRA, S. Sensitivity of simulated South America climate to the land surfaces schemes in RegCM4. **Climate Dynamics**, v. 48, p. 1-13, 2017.

LOBELL, D. B.; FIELD, C. B. Global scale climate-crop yield relationships and the impacts of recent warming. **Environmental Research Letters**, v. 2, 2007.

LODH, A. Reassessment of land-atmosphere interactions over India during summer monsoon using state-of-the-art regional climate models. **Theoretical and Applied Climatology**, v. 142, p. 1649-1673, 2020.

LORENZ, E. N. A study of the predictability of a 28-variable atmospheric model. **Tellus**, v. 17, p. 321-333, 1965.

LORENZ, E. N. Atmospheric predictability experiments with a large numerical model. **Tellus**, v. 34, p. 505-513, 1982.

LOWE, R.; BAILEY, T. C.; STEPHENSON, D. B.; GRAHAM, R. J.; COELHO, C. A. S.; CARVALHO, M. S.; BARCELLOS, C. Spatio-temporal Modelling of climate-sensitive disease

risk: towards an early warning system for dengue in Brazil. **Computers & Geosciences**, v. 37, p. 371-381, 2011.

LOWE, R.; GARCÍA-DÍEZ, M.; BALLESTER, J.; CRESWICK, J.; ROBINE, J.-M.; HERRMANN, F. R.; RODÓ, X. Evaluation of an early-warning system for heat wave-related mortality in Europe: implications for sub-seasonal to seasonal forecasting and climate services. **International Journal of Environmental Research and Public Health**, v. 13, 206, 2016.

LÚCIO, P. S.; SILVA, F. D. S.; FORTES, L. T. G.; SANTOS, L. A. R.; FERREIRA, D. B.; SALVADOR, M. A.; BALBINO, H. T.; SARMANHO, G. F.; SANTOS, L. S. F. C.; LUCAS, E. W. M.; BARBOSA, T. F.; SILVA DIAS, P. L. Um modelo estocástico combinado de previsão sazonal para a precipitação no Brasil. **Revista Brasileira de Meteorologia**, v. 25, p. 70-87, 2010.

MA, H-Y.; SIONGCO, A. C.; KLEIN, S. A.; XIE, S.; KARSPECK, A. R.; RAEDER, K.; ANDERSON, J. L.; LEE, J.; KIRTMAN, B. P.; MERRYFIELD, W. J.; MURAKAMI, H.; TRIBBIA, J. J. On the correspondence between seasonal forecast biases and long-term climate biases in sea surface temperature. **Journal of Climate**, v. 34, p. 427-446, 2021.

MACHADO, R. D.; DA ROCHA, R. P. Previsões climáticas sazonais sobre o Brasil: avaliação do RegCM3 aninhado no modelo global CPTEC/COLA. **Revista Brasileira de Meteorologia**, v. 26, p. 121-136, 2011.

MACHADO, L. A. T.; FERREIRA, N. J.; LAURENT, H.; DIEDHIOU, A. Distúrbios ondulatórios de leste. *In*: CAVALCANTI, I. F. A.; FERREIRA, N. J.; SILVA, M. G. A. J.; SILVA DIAS, M. A. F. **Tempo e Clima no Brasil**. São Paulo: Oficina de Textos, 2009, p. 61-74.

MACLEOD, D.; KLASSEN, S. Seasonal forecasts 101. **Building Resilience and Adaptation to Climate Extremes and Disasters**, Issue nº 1, p.3-23, 2019.

MADEC, G. NEMO Ocean Engine. 2016.

MANZANAS, R.; BEDIA, J.; MAGARIÑO, M. E.; FERNÁNDEZ, J.; COFIÑO, A. S.; GUTIÉRREZ, J. M. Preliminary validation of the seasonal forecasting systems included in the SPECS-EUPORIAS Data Portal: the ECMWF System4 Hindcast. Santander Meteorology Group (CSIC-UC) – Technical notes, 2013.

MARDONES, P.; WONG, Z.; CONTRERAS-ROJAS, J.; MUÑOZ, R.; HERNÁNDEZ, E.; SOBARZO, M. Upwelling shadows driven by the Low-Level Jet along the subtropical west coast of South America: Gulf of Arauco, Chile. **Journal of Geophysical Research: Oceans**, 2021.

MARENGO, J. A. Interannual variability of deep convection over the tropical South American sector as deduced from ISCCP C2 data. **International Journal of Climatology**, v. 15, p. 995-1010, 1995.

MARENGO, J. A.; ALVES, L. M.; SOARES, W. R.; RODRIGUEZ, D. A.; CAMARGO, H.; RIVEROS, M. P.; PABLÓ, A. D. Two contrasting severe seasonal extremes in tropical South America in 2012: flood in Amazonia and drought in Northeast Brazil. **Journal of Climate**, v, 26, p. 9137-9154, 2013.

MARENGO, J. A.; ALVES, L. M.; ALVALA, R. C. S.; CUNHA, A. P.; BRITO, S.; MORAES, O. L. L. Climatic characteristics of the 2010-2016 drought in the semiarid Northeast Brazil region. **Anais da Academia Brasileira de Ciências**, v. 90, p. 1973-1985, 2018.

MARENGO, J.A.; AMBRIZZI, T.; BARRETO, N.; CUNHA, A. P.; RAMOS, A. M.; SKANSI, M.; CARPIO, J. M.; SALINAS, R. The heat wave of October 2020 in central South America. **International Journal of Climatology**, Early View, 2021.

MARENGO, J. A.; AMBRIZZI, T.; SOARES, W. R. Jato de baixos níveis ao longo dos Andes. *In*: CAVALCANTI, I. F. A.; FERREIRA, N. J.; SILVA, M. G. A. J.; SILVA DIAS, M. A. F. **Tempo e Clima no Brasil**. São Paulo: Oficina de Textos, 2009, p. 169-180.

MARENGO, J. A.; CAVALCANTI, I. F. A.; SATYAMURTY, P.; TROSNIKOV, I.; NOBRE, C. A.; BONATTI, J. P.; CAMARGO, H.; SAMPAIO, G.; SANCHES, M. B.; MANZI, A. O.; CASTRO, C. A. C.; D'ALMEIDA, C.; PEZZI, L. P.; CANDIDO, L. Assessment of regional seasonal rainfall predictability using the CPTEC/COLA atmospheric GCM. **Climate Dynamics**, v. 21, p. 459-475, 2003.

MARENGO, J. A.; LIEBMANN, B.; GRIMM, A. M.; MISRA, V.; SILVA DIAS, P. L.; CAVALCANTI, I. F. A.; CARVALHO, L. M. V.; BERBERY, E. H.; AMBRIZZI, T.; VERA, C. S.; SAULO, A. C.; NOGUES-PAEGLE, J.; ZIPSER, E.; SETH, A.; ALVES, L. M. Recent developments on the South American monsoon system. **International Journal of Climatology**, v. 32, p. 1-21, 2012.

MARENGO, J. A.; NOBRE, C. A.; CULF, A. D. Climatic impacts of “friagens” in forested and deforested areas of the Amazon Basin. **Journal of Applied Meteorology**, v. 36, p. 1553-1566, 1997.

MARENGO, J. A.; NOBRE, C. A.; TOMASELLA, J.; OYAMA, M. D.; OLIVEIRA, G. S.; OLIVEIRA, R.; CAMARGO, H.; ALVES, L. M.; BROWN, I. F. The drought of Amazonia in 2005. **Journal of Climate**, v. 21, p. 495-516, 2008.

MARENGO, J. A.; SOARES, W. R.; SAULO, C.; NICOLINI, M. Climatology of the low-level jets east of the Andes as derived from NCEP-NCAR reanalyses: characteristics and temporal variability. **Journal of Climate**, v. 17, p. 2261-2280, 2004.

MARRAFON, V.; REBOITA, M. S. Características da precipitação na América do Sul reveladas através de índices climáticos. **Revista Brasileira de Climatologia**, v. 26, 2020.

MARTINS, M. A.; TOMASELLA, J.; RODRIGUEZ, D. A.; ALVALÁ, R. C. S.; GIAROLLA, A.; GAROFOLO, L. I.; SIQUEIRA JÚNIOR, J. L.; PAOLICCHI, L. T. L. C.; PINTO, G. L. N. Improving drought management in the Brazilian semiarid though crop forecasting. **Agricultural Systems**, v. 160, p. 21-30, 2018.

MEEHL, G. A.; RICHTER, J. H.; TENG, H.; CAPOTONDI, A.; COBB, K.; DOBLAS-REYES, F.; DONAT, M. G.; ENGLAND, M. H.; FYFE, J. C.; HAN, W.; KIM, H.; KIRTMAN, B. P.; KUSHNIR, Y.; LOVENDUSKI, N. S.; MANN, M. E.; MERRYFIELD, W. J.; NIEVES, V.; PEGION, K.; ROSENBLOOM, N.; SANCHEZ, S. C.; SCAIFE, A. A.; SMITH, D.; SUBRAMANIAN, A. C.; SUN, L.; THOMPSON, D.; UMMENHOFER, C. C.; XIE, S. P. Initialized Earth System prediction from subseasonal to decadal timescales. **Nature Reviews Earth & Environment**, v. 2, p. 340–357, 2021.

MENDES, D.; SOUZA, E.P.; MARENGO, J. A.; MENDES, M.C.D. Climatology of extratropical cyclones over the South American-southern oceans sector. **Theoretical and Applied Climatology**, v. 100, p. 239-250, 2010.

MERRYFIELD, W. J.; LEE, W. -S.; BOER, G. J.; KHARIN, V. V.; SCINOCCA, J. F.; FLATO, G. M.; AJAYAMOHAN, R. S.; FYFE, J. C. The Canadian seasonal to interannual prediction system. Part 1: models and initialization. **Monthly Weather Review**, v. 141, p. 2910-2945, 2013.

MESEGUER-RUIZ, O.; NICOLA, C.; GUIJARRO, J. A.; SARRICOLEA, P. Weather regimes linked to daily precipitation anomalies in Northern Chile. **Atmospheric Research**, v. 236, 104802, 2020a.

MESEGUER-RUIZ, O.; PONCE-PHILIMON, P. I.; BALTAZAR, A.; GUIJARRO, J. A.; SERRANO-NOTIVOLI, R.; CANTOS, J. O.; MARTIN-VIDE, J.; SARRICOLEA, P. Synoptic attributions of extreme precipitation in the Atacama Desert (Chile). **Climate Dynamics**, v. 55, p. 3431-3444, 2020b.

MISRA, V. Understanding the predictability of seasonal precipitation over northeast Brazil. **Tellus A: Dynamic Meteorology and Oceanography**, v. 58, p. 37-319, 2006.

MISRA, V.; DIRMEYER, P. A.; KIRTMAN, B. P. Dynamic downscaling of seasonal simulations over South America. **Journal of Climate**, v. 16, p. 103-117, 2003.

MOLTENI, F.; STOCKDALE, T.; BALSAMEDA, M.; BALSAMO, G.; BUIZZA, R.; FERRANTI, L.; MAGNUSSON, L.; MOGENSEN, K.; PALMER, T.; VITART, F. The new ECMWF seasonal forecast system (System 4). **ECMWF Technical Memorandum**, n. 656, 2011, 44 p.

MONTGOMERY, D. C.; JENNINGS, C. L.; KULAHCI, M. **Introduction to time series analysis and forecasting.** New Jersey: John Wiley & Sons, 2008, 672 p.

MONTINI, T. L.; JONES, C.; CARVALHO, L. M. The South American low-level jet: a new climatology, variability and changes. Journal of Geophysical Research: **Atmospheres**, v. 124, p. 1200-1218, 2020.

MORAES, F. D. S.; AQUINO, F. E.; MOTE, T. L.; DURKEE, J. D.; MATTINGLY, K. S. Atmospheric characteristics favorable for the development of mesoscale convective complexes in Southern Brazil. **Climate Research**, v. 80, p. 43-58, 2020.

MORAIS, M. D. C.; GAN, M. A.; YOSHIDA, M. C. Features of the upper tropospheric cyclonic vortices of Northeast Brazil in life cycle stages. **International Journal of Climatology**, v. 41, p. E39-E58, 2020.

MORCRETTE, J. J. BARKER, H. W.; COLE, J. N. S.; IACONO, M. J.; PINCUS, R. Impact of a new radiation package, McRad, in the ECMWF Integrated Forecast System. **Monthly Weather Review**, v. 136, p. 4773-4798, 2008.

MORETO, V. B.; ROLIM, G. S.; ESTEVES, J. T.; VANUYTRECHT, E.; CHOU, S. C. Sugarcane decision-making support using ETA Model precipitation forecasts. **Meteorology and Atmospheric Physics**, 2020.

MORETTIN, P. A.; BUSSAB, W. O. **Estatística Básica**. São Paulo: Editora Saraiva, 2017, 568 p.

MORSE, A. P.; DOBLAS-REYES, F.; HOSHEN, M.; HAGEDORN, R.; PALMER, T. N. A forecast quality assessment of an end-to-end probabilistic multi-model seasonal forecast system using a malaria model. **Tellus**, v. 57, p. 64–475, 2005.

MOURA, A. D.; HASTENRATH, S. Climate prediction for Brazil's Nordeste: performance of empirical and numerical modeling methods. **Journal of Climate**, v. 17, p. 2667-2672, 2004.

MOURA, A. D.; SHUKLA, J. On the dynamics of droughts in the Northeast Brazil: observations, theory and numerical experiments with a general circulation model. **Journal of the Atmospheric Sciences**, v. 38, p. 2653-2675, 1981.

NASCIMENTO, M. G.; HERDIES, D. L.; SOUZA, D. O. The South American water balance: the influence of low-level jets. **Journal of Climate**, v. 39, p. 1429-1449, 2016.

NERY, J. T.; CARFAN, C. Re-analysis of pluvial precipitation in southern Brazil. **Atmósfera**, v. 27, p. 103-115, 2014.

NESTARES, V. J. A. **Lorenz energetic applied to understanding of squall lines propagation over the Amazon Basin.** Instituto de Astronomia e Geofísica. Universidade de São Paulo. Dissertação de Mestrado em Meteorologia. 90f. 2017.

NETO, A. C. A.; SATYAMURTY, P.; CORREIA, F. W. Some observed characteristics of frontal systems in the Amazon Basin. **Meteorological Applications**, v. 22, p. 617-635, 2015.

NIELSEN, D. M.; BELÉM, A. L.; MARTON, E.; CATALDI, M. Dynamics-based regression models for the South Atlantic Convergence Zone. **Climate Dynamics**, v. 52, p. 5527-5553, 2019.

NIMER, E. **Climatologia do Brasil**. Rio de Janeiro: Fundação Instituto Brasileiro de Geografia e Estatística. 1989, 421 p.

OCEAN5: The ECMWF ocean reanalysis system and its real-time analysis component. 2020.

OKUMURA, Y. M.; DESER, C. Asymmetry in the duration of El Niño and La Niña. **Journal of Climate**, v. 23, p. 5826-5843, 2010.

OLIVEIRA, G.S.; SATYAMURTY, P. O El Niño de 1997/98: evolução e impactos no Brasil. *In*: Congresso Brasileiro de Meteorologia, 7, 1998, Brasília. **Anais** [...]. Brasília, 1998.

OLIVEIRA, F. P.; OYAMA, M. D. Squall-line initiation over the northern coast of Brazil in March: observational features. **Meteorological Applications**, v. 27, e1799, 2019.

OSMAN, M.; COELHO, C. A. S.; VERA, C. S. Calibration and combination of seasonal precipitation forecasts over South America using Ensemble Regression. **Climate Dynamics**, 2021.

OSMAN, M.; VERA, C. S. Climate predictability and prediction skill on seasonal time scales over South America from CHFP models. **Climate Dynamics**, v. 49, p. 2365-2383, 2017.

OTTO, F. E. L.; COELHO, C. A. S.; KING, A.; PEREZ, E. C.; WADA, Y.; VAN OLDENBORGH, G. J.; HAARSMA, R.; HAUSTEIN, K.; UHE, P.; VAN AALST, M.; ARAVEQUIA, J. A.; ALMEIDA, W.; CULLEN, H. Factors other than climate change, main drivers of 2014/2015 water shortage in southeast Brazil. **Bulletin of the American Meteorological Society**, v. 96, n. 12, 2015.

PAIVA, L. F. G.; MONTENEGRO, S. M.; CATALDI, M. Prediction of monthly flows for Três Marias reservoir (São Francisco river basin) using the CFS climate forecast model. **Revista Brasileira de Recursos Hídricos**, v. 25, e16, 2020.

PAIXÃO, E. B.; GANDU, A. W. Caracterização do vórtice ciclônico de ar superior no Nordeste Brasileiro. *In*: Congresso Brasileiro de Meteorologia, 9, 2000, Rio de Janeiro. **Anais** [...]. Rio de Janeiro, 2000, p. 860-865.

PALIN, E. J.; SCAIFE, A. A.; WALLACE, E.; POPE, E. C.; ARRIBAS, A.; BROOKSHAW, A. Skillful seasonal forecasts of winter disruption to the UK transport system. **Journal of Applied Meteorology and Climatology**, v. 55, p. 325–344, 2016.

PALMÉN, E.; NEWTON, C. W. **Atmospheric circulation systems – Their structure and physical interpretation**. New York: Academic Press, 1969, 603 p.

PALMER, T. N.; ANDERSON, L. T. The prospects for seasonal forecasting – a review paper. **Quarterly Journal of Royal Meteorological Society**, v. 120, p. 755-793, 1994.

PASCALE, S.; CARVALHO, L. M. V.; ADAMS, D. K.; CASTRO, C. L.; CAVALCANTI, I. F. A. Current and future variations of the Monsoons of the Americas in a warming climate. **Current Climate Change Reports**, v. 5, p. 125-144, 2019.

PATIL, M. K. Change in seasonality index of rainfall in Sangli district. **Indian Streams Research Journal**, v. 5, p. 1-7, 2015.

PEDRON, I. T.; SILVA DIAS, M. A. F.; DIAS, S. P.; CARVALHO, L. M. V.; FREITAS, E. D. Trends and variability in extremes of precipitation in Curitiba – Southern Brazil. **International Journal of Climatology**, v. 37, p. 1250-1264, 2016.

PEGION, K.; KUMAR, A. Does an ENSO-conditional skill mask improve seasonal predictions? **Monthly Weather Review**, v. 141, p. 4515-4533, 2013.

PEIXOTO, J. P.; OORT, A. H. **Physics of climate**. New York: American Institute of Physics. 1992, 520 p.

PENNA, A. C.; TORRES, R. R.; GARCIA, S. R.; MARENGO, J. A. Moisture flows on Southeastern Brazil: present and future climate. **International Journal of Climatology**, v. 41, p. E935-951, 2021.

PEREIRA, G.; CARDOZO, F. S.; NEGREIROS, A. B.; ZANIN, G. D.; COSTA, J. C.; LIMA, T. E. R.; RICARDO, R. P.; RAMOS, R. C. Variabilidade da precipitação no estado de Minas Gerais no período de 1981 a 2017. **Revista Brasileira de Climatologia**, v. 213, 2018.

PÉREZ, A. R.; ORTIZ, J. C. R.; BEJARANO, L. F. A.; OTERO, L. D.; RESTREPO, J. C. L.; FRANCO, A. H. Sea breeze in the Colombian Caribbean coast. **Atmósfera**, v. 31, p. 389-406, 2018.

PEZZI, L. P.; CAVALCANTI, I. F. A. The relative importance of ENSO and tropical Atlantic sea precipitation over South America: a numerical study. **Climate Dynamics**, v. 17, p. 205-212, 2001.

PIEDRA-BONILLA, E. B.; DA CUNHA, D. A.; BRAGA, M. J. Climate variability and crop diversification in Brazil: an ordered probit analysis. **Journal of Cleaner Production**, v. 256, p. 1-10, 2020.

PIERSANTE, J. O.; RASMUSSEN, K. L.; SCHUMACHER, R. S.; ROWE, A. K. MCMURDIE, L. A. A synoptic evolution comparison of the smallest and largest MCSs in subtropical South America between spring and summer. **Monthly Weather Review**, v. 149, p. 1943-1966, 2021.

PINHEIRO, H. R.; HODGES, K. I.; GAN, M. A.; FERREIRA, N. J. A new perspective of the climatological features of upper-level cut-off lows in the Southern Hemisphere. **Climate Dynamics**, v. 48, p. 541-559, 2016.

PORTMANN, R.; SPRENGER, M.; WERNLI, H. The three-dimensional life cycles of potential vorticity cutoffs: a global and selected regional climatologies in ERA-Interim (1979-2018). **Weather and Climate Dynamics**, v. 2, p. 507-534, 2021.

PRADO, L. F.; WAINER, I.; YOKOYAMA, E.; KHODRI, M.; GARNIER, J. Changes in summer precipitation variability in central Brazil over the past eight decades. **International Journal of Climatology**, v. 8, p. 4171-4186, 2021.

PRESS, W. H.; TEUKOLSKY, S. A.; VETTERLING, W. T. FLANNERY, B. P. **Numerical recipes in C: the art of scientific computing**. Cambridge: Cambridge University Press, 2007, 994 p.

QUADRO, M. F. L.; SILVA DIAS, M. A. F.; HERDIES, D. L.; GONÇALVES, L. G. G. Análise climatológica da precipitação e do transporte de umidade na região da ZCAS através da nova geração de reanálises. **Revista Brasileira de Meteorologia**, v. 27, p. 152-162, 2012.

RAJAGOPALAN, B.; LALL, U.; ZEBIAK, S. E. Categorical climate forecasts through regularization and optimal combination of multiple GCM ensembles. **Monthly Weather Review**, v. 130, p. 1792-1811, 2002.

RAMÍREZ, M. C. V.; KAYANO, M. T.; FERREIRA, N. J. Statistical Analysis of upper tropospheric vortices in the vicinity of Northeast Brazil during the 1980-1989 period. **Atmósfera**, v. 12, p 75-88, 1999.

RAO, V. B.; HADA, K. Characteristics of rainfall over Brazil: annual variations and connections with the Southern Oscillation. **Theoretical and Applied Climatology**, v. 42, p. 81-91, 1990.

RASMUSSEN, K. L.; CHAPLIN, M. M.; ZULUAGA, M. D.; HOUZE JR., R. A. Contribution of extreme convective storms to rainfall in South America. **Journal of Hydrometeorology**, v. 17, p. 353-367, 2016.

REBOITA, M. S.; AMBRIZZI, T.; CRESPO, N. M.; DUTRA, L. M. M.; FERREIRA, G. W. S.; REHBEIN, A.; DRUMOND, A.; DA ROCHA, R. P.; SOUZA, C. A. Impacts of teleconnection patterns on South America climate. **Annals of the New York Academy of Sciences**, 2021.

REBOITA, M. S.; AMBRIZZI, T.; DA ROCHA, R. P. Relationship between the Southern Annular Mode and Southern Atmospheric Systems. **Revista Brasileira de Meteorologia**, v. 24, p. 48-55, 2009.

REBOITA, M. S.; AMBRIZZI, T.; SILVA, B.; PINHEIRO, R.; DA ROCHA, R. P. The South Atlantic Subtropical Anticyclone: present and future climate. **Frontiers in Earth Science**, v. 7, 2019.

REBOITA, M. S.; ASSIREU, A.; SILVA, L. C.; RIOS, N. Evidências de circulação de brisa vale-montanha na Serra da Mantiqueira: cidade de Itajubá – MG. **Ciência e Natura**, v. 36, p. 61-71, 2014a.

REBOITA, M. S.; CRESPO, N. M.; DUTRA, L. M. M.; SILVA, B. A.; CAPUCIN, B. C.; DA ROCHA, R. P. Iba: the first pure tropical cyclogenesis over the western South Atlantic ocean. **Journal of Geophysical Research: Atmospheres**, v. 126, e2020JD033431, 2020.

REBOITA, M. S.; CRESPO, N. M.; TORRES, J. A.; REALE, M.; DA ROCHA, R. P.; GIORGI, F.; COPPOLA, E. Future changes in winter explosive cyclones over the Southern Hemisphere domains from the CORDEX-CORE ensemble. **Climate Dynamics**, v. 57, 3303-3322, 2021b.

REBOITA, M. S.; DA ROCHA, R. P.; DIAS, C. G.; YNOUE, R. Y. Climate projections for South America: RegCM3 driven by HadCM3 and ECHAM5. **Advances in Meteorology**, v. 2014, 376738, 2014b.

REBOITA, M.S.; DA ROCHA, R. P.; OLIVEIRA, D. M. Key features and adverse weather of the named subtropical cyclones over the southwestern South Atlantic ocean. **Atmosphere**, v. 10, 6, 20149.

REBOITA, M. S.; DIAS, C. G.; DUTRA, L. M. M.; DA ROCHA, R. P.; LLOPART, M. Previsão climática sazonal para o Brasil obtida através de modelos climáticos globais e regional. **Revista Brasileira de Meteorologia**, v. 33, n. 2, p. 207-224, 2018.

REBOITA, M. S.; GAN, M. A.; DA ROCHA, R. P.; AMBRIZZI, T. Regimes de precipitação na América do Sul: uma revisão bibliográfica. **Revista Brasileira de Meteorologia**, v. 25, p. 184-204, 2010a.

REBOITA, M. S.; KRUSCHE, N.; AMBRIZZI, T.; DA ROCHA, R. P. Entendendo o tempo e o clima na América da Sul. **Terrae Didatica**, v. 8, p. 34-50, 2012.

REBOITA, M. S.; KRUSCHE, N.; PICCOLI, H. C. Climate variability in Rio Grande, RS, Brazil: a quantitative Analysis of contributions due to atmospheric systems. **Revista Brasileira de Meteorologia**, v. 21, p. 256-270, 2006.

REBOITA, M. S.; NIETO, R.; GIMENO, L.; DA ROCHA, R. P.; AMBRIZZI, T.; GARREAUD, R.; KRÜGER, L. F. Climatological features of cutoff low systems in the Southern Hemisphere. **Journal of Geophysical Research**, v. 115, p. 1-15, 2010b.

REBOITA, M. S.; OLIVEIRA, D. M.; FREITAS, C. H.; OLIVEIRA, G. M.; PEREIRA, R. A. A. Anomalias dos padrões sinóticos da atmosfera na América do Sul nos meses de janeiro de 2014 e 2015. **Revista Brasileira de Energias Renováveis**, v. 4, p. 01-12, 2015.

REBOITA, M. S.; RODRIGUES, M.; ARMANDO, R. P.; FREITAS, C.; MARTINS, D.; MILLER, G. Causas da semi-aridez do sertão nordestino. **Revista Brasileira de Climatologia**, v. 19, p. 254-277, 2016.

REHBEIN, A.; DUTRA, L. M. M.; AMBRIZZI, T.; DA ROCHA, R. P.; REBOITA, M. S.; SILVA, G. A. M.; GOZZO, L. P.; TOMAZIELLO, A. C. N.; CAMPOS, J. L. P. S.; MAYTA, V. R. C.; CRESPO, N. M.; BUENO, P. G.; NESTARES, V. J. A.; MACHADO, L. T.; DE JESUS, E. M.; PAMPUCH, L. A. P.; CUSTÓDIO, M. S.; CARPENEDO, C. B. Severe Weather events over southeastern Brazil during the **2016** season. **Advances in Meteorology**, v. 2018, 4878503, 2018.

RIBEIRO, F. N. D.; OLIVEIRA, A. P.; SOARES, J.; MIRANDA, R. M.; BARLAGE, M.; CHEN, F. Effect of sea breeze propagation on the urban boundary layer of the metropolitan region of São Paulo, Brazil. **Atmospheric Research**, v. 214, p. 174-188, 2018.

RISBEY, J. S.; SQUIRE, D. T.; BLACK, A. S.; DELSOLE, T.; LEPORE. C.; MATEAR, R. J.; MONSELESAN, D. P.; MOORE, T. S.; RICHARDSON, D.; SCHEPEN, A.; TIPPETT, M. K.; TOZER, C. R. Standard assessments of climate forecast skill can be misleading. **Nature Communications**, v. 12, 4346, 2021.

ROBERTS, P. S.; WERNSTEDT, K. Using climate forecasts across a state's emergency management network. **Natural Hazards Review**, v. 17, n. 3, 2016.

RODRIGUES, L. R. L.; DOBLAS-REYES, F. J.; COELHO, C. A. S. Multi-model calibration and combination of tropical seasonal sea surface temperature forecasts. **Climate Dynamics**, v. 42, p. 597-616, 2014.

RODRIGUES, M. L. G.; FRANCO, D.; SUGAHARA, S. Climatologia de frentes frias no litoral de Santa Catarina. **Revista Brasileira de Geofísica**, v. 22, p. 135-151, 2004.

RODRIGUES, R. R.; HAARSMA, R. J.; CAMPOS, E. J. D.; AMBRIZZI, T. The impacts of inter-El Niño variability on the tropical Atlantic and Northeast Brazil climate. **Journal of Climate**, v. 24, p. 3402-3422, 2011.

RODRIGUES, R. R.; MCPHADEN, M. J. Why did the 2011-2012 La Niña cause a severe drought in the Brazilian Northeast? **Geophysical Research Letters**, v. 41, p. 1012-1018, 2014.

RODRIGUES, R. R.; TASCHETTO, A. S.; GUPTA, A. S.; FOLTZ, G. R. Common cause for severe drought in South America and marine heatwaves in the South Atlantic. **Nature Geoscience**, v. 12, p. 620-626, 2019.

RODRIGUES, R. R.; WOOLINGS, T. Impact of atmospheric blocking on South America in austral summer. **Journal of Climate**, v. 30, p. 1821-1837, 2017.

ROPELEWSKI, C. F.; HALPERT, M. S. Global and regional scale precipitation patterns associated with the El Niño/Southern Oscillation. **Monthly Weather Review**, v. 115, p. 1606-1626, 1987.

ROWELL, D. P. Assessing potential seasonal predictability with an ensemble of multidecadal GCM simulations. **Journal of Climate**, v. 11, p. 109-120, 1998.

RYDBEK, A. V.; MALONEY, E. D.; ALAKA JR., G. J. In situ initiation of East Pacific easterly waves in a regional model. **Journal of the Atmospheric Sciences**, v. 74, p. 333-351, 2017.

SAHA, S.; MOORTHI, S.; WU, X.; WANG, J.; NADIGA, S.; TRIPP, P.; BEHRINGER, D.; HOU, Y. -T.; CHUANG, H. -Y.; IREDELL, M.; EK, M.; MENG, J.; YANG, R.; MENDEZ, M. P.; VAN DEN DOOL, H.; ZHANG, Q.; WANG, W.; CHEN, M.; BECKER, E. The NCEP climate forecast system version 2. **Journal of Climate**, v. 27, p. 2185-2208, 2014.

SALIO, P.; NICOLINI, M.; ZIPSER, E. J. Mesoscale convective systems over Southeastern South America and their relationship with the South American Low-Level Jet. **Monthly Weather Review**, v. 135, p. 1290-1309, 2007.

SAMPAIO, G.; SILVA DIAS, P. L. Evolução dos modelos climáticos e de previsão de tempo e clima. **Revista USP – Dossiê Clima**, n. 103, p. 41-54, 2014.

SANTOS, E. B.; FREITAS, E. D.; RAFEE, S. A. A.; FUJITA, T.; RUDKE, A. P.; MARTINS, L. D.; DE SOUZA, R. A. F.; MARTINS, J. A. Spatio-temporal variability of wet and drought events in the Paraná River basin – Brazil and its association with the El Niño-Southern oscillation phenomenon. **International Journal of Climatology**, v. 41, p. 4879-4897, 2021.

SANTOSO, A.; ENGLAND, M. H.; CAI, W. Impact of Indo-Pacific feedback interactions on ENSO dynamics diagnosed using ensemble climate simulations. **Journal of Climate**, v. 25. p. 7743-7763, 2012.

SATYAMURTY, P.; NOBRE, C. A.; SILVA DIAS, P. L. South America. *In*: KAROLY, D. J.; VINCENT, D. G. **Meteorology of the Southern Hemisphere**. Boston: American Meteorological Society, 1998, p. 119-139.

SATYAMURTY, P.; ROSA, M. B. Synoptic climatology of tropical and subtropical South America and adjoining seas as inferred from GOES satellite imagery. **International Journal of Climatology**, v. 40, p. 378-399, 2019.

SATYAMURTY, P.; SELUCHI, M. E. Characteristics and structure of an upper air cold vortex in the subtropics of South America. **Meteorology and Atmospheric Physics**, v. 96, p. 203-220, 2007.

SCAIFE, A. A.; ATHANASSIADOU, M.; ANDREWS, M.; ARRIBAS, A.; BALDWIN, M.; DUNSTONE, N.; KNIGHT, J.; MACLACHLAN, C.; MANZINI, E.; MÜLLER, W.; POHLMANN, H.; SMITH, D.; STOCKDALE, T.; WILLIAMS, A. Predictability of the quasi-biennal oscillation and its northern winter teleconnection on seasonal to decadal timescales. **Geophysical Research Letters**, v. 41, p. 1752-1758, 2014.

SCHEPEN, A.; WANG, Q. J.; ROBERTSON, D. E. Combining the strengths of statistical and dynamical modeling approaches for forecasting Australian seasonal rainfall. **Journal of Geophysical Research**, v. 117, D20107, 2012.

SHAFIEE-JOOD, M.; CAI, X.; CHEN, L.; LIANG, X. Z.; KUMAR, P. Assessing the value of seasonal climate forecast information through an end-to-end forecasting framework: application to U.S. 2012 drought in central Illinois. **Water Resources Research**, v. 50, p. 6592–6609, 2014.

SHIMIZU, M.H.; ANOCHI, J.A.; KAYANO, M. T. Precipitation patterns over northern Brazil basin: climatology, trends, and associated mechanisms. **Theoretical and Applied Climatology**, 2021.

SHUKLA, J. Predictability in the midst of chaos: a scientific basis for climate forecasting. **Science**, v. 282, p. 728-731, 1998.

SHUKLA, J.; ANDERSON, J.; BAUMHEFNER, D.; BRANKOVIĆ, Č.; CHANG, Y.; KALNAY, E.; MARX, L.; PALMER, T.; PAOLINO, D.; PLOSHAY, J.; SCHUBERT, S.;

STRAUS, D.; SUAREZ, M.; TRIBBIA, J. Dynamical seasonal prediction. **Bulletin of the American Meteorological Society**, v. 81, n. 11, p. 2593-2606, 2000.

SHUKLA, J.; KINTER, J. Predictabilty of seasonal climate variations: a pedagogical review. *In*: PALMER, T.; HAGEDORN, R. **Predictability of Weather and Climate**. Cambridge: Cambridge University Press, 2006, p. 306-341.

SHUKLA, J.; PAOLINO, D. A.; STRAUS, D. M.; DE WITT, D. G.; FENNESSY, M.; KINTER, J. L.; MARX, L.; MO, R. Dynamical seasonal predictions with the COLA atmospheric model. **Quarterly Journal of Royal Meteorological Society**, v. 126, p. 2265-2291, 2000.

SILVA, B. F. P.; DA ROCHA, R. P.; GOMES, H. B. Easterly waves disturbances activity over the eastern Northeast Brazil. **Revista Científica Foz**, v. 3, 2020.

SILVA, E. D.; REBOITA, M. S. Estudo da precipitação no estado de Minas Gerais – MG. **Revista Brasileira de Climatologia**, v. 13, p. 120-136, 2013.

SILVA, G. A. M.; AMBRIZZI, T. Inter-El Niño variability and its impact on the South American low-level jet east of the Andes during austral summer – two case studies. **Advances in Geosciences**, v. 6, p. 283-287, 2006.

SILVA, G. A. M.; DUTRA, L. M. M.; DA ROCHA, R. P.; AMBRIZZI, T.; LEIVA, E. Preliminary analysis on the global features of the NCEP CFSv2 seasonal hindcasts. **Advances in Meteorology,** v. 2014, 695067, 2014.

SILVA, R. P.; REBOITA, M. S.; ESCOBAR, G. C. J. Caracterização da zona de convergência do Atlântico sul em campos atmosféricos recentes. **Revista Brasileira de Climatologia**, v. 25, p. 355-377, 2019.

SILVA DIAS, M. A. F. Sistemas de mesoescala e previsão de tempo a curto prazo. **Revista Brasileira de Meteorologia**, v. 2, p. 133-150, 1987.

SILVA DIAS, M. A. F.; ROZANTE, J. R.; MACHADO, L. A. T. Complexos convectivos de mesoescala na América do Sul. *In*: CAVALCANTI, I. F. A.; FERREIRA, N. J.; SILVA, M. G. A. J.; SILVA DIAS, M. A. F. **Tempo e Clima no Brasil**. São Paulo: Oficina de Textos, 2009, p. 181-194.

SOLMAN, S. A.; SANCHEZ, E.; SAMUELSSON, P.; DA ROCHA, R. P.; LI, L.; MARENGO. J. A.; PESSAEG, N. L.; REMEDIO, A. R. C.; CHOU, S. C.; BERBERY, H.; LE TREUT, H.; CASTRO, M.; JACOB, D. Evaluation of an ensemble of regional climate model simulations over

South America driven by the ERA-Interim reanalysis: model performance and uncertainties. **Climate Dynamics**, v. 41, p. 1139-1157, 2013.

SONKA, S. T.; CHANGNON, JR., S. A.; HOFING, S. L. How agribusiness uses climate predictions: implications for climate research and provision of predictions. **Bulletin of the American Meteorological Society**, v. 73, n. 12, p. 1999-2008, 1992.

SOUSA, A. C. **Análise de tendências e fatores determinantes da intensificação de sistemas convectivos de mesoescala e linhas de instabilidade na costa norte-nordeste da América do Sul.** Instituto Nacional de Pesquisas da Amazônia. Universidade do Estado do Amazonas. Tese de Doutorado em Clima e Ambiente. 139f. 2020.

SOUSA, A. C.; CANDIDO, L. A.; SATYAMURTY, P. Convective cloud clusters and squall lines along the coastal Amazon. **Monthly Weather Review**, v. 149, p. 3589-3608, 2021.

STEFANOVA, L.; KRISHNAMURTI, T. N. Interpretation of seasonal climate forecast using Brier skill score, the Florida State University Superensemble, and the AMIP-1 dataset. **Journal of Climate**, v. 15, p. 537-544, 2002.

STENSRUD, D. Importance of low-level jets to climate: a review. **Journal of Climate**, v. 9, p. 1698-1711, 1996.

STONE, R. C.; MEINKE, H. Operational seasonal forecasting of crop performance. **Philosophical Transactions of The Royal Society B**, v. 360, p. 2109-2124, 2005.

SUN, X.; COOK, K. H.; VIZY, E. K. The South Atlantic Subtropical High: climatology and interannual variability. **Journal of Climate**, v. 30, p. 3279-3296, 2017.

TASCHETTO, A. S.; SEN GUPTA, A.; JOURDAIN, N. C.; SANTOSO, A. Cold tongue and warm pool ENSO events in CMIP5: mean state and future projections. **Journal of Climate**, v. 27, p. 2861-2885, 2014.

TEDESCHI, R. G.; CAVALCANTI, I. F. A.; GRIMM, A. M. Influences of two types of ENSO on South American precipitation. **International Journal of Climatology**, v. 33, p. 1382-1400, 2013.

TEDESCHI, R. G.; COLLINS, M. The influence of ENSO on South American precipitation during austral summer and autumn in observations and models. **International Journal of Climatology**, v. 36, p. 618-635, 2016.

TEODORO, T. A.; REBOITA, M. S.; ESCOBAR, G. C. J. Caracterização da banda dupla da Zona de Convergência Intertropical (ZCIT) no oceano Atlântico. **Anuário do Instituto de Geociências**, v. 42, p. 282-298, 2019.

TEODORO, T. A.; REBOITA, M. S.; LLOPART, M.; DA ROCHA, R. P.; ASHFAQ, M. Climate change impacts on the South American monsoon system and its surface-atmosphere processes through RegCM4 Cordex-CORE Projections. **Earth Systems and Environment**, v. 5. P. 825-847, 2021.

THOMSON, M. C.; DOBLAS-REYES, F. J.; MASON, S. J.; HAGEDORN, R.; CONNOR, S. J.; PHINDELA, T.; MORSE, A. P.; PALMER, T. N. Malaria early warnings based on seasonal climate forecasts from multi-model ensembles. **Nature**, v. 439, p. 576-579, 2006.

TIEDTKE, M. A comprehensive mass flux scheme for cumulus parameterization in large-scale models. **Monthly Weather Review**, v. 117, p. 1779-1800, 1989.

TIEDTKE, M. Representation of clouds in large-scale models. **Monthly Weather Review**, v. 121, p. 3040-3061, 1993.

TIETSCHE, S.; BALSAMEDA, M. A.; ZUO, H.; MOGENSEN, K. Arctic sea ice in the global eddy-permitting Ocean Reanalysis ORAP5**. Climate Dynamics**, v. 11. P. 775-789, 2017.

TOL, R. S. J. The economic effects of climate change. **Journal of Economic Perspectives**, v. 23, n. 2, p. 29-51, 2009.

TOL, R. S. J. The economic impacts of climate change. **Review of Environmental Economics and Policy**, p. 1-12, 2018.

TOMMASI, D.; STOCK, C.; PEGION, K.; VECCHI, G.; METHOT, R. D.; ALEXANDER, M.; CHECKLEY, D. Improved management of small pelagic fisheries through seasonal climate prediction. **Ecological Applications**, v. 27, n. 2, p. 378-388, 2017.

TORRALBA, V.; DOBLAS-REYES, F. J.; MACLEOD, D.; CHRISTEL, I.; DAVIS, M. Seasonal climate prediction: a new source of information for the management of wind energy resources. **Journal of Applied Meteorology and Climatology**, v. 56, p. 1231-1247, 2017.

TORRES, F. L. R.; FERREIRA, G. W. S.; KUKI, C. A.; VASCONCELLOS, B. T. C.; FREITAS, A. A.; SILVA, P. N.; SOUZA, C. A.; REBOITA, M. S. Validação de diferentes bases de dados de precipitação nas bacias hidrográficas do Sapucaí e São Francisco. **Revista Brasileira de Climatologia**, v. 27, p. 368-404, 2020.

TORRES, R. R.; FERREIRA, N. J. Case studies of easterly waves disturbances over Northeast Brazil using the Eta model. **Weather and Forecasting**, v. 25, p. 225-235, 2011.

TOWNER, J.; CLOKE, H.L.; ZSOTER, E.; FLAMIG, Z.; HOCH, J. M.; BAZO, J.; PEREZ, E. C.; STEPHENS, E. M. Assessing the performance of global hydrological models for capturing peak rivers flows in the Amazon basin. **Hydrology and Earth System Sciences**, v. 23, p. 3057-3080, 2019.

TROCCOLI, A. Seasonal climate forecasting. **Meteorological Applications**, v. 17, p. 251-268, 2010.

TRUCCOLO, E. C. Assessment of the wind behavior in the northern coast of Santa Catarina. **Revista Brasileira de Meteorologia**, v. 26, p. 451-460, 2011.

TURCO, M.; MARCOS-MATAMOROS, R.; CASTRO, X.; CANYAMERAS, E.; LLASAT, M. C. Seasonal prediction of climate-driven fire risk for decision-making and operational applications in a Mediterranean region. **Science of the Total Environment**, v. 676, p. 577-583, 2019.

URREA, V.; OCHOA, A.; MESA, O. Seasonality of rainfall in Colombia. **Water Resources Research**, v. 55, p. 4149-4162, 2019.

UTIDA, G.; CRUZ, F. W.; ETORNEAU, J.; BOULOUBASSI, I. SCHFUB, E.; VUILLE, M.; NOVELLO, V. F.; PRADO, L. F.; SIFEDDINE, A.; KLEIN, V.; ZULAR, A.; VIANA, J. C. C.; TURCQ, B. Tropical South Atlantic influence on Northeastern Brazil precipitation and ITCZ displacement during the past 2300 years. **Scientific Reports**, v. 9, 1698, 2019.

UVO, C. B.; REPELLI, C. A.; ZEBIAK, S. E.; KUSHNIR, Y. The relationships between tropical Pacific and Atlantic SST and Northeast Brazil monthly precipitation. **Journal of Climate**, v. 11, p. 551-562, 1998.

VAJDA, A.; HYVÄRINEN, O. Development of seasonal climate outlooks for agriculture in Finland. **Advances in Science and Research**, v. 17, p. 269-277, 2020.

VAN OLDENBORGH, G. J.; BALSAMEDA, M. A.; FERRANTI, L.; STOCKDALE, T. N.; ANDERSON, D. L. T. Did the ECMWF seasonal forecast model outperform statistical ENSO forecast models over the last 15 years? **Journal of Climate**, v. 18. p. 3240-3249, 2005a.

VAN OLDENBORGH, G. J.; BALSAMEDA, M. A.; FERRANTI, L.; STOCKDALE, T. N.; ANDERSON, D. L. T. Evaluation of atmospheric fields from the ECMWF seasonal forecasts over a 15-year period. **Journal of Climate**, v. 18. p. 3250-3269, 2005b.

VALDÉS-PINEDA, R.; VALDÉS, J. B.; DIAZ, H. F.; PIZARRO-TAPIA, R. Analysis of Spatio-temporal changes in annual and seasonal precipitation variability in South America-Chile and related ocean-atmosphere circulation-patterns. **International Journal of Climatology**, v. 36, p. 2979-3001, 2016.

VELOSO, J. M. V. Analysis of an extreme precipitation event in the Atacama Desert on January 2020 and its relationship to humidity advection along the Southeast Pacific. **Atmósfera**, 2021.

VEMADO, F.; FILHO, A. J. P. Severe Weather caused by heat island and sea breeze effects in the metropolitan area of São Paulo, Brazil. **Advances in Meteorology**, v. 2016, 8364134, 2016.

VERA, C.; HIGGINS, W.; AMBRIZZI, T.; AMADOR, J.; GARREAUD, R.; GOCHIS, D.; GUTZLER, D.; LETTENMAIER, D.; MARENGO, J.; MECHOSO, C. R.; NOGUES-PAEGLE, J. SILVA DIAS, P. L.; ZHANG, C. Toward a unified view of the American monsoon system. **Journal of Climate**, v. 19, p. 4977-5000, 2006.

VIALE, M.; BIANCHI, E.; CARA, L.; RUIZ, L. E.; VILLALBA, R.; PITTE, P.; MASIOKAS, M.; RIVERA, J.; ZALAZAR, L. Contrasting climate at both sides of the Andes in Argentina and Chile. **Frontiers in Environmental Science**, v. 7, 69, 2019.

VIEGAS, J.; ANDREOLI, R. V.; KAYANO, M. T.; CANDIDO, L. A.; SOUZA, R. A. F.; HALL, D. H.; SOUZA, A. C.; GARCIA, S. R.; TEMOTEO, G. G.; VALENTIN, W. I. D. Caracterização dos diferentes tipos de El Niño e seus impactos na América do Sul a partir de dados observados e modelados. **Revista Brasileira de Meteorologia**, v. 34, n. 1, p. 43-67, 2019.

VIRJI, H. A preliminary study of summertime tropospheric circulation patterns over South America estimated from cloud winds. **Monthly Weather Review**, v. 109, p. 599-610, 1981.

VITART, F.; ROBERTSON, A. W. Introduction: Why sub-seasonal to seasonal prediction (S2S)? *In*: ROBERTSON, A. W.; VITART, F. **Sub-Seasonal to Seasonal Prediction – The Gap Between Weather and Climate Forecasting**. Elsevier, 2019, p. 3-15.

VITERBO, P.; BELJAARS, A. C. M. An improved land surface parameterization scheme in the ECMWF model and its validation. **Journal of Climate**, v. 8, p. 2716-2748, 1995.

WALLACE, J. M.; HOBBS, P. V. **Atmospheric science – An introductory survey**. New York: Academic Press, 2006, 483 p.

WALSH, R. P. D.; LAWLER, D. M. Rainfall seasonality: description, spatial patterns and change through time. **Weather**, v. 36, p. 201-208, 1981.

WANG, B.; LEE, J. -Y.; KANG, I. -S.; SHUKLA, J.; PARK, C. -K.; KUMAR, A.; SCHEMM, J.; COCKE, S.; KUG, J. -S.; LUO, J. -J.; ZHOU, T.; WANG, B.; FU, X.; YUN, W. -T.; ALVES, O.; JIN, E. K.; KINTER, J.; KIRTMAN, B.; KRISHNAMURTI, T.; LAU, N. C.; LAU, W.; LIU, P.; PEGION, P.; ROSATI, T.; SCHUBERT, S.; STERN, W.; SUAREZ, M.; YAMAGATA, T. Advance and prospectus of seasonal prediction: assessment of the APCC/CliPAS 14-model ensemble retrospective seasonal prediction (1980-2004). **Climate Dynamics**, v. 33, p. 93-117, 2009.

WANG, C. Three-ocean interactions and climate variability: a review and perspective. **Climate Dynamics,** v. 53, p. 5119-5136, 2019.

WANG, W.; CHEN, M.; KUMAR, A. An assessment of the CFS real-time seasonal forecasts. **Weather and Forecasting**, v. 25, p. 950-969, 2010.

WANG, X-Y.; LI, X.; ZHU, J.; TANAJURA, C. A. S. The strengthening of Amazonian precipitation during the wet season driven by tropical sea surface temperature forcing. **Environmental Research Letters**, 13, 0940115, 2018.

WEBER, N. J.; MASS, C. F. Evaluating CFSv2 sub-seasonal forecast skill with an emphasis on tropical convection. **Monthly Weather Review**, v. 145, p. 3795-3815, 2017.

WEBER, T. M.; DERECZYNSKI, C. P.; SOUZA, R. H. S.; CHOU, S. C.; BUSTAMANTE, J. F.; NETO, A. C. P. Investigação da previsibilidade sazonal da precipitação na região do Alto São Francisco em Minas Gerais. **Anuário do Instituto de Geociências**, v. 38, n. 2, p. 24-36, 2015.

WEBSTER, P. J. Response of the tropical atmosphere to local, steady forcing. **Monthly Weather Review**, v. 100, n. 7, p. 518-541, 1972.

WEIGEL, A. P.; BAGGENSTOS, D.; LINIGER, M. A.; VITART, F.; APPENZELLER, C. Probabilistic verification of monthly temperature forecasts. **Monthly Weather Review**, v. 136, p. 5162-5182, 2008.

WEISHEIMER, A.; PALMER, T. N. On the reliability of seasonal climate forecasts. **Journal of the Royal Society Interface**, v. 11, 20131162, 2014.

WHEELER, T.; VON BRAUN, J. Climate change impacts on global food security. **Science**, v. 341, p. 508-513, 2013.

WIEDERMANN, M.; SIEGMUND, J. F.; DONGES, J. F.; DONNER, R. V. Differential imprints of distinct ENSO flavors in global patterns of very low and high seasonal precipitation. **Frontiers in Climate**, v. 3, 618548, 2021.

WILKS, D. S. **Statistical methods in the atmospheric sciences**. Cambridge: Cambridge University Press, 2006, 630 p.

WILLMOTT, C. J. On the validation of models. **Physical Geography**, v. 2, p. 184-194, 1981.

WU, H.; ZOU, Y.; ALVEZ, L. M.; MACAU, E. E. N.; SAMPAIO, G.; MARENGO, J. A. Uncovering episodic influence of oceans on extreme drought events in Northeast Brazil by ordinal partition network approaches. **Chaos**, v. 30, 053104, 2020.

YEPES, J.; POVED, G.; MEJÍA, J.F.; MORENO, L.; RUEDA, C. CHOCO-JEX – A Research experiment focused on the Chocó low-level jet over the far eastern Pacific and western Colombia. **Bulletin of the American Meteorological Society**, v. 100, p. 779-796, 2019.

YNOUE, R. Y.; REBOITA, M. S.; AMBRIZZI, T.; SILVA, G. A. M. **Meteorologia: noções básicas**. São Paulo: Oficina de Textos, 2017, 182 p.

YUAN, X.; WOOD, E. F.; LUO, L.; PAN, M. A first look at Climate Forecast System version 2 (CFSv2) for hydrological seasonal prediction. **Geophysical Research Letters**, v. 38, L13402, 2011.

XU, K.; SU, J. Z.; ZHU, C. W.; The natural oscillation of two types of ENSO events based on analyses of CMIP5 model control runs. **Advances in Atmospheric Sciences**, v. 31, p. 801-813, 2014.

ZHOU, J.; LAU, K. M. Does monsoon climate exist over South America? **Journal of Climate**, v. 11, p. 1020-1040, 1998.

ZIERVOGEL, G.; BITHELL, M.; WASHINGTON, R.; DOWNING, T. Agent-based social simulation: a method for assessing the impact of seasonal climate forecast applications among smallholder farmers. **Agricultural Systems**, v. 83, p. 1-26, 2005.

ZOU, Y.; XI, X. An ongoing cooling in the eastern Pacific linked to eastward migrations of the Southeast Pacific Subtropical Anticyclone. **Environmental Research Letters**, v. 16, 034020, 2021.

ZUO, H.; BALSAMEDA, M. A.; BOISSESON, E.; HIRAHARA, S.; CHRUST, M.; ROSNAY, P. A generic ensemble generation scheme for data assimilation and ocean analysis. **ECMWF Technical Memorandum**, n. 795, 2017.

ZUO, H.; BALSAMEDA, M. A.; MOGENSEN, K. The new eddy-permitting ORAP5 Ocean Reanalysis: description, evaluation and uncertainties in climate signals. **Climate Dynamics**, v. 49, p. 791-811, 2017.

APPENDIX

→ Access to the work

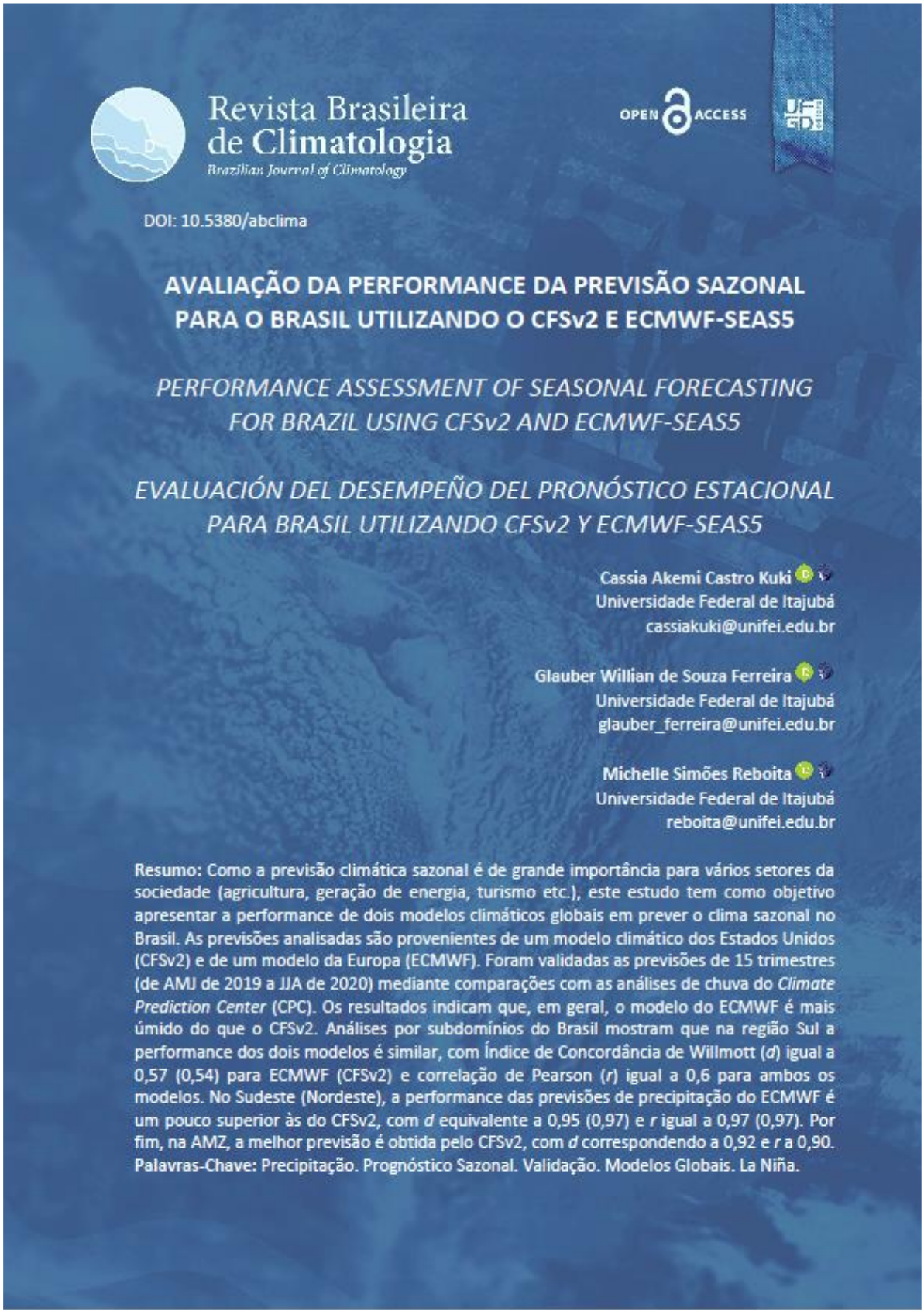

Revista Brasileira de Climatologia
Brazilian Journal of Climatology
OPEN ACCESS
DOI: 10.5380/abclima

AVALIAÇÃO DA PERFORMANCE DA PREVISÃO SAZONAL PARA O BRASIL UTILIZANDO O CFSv2 E ECMWF-SEAS5

PERFORMANCE ASSESSMENT OF SEASONAL FORECASTING FOR BRAZIL USING CFSv2 AND ECMWF-SEAS5

EVALUACIÓN DEL DESEMPEÑO DEL PRONÓSTICO ESTACIONAL PARA BRASIL UTILIZANDO CFSv2 Y ECMWF-SEAS5

Cassia Akemi Castro Kuki
Universidade Federal de Itajubá
cassiakuki@unifei.edu.br

Glauber Willian de Souza Ferreira
Universidade Federal de Itajubá
glauber_ferreira@unifei.edu.br

Michelle Simões Reboita
Universidade Federal de Itajubá
reboita@unifei.edu.br

Resumo: Como a previsão climática sazonal é de grande importância para vários setores da sociedade (agricultura, geração de energia, turismo etc.), este estudo tem como objetivo apresentar a performance de dois modelos climáticos globais em prever o clima sazonal no Brasil. As previsões analisadas são provenientes de um modelo climático dos Estados Unidos (CFSv2) e de um modelo da Europa (ECMWF). Foram validadas as previsões de 15 trimestres (de AMJ de 2019 a JJA de 2020) mediante comparações com as análises de chuva do *Climate Prediction Center* (CPC). Os resultados indicam que, em geral, o modelo do ECMWF é mais úmido do que o CFSv2. Análises por subdomínios do Brasil mostram que na região Sul a performance dos dois modelos é similar, com Índice de Concordância de Willmott (*d*) igual a 0,57 (0,54) para ECMWF (CFSv2) e correlação de Pearson (*r*) igual a 0,6 para ambos os modelos. No Sudeste (Nordeste), a performance das previsões de precipitação do ECMWF é um pouco superior às do CFSv2, com *d* equivalente a 0,95 (0,97) e *r* igual a 0,97 (0,97). Por fim, na AMZ, a melhor previsão é obtida pelo CFSv2, com *d* correspondendo a 0,92 e *r* a 0,90.
Palavras-Chave: Precipitação. Prognóstico Sazonal. Validação. Modelos Globais. La Niña.

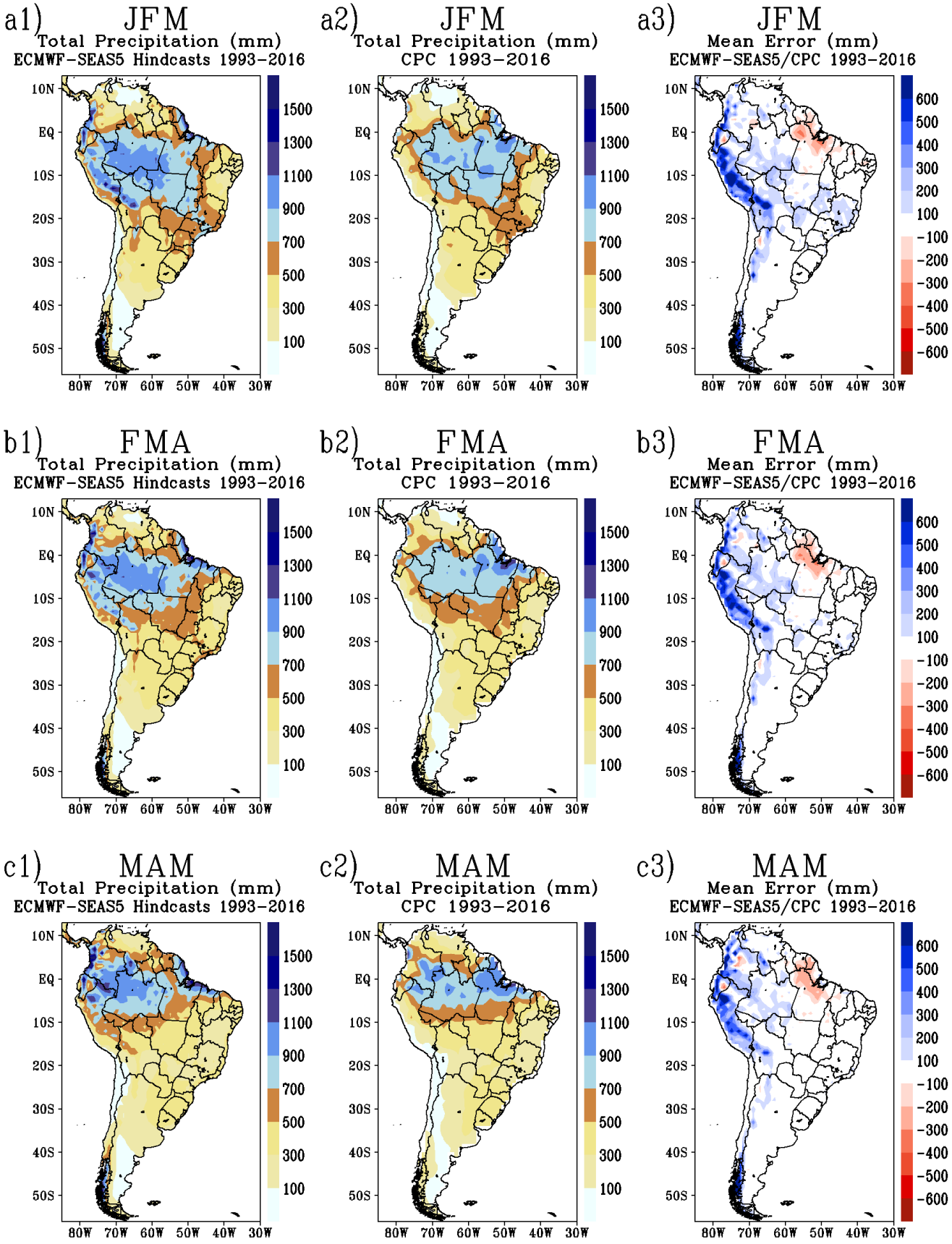

Figure A1 – Left column: seasonal total precipitation (mm) derived from the ECMWF-SEAS5 hindcasts, averaged for 1993-2016 and over the 25 ensemble members. Center column: CPC seasonal total precipitation (mm) averaged over 1993-2016. Right column: seasonal total precipitation mean errors (mm) obtained by the difference between ECMWF-SEAS5 and CPC and averaged over 1993-2016.

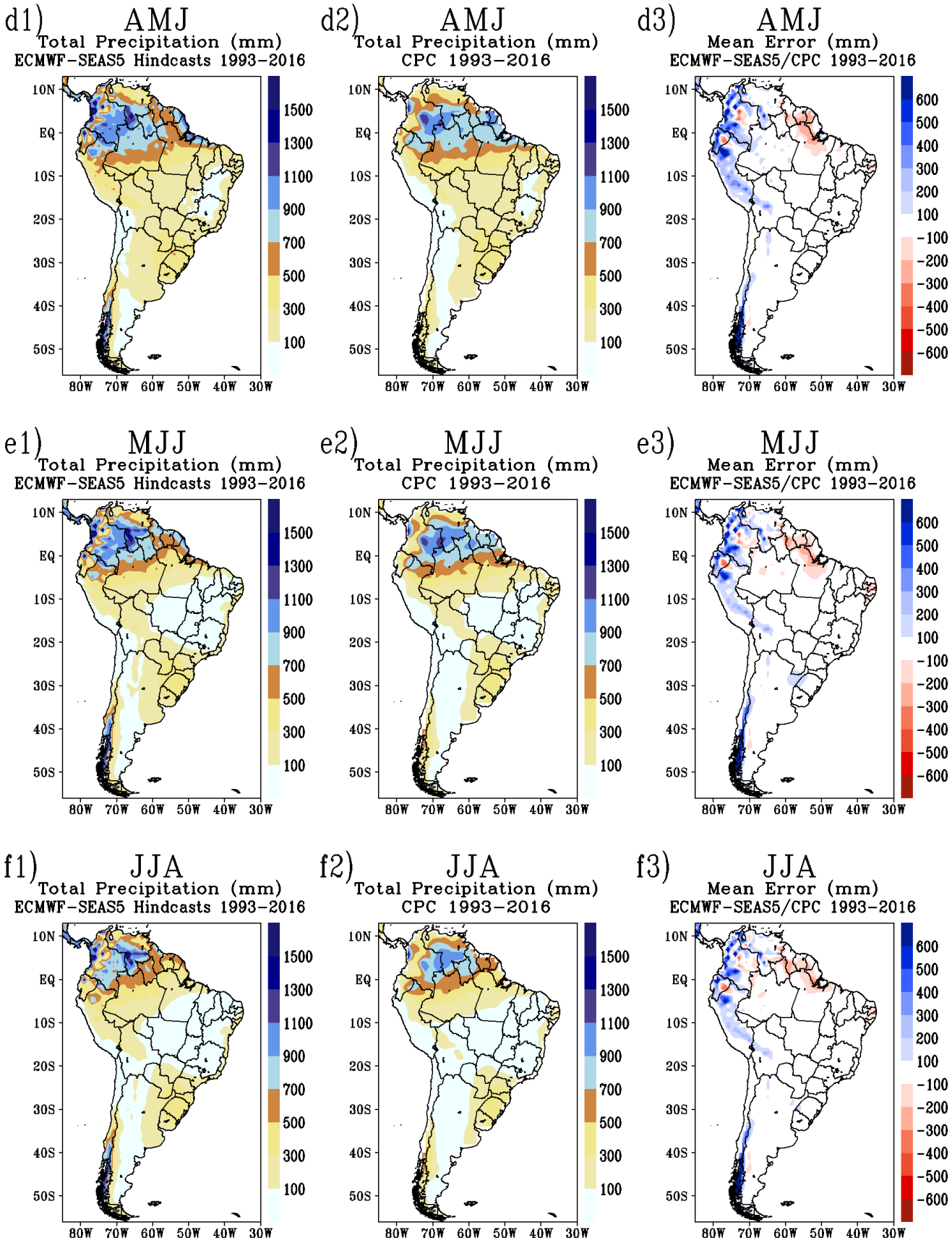

Figure A1 – continued.

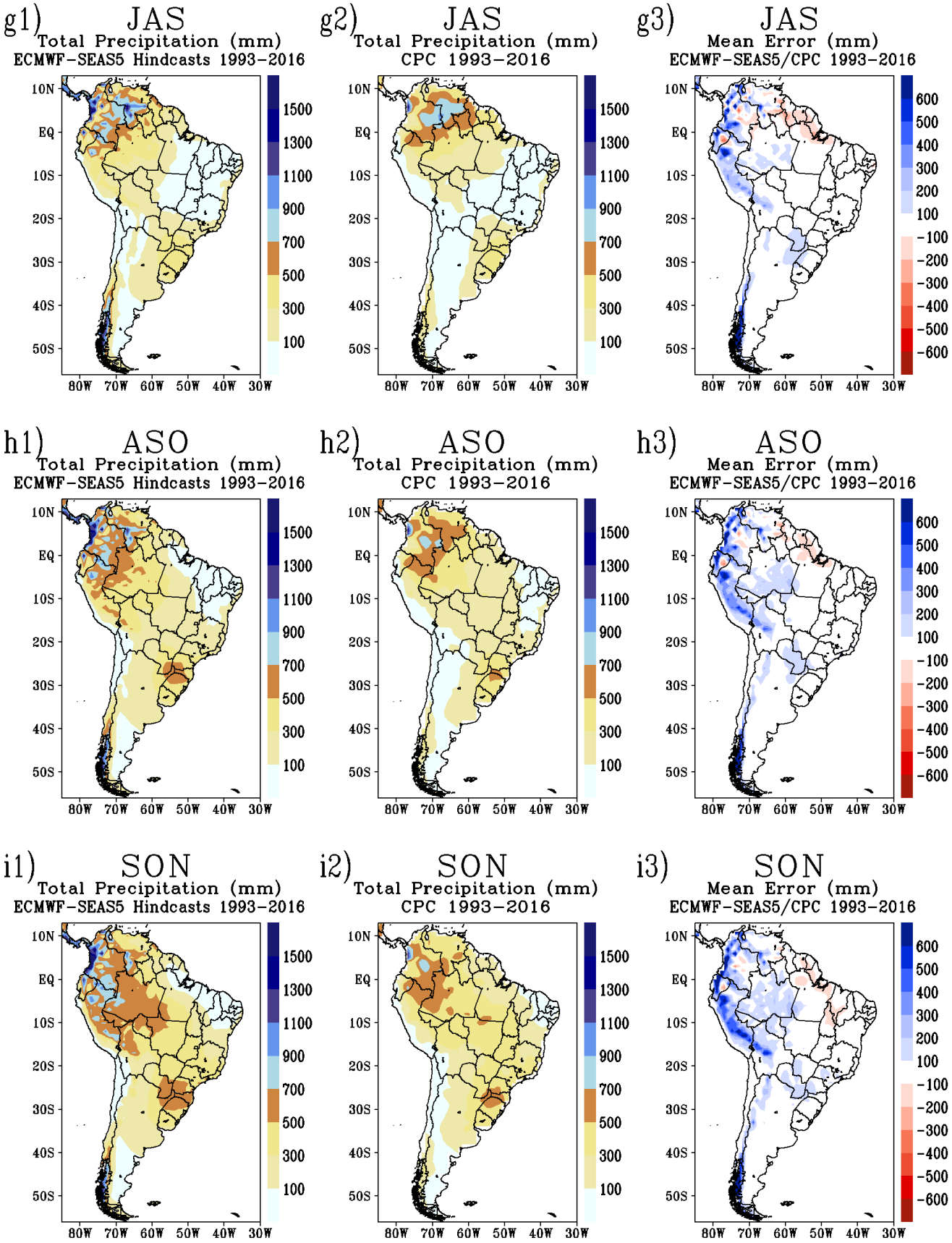

Figure A1 – continued.

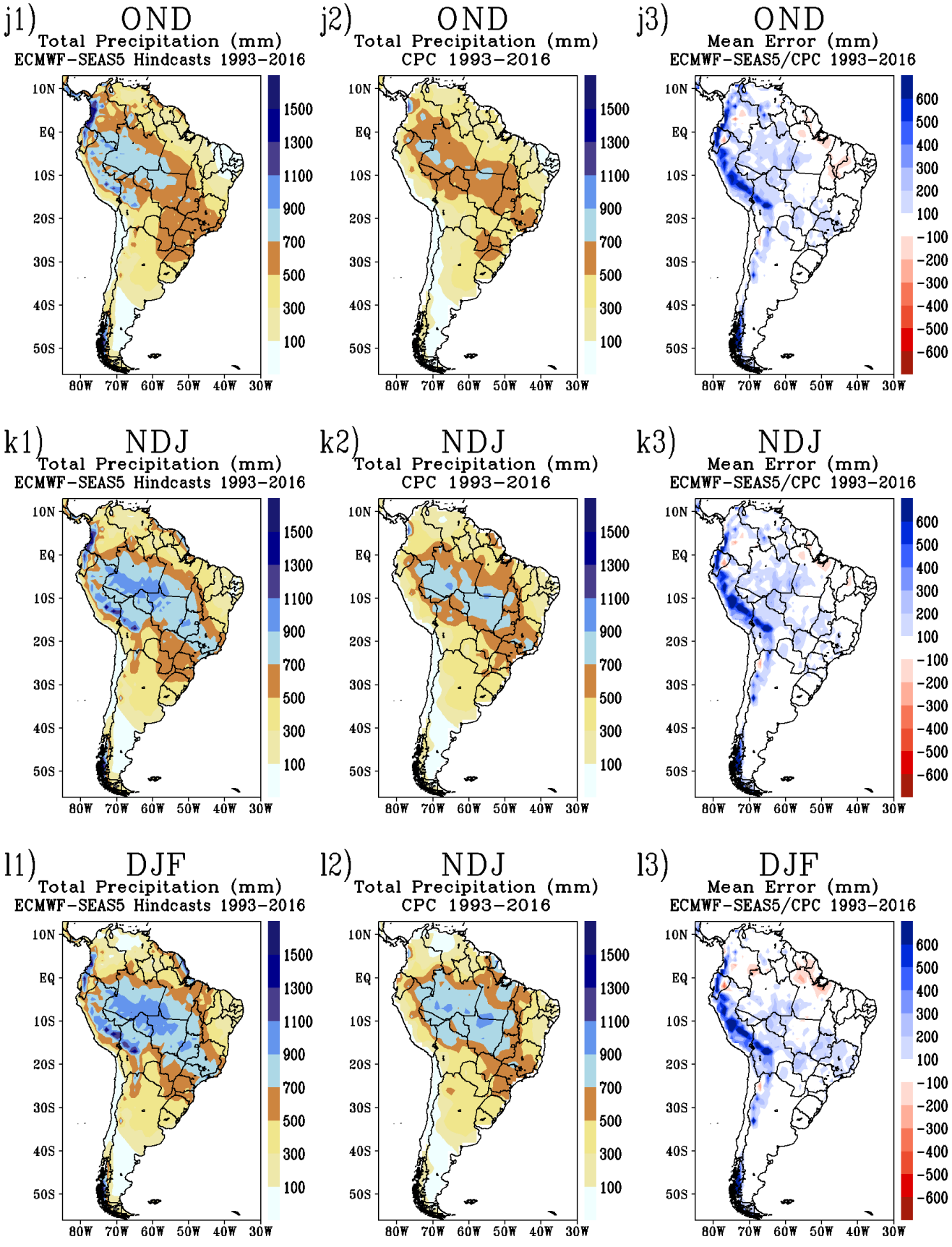

Figure A1 – continued.

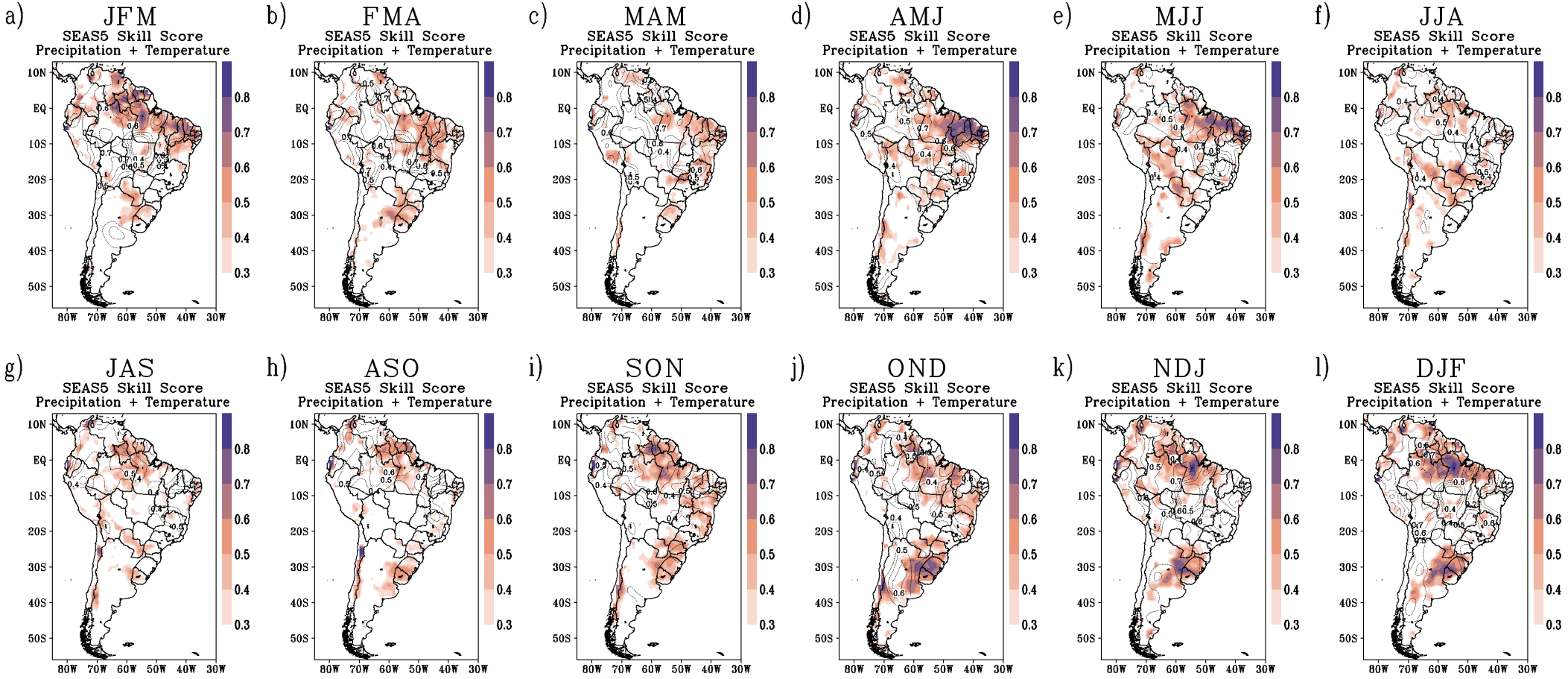

Figure A2 – Seasonal precipitation (colours) and temperature (contours) anomaly skill scores for the SEAS5 hindcasts. Trimesters correspond to reforecasts from the 1–3-month lead times. Only scores equal to or above 0.3 are shown. The score is nondimensional.

	SOUTHEAST BRAZIL - MEAN STATISTICS 1993-2016 - PREC							
	BIAS	R²	*r*	*d*	MAE	RMSE	RE	KGE
JFM	0,0000006167	0,0402	-0,2	0,143	0,81	1,067	14,93	-0,434
FMA	-0,0000001413	0,0360	0,19	0,257	0,683	0,862	19,92	-0,115
MAM	0,0000000941	0,0015	-0,039	0,302	0,469	0,545	16,89	-0,243
AMJ	0,0000001379	0,1135	0,337	0,434	0,455	0,553	25,42	0,059
MJJ	-0,0000000604	0,0223	0,149	0,397	0,472	0,539	30,86	-0,002
JJA	-0,0000001542	0,1773	0,421	0,608	0,276	0,361	26,92	0,326
JAS	-0,0000001167	0,0000	-0,004	0,279	0,494	0,651	41,15	-0,167
ASO	0,0000001829	0,1022	0,32	0,441	0,626	0,704	35,26	0,119
SON	-0,0000000646	0,1364	0,369	0,485	0,559	0,685	17,87	0,108
OND	0,0000000021	0,0171	0,131	0,283	0,699	0,784	15,19	-0,119
NDJ	0,0000002387	0,1911	-0,437	0,049	0,897	1,186	13,95	-0,659
DJF	-0,0000001312	0,1290	0,359	0,363	0,87	1,048	13,82	0,011

	SOUTHEAST BRAZIL - MEAN STATISTICS 2017-2020 - PREC							
	BIAS	R²	*r*	*d*	MAE	RMSE	RE	KGE
JFM	1,02790095	0,0247	-0,157	0,446	1,028	1,297	25,65	-0,123
FMA	0,372710375	0,3095	-0,556	0,42	0,561	0,581	35,21	-0,948
MAM	0,389835475	0,5486	0,741	0,542	0,57	0,705	29,34	0,14
AMJ	0,29079861	0,0341	0,185	0,387	0,666	0,716	44,84	-0,187
MJJ	0,358372175	0,0756	-0,275	0,401	0,503	0,58	51,32	-0,554
JJA	0,2439441	0,1687	-0,411	0,373	0,298	0,354	40,53	-0,566
JAS	0,5122905	0,1019	0,319	0,413	0,512	0,594	75,26	0,006
ASO	0,19150875	0,9285	0,964	0,607	0,545	0,58	44,6	0,17
SON	0,4587037	0,0180	0,134	0,452	0,81	1,044	41,48	-0,238
OND	0,62973734	0,1015	-0,319	0,453	0,868	1,127	25,21	-0,286
NDJ	1,491856275	0,0590	0,243	0,47	1,492	1,74	16,95	0,219
DJF	1,342939625	0,3044	-0,552	0,433	1,343	1,616	27,23	-0,446

	SOUTHEAST BRAZIL - MEAN STATISTICS 1993-2016 - TEMP							
	BIAS	R²	*r*	*d*	MAE	RMSE	RE	KGE
JFM	-0,0000001083	0,068	0,26	0,549	0,383	0,484	4,606	0,163
FMA	0,0000000975	0,065	0,254	0,538	0,395	0,519	2,41	0,206
MAM	0,0000001708	0,026	0,16	0,466	0,47	0,618	3,495	0,137
AMJ	0,0000000292	0,115	0,339	0,59	0,422	0,558	6,111	0,275
MJJ	0,0000000808	0,091	0,301	0,491	0,411	0,514	5,584	0,283
JJA	-0,0000000167	0,029	0,17	0,467	0,474	0,596	2,791	0,16
JAS	-0,0000001813	0,012	-0,108	0,319	0,562	0,705	6,901	-0,143
ASO	0,0000000167	0,08	0,283	0,521	0,511	0,597	9,471	0,196
SON	0,0000000333	0,202	0,449	0,644	0,514	0,593	9,102	0,309
OND	0,0000000542	0,139	0,372	0,584	0,468	0,626	8,366	0,301
NDJ	-0,0000005292	0,311	0,558	0,754	0,381	0,472	7,524	0,543
DJF	0,0000022563	0,335	0,579	0,753	0,363	0,437	6,622	0,549

	SOUTHEAST BRAZIL - MEAN STATISTICS 2017-2020 - TEMP							
	BIAS	R²	*r*	*d*	MAE	RMSE	RE	KGE
JFM	-0,0093361	0,01	0,101	0,434	0,293	0,343	4,486	-0,684
FMA	0,51858205	0,03	0,173	0,353	0,555	0,63	1,345	0,125
MAM	-0,18024785	0,103	-0,322	0,285	0,365	0,448	2,438	-0,407
AMJ	-0,4072945	0,076	0,275	0,231	0,479	0,556	4,309	0,032
MJJ	-0,3946555	0,391	-0,625	0,283	0,585	0,711	3,775	-0,693
JJA	0,33191685	0,466	-0,683	0,061	0,866	0,931	3,604	-0,756
JAS	0,06443545	0,006	-0,077	0,161	0,681	0,776	6,284	-0,396
ASO	-0,14305775	0,235	0,485	0,487	0,646	0,695	9,911	0,186
SON	-0,5289857	0,24	0,49	0,579	0,53	0,844	11,1	0,219
OND	0,1085821	0,206	0,454	0,605	0,347	0,414	7,804	0,44
NDJ	0,15604945	0,073	0,269	0,507	0,322	0,422	6,66	0,246
DJF	-0,055508225	0,062	-0,249	0,326	0,438	0,491	6,579	-0,31

	AMAZON - MEAN STATISTICS 1993-2016 - PREC							
	BIAS	R²	*r*	*d*	MAE	RMSE	RE	KGE
JFM	-0,0000003817	0,0046	0,068	0,2264	0,7429	0,9626	13,84	-0,201
FMA	-0,0000004250	0,0661	0,2571	0,3448	0,757	0,9034	14,28	-0,046
MAM	-0,0000002129	0,0389	0,1973	0,2739	0,6345	0,7708	14,97	-0,107
AMJ	0,0000001171	0,4063	0,6374	0,5998	0,4163	0,4958	14,87	0,257
MJJ	-0,0000000583	0,3298	0,5743	0,6145	0,2326	0,2974	15,7	0,283
JJA	-0,0000000375	0,1415	0,3761	0,5727	0,2268	0,277	27,9	0,201
JAS	0,0000001542	0,0973	0,3119	0,5555	0,3354	0,4133	48,58	0,123
ASO	-0,0000000925	0,0496	0,2227	0,3996	0,4762	0,5849	39,5	-0,06
SON	-0,0000000375	0,1322	0,3637	0,5621	0,5638	0,6946	26,57	0,167
OND	0,0000001083	0,1498	0,387	0,5157	0,6657	0,9256	22,42	0,137
NDJ	-0,0000004500	0,1729	0,4158	0,514	0,6666	0,9505	19,22	0,17
DJF	0,0000000787	0,0898	0,2997	0,4156	0,8359	1,0504	15,88	0,022

	AMAZON - MEAN STATISTICS 2017-2020 - PREC							
	BIAS	R²	*r*	*d*	MAE	RMSE	RE	KGE
JFM	1,338032	0,0164	0,1281	0,3126	1,338	1,4463	31,16	0,025
FMA	0,718277	0,4995	-0,707	0,2879	0,7183	0,8057	32,26	-4,069
MAM	0,51431625	0,3729	0,6107	0,4793	0,5855	0,658	20,83	0,099
AMJ	0,234490638	0,6295	-0,793	0,271	0,4595	0,4955	19,4	-0,981
MJJ	0,346441	0,7021	-0,838	0,1845	0,4544	0,4784	34,54	-0,906
JJA	0,3410278	0,323	0,5684	0,1112	0,341	0,3532	56,85	-2,293
JAS	0,49875981	0,1025	-0,32	0,238	0,4988	0,5739	97,61	-0,684
ASO	0,5486259	0,9194	0,9589	0,5809	0,5486	0,5793	67,24	0,201
SON	0,97399715	0,5939	0,7706	0,5104	0,974	1,0826	56,93	0,093
OND	1,09334275	0,114	0,3377	0,5244	1,0933	1,3387	38,63	-0,418
NDJ	1,7260184	0,1025	0,3201	0,4473	1,726	1,9063	35,26	0,074
DJF	1,59063915	0,1358	0,3685	0,4318	1,5906	1,8235	37,81	-0,102

	AMAZON - MEAN STATISTICS 1993-2016 - TEMP							
	BIAS	R²	*r*	*d*	MAE	RMSE	RE	KGE
JFM	0,0000001083	0,5218	0,7224	0,8366	0,2894	0,3413	4,92	0,222
FMA	0,0000002554	0,4745	0,6889	0,8185	0,3274	0,3732	5,786	0,646
MAM	0,0000000250	0,3498	0,5915	0,7573	0,324	0,4327	5,765	0,569
AMJ	-0,0240616500	0,2867	0,5354	0,7145	0,3985	0,5045	5,076	0,514
MJJ	0,0000000625	0,2943	0,5425	0,7104	0,3871	0,4755	3,926	0,46
JJA	-0,0000000433	0,1535	0,3918	0,5797	0,5087	0,59	4,535	0,297
JAS	-0,0000000229	0,1357	0,3684	0,5383	0,4892	0,6094	4,831	0,203
ASO	0,0000001754	0,1388	0,3725	0,5975	0,4844	0,6246	4,542	0,308
SON	0,0000000458	0,3509	0,5924	0,7601	0,3809	0,4791	3,159	0,509
OND	-0,0000008875	0,3619	0,6016	0,7783	0,3161	0,4054	3,016	0,595
NDJ	0,0000000371	0,4268	0,6533	0,7957	0,3013	0,3824	3,557	0,646
DJF	0,0000000750	0,5793	0,7611	0,864	0,2402	0,2967	4,409	0,739

	AMAZON - MEAN STATISTICS 2017-2020 - TEMP							
	BIAS	R²	*r*	*d*	MAE	RMSE	RE	KGE
JFM	-0,314471825	0,5607	0,7488	0,5467	0,3145	0,3475	6,344	0,234
FMA	-0,2771589	0,792	0,89	0,6658	0,2772	0,2915	6,71	0,816
MAM	-0,30229835	0,0057	0,0756	0,4606	0,4034	0,4417	6,766	0,064
AMJ	-0,266974875	0,2149	0,4635	0,6226	0,3667	0,4498	5,978	0,282
MJJ	-0,418155	0,2487	0,4987	0,5985	0,4182	0,5264	5,432	0,449
JJA	-0,245963425	0,9711	0,9855	0,712	0,3655	0,3786	5,369	0,334
JAS	-0,39574775	0,8349	0,9137	0,6703	0,3957	0,4429	6,153	0,535
ASO	-0,37884875	0,9932	0,9966	0,7176	0,3788	0,4094	5,762	0,585
SON	-0,47634675	0,7025	0,8381	0,6527	0,4763	0,524	4,7	0,8
OND	0,1211853	0,151	0,3885	0,6364	0,3897	0,4125	2,476	0,364
NDJ	-0,10167775	0,6211	0,7881	0,831	0,1462	0,1679	3,861	0,758
DJF	-0,16721475	0,7184	0,8476	0,622	0,1672	0,2178	4,971	0,364

	NORTHEAST BRAZIL - MEAN STATISTICS 1993-2016 - PREC							
	BIAS	R^2	*r*	*d*	MAE	RMSE	RE	KGE
JFM	0,0000001517	0,465	0,682	0,728	0,696	0,862	16,82	0,415
FMA	-0,0000000750	0,195	0,441	0,605	0,955	1,17	29,02	0,245
MAM	-0,0000003625	0,469	0,685	0,779	0,753	0,966	30,52	0,492
AMJ	-0,0000000212	0,65	0,806	0,85	0,483	0,627	23,23	0,595
MJJ	-0,0000002375	0,683	0,826	0,861	0,267	0,311	17,37	0,565
JJA	-0,0000000125	0,38	0,616	0,699	0,189	0,217	23,97	0,329
JAS	-0,0000000461	0,211	0,459	0,455	0,132	0,192	16,76	0,121
ASO	0,0000000417	0,096	0,31	0,262	0,231	0,326	31,95	-0,078
SON	-0,0000000604	0,275	0,525	0,468	0,259	0,368	28,85	0,1
OND	-0,0000000516	0,285	0,534	0,63	0,331	0,425	30,08	0,23
NDJ	-0,0000000975	0,02	0,142	0,315	0,645	0,885	24,24	-0,056
DJF	-0,0000000708	0,081	0,284	0,441	0,724	1,011	18,45	0,106

	NORTHEAST BRAZIL - MEAN STATISTICS 2017-2020 - PREC							
	BIAS	R^2	*r*	*d*	MAE	RMSE	RE	KGE
JFM	0,6544635	0,152	0,39	0,5	1,118	1,486	27,03	-0,057
FMA	0,09754015	0,181	0,426	0,629	0,613	0,66	23	-0,19
MAM	0,0400115	0,887	0,942	0,947	0,264	0,304	14,16	0,61
AMJ	0,416551015	0,297	0,545	0,513	0,422	0,57	21,12	-0,022
MJJ	0,39418955	0,095	0,308	0,387	0,402	0,478	22,1	0,272
JJA	0,135354265	0,014	-0,118	0,376	0,195	0,254	28,5	-0,331
JAS	0,099491383	0,189	0,434	0,434	0,18	0,191	23,79	0,165
ASO	0,142334525	0,965	0,982	0,17	0,142	0,142	10,73	0,863
SON	0,1034699	0,353	0,594	0,497	0,225	0,229	19,09	0,164
OND	0,235502425	0,702	0,838	0,604	0,384	0,405	19,13	0,269
NDJ	0,620577875	0,968	0,984	0,507	0,621	0,624	11,41	0,301
DJF	0,66097225	0,135	0,368	0,415	0,78	0,872	25,03	0,35

	NORTHEAST BRAZIL - MEAN STATISTICS 1993-2016 - TEMP							
	BIAS	R^2	*r*	*d*	MAE	RMSE	RE	KGE
JFM	0,0000004933	0,379	0,615	0,763	0,355	0,433	2,351	-0,057
FMA	-0,0000000750	0,303	0,551	0,715	0,396	0,473	2,687	0,467
MAM	-0,0000001750	0,506	0,711	0,822	0,343	0,432	2,818	0,647
AMJ	0,0000003025	0,467	0,683	0,818	0,357	0,466	1,453	0,686
MJJ	-0,0000000637	0,666	0,816	0,9	0,277	0,338	1,392	0,809
JJA	0,0000002021	0,591	0,769	0,874	0,248	0,301	1,044	0,768
JAS	-0,0000000401	0,499	0,706	0,834	0,215	0,28	2,669	0,701
ASO	-0,0000000300	0,651	0,807	0,879	0,167	0,2	4,819	0,707
SON	-0,0000000458	0,552	0,743	0,79	0,264	0,299	4,388	0,5
OND	-0,0000000188	0,588	0,767	0,788	0,277	0,333	2,19	0,487
NDJ	-0,0000000708	0,49	0,7	0,805	0,33	0,372	1,152	0,594
DJF	-0,0000000625	0,393	0,627	0,787	0,304	0,39	1,077	0,609

	NORTHEAST BRAZIL - MEAN STATISTICS 2017-2020 - TEMP							
	BIAS	R^2	*r*	*d*	MAE	RMSE	RE	KGE
JFM	0,3037333	0,059	-0,244	0,388	0,532	0,578	0,995	0,444
FMA	0,6790134	0,21	0,459	0,452	0,679	0,74	0,886	0,174
MAM	0,545765675	0,839	0,916	0,614	0,546	0,579	0,654	0,57
AMJ	0,39390675	0,416	0,645	0,622	0,394	0,489	1,199	0,433
MJJ	0,326925825	0,007	-0,084	0,42	0,327	0,397	2,362	-0,145
JJA	0,56699555	0,811	-0,9	0,061	0,626	0,71	2,736	-1,126
JAS	0,515599815	0,343	-0,586	0,185	0,66	0,767	2,059	-0,592
ASO	0,12679085	0,177	-0,421	0,155	0,367	0,395	4,353	-0,511
SON	0,063730275	0,139	0,373	0,413	0,189	0,253	4,189	0,067
OND	0,095208353	0,828	0,91	0,708	0,225	0,255	1,836	0,328
NDJ	0,235716625	0,114	0,338	0,497	0,31	0,365	1,174	0,073
DJF	0,345801675	0,037	-0,192	0,369	0,424	0,467	1,512	-0,222

	SOUTH BRAZIL - MEAN STATISTICS 1993-2016 - PREC							
	BIAS	R^2	*r*	*d*	MAE	RMSE	RE	KGE
JFM	-0,0000001208	0,203	0,451	0,466	0,905	1,1	21,6	0,119
FMA	-0,0000001258	0,309	0,556	0,563	0,934	1,086	19,88	0,224
MAM	0,0000004417	0,339	0,582	0,671	0,72	0,904	19,48	0,361
AMJ	0,0000004292	0,113	0,336	0,54	0,702	0,85	21,89	0,185
MJJ	-0,0000003592	0,083	0,288	0,511	0,592	0,707	24,12	0,13
JJA	-0,0000001742	0,089	0,299	0,512	0,457	0,559	21,41	0,214
JAS	-0,0000002042	0,088	0,296	0,469	0,555	0,721	32,45	0,033
ASO	-0,0000002225	0,222	0,472	0,594	0,638	0,759	22,75	0,25
SON	0,0000001833	0,35	0,591	0,672	0,659	0,904	20,15	0,366
OND	0,0000005083	0,557	0,746	0,756	0,843	1,028	17,77	0,438
NDJ	0,0000001667	0,523	0,723	0,765	0,742	0,97	17,56	0,473
DJF	0,0000006375	0,605	0,778	0,676	0,823	0,991	19,09	0,31

	SOUTH BRAZIL - MEAN STATISTICS 2017-2020 - PREC							
	BIAS	R^2	*r*	*d*	MAE	RMSE	RE	KGE
JFM	0,29140725	0,325	0,570	0,506	0,691	0,727	17,19	0,229
FMA	0,73468705	0,378	0,615	0,476	1,322	1,474	36,13	0,743
MAM	-0,14174985	0,894	0,945	0,255	1,369	1,506	36,19	0,067
AMJ	-0,214009925	0,461	0,679	0,618	0,694	0,954	19,29	0,311
MJJ	-0,220199775	0,367	0,606	0,659	0,287	0,347	8,212	0,339
JJA	0,567725325	0,517	-0,719	0,289	0,653	0,859	43,16	-0,789
JAS	0,646257758	0,220	-0,469	0,383	0,646	0,846	55,52	-0,626
ASO	0,6660738	0,035	0,188	0,458	0,974	1,219	47,57	-0,271
SON	0,740607925	0,270	0,520	0,471	0,952	1,228	40,63	0,008
OND	0,870703625	0,593	0,770	0,531	0,871	1,048	25,48	0,283
NDJ	-0,09450625	0,245	0,495	0,575	0,51	0,639	16,67	-0,33
DJF	0,419342225	0,317	-0,563	0,233	0,856	0,878	17,03	-0,736

	SOUTH BRAZIL - MEAN STATISTICS 1993-2016 - TEMP							
	BIAS	R^2	*r*	*d*	MAE	RMSE	RE	KGE
JFM	-0,0000000083	0,0107	-0,104	0,313	0,444	0,572	3,248	-0,223
FMA	-0,0000002917	0,051	0,226	0,42	0,459	0,604	3,182	0,111
MAM	0,0000000917	0,0015	0,038	0,376	0,54	0,677	9,36	-0,026
AMJ	0,0000003667	0,1286	0,359	0,562	0,457	0,594	13,33	0,181
MJJ	0,0000000896	0,0085	-0,092	0,296	0,821	1,012	11,47	-0,22
JJA	0,0000002458	0,0072	0,085	0,408	0,852	1,012	5,591	-0,055
JAS	-0,0000003521	0,0283	0,168	0,463	0,746	0,882	7,52	0,062
ASO	0,0000000163	0,0002	0,014	0,354	0,789	0,879	13,43	-0,036
SON	0,0000000000	0,0871	0,295	0,574	0,522	0,682	14,42	0,286
OND	0,0000001204	0,1943	0,441	0,673	0,446	0,535	14,8	0,408
NDJ	-0,0000000550	0,1549	0,394	0,595	0,366	0,433	12,01	0,303
DJF	0,0000004475	0,1097	0,331	0,533	0,416	0,49	7,982	0,256

	SOUTH BRAZIL - MEAN STATISTICS 2017-2020 - TEMP							
	BIAS	R^2	*r*	*d*	MAE	RMSE	RE	KGE
JFM	0,23615755	0,2375	0,487	0,611	0,258	0,351	2,639	0,174
FMA	0,18652895	0,3539	-0,595	0	0,504	0,527	3,574	-0,669
MAM	-0,32385275	0,6873	-0,829	0,211	0,559	0,715	7,52	-0,957
AMJ	-0,486372	0,1607	-0,401	0,367	0,657	0,837	10,02	-0,608
MJJ	-0,515018725	0,747	0,864	0,593	0,582	0,767	7,502	0,18
JJA	0,23038725	0,3265	-0,571	0,16	0,988	1,274	6,59	-0,705
JAS	-0,422608075	0,2091	0,457	0,499	0,712	0,941	9,572	0,144
ASO	-0,365084325	0,7976	0,893	0,678	0,499	0,555	15,04	0,341
SON	-0,23138025	0,1933	-0,44	0,167	0,382	0,408	15	-0,455
OND	-0,005600425	0,558	-0,747	0,102	0,473	0,62	14,56	-0,778
NDJ	0,12178745	0,0092	0,096	0,477	0,418	0,437	11,39	0,078
DJF	0,36142165	0,3072	-0,554	0,224	0,426	0,564	6,558	-0,571

	SOUTHEASTERN SOUTH AMERICA - MEAN STATISTICS 1993-2016 - PREC							
	BIAS	R^2	*r*	*d*	MAE	RMSE	RE	KGE
JFM	-0,0000005262	0,0051	-0,072	0,235	0,7269	0,829	21,436	-0,184
FMA	0,0000005875	0,1122	0,3349	0,4731	0,6192	0,7138	19,821	0,0822
MAM	-0,0000001756	0,092	0,3034	0,3931	0,6095	0,7513	20,412	0,0128
AMJ	-0,0000003083	0,0865	0,2942	0,3721	0,5062	0,7549	27,314	-0,01
MJJ	0,0000000004	0,003	0,055	0,3691	0,3997	0,5511	32,156	-0,128
JJA	0,0000000925	0,162	0,4024	0,4261	0,3514	0,4306	36,477	0,0597
JAS	-0,0000000304	0,2231	0,4724	0,4825	0,3807	0,4693	33,818	0,1274
ASO	-0,0000002463	0,3329	0,577	0,4123	0,5988	0,7779	24,903	0,1115
SON	-0,0000004371	0,1654	0,4067	0,447	0,6338	0,7417	19,804	0,0922
OND	-0,0000002327	0,4308	0,6564	0,519	0,7458	0,8768	22,516	0,1873
NDJ	0,0000000667	0,2711	0,5207	0,597	0,5276	0,6781	20,767	0,2611
DJF	0,0000154208	0,3753	0,6126	0,6378	0,4586	0,6372	18,732	0,2882

	SOUTHEASTERN SOUTH AMERICA - MEAN STATISTICS 2017-2020 - PREC							
	BIAS	R^2	*r*	*d*	MAE	RMSE	RE	KGE
JFM	0,54400205	0,0004	-0,021	0,1486	0,6768	0,8904	24,201	-0,199
FMA	0,451655725	0,0031	-0,056	0,4133	0,9777	1,1565	32,465	-0,342
MAM	0,053404975	0,17	0,4123	0,4483	0,5086	0,6088	20,436	0,108
AMJ	-0,20679487	0,2309	-0,48	0,291	0,3623	0,4531	14,461	-0,216
MJJ	-0,1416806	0,615	0,7842	0,5861	0,3096	0,3399	15,397	0,2105
JJA	-0,254378025	0,0058	0,0762	0,4907	0,334	0,4263	18,765	-0,209
JAS	-0,266609175	0,1337	0,3657	0,3566	0,852	0,9243	47,316	-0,107
ASO	-0,115884925	0,4663	0,6829	0,3574	0,4723	0,6321	16,347	0,0933
SON	0,32302819	0,4488	0,6699	0,5307	0,3392	0,4622	11,698	0,1645
OND	0,535449675	0,907	0,9524	0,5585	0,6695	0,8378	22,941	0,1294
NDJ	0,152625	0,5301	0,7281	0,5446	0,948	1,0302	17,828	0,1927
DJF	0,43254115	0,4327	0,6578	0,5066	0,8845	0,9592	20,243	0,068

	SOUTHEASTERN SOUTH AMERICA - MEAN STATISTICS 1993-2016 - TEMP							
	BIAS	R^2	*r*	*d*	MAE	RMSE	RE	KGE
JFM	0,0000001208	0,2698	0,5194	0,6685	0,4422	0,5148	3,415	0,332
FMA	0,0000000154	0,1324	0,3639	0,5913	0,4986	0,635	6,241	0,365
MAM	-0,0000000833	0,0331	0,182	0,4188	0,5416	0,6765	14,36	0,022
AMJ	-0,0000001937	0,0283	0,1682	0,3876	0,5138	0,6722	23	-0,011
MJJ	0,0000004583	0,0039	0,0627	0,3641	0,6376	0,848	22,81	-0,142
JJA	0,0000003333	0,0762	0,2761	0,4314	0,6031	0,7811	8,919	0,048
JAS	-0,0000003500	0,0518	0,2276	0,4445	0,5407	0,6386	10,149	0,040
ASO	0,0000000167	0,0056	-0,075	0,3347	0,5782	0,7043	21,9	-0,128
SON	0,0000005446	0,0000	-0,0005	0,363	0,527	0,6532	24,52	-0,128
OND	-0,0000001058	0,1945	0,441	0,6022	0,4607	0,5311	23,84	0,23
NDJ	-0,0000000750	0,2702	0,5198	0,6246	0,4814	0,5607	19,06	0,252
DJF	0,0000003375	0,0736	0,2714	0,4933	0,5219	0,6238	11,79	0,089

	SOUTHEASTERN SOUTH AMERICA - MEAN STATISTICS 2017-2020 - TEMP							
	BIAS	R^2	*r*	*d*	MAE	RMSE	RE	KGE
JFM	0,17622865	0,1437	0,379	0,7479	0,414	0,4646	2,51	0,081
FMA	-0,345565075	0,7521	0,8673	0,6128	0,4701	0,5139	4,094	0,279
MAM	-0,27205575	0,3401	0,5831	0,9423	0,3659	0,4689	12,01	0,367
AMJ	-0,29160325	0,034	-0,184	0,2985	0,4452	0,5883	19,22	-0,228
MJJ	-0,072260325	0,0179	-0,134	0,1127	0,6451	0,6668	20,73	-0,411
JJA	0,174926875	0,0045	0,0667	0,4049	0,6578	0,9117	10,25	-0,16
JAS	-0,10555575	0,1222	-0,35	0,1121	0,7849	0,8598	10,55	-0,453
ASO	0,07850675	0,8357	0,9142	0,9399	0,1679	0,1737	21,32	0,744
SON	0,40220325	0,4746	-0,689	0,36	0,4022	0,5706	21,9	-0,775
OND	0,287452525	0,9975	-0,999	0,1706	0,4883	0,5353	23,84	0,23
NDJ	0,077831925	0,5834	0,7638	0,8316	0,1599	0,1936	18,68	0,576
DJF	0,23479125	0,0218	-0,148	0,1453	0,5238	0,5264	10,82	-0,249

	NORTHERN SOUTH AMERICA- MEAN STATISTICS 1993-2016 - PREC							
	BIAS	R²	*r*	*d*	MAE	RMSE	RE	KGE
JFM	-0,0000001667	0,601	0,775	0,872	0,572	0,692	12,69	0,73
FMA	0,0000003108	0,101	0,318	0,586	0,81	0,984	14,68	0,299
MAM	-0,0000008375	0,005	0,073	0,314	1,151	1,297	16,45	-0,128
AMJ	-0,0000001000	0,035	0,186	0,352	1,242	1,444	14,66	-0,088
MJJ	0,0000001937	0,051	0,225	0,295	1,202	1,42	14,02	-0,074
JJA	0,0000003125	0,163	0,403	0,543	0,985	1,182	14,24	0,181
JAS	-0,0000000917	0,186	0,431	0,533	0,989	1,064	16,13	0,199
ASO	-0,0000007108	0,227	0,477	0,589	0,857	0,953	18,61	0,247
SON	-0,0000000242	0,295	0,544	0,6	0,771	0,868	21,61	0,274
OND	0,0000003125	0,428	0,655	0,755	0,517	0,63	24,58	0,466
NDJ	0,0000004542	0,484	0,696	0,787	0,63	0,752	23,93	0,516
DJF	-0,0000005042	0,642	0,801	0,85	0,586	0,711	12,68	0,605

	NORTHERN SOUTH AMERICA - MEAN STATISTICS 2017-2020 - PREC							
	BIAS	R²	*r*	*d*	MAE	RMSE	RE	KGE
JFM	1,164851	0,385	0,62	0,634	1,249	1,568	41,8	0,48
FMA	1,2517605	0,213	0,462	0,393	1,252	1,41	37,32	0,323
MAM	1,68449205	0,015	-0,124	0,882	1,684	1,926	36,44	-0,291
AMJ	1,9406137	0,146	0,382	0,433	1,941	2,169	28,8	0,064
MJJ	1,927156225	0,631	0,794	0,403	1,927	2,01	22,11	0,304
JJA	1,88163	0,797	0,893	0,346	1,882	1,901	21,66	0,625
JAS	1,391443025	0,117	0,341	0,312	1,391	1,44	17,66	0,28
ASO	1,256006525	0,317	0,563	0,29	1,256	1,275	33,49	0,169
SON	1,04205115	0,388	0,623	0,307	1,042	1,065	43,31	0,165
OND	0,899321475	0,09	0,3	0,395	0,899	0,953	52,51	-0,066
NDJ	0,70400055	0,482	0,694	0,671	0,704	0,937	42,61	0,295
DJF	1,260541	0,659	0,812	0,606	1,261	1,352	38,17	0,531

	NORTHERN SOUTH AMERICA - MEAN STATISTICS 1993-2016 - TEMP							
	BIAS	R²	*r*	*d*	MAE	RMSE	RE	KGE
JFM	-0,0000001612	0,718	0,847	0,919	0,259	0,311	5,721	0,834
FMA	-0,0000003688	0,652	0,807	0,845	0,342	0,442	5,413	0,386
MAM	0,0000000533	0,466	0,683	0,732	0,39	0,47	4,872	0,089
AMJ	-0,0000001583	0,258	0,508	0,654	0,281	0,416	4,943	0,113
MJJ	0,0000002317	0,225	0,474	0,699	0,261	0,324	5,675	0,451
JJA	-0,0000001779	0,261	0,511	0,719	0,263	0,314	7,198	0,499
JAS	-0,0000001229	0,365	0,604	0,766	0,239	0,295	8,072	0,55
ASO	0,0000000236	0,59	0,768	0,861	0,207	0,257	7,855	0,696
SON	-0,0000001083	0,569	0,754	0,865	0,235	0,288	6,041	0,746
OND	-0,0000000663	0,465	0,682	0,819	0,253	0,336	5,065	0,663
NDJ	0,0000000492	0,472	0,687	0,821	0,28	0,371	5,106	0,682
DJF	0,0000000583	0,634	0,796	0,886	0,245	0,314	5,746	0,749

	NORTHERN SOUTH AMERICA - MEAN STATISTICS 2017-2020 - TEMP							
	BIAS	R²	*r*	*d*	MAE	RMSE	RE	KGE
JFM	-0,25466675	0,86	0,927	0,891	0,255	0,291	6,575	0,781
FMA	-0,075518425	0,641	0,801	0,88	0,246	0,286	5,607	0,778
MAM	0,12548615	0,683	0,826	0,887	0,224	0,28	4,346	0,44
AMJ	0,349731375	0,91	0,954	0,671	0,35	0,414	3,601	0,076
MJJ	0,16479625	0,444	0,666	0,757	0,236	0,284	5,027	0,629
JJA	0,0792932	0,031	0,177	0,519	0,271	0,317	6,857	0,133
JAS	0,01236225	0,02	-0,142	0,264	0,3	0,357	7,954	-0,234
ASO	0,0626895	0,054	-0,232	0,35	0,306	0,324	7,546	-0,334
SON	0,000111057	0,439	-0,663	0,146	0,255	0,34	5,978	-0,664
OND	0,130081225	0,539	-0,734	0,055	0,271	0,287	4,548	-1,004
NDJ	-0,02386693	0,712	-0,844	0	0,174	0,206	5,159	-0,985
DJF	-0,077215315	0,088	0,297	0,531	0,221	0,293	5,984	0,219

This section presents a tutorial demonstrating the steps for selecting and obtaining SEAS5 data. Initially, access the website https://cds.climate.copernicus.eu/cdsapp#!/dataset/seasonal-original-single-levels?tab=form. There will be two sets of data labelled as “daily data”. These contain daily or sub-daily frequency (6h, 12h or 24h). The results of the different forecasting systems are available both for real-time forecasts (from 2017) and for retrospective forecasts or hindcasts (covering the 1993-2016 period). Please note that all available individual members (ensemble members) will be provided in each requested set. The real-time prediction set contains surface (or single level) parameters, while the hindcast set contains variables at 11 pressure levels covering layers from 925 hPa up to 10 hPa.

First, the institution that provides the forecasting system of interest must be selected.

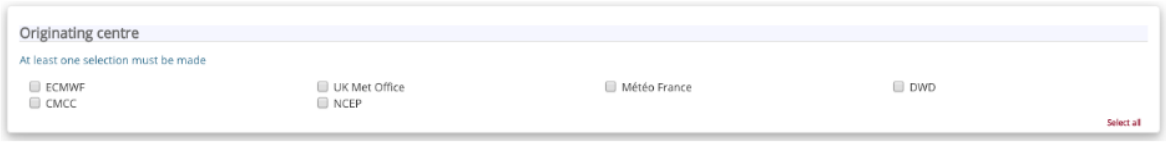

Next, the forecast system version of interest must be selected. Each centre is assigned as a numerical value, and the available values are different for each forecast delivery centre. It should be noted that there may be more than one system available for a single forecast centre for a given start date. Also, the user must match the seasonal forecasts to the hindcasts of interest using the same system for both sets.

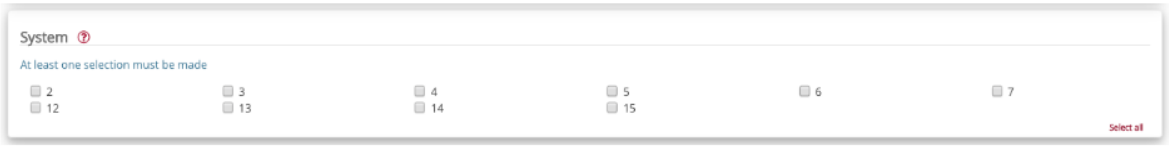

Then the user must select the parameters of interest.

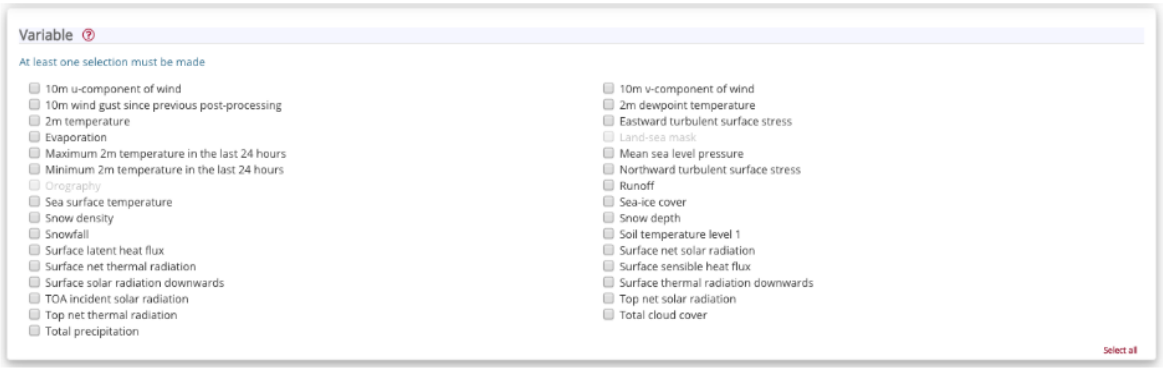

In this step, the user must select the year of the start date of the model of interest. Note that there may be differences in the options available depending on the selection of forecast or hindcasts years. In addition, the user must employ the hindcast data to obtain a more consistent use of the forecast data. It is emphasized again that the sets of predictions and hindcasts must be paired, using the same system for both sets.

Next, the user must select the month of the start date of the model round of interest.

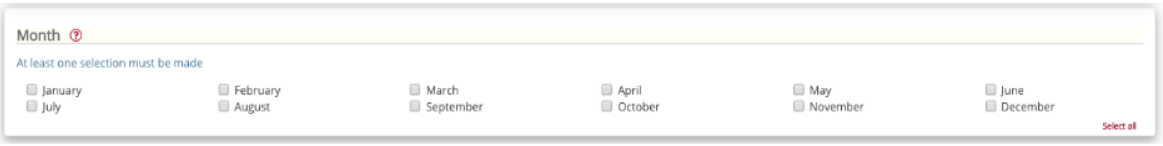

The start date (day) of the model run of interest is selected. However, due to different production schedules, available dates may differ between forecasts and hindcasts and between different forecast centres.

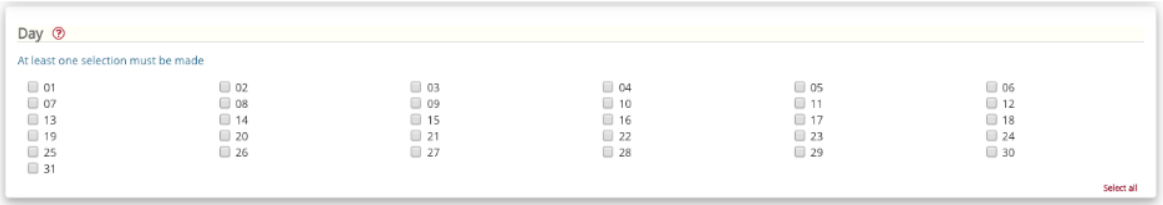

Next, the user must select the lead time of interest. This lead time is the time, in hours, since the boot date. Note that some variables are available every 6 hours and other every 24 hours. This information is available in the complete list of parameters in the official documentation and the summary table on the data collection page. Finally, it should be noted that the minimum time horizon for outputs is six months, but this extension may change depending on the forecasting centre.

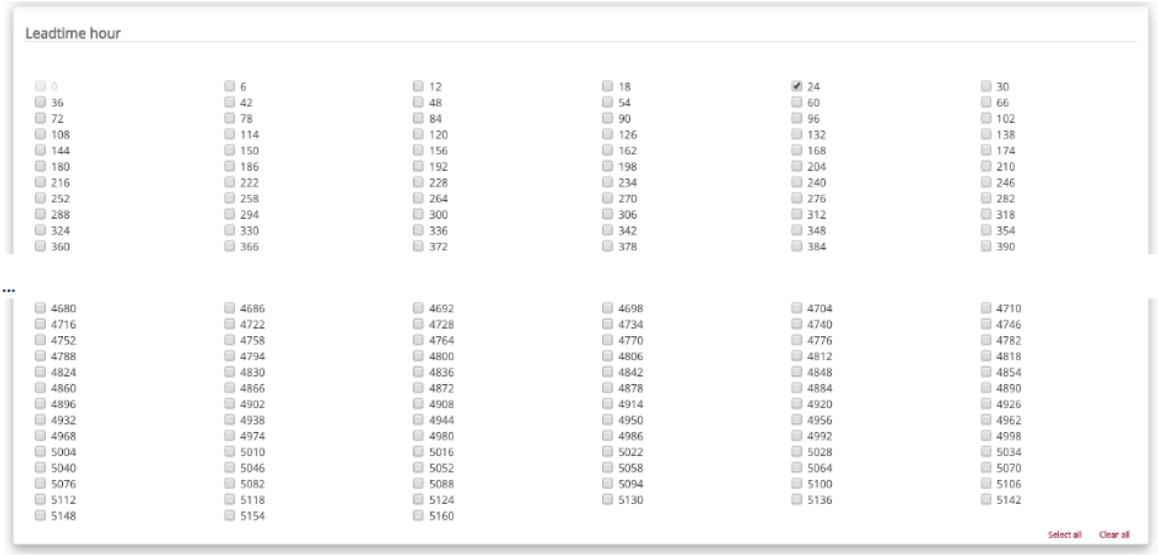

The user must select the area of interest, which can be a global field (comprising the entire available area) or a regional selection, by providing the latitude and longitude coordinates of the borders.

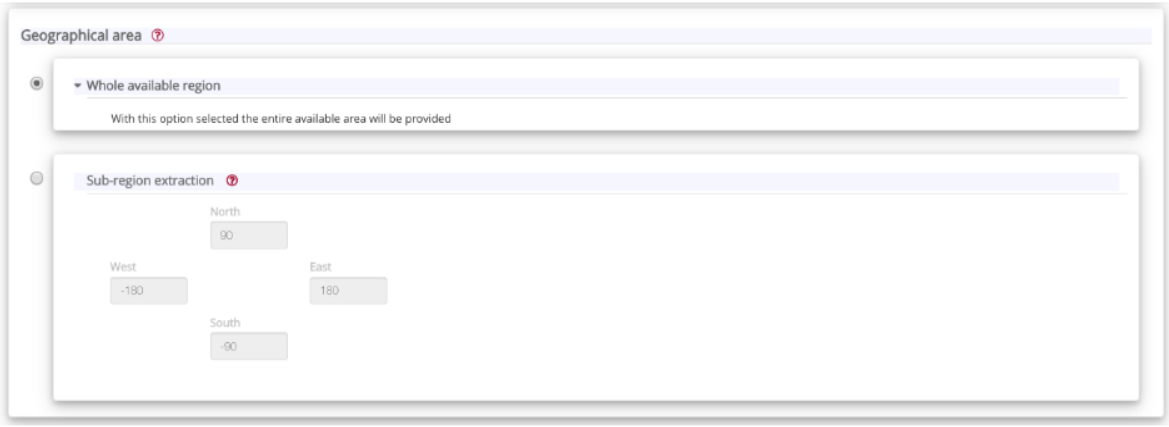

The user can select the format of the data provided. Currently, C3S forecast datasets are only available in GRIB format.

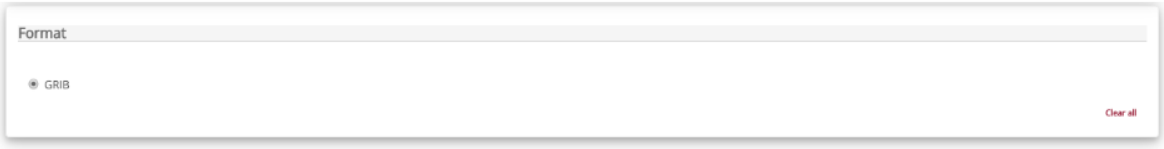

Finally, the user must accept the Copernicus User License terms and conditions to access seasonal forecast data and hindcasts.